Role of the AhR-Repressor and AhR-dependent CYP1 Monooxygenases in Immune Cells Regulation

Dissertation

zur

Erlangung des Doktorgrades (Dr. rer. nat.)

der

Mathematisch-Naturwissenschaftlichen Fakultät

der

Rheinischen Friedrich-Wilhelms-Universität Bonn

vorgelegt von

Irina Iriady

aus

Jakarta, Indonesien

Bonn, Februar 2024

Angefertigt mit Genehmigung der Mathematisch-Naturwissenschaftlichen Fakultät der Rheinischen Friedrich-Wilhelms-Universität Bonn

Gutachterin/Betreuerin : Prof. Dr. Irmgard Förster

Gutachter : Prof. Dr. Christoph Wilhelm

Tag der Promotion: 09.10.2024

Erscheinungsjahr: 2024

Table of Contents

1. Introduction	1
1.1. The immune system	1
1.1.1. Innate immune system	1
1.1.2. Adaptive immune system	2
1.2. Tissue specific regulation of immune response	3
1.1.3. Immune regulation in the intestine	4
1.1.3.1. Intestinal epithelial layer	4
1.1.3.2. Intestinal myeloid and lymphoid cells in the lamina propr	ia 5
1.1.3.3. Intestinal innate lymphoid cells	6
1.1.3.4. Peyer's patches	7
1.1.4. Immune regulation in liver	8
1.1.5. Immune regulation in adipose tissue	10
1.2. Stromal-immune cell cross-talk influences the tissue microenvironmen	t 14
1.3. Diet-induced obesity and its implications on metabolism	15
1.4. DIO impacts organ function which involves alterations of immune cell	ratios and functions 16
1.5. The properties of the AhR/AhRR signaling pathway	17
1.6. The diversity of AhR ligands	19
1.7. Canonical and non-canonical AhR signaling pathways	20
1.8. Expression and physiological functions of AhR and its target genes	23
1.8.1. Function of AhR signaling in lipid metabolism and DIO	24
2. Aim of the Thesis	26
3. Materials	27
3.1. Equipments	27
3.2. Consumables	29
3.3. Chemicals	30
3.4. Solutions	32
3.5. Enzymes	33
3.6. Kits	33
3.7. Antibodies	
3.7.1. Antibodies for FACS	33
3.7.2. Antibodies for Histology	35

	3.7.3.	Antibodies for Western Blot	
	3.8. PCF	R Primers	36
	3.9. qPC	CR reagents	37
	3.10.Mou	use Diets	37
	3.11.Soft	tware	37
	3.12. Ani	mals	38
	3.13.Gen	neration of AhRRE/E and Triple CYP-deficient mice	38
4	. Meth	ods	39
	4.1. Ani	mal Experiments	39
	4.1.1.	Genomic DNA isolation and gel electrophoresis	
	4.1.2.	In vivo Ligand Stimulation with 3MC	
	4.1.3.	High-fat diet experiment40	
	4.1.4.	Glucose-tolerance test	
	4.1.5.	Generation of bone-marrow-derived DC	40
	4.2. Hep	G2 and HEK293T cell culture	41
	4.3. Cell	stimulations with LPS and AhR ligands	41
	4.4. mR	NA decay	41
	4.5. Hist	tology	41
	4.5.1.	Tissue preparation for cryosections	
	4.5.2.	Tissue preparation for paraffin sections	
	4.5.3.	Immunofluorescence staining	
	4.5.4.	Hematoxylin and Eosin (H&E) staining	
	4.5.5.	Picrosirius red staining	
	4.5.6.	Oil-Red-O staining43	
	4.5.7.	Microscopy44	
	4.5.8.	Spatial Phenotyping44	
	4.6. Sing	gle cell suspensions from various tissue for FACS analysis	44
	4.6.1.	Small Intestine (Lamina Propria and IEL)44	
	4.6.2.	WATg (stromal vascular fraction)	
	4.6.3.	Adult murine ear skin	
	4.6.4.	Neonatal murine epidermis	
	4.6.5.	Isolation of immune cells from Liver46	
	4.6.6.	Isolation of immune cells from Spleen46	

4.7. FACS staining	46
4.7.1. LIVE/DEAD® Fixable Dead Cell Staining	47
4.7.2. Fixation of cells for flow cytometric analysis or intracellular staining	47
4.8. Western Blot	47
4.9. Real Time Quantitative PCR (qPCR)	47
4.9.1. RNA isolation	47
4.9.2. cDNA synthesis	48
4.9.3. qPCR	48
4.9.4. Comparative Ct Method Quantification	49
4.10. Luciferase assay	50
4.11.FAT scoring for WATg fibrosis	50
4.12. Statistical analysis	50
. Results	51
5.1. Validation of AhRR-V5 protein expression in mice	51
5.2. Determination of the optimal concentration and activation time point of difference 57	ent AhR ligands
5.3. Visualization of AhRR-Expressing Cell Subsets in Different Organs Under	62
Steady-State Conditions	62
5.3.1. AhRR expression and analysis of cell subsets in the small intestine	63
5.3.2. AhRR expression and analysis of cell subsets in the skin	67
5.3.3. AhRR expression and analysis of cell subsets in the liver	75
5.3.4. AhRR expression and analysis of cell subsets in the Stromal Vascular Fra WATg 82	ction of
5.3.5. AhRR expression and analysis of cell subsets in the gallbladder	85
5.3.6. AhRR expression and analysis of cell subsets in the spleen	88
5.3.7. AhRR expression and analysis of cell subsets in bone-marrow-derived DO 95	C (BMDC)
5.4. AhR ligand application enhances AhRR expression in multiple cell subsets of pounder physiological conditions	
5.4.1. AhRR expression in small intestine	99
5.4.1.1. AhRR expression in IEL	100
5.4.1.2. AhRR expression in the lamina propria of SI	105
5.4.2. AhRR expression in Liver	109
5.4.3. AhRR expression in gonadal white adipose tissue (WATg)	115
5.1.5. Thirtt expression in gondant white despose tissue (WTTg)	

5.5.2. Cellular composition of the small intestinal intraepithelial lymphocytes and lamin propria after HFD challenge	
5.5.2.1. Cellular compositions of IEL	125
5.5.2.2. Cellular composition in SI Lamina Propria	127
5.5.3. AhRR and CYP-dependent cellular and metabolic alterations in the liver after died challenge	•
5.5.4. AhRR and CYP-dependent cellular and metabolic alterations in WATg after dieta challenge	•
6. Discussion	150
6.1. Validation of AhRR-V5 protein expression in mice	150
6.2. Expression kinetics of <i>Ahr</i> and its target genes after stimulation with different AhR 152	ligands
6.3. Increased AhR signaling through elimination of CYP- and/or AhRR- mediated n feedback regulation	_
6.3.1. Triple CYP deficiency enhanced AhRR expression in immune and stromal non-immune cells in different organs	55
6.3.2. Lack of AhRR and/or deficiency of the three AhR-dependent CYP enzymes alters the frequency of immune cell subsets	
6.3.3. Deficiency for AhRR and Triple CYP inhibit proliferation of skin epidermal DET under physiological conditions	
6.4. 3MC treatment in vivo can upregulate AhRR expression in myeloid cells of various 162	organs
6.4.1. 3MC activates AhR and induces AhR target genes on mRNA level in several peripheral organs	63
6.4.2. AhRR expression is induced by 3MC treatment in immune cells in several peripheral organs	54
6.4.3. 3MC treatment alters the frequency of eosinophils and double negative ATM in WATg SVF	67
6.5. Dysregulated AhR signaling affects the onset of obesity and immune cell frequencies	167
6.5.1. Purified diets significantly reduce AhRR/EGFP expression10	58
6.5.2. Ablation of AhRR but not Triple CYP protects against weight gain and liver steatosis	70
6.5.3. HFD did not lead to extensive fibrosis in liver and WATg1	73
6.5.4. Ablation of AhRR and/or Triple CYP deficiency alters immune cell frequencies a dietary challenge	
6.5.4.1. Ablation of AhRR reduces the lamina propria Mo-Mac after HFD	174

7. Refere	ences		182
6.6 Concl	lusion		181
6	5.4.3.	HFD alters both lymphoid and myeloid immune compartments in WATg	178
		DIO and dysregulated AhR signaling alter the frequencies of hepatic KC an	

Abstract

The Aryl hydrocarbon receptor (AhR) is a transcription factor that can be activated by various polyaromatic ligands and plays an important role in immune regulatory processes. AhR activity is regulated through the AhR-repressor (AhRR), which is involved in the regulation of immune responses according to our previous results. Apart from the AhRR, Cytochrome P450 enzymes, particularly CYP1A1, CYP1A2, and CYP1B1 also regulate AhR activity by metabolizing AhR ligands, hence curtailing the duration of AhR activation. Thus, we hypothesized that the depletion of these three CYP enzymes increases AhR's ligand bioavailability and hence AhRR expression, affecting immune cell subsets under physiological and perturbed condition, such as Diet-Induced Obesity (DIO). To prove this, we crossed *Cyp1a1-*, *Cyp1a2-*, and *Cyp1b1* (Triple CYP)-deficient mice with AhRR^{E/E} mice that harbor an EGFP knock-in allele in the endogenous *Ahrr* locus (Triple CYP-KO AhRR^{E/E}).

This dissertation demonstrated that the ablation of AhRR and the three AhR-dependent CYP enzymes enhanced AhR activation more than AhRR ablation alone, as shown by the presence of more AhRR/EGFP-expressing immune cells in various peripheral organs, such as small intestine (SI), liver, and gonadal white adipose tissue (WATg). Our previous findings showed that no AhRR/EGFP was detected in the liver of AhRR^{E/E} mice both in immune- and non-immune cells. However, in Triple CYP-KO AhRR^{E/E} mice, AhRR/EGFP expression was detected not only in immune-, but also non-immune cells in the liver. Furthermore, *in vivo* treatment with 3- Methylcholanthrene (3MC), a potent AhR ligand, increased AhR activation and hence AhRR/EGFP expression in several immune cells of Triple CYP-KO AhRR^{E/E} mice, particularly in liver and WATg, suggesting that AhR ligand stimulation promoted AhRR expression in an organ- and cell-specific manner. Besides, this treatment also altered the frequencies of eosinophils and adipose tissue macrophages of type 3 (ATM3) in WATg,

Due to the role of AhR signaling in immunometabolism, the physiological parameters (e.g., body weight, blood glucose, and liver enzymes), as well as the frequencies of immune cells and AhRR-expressing immune cells in the context of diet-induced obesity (DIO), were also investigated. It was shown that following 14 weeks feeding high fat diet (HFD), the ablation of AhRR ameliorated the DIO onset, as AhRR^{E/E} and Triple CYP-KO AhRR^{E/E} mice had reduced body- and liver-weight gain, as well as higher insulin sensitivity compared to the WT and Triple CYP-KO mice, respectively. Furthermore, HFD in combination with the ablation

of AhRR and/or Triple CYP also altered both myeloid and lymphoid immune subsets mostly in liver and WATg.

Overall, the results of this dissertation highlighted the effects of dysregulated AhR signaling on the immune cell subsets not only under physiological conditions, but also in response to ligand stimulation and overnutrition.

List of Abbreviation

2,3,7,8-tetrachlordibenzo-ρ-dioxin c	TCDD
3-Methylcholanthrene	3MC
3,3'-Diindolylmethane	DIM
4',6-diamidino-2-phenylindole	DAPI
6-formylindolo[3,2-b]carbazol	FICZ
AhR nuclear translocator	ARNT
AhR repressor	AhRR
Antigen presenting cell	APC
Aryl hydrocarbon receptor	AhR
Antimicrobial peptide	AMP
Antioxidant response element	ARE
Adipose tissue eosinophils	ATE
Adipose tissue macrophages	ATM
Benzo[a]pyrene	B[a]P
Bone marrow-derived dendritic cells	BMDC
Basic helix-loop-helix	bHLH
Brown adipose tissue	BAT
C-C chemokine receptor	CCR
Cluster of differentiation	CD
Control diet	CD
Cytochrome P450	CYP
Danger-associated molecular patterns	DAMPs

Dendritic cell	DC
Dendritic epidermal T cell	DETC
Diet induced obesity	DIO
Dextran sodium sulfate	DSS
Dioxin response element	DRE
Enzyme-linked Immunosorbent Assay	ELISA
Epithelial cell adhesion molecule	EPCAM
Granulocyte macrophage colony-stimulating factor	GM-CSF
High-fat diet	HFD
Indole-3-carbinol	I3C
Indolo[3,2-b]carbazole	ICZ
Interferon	IFN
Interleukin	IL
Intestinal epithelial cell	IEC
Intraepithelial lymphocyte	IEL
Innate lymphoid cells	ILC
Intestinal stem cells	ISC
Lipid Associated Macrophages	LAM
Lamina propria mononuclear cells	LPMC
Liver sinusoidal endothelial cells	LSEC
Nuclear factor erythroid 2-related factor 2	Nrf2
Nuclear factor-κB	NF-κB
Platelet-derived growth factor receptor	PDGFR

Platelet endothelial cell adhesion molecule	PECAM
Perivascular adipose tissue	PVAT
Perivascular macrophages	PVM
Smooth muscle actin	SMA
Subcutaneous adipose tissue	SAT
T cell receptor	TCR
TCDD-inducible poly (ADP-ribose) polymerase	TiPARP
Tristetraprolin	TTP
Visceral adipose tissue	VAT
Gonadal White Adipose Tissue	WATg
Xenobiotic response element	XRE

List of Figures

Fig. 1.1 The structure and functional domains of AhR, AhRR, and ARNT	19
Fig. 1.2 Schematic representation of the canonical and non-canonical AhR signaling pathways	22
Fig. 5.1 AhRR expression in BMDC is not detectable by western blot	52
Fig. 5.2 The peak of Ttp expression coincides with the peak of Ahrr expression	55
Fig. 5.3 The mRNA decay rates of AhR and its target genes	55
Fig. 5.4 3MC is the most potent stimulus to induce the expression of most AhR target genes	58
Fig. 5.5 Cyp1a1 expression was highest among all target genes following 3MC stimulation	61
Fig. 5.6. Enhanced AhRR/EGFP Expression in the Small Intestine of Triple CYP-KO AhRR ^{E/E}	
Fig. 5.7. Enhanced AhRR/EGFP expression in the back skin of Triple CYP EE mice on a histol level	ogical
Fig. 5.8. Gating strategies for myeloid and lymphocytes subsets in the ear skin	69
Fig. 5.9. Elevated cDC2 frequency and AhRR/EGFP expression in all myeloid subsets in the sk	in of
Triple CYP AhRR EE mice.	70
Fig. 5.10 Ablation of AhRR reduces the frequency of DETC	72
Fig. 5.11 Confirmation of AhRR-expression in DETC of back skin	73
Fig. 5.12 Ablation of the three AhR-dependent CYP enzymes and AhRR reduced the frequency	
proliferating DETC in mice on day 2 post-natal	74
Fig. 5.13 AhRR/EGFP expression in the liver is observed in Triple CYP EE but not AhRR EE i	
on a histological level. Expression of AhRR/EGFP in.	79
Fig. 5.14 Gating strategies for myeloid and lymphocyte subsets in the liver	79
Fig. 5.15 Ablation of AhRR or the three AhR-dependent CYP enzymes did not cause significant	ıt
differences in lymphocyte and myeloid subsets	80
Fig. 5.16 AhRR/EGFP is expressed in hepatic immune cell subsets	81
Fig. 5.17 Gating strategies for myeloid and lymphocyte subsets in the SVF of WATg	82
Fig. 5.18 Enhanced expression of AhRR/EGFP in Triple CYP EE mice did not lead to significa	nt
changes in the frequencies of myeloid cells in WATg.	84
Fig. 5.19 Neither deficiency of AhRR- nor AhR-dependent CYP enzymes led to significant cha	nges
in lymphocyte subsets in WATg	85
Fig.5.20 AhRR/EGFP is expressed in the gallbladder of Triple CYP AhRR ^{E/E} mice	86
Fig. 5.21 The AhRR/EGEP-expressing cells in the gallbladder are CD34 ⁺ stromal cells	87

Fig. 5.22 Enhanced AhRR expression is observed in the spleen Triple CYP EE mice on histological	al
level.	. 89
Fig. 5.23 Gating strategies for myeloid and lymphocyte subsets in spleen.	. 90
Fig. 5.24 Deficiency in either AhRR or the three AhR-dependent CYP enzymes can elevate the	
frequency of NK cells.	. 92
Fig. 5.25 Deficiency in neither AhRR nor Triple CYP alters the frequency of T cells in the spleen.	. 92
Fig. 5.26 . Triple CYP deficiency enhanced AhRR/EGFP expression in the splenic myeloid cell	
subsets in Triple CYP AhRR ^{E/E} mice.	. 93
Fig. 5.27 AhRR/EGFP expression in splenic T-lymphocytes subsets was detected in Triple CYP	
AhRR ^{E/E} and not in AhRR ^{E/E} mice.	. 93
Fig. 5.28 AhRR/EGFP is expressed in T- and B cells, but not in SIGNR1 ⁺ marginal zone	
macrophages.	. 94
Fig. 5.29 Gating strategies for myeloid subsets in BMDC	. 95
Fig. 5.30 The absence of both AhRR and Triple CYP reduced GM-Macs frequency.	. 96
Fig. 5.31 LPS-mediated downregulation of CD115 in BMDC of WT mice.	. 97
Fig. 5.32 Comparable AhRR/EGFP expression was detected in the BMDC subsets of Triple CYP	
AhRRE/E and AhRRE/E mice regardless of the treatments	. 98
Fig. 5.33 AhR and its target genes in SI 16 hours post in vivo 3MC treatment.	. 99
Fig. 5.34 Gating strategies for IEL of S.I	100
Fig. 5.35 3MC does not alter the frequencies of the cell subsets	101
Fig. 5.36 3MC does not increase the frequencies of AhRR-expressing IEL.	102
Fig. 5.37 Minimum expression of AhRR in IEC was observed in intestinal epithelia of 3MC-treate	d
Triple CYP-KO AhRR ^{E/E} mouse	104
Fig. 5.38 There is no difference in MFI between genotypes and treatment groups	105
Fig. 5.39 The gating strategy of small intestinal lamina propria	105
Fig. 5.40 3MC does not alter myeloid and lymphoid cell subsets in SI lamina propria	106
Fig. 5.41 The frequencies of AhRR-expressing macrophages and Mo-Mac were increased by 3MC	
Fig. 5.42 Fluorescence intensity of AhRR-expressing immune cells was not significantly increased	l by
3MC	
Fig. 5.43 AhRR expression in SI in control and 3MC-treated mice	
Fig. 5.44. The expression of AhR and its target genes in liver 16 hours post in vivo 3MC treatment	
	110

Fig. 5.45 Gating strategies for myeloid and lymphocyte subsets in the liver	111
Fig. 5.46 Acute 3MC treatment did not cause significant differences in frequencies of lymphocyt	tes
and myeloid subsets.	112
Fig. 5.47 Acute 3MC-treatment increased the frequencies and the MFI of AhRR-expressing imm	nune
cells	114
Fig. 5.48 3MC does not enhance AhRR expression or its intensity in intrahepatic vessels	115
Fig. 5.49 Gating strategy of myeloid subsets in the SVF of WATg	116
Fig. 5.50 3MC increased the frequency of ATM3 in AhRR ^{E/E} mice	116
Fig. 5.51 3MC significantly increases the frequency of AhRR-expressing Eosinophils in Triple C KO AhRR ^{E/E} mice	
Fig. 5.52 3MC enhances the MFI of AhRR(EGFP expression of some of the myeloid subsets	119
Fig. 5.53 Tissue autofluorescence was observed in the cryosections of WATg	120
Fig. 5.54 Loss of AhRR reduced weight gain and increased glucose tolerance.	124
Fig. 5.55 HFD does not alter the frequencies of cell subsets in intestinal epithelium	125
Fig. 5.56. HFD does not increase the frequencies of AhRR-expressing IEL	127
Fig. 5.57 Gating strategy of lymphocytes in SI lamina propria.	127
Fig. 5.58 HFD only slightly altered the frequencies of $T\gamma\delta$ and Mo-Mac in SI lamina propria	129
Fig. 5.59 HFD markedly reduced the frequencies of AhRR-expressing immune cells in SI lamina	ı
propria	130
Fig. 5.60 AhRR expression in SI of CD- HFD-fed mice.	132
	133
Fig. 5.61 Loss of Triple CYP enzymes increased liver weight and hepatic Ahrr expression	
Fig. 5.61 Loss of Triple CYP enzymes increased liver weight and hepatic Ahrr expression	135
Fig. 5.62 Liver histology in response to HFD and CD feeding	136
Fig. 5.62 Liver histology in response to HFD and CD feeding	136 137
Fig. 5.62 Liver histology in response to HFD and CD feeding	136 137 139
Fig. 5.62 Liver histology in response to HFD and CD feeding	136 137 139 140 ells.
Fig. 5.62 Liver histology in response to HFD and CD feeding	136 137 139 140 ells. 140
Fig. 5.62 Liver histology in response to HFD and CD feeding	136 137 139 140 ells. 140
Fig. 5.62 Liver histology in response to HFD and CD feeding	136 137 139 140 ells. 140 142
Fig. 5.62 Liver histology in response to HFD and CD feeding	136 137 139 140 ells. 140 142 143

Fig. 5.73 HFD and CD diminished AhRR-expressing immune cells in WATg SVF	149
List of Tables	
Table 1.1 Subpopulations of murine ATM. Table is adapted from Morris et al., 2011.	12
Table 1.2 Newly identified murine ATM subsets. Table is adapted from Li et al., 2023	13
Table 3.1. Equipments	. 27
Table 3.2 Consumables	. 29
Table 3.3. Chemicals	. 30
Table 3.4. Solutions	. 32
Table 3.5. Enzymes	33
Table 3.6. Kits	. 33
Table 3.7 FACS antibody list	33
Table 3.8 Histology antibody list	. 35
Table 3.9 Western blot antibodies list	35

1. Introduction

1.1. The immune system

Organisms are challenged with pathogens throughout their lifetime. The immune system consists of various organs, cells and molecules that work in concert to protect the body against diseases. The immune system is a complex and interactive network that takes on various tasks to confer effective protection against diseases that are caused by pathogens or other harmful stimuli. A healthy immune system needs to fulfill four basic principles (Lentz & Feezor, 2003). First, it must detect and fight off infection by employing immune effector functions. Second, it must be able to distinguish the host's own cells from foreign cells, hence preventing the former from being attacked. Third, it must prevent recurring disease due to infection caused by the same pathogen, by generating immunological memory. Fourth, it should limit its own response following pathogen removal and resolution of an infection. Inactivity of the immune system can lead to chronic infections and immunodeficiencies, whereas exaggerated reactions may result in allergy and autoimmune diseases. Based on the specificity of the response and chronological order of its induction, the immune system can be divided into innate and adaptive immunity. These two parts consist of different cell types that have various functions to confer protection. Nonetheless, both the innate and adaptive immune system are closely interconnected.

1.1.1. Innate immune system

The innate immune system is the first line of defense against pathogens when they infiltrate the body. From the evolutionary perspective, it is the oldest part of the immune system and it is a highly conserved system. Its action has limited specificity; it responds through a restricted set of receptors with conserved signaling pathways to all pathogens and foreign substances. However, it only keeps pathogens at bay and its response *per se* mostly does not resolve the disease. Moreover, it wards off pathogens by conferring multiple layers of protection (Delves & Roitt, 2000; Janeway, 1992). First, physical barriers like skin, nasal hair, eyelashes, tight junctions, and mucous. Second, chemical barriers, such as pH regulation and antimicrobial molecules (e.g., IgA, lysozyme, pepsin, β-defensins). Third, biological barriers, such as the

microbiome. Upon barrier breaching, innate immune cells phagocytose the invading pathogen, leading to release of cytokines or other inflammatory mediators assigned to the innate immune system. The latter ranges from inflammation-related serum proteins, antimicrobial peptides (AMP), the complement system, to cytokines and chemokines. Innate immune cells are for instance neutrophils, dendritic cells (DC), monocytes, and macrophages. Together with other innate immune cells, such as innate lymphoid cells (ILCs) and mast cells, they endow the organism with immediate protection. In addition, the innate immune system is equipped with a variety of receptors to recognize pathogen-associated molecular patterns (PAMPs) present on many microorganisms as well as danger-associated molecular patterns (DAMPS). These pattern recognition receptors (PRRs) do not only exist on the cell membrane but are also widely distributed in intracellular compartment membranes and in the cytoplasm (Li & Wu, 2021). Activation of most PRRs recruits signaling adaptors that control processes like the induction of local inflammation, recruitment of further effector cells, restriction of a local infection and finally triggering of an adaptive immune response (Janeway, 1992). However, the innate immune system lacks classical immunological memory, meaning it responds uniformly, irrespective of how many times a specific infectious agent is encountered. Interestingly, this concept has recently been challenged. The term "trained immunity" is coined to describe a phenomenon, in which organisms lacking adaptive immunity have been shown to develop resistance to reinfections (Netea et al., 2016). This could be achieved by epigenetic and metabolic reprogramming, e.g., histone methylation and acetylation of genes involved in innate immune responses. This may also be the underlying reason why BCG vaccination in African children also reduced other non-tuberculous infections (Garly et al., 2003). Furthermore, the innate immune system cannot provide specificity against individual pathogens, which depends on activation of the adaptive immune system by antigen presenting cells (APC) (Delves & Roitt, 2000).

1.1.2. Adaptive immune system

The adaptive immune response plays a crucial role during pathogen clearance and disease resolution. Antigen presentation by APC eventually triggers the adaptive immune response by their expression of co-stimulatory molecules and the APC-induced alteration of the cytokine microenvironment. Adaptive immunity involves selection and expansion of lymphocytes, bearing receptors with high specificity for foreign antigens. These receptors allow for a fine

discrimination between self and non-self. Additional central features of the adaptive immune system are the precise elimination of pathogens and pathogen-infected cells and the creation of immunological memory that provides protection against re-infection (Kaech et al., 2002). The two main cell types of the adaptive immune system are T- and B lymphocytes To fulfill their function, adaptive immune cells need to recognize pathogens as well as pathogen-derived peptides presented in the context of major histocompatibility complex (MHC) molecules on the surface of APC to generate pathogen-specific antibodies or activation of T cells with appropriate T-cell receptors (TCRs). This process requires the maturation of B-cell receptors (BCRs) and clonal expansion of pathogen-specific B- and T cells, leading to a slower response time compared to innate immune responses. T lymphocytes, which mature in the thymus are the effectors of the cellular immune response and can be functionally divided into subsets either assisting other cells in immunological processes (CD4⁺ T cells) or directly destroying virus-infected cells or tumor cells (CD8⁺ T cells) (Bonilla & Oettgen, 2010). B lymphocytes, which arise in the bone marrow, develop into antibody producing plasma cells directed by signals from CD4⁺ helper T cells. Antibodies form the humoral component of the adaptive immune system and are used to neutralize pathogens, immobilize antigens for phagocytosis and activate the complement system (Bonilla & Oettgen, 2010; Janeway et al., 2001).

1.2. Tissue specific regulation of immune response

As mentioned above, activation of PRRs leads to a cascade of immunological processes, such as secretion of inflammatory and recruitment of effector cells. It has been shown, however, that different pathogen entry routes lead to different outcomes of adaptive immunity, even though they likely activate a similar PRR repertoire (Hu & Pasare, 2013). For instance, the mucosal route of infection seems to favor Th17 over Th1 response. *Francisella tularensis* infection via the intranasal and intradermal routes favor Th17 and Th1 responses, respectively (Woolard et al., 2008). Similarly, oral infection with *Yersinia enterocolitica* also promotes Th17 response, whereas systemic infection with the same pathogen promotes Th1 responses (DePaolo et al., 2012). Hence, the unique regulation of immune response in several peripheral organs, such as small intestine (SI), liver, and gonadal white adipose tissue (WATg) will be delineated in the following sections.

1.1.3. Immune regulation in the intestine

1.1.3.1. Intestinal epithelial layer

Most pathogens enter via the mucosal surface, either in the mucosal membrane of the respiratory-, the urogenital-, or the gastrointestinal tract (Quintana-Hayashi et al., 2018). The gastrointestinal tract represents the largest mucosal surface in the human body; the SI of humans has a surface area of around 400m^2 (Janeway et al., 2001). It is also exposed to the heaviest burden of antigens derived from the environment or diets, leading to the development of distinct commensal niches (Belkaid & Naik, 2013; Mestecky et al., 1999). Due to this constant antigen exposure, the intestine, like other barrier organs, has developed a finely tuned local immunosurveillance system that is also highly compartmentalized (Belkaid & Naik, 2013). Anatomically, the intestinal barrier contains the epithelial layer that is mostly made up of intestinal epithelial cells (IEC) and the lamina propria of the mucosa. Both harbor diffuse mucosa-associated lymphoid tissue that consists of leukocytes, such as intraepithelial lymphocytes (IEL) and lamina propria mononuclear cells (LPMC).

The majority of the IEL have cytotoxic properties and they express effector cytokines, such as interferon gamma (IFNy), interleukin-2 (IL-2), IL-4 or IL-17. In general, IEL maintain the intestinal barrier and keep pathogens at bay. IEL are located at the basement membrane between enterocytes and they are composed of antigen-experienced T cells of both the TCR $\gamma\delta^+$ and conventional TCRαβ⁺ lineages (Goodman & Lefrançois, 1988). Most of these cells express CD8 rather than CD4 and a large fraction of them expresses a CD8αα homodimer as co-receptor, which is essentially not found in any other location (Hayday et al., 2001). IEL can be further divided into natural IEL (CD8 $\alpha\alpha^+$ TCR $\gamma\delta^+$ and TCR β^+) that differentiate in the thymus, and induced IEL (CD8 $\alpha\beta^+$ TCR β^+) that differentiate in the periphery (Cheroutre et al., 2011; Park et al., 2019). Natural IEL acquire their intestinal homing properties in the thymus and dominate the intestinal epithelium early in life. In the thymus, they develop from non-MHC restricted triple-positive thymocytes and subsequently migrate to the intestine as CD8α⁻CD8β⁻CD4⁻ cells where they undergo further differentiation (Hayday et al., 2001). Meanwhile, induced IEL numbers increase with age. As they become activated in the periphery, they obtain signals to migrate to the intestine and eventually surpass natural IEL (Park et al., 2019).

1.1.3.2. Intestinal myeloid and lymphoid cells in the lamina propria

The other part of the intestinal layer is the lamina propria, which is made up of connective tissue between the epithelium and muscularis mucosae. This layer contains both immune and non-immune cells. The immune cell compartment of the lamina propria harbors a huge number of lymphoid and myeloid cells including B cells, T cells and numerous innate immune cells such as DC, macrophages, eosinophils and mast cells. CD4⁺ T cells are more abundant compared to CD8⁺ T cells with a ratio of two to one. They are mostly classified as conventional T cells primed in secondary lymphoid organs displaying an effector memory phenotype (CD45RO⁺ CCR7⁻ CD62L⁻). Nevertheless, the CD4⁺ T cell compartment is highly diverse with regional differences in distribution and function along the intestine (Mowat & Agace, 2014). These T cells might have regulatory functions and therefore be involved in maintenance of tolerance to environmental antigens. Lamina propria CD8⁺ T cells can have potent cytolytic activity acting as antigen experienced true effector cells (Aguilera-Montilla et al., 2004).

The presence of large numbers of APC, such as macrophages and DC in the lamina propria may suggest that antigens crossing the epithelium are processed and presented to CD4⁺ T cells. DC sample antigens from the intestine, then migrate to the mesenteric lymph nodes (mLN) and initiate adaptive immune responses by priming of naïve T cells. Intestinal DC, like the ones in other organs, are identified by their co-expression of CD11c and major histocompatibility complex class II (MHCII), as well as their lack of F4/80 expression. The majority of intestinal DC express integrin $\alpha_E \beta_7$ (CD103). Intestinal DC can be further divided by their CD11b and CD103 expression into CD103 CD11c, CD103 CD11b and CD103⁺CD11b⁻ DC. A poorly defined CD103⁻CD11b⁺ DC subset is also found in intestinal lamina propria (Bain et al., 2017). All four subsets can also be located in gut-draining afferent lymph and are all derived from a committed FMS-like tyrosine kinase 3 ligand (Flt3L)dependent precursor (McDole et al., 2012). The CD103⁺ DC subsets induce Treg development but can also prime Th17 or Th1 cells if readily activated. Meanwhile, CD103⁻ intestinal DC are more immunogenic, inducing effector Th1 and Th17 cells (Bekiaris et al., 2014; Cerovic et al., 2014). Gut-resident DC, particularly CD103⁺ DC, have the unique ability to induce expression of gut-homing adhesion molecules during T cell priming (Hue et al., 2006; Johansson-Lindbom et al., 2005).

Furthermore, intestinal macrophages, also belonging to mononuclear phagocytes, are identified by their expression of F4/80, CD64, and CX3CR1. On top of that, intestinal macrophages also express CD11c (Bradford et al., 2011). Although these cells are present throughout the whole intestine, their abundance increases towards the colon (Bain & Mowat, 2014; Nagashima et al., 1996). In most tissues, macrophages arise from yolk sac and fetal liver progenitors, which seed tissues during embryonic development and subsequent in situ selfrenewal ensures constant macrophage replenishment (Stremmel et al., 2018). This mechanism has been verified for microglia, lung alveolar macrophages, liver Kupffer cells (KC) and epidermal Langerhans cells, whereas macrophages in the intestine need constant replenishment from circulating blood monocytes (Bain et al., 2014). Ly6Chi monocytes enter the intestinal mucosa, where they differentiate into CX3CR1hi macrophages. During this process, precursors upregulate MHCII, F4/80, CD64 and CX3CR1 but downregulate Ly6C (Bain et al., 2013; Cerovic et al., 2014). Furthermore, intestinal APC have also been shown to produce larger amounts of IL-23 than APC in the periphery (e.g. spleen), which stimulates the production of pro-inflammatory cytokines like TNF, IL-1β, and IL-17 from Th17 cells (Bunte & Beikler, 2019). This may explain the differential regulation of immune cells in different organs.

1.1.3.3. Intestinal innate lymphoid cells

Innate lymphoid cells (ILCs) are a subset of mucosal lymphocytes that gained more attention and interest in recent years. These cells are enriched at barrier surfaces and lack antigenspecific receptors found on T and B cells. They further lack myeloid cell- and DC-specific phenotypic markers and display a lymphoid morphology (Spits & Cupedo, 2012). Development of ILCs depends on expression of the common cytokine receptor γ -chain and the transcriptional repressor inhibitor of DNA binding 2 (ID2). Further, all subsets rely on signaling via the IL-7 receptor subunit- α (IL-7R α) for their development and maintenance. Like T helper cell subsets, ILCs are subdivided into different groups based on expression of specific transcription factors and effector cytokines.

Group 1 ILCs are primarily characterized by production and release of IFNγ upon stimulation with IL-12 and IL-18. They consist of NK cells and other ILC1s. NK cell development is regulated by the transcription factors T-bet and eomesodermin (Eomes). NK cells are

characterized by their cytotoxic function, and are therefore considered as the innate counterpart of CD8⁺ cytotoxic T cells (Fuchs et al., 2013; Klose et al., 2013). The other ILC1s are developmentally dependent on expression of T-bet but not of Eomes and produce IFNγ but no Th2- or Th17-cell-associated cytokines. (McKenzie et al., 2014; Spits & Cupedo, 2012).

Group 2 ILCs are distinguished from other ILCs by production of the Th2-associated cytokines IL-4, IL-13, and IL-5 upon stimulation with IL-25, IL-33 or thymic stromal lymphopoietin (TSLP). Like Th2 cells, ILC2s require expression of the transcription factor GATA3 for development and function. Moreover, their development is also dependent on the expression of the transcription factor RORα. Different studies have shown importance of ILC2s in mediating resistance to certain helminths and nematodes. Due to their broad cytokine production profile, including IL-9 and amphiregulin, ILC2s are also involved in metabolic processes, tissue repair, alternative macrophage activation, thermoregulation and mucus production (Eberl et al., 2015; McKenzie et al., 2014).

Group 3 ILCs are identified by their ability to produce the IL-17 and IL-22 cytokines. They additionally release lymphotoxins and granulocyte macrophage colony-stimulating factor (GM-CSF). Group 3 ILCs can be further sub-classified into three different categories. Lymphoid tissue inducer cells (LTi cells) are a prototypic ILC3 family member and are essential for the formation of secondary lymphoid organs. The remaining ILC3s are further phenotypically subdivided into NKp46⁺ and NKp46– ILC3s. All subgroups consistently produce IL-22 and IL-17 upon stimulation with IL-23 and IL-1β, and their development and function depends on RORγt (Klose et al., 2013). However, only NKp46–ILC3 express the Th1 transcription factor T-bet and produce IFNγ, which is an important mediator of pathology in a mouse model of colitis (Buonocore et al., 2010). In addition, LTi cells and NKp46⁺ ILC3s depend on expression of the AhR for development and optimal maintenance. (Eberl et al., 2015; McKenzie et al., 2014; Spits & Cupedo, 2012).

1.1.3.4. Peyer's patches

In the intestinal lamina propria, there are also secondary lymphoid structures called Peyer's patches (PP). PP consist of large B cell follicles and interpolated T cell areas. They are separated from the intestinal lumen by the follicle associated epithelium (FAE) and the subepithelial dome, a diffuse area directly below the epithelium, which is rich in DC, T cells

and B cells. Specialized epithelial cells in the FAE, the so called microfold (M) cells, are very potent in transcytosing antigen from epithelial surfaces of the gastrointestinal tract. These antigens can subsequently be taken up and sampled by DC / macrophages, located directly below the M cells in the PP dome region. (Bain & Schridde, 2018; Mowat, 2003; Randall & Mebius, 2014)

1.1.4. Immune regulation in liver

Despite its primary role in metabolism, nutrient storage, and detoxification, the liver also harbors a diverse immune cell repertoire as well as non-hematopoietic cell populations that mediate complex immunological activity (Crispe, 2009). Like the intestine, the hepatic immune system has to keep the balance between tolerating harmless molecules and recognizing possible infectious agents, malignant cells or tissue damage. In addition, multiple populations of non-hematopoietic liver cells, including liver sinusoidal endothelial cells (LSEC) and stellate cells located in the subendothelial space, as well as liver parenchymal cells, take on the function of APC if immunosuppressive cytokines and inhibitory cell surface ligands are present. This often result in tolerance. Some pathogens like Hepatitis C virus and the malaria parasite, exploit such tolerance, and subsequently establish persistent infection (Crispe, 2009). Dynamic metabolic and tissue remodeling activities, combined with constant exposure to microbial products, results in persistent, tightly-controlled inflammation even in healthy liver (Robinson et al., 2016). When such controlled inflammation is dysregulated, it can lead to organ damage and pathology.

From the anatomical perspective, the low pressure blood flow, fenestrated endothelium and lack of a basement membrane also allows intimate interactions between resident immune cells and non-hematopoietic hepatic cells (Wisse et al., 1996). Hepatocytes and KC, the liver-resident macrophages, express PRR that can bind to MAMPs and DAMPs entering the liver from the blood via the portal vein (Janeway, 1992; Kubes & Mehal, 2012). In the myeloid compartment, KC are the most predominant cell subset and account for almost a third of the non-parenchymal cells in the liver (Bilzer et al., 2006). Other subsets of macrophages include liver capsular macrophages (LCM), biliary-tree-associated macrophages, as well as peritoneal macrophages and Mo-Mac (Elchaninov et al., 2022). The latter two subsets are normally recruited during infection (Cassado et al., 2015; Louwe et al., 2020). KC are mainly identified

by their high expression of F4/80, intermediate CD11b expression, as well as Tim4, Clec4F, CD206, and CD163 expression. Some publications show that there might be two KC subsets; the more predominant CD206^{lo} ESAM⁻ (KC1) and the less frequent CD206^{hi} ESAM⁺ (KC2) (Blériot et al., 2021; De Simone et al., 2021). This finding is still debatable, however, as both CD206 and ESAM are also expressed by LSEC. As LSEC are closely associated with KC, they might contaminate sorted KC populations (Hume et al., 2022). In general, KC are mainly involved in maintaining liver homeostasis, but are also important for immune regulation, tissue repair and liver regeneration. They are capable of inducing cytokine-, Toll-like receptor (TLR), RIG-like receptor and NOD-like receptor signaling (Robinson et al., 2016). KC can also mediate phagocytosis, as they express an array of PRR, complement receptors, and Fc receptors. Regarding the other macrophages subsets, LCM express F4/80, CD14, CD64 and CD207. They confer protection against infiltrating pathogens from the abdominal cavity (Sierro et al., 2017). Peritoneal macrophages are normally recruited upon infection and they express CD102 and GATA6, whereas biliary-tree associated macrophages express glycoprotein non-metastatic protein B (Gpnmb) (Remmerie, Martens, Thoné, et al., 2020). The role of peritoneal and biliary-tree associated macrophages are not as well-understood as the other two macrophages subsets (Elchaninov et al., 2022). During inflammation, monocytes are recruited and some of them give rise to monocyte-derived macrophages (Mo-Mac) that express CD11b, F4/80, and Ly6C. Even though Mo-Mac also express CD11b and F4/80, Mo-Mac express higher levels of CD11b and slightly lower levels of F4/80 compared to KC (Haldar & Murphy, 2014; Movita et al., 2012). Apart from macrophages, DC also contribute to the liver myeloid subset in healthy liver, and they encompass conventional DC (cDC) and plasmacytoid DC (pDC). Hepatic DC populations are described as phenotypically immature although they can stimulate strong T-cell responses depending on the stimuli (Thomson & Knolle, 2010). A subpopulation of human hepatic CD141⁺ DC have been shown to be potent cytokine producers and activators of T cells (Kelly et al., 2014). Granulocytic cells, such as neutrophils, are thought to be largely absent in the healthy liver, only accumulating in response to infection and inflammation (Gregory et al., 1996). Pertaining to the hepatic lymphocytes, they largely consist of natural killer (NK) cells, NK T cells (NKT), as well as mucosal associated invariant T cells (MAIT) and TCRγδ cells. The NKT cell subset also encompasses the CD1d-restricted invariant NKT cells (Robinson et al., 2016). The NK cells are part of ILC1, whereas the others belong to the unconventional T cells. Both groups are potent cytokine producers and influence both innate and adaptive immune responses in the liver (Borger et al., 2019; Zhang & Huang, 2017). In the mouse, NKT cells and NK cells make up 40% and 10% of total liver lymphocytes, respectively (Gao et al., 2008). Apart from innate lymphocytes, adaptive lymphocytes, such as CD4⁺ and CD8⁺ T cells, as well as B cells are also abundantly expressed in liver. The liver is particularly enriched in CD8⁺ T cells, activated T cells and memory T cells (Norris et al., 1998). Specific hepatic B cell subpopulations, such as the innate-like CD5⁺ B cell population, are further expanded in the liver during hepatotropic viral infection (Curry et al., 2003; Racanelli et al., 2001).

1.1.5. Immune regulation in adipose tissue

Adipose tissue (AT) is partially composed of adipocytes; they make up more than 90% of adipose tissue volume but represent less than 50% of its cellular content (Corvera, 2021). Apart from adipocytes, AT also contains a stromal vascular fraction (SVF). In lean mice, the SVF is comprised of endothelial cells, fibroblasts, pericytes, preadipocytes, mesenchymal stem cells, progenitor cells as well as numerous immune cells including anti-inflammatory immunoregulatory T cells, Tregs, ILC2, alternatively activated macrophages, and eosinophils (Ahima & Flier, 2000; Blaszczak et al., 2021). These cells work in concert to ensure the homeostasis within the AT including systemic insulin sensitivity.

AT is generally divided into white and brown AT (WAT and BAT, respectively). BAT is enriched in mitochondria and it expresses uncoupling protein 1 (UCP1), which allows it to modulate energy expenditure and thermogenesis (Townsend & Tseng, 2012). BAT is more predominantly found in newborns and infants, and it transform to WAT as we age. Meanwhile, WAT is the primary nutrient-sensing organ and energy storage site in our body, as WAT adipocytes are composed of large unilocular lipid droplets containing triacylglycerols and neutral free fatty acids (FFAs) (Harwood, 2012; Wensveen et al., 2015). Adipocytes release fatty acids into the circulation when glucose is limiting. These fatty acids are generated by breaking down triacylglycerols that contain more energy per unit mass than do carbohydrates and can essentially be stored anhydrously (Cox & Geissmann, 2020). WAT is further divided into two forms, subcutaneous AT (SAT) and visceral AT (VAT) (found close to and around the abdominal organs) (Wayne et al., 2020). In general, VAT accumulation associates with an

increased metabolic risk and overall mortality (Mittal, 2019). For the latter, there are six visceral fat depots, they are perirenal, gonadal, epicardial, retroperitoneal, omental, and mesenteric. These different depots are differentially affected by HFD feeding. Interestingly, gonadal white adipose tissue (WATg) seems to have a more limited lipid storage capacity compared to SAT and mesenteric VAT, as a study performed on mice showed that the WATg stopped expanding in size after the mice reached a body weight of around 40 g. This is also the point, where WATg crown-like structure (CLS) formation, liver steatosis and insulin resistance occurred (van Beek et al., 2015).

Both BAT and WAT can act as endocrine organs, as they can secrete an array of hormones called adipokines. Adipokines are involved in maintaining energy homeostasis by modulating food intake, energy expenditure, carbohydrate and lipid metabolism, blood pressure, blood coagulation, and inflammation (Harwood, 2012; Wensveen et al., 2015). Most adipokines are secreted by adipocytes, but they can also be produced by resident macrophages and other cells of the SVF. They control adipocyte metabolism, as well as energy homeostasis in multiple organs through their autocrine, paracrine, and endocrine functions (Deng & Scherer, 2010; Harwood, 2012). Adiponectin and leptin counteract each other to maintain WAT homeostasis. Adiponectin is the most abundant adipokine in the circulation and its levels are inversely correlated to BMI, triglyceride levels, and insulin resistance (Arita et al., 1999; Kadowaki et al., 2006). Adiponectin is an endogenous insulin sensitizer of tissues including the skeletal muscle and liver. Injection of mice with recombinant adiponectin results in decreased blood glucose levels (Berg et al., 2001) by increasing fatty acid oxidation and stimulating glucose utilization via the activation of AMPK (Yamauchi et al., 2001, 2002). On the contrary, elevated circulating leptin is associated with obesity, although obese patients are generally resistant to leptin's effects. Leptin acts on cells in specific hypothalamic nuclei that express the long form of the leptin receptor (ObRb) and mediate downstream signaling pathways to control appetite and energy expenditure (Kwon et al., 2016). Another well studied adipokine is Resistin, which was first discovered involved in obesity-mediated insulin resistance (Steppan et al., 2001). Resistin plays a role in the suppression of insulin-mediated signaling in adipocytes by activating SOCS3, an inhibitor of insulin signaling (Steppan et al., 2005).

In lean mice, DC play an anti-inflammatory role in AT. The upregulation of the WNT/β-catenin pathway in cDC1 promotes IL-10 production, while overexpression of PPARγ, a

transcription factor that controls adipocyte differentiation and adipogenesis in cDC2 contains the outbreak of local inflammatory responses (Longo et al., 2019; Macdougall et al., 2018). cDC2 can also directly upregulate PPARy signaling to limit pro-inflammatory signaling cascades (Macdougall et al., 2018; Trim & Lynch, 2022). However, specific depletion (Zbtb46^{cre}) of either PPARγ or β-catenin in DC does not significantly impact AT homeostasis in mice fed a normal diet (Redondo-Urzainqui et al., 2023). For macrophages, there are different subsets of ATM that exert various functions depending on the physiological condition, as shown in **Table 1.1**. ATM can be distinguished by their expression of CD11c and CD206 (Li et al., 2023; Morris et al., 2011). ATM1a and ATM1b are the classically activated macrophages that express CD11c, whereas ATM2 and 3 do not express CD11c and they are CD206⁺ or CD206⁻, respectively. ATM2 can produce inflammatory cytokines but the expression of CD206 has been perceived as a marker of alternatively activated phenotype and CD206⁺ M2-like macrophages modulate insulin sensitivity by inhibiting proliferation and differentiation of adipocyte progenitors (Li et al., 2023; Nawaz et al., 2017). In addition, several other subtypes have been more recently identified using other markers, such as CD9, Trem2, CD36, and Ferroportin/SLC40a1 among others as shown in **Table 1.2** (Li et al., 2023). Moreover, Bailin et al. (Bailin et al., 2022) suggested that CD206⁺ CD11c⁻ ATMs are primarily perivascular macrophages (PVM), whereas intermediate macrophages (IM) are among the CD206⁻ CD11c⁺ population, and lipid-associated macrophages (LAM) are within the CD11c⁺ cell subset. Nevertheless, this ATM classification is not as clear and elaborate as the previous ones.

Table 1.1 Subpopulations of murine ATM. Table is adapted from Morris et al., 2011.

Macrophage	Characteristics	Functions
subsets		
ATM1a	CD11b+, CD206 ⁻ CD11c ⁺	Pro-inflammatory; localize to CLS and
		secrete inflammatory factors including
ATM1b	CD11b+, CD206+ CD11c ⁺	TNF- α , IL-1 β , IL-6, and NO

ATM2	CD206+ CD11c- CD163	Anti-inflammatory; localize in the interstitial space and secrete anti-inflammatory cytokines, such as IL-4 and IL-10
ATM3	CD11b+, CD206- CD11c-	Express Ccr7, localize to CLS

Table 1.2 Newly identified murine ATM subsets. Table is adapted from Li et al., 2023.

Macrophage subsets	Characteristics	Functions
CD9+ ATM	CD11b+, Ly6c-, CD9+	Pro-inflammatory, promote
		obesity, localize to CLS
Lipid-associated	CD9+, CD63+, Trem2+,	Localize to CLS, counteract
macrophages (LAM)	CD9, LIPA, Fabp4, Fabp5	inflammation and adipocyte
		hypertrophy
Metabolically-activated	ABCA1, Plin2, CD36	Remove dead adipocytes by
macrophages (MMe)		lysosomal exocytosis,
		localize to CLS
MFe ^{hi}	CD163, CD11chi CD206lo,	store iron, regulate iron-
	SLC40a1, TFRC, FTL1, and	handling genes, and protect
	MGL1/2	adipocytes from iron
		overload

resident ATM in lean mice express markers of alternatively activated macrophages like CD206 and CD163, but not CD11c (Wentworth et al., 2010). CD11c⁺ ATM are more lipid-rich, are antigen presenting, and overlap with monocyte signatures (Muir et al., 2022). However, CD206⁺ CD11c⁻ ATM were increased in diabetic patients, were scavenger receptor–rich with low intracellular lipids, and they secreted proinflammatory cytokines (Muir et al., 2022). In terms of localization, CD206⁻ CD11c⁺ ATM can form 'crown' aggregates or crown-like structures (CLS). CD206⁺ CD11c⁻ ATMs concentrate in vascularized lymphoid clusters adjacent to CD206⁻ CD11c⁺ ATM, whereas CD206⁺ CD11c⁺ are more solitary and distributed

between adipocytes (Muir et al., 2022.; Wentworth et al., 2010). ATM can also be distinguished by their expression of Tim4, CD163, and MHCII. Based on lineage tracing and inducible labeling, Tim4⁺ ATM are of embryonic origin, whereas CD163⁺ and Tim4- ATM originate from bone marrow-derived monocytes and are dependent on *Ccr2* in mice, hence further supporting their origin (Etzerodt et al., 2020; Félix et al., 2021).

Apart from macrophages, eosinophils, ILC2, and immunomodulatory Tregs also play a role in WAT homeostasis. In WAT, eosinophils regulate axonal plasticity, leading to enhanced sympathetic innervation and they also promote energy expenditure (Meng et al., 2022). Eosinophils are recruited into WAT by ILC2, which produce IL-5 and IL-13 in response to IL-33 (Hams et al., 2013; Molofsky et al., 2013). ILC2 together with Tregs as well as eosinophils and alternatively activated macrophages play a role in suppressing adipose tissue inflammation (Misawa et al., 2022). AT-resident Tregs highly express the transcription factors GATA3 and peroxisome proliferator-activated receptor γ (PPAR γ). Treg proliferation is directly stimulated by IL-33, as adipose tissue Tregs highly express the IL-33 receptor ST2 (Cipolletta et al., 2012; Kolodin et al., 2015). This can also mediated by ILC2 through ICOSL and OX40L signaling in response to IL-33 (Halim et al., 2018).

Many cells in the myeloid and lymphoid subsets express at least one form of leptin receptor, therefore they can respond to adipokines. In the myeloid cell subset, leptin increases the proliferation of monocytes and induces the expression of inflammatory cytokines (TNF- α and IL-6) and activation markers (Santos-Alvarez et al., 1999). Leptin also acts on eosinophils by inducing the production of inflammatory cytokines, including IL-1 β , IL-6, and MCP-1 (Wong et al., 2007). In T lymphocytes, leptin acts as a negative signal for proliferation of thymus-derived Tregs (De Rosa et al., 2007). Contrary to leptin, adiponectin suppresses the production of TNF- α and IL-6 in monocytes/macrophages in the AT (Ohashi et al., 2010). Adipocyte-derived adiponectin is also responsible for the reduction of IFN- γ and IL-17-producing T lymphocytes in mice fed a normal diet (Surendar et al., 2019). Therefore, adipokines are also involved in shaping the immune response and pathophysiology of DIO.

1.2. Stromal-immune cell cross-talk influences the tissue microenvironment

In many organs, stromal-immune cell cross-talk has been reported to shape immune responses and affect disease progression, depending on the stimuli. In the intestine, the non-immune compartment consists of lymphatics and blood vessels that are embedded into smooth muscle cells, pericytes lining the blood vessels, fibroblasts, trophocytes, telocytes, intestinal stem cells (ISC) residing in the epithelial crypts, and the underlying myocytes (McCarthy et al., 2020). Trophocytes refer to a CD81⁺ PDGFR α^{lo} expressing cell subset located near the basal membrane. They secrete Gremlin1 and contribute to ISC maintenance. Telocytes are PDGFR α^{hi} expressing cells with sub-epithelial localization, and they are distinct from the CD34⁺ PDGFR α^{lo} cells that occupy the same space. These cells also express the prodifferentiation factors Bmp5 and 7 (Kaestner, 2019; McCarthy et al., 2020). Intestinal stromal cells also interact with the immune cells via IL-6 and they can also secrete inflammatory factors in response to inflammatory stimuli (West, 2019). For instance, intestinal fibroblast are sensitive to Oncostatin M (OSM) and either OSM or TNF stimulation can lead to secretion of various inflammatory factors, such as CCL2, CXCL10, and IL-6 (West et al., 2017).

In liver, LSECs can trigger steatosis, inflammatory responses, and fibrogenesis via communication with surrounding sinusoidal cells. This plays a role in the progression of NASH to liver fibrosis, as formation of capillaries and dysfunction of LSECs appear in the early stage of NASH. At this stage, LSECs acquire a pro-inflammatory phenotype; they recruit immune cells including neutrophils, monocytes and lymphocytes to the hepatic microenvironment, promoting HC steatosis and cell death, activating hepatic stellate cells (HSC) and KC, and promoting liver fibrosis. LSEC express scavenger- and mannose receptors. The latter can bind to glycoproteins and microbial glycans (Du & Wang, 2022). LSEC are perceived as the gatekeepers of hepatic immunity, as they are the first site that microbial and food antigens derived from the gastrointestinal tract encounter upon entry via the portal vein. Together with KC, LSEC scavenge and clean soluble antigens within the hepatic sinusoids. (Shetty et al., 2018).

1.3. Diet-induced obesity and its implications on metabolism

Obesity is a complex and chronic disease that involves many pathophysiological changes, due to alterations in environment. Obesity can be caused by genetic factors, diet, age, and a combination of these factors; of special relevance for this thesis is diet-induced obesity (DIO). DIO occurs when energy intake exceeds energy expenditure (Singla et al., 2010). Excessive energy intake disrupts the feeding regulatory centers in the central nervous system (CNS),

particularly the hypothalamic signaling pathway, which eventually affects the mobilization of fat depots (Kennedy, 1953; Woods et al., 1998). Leptin, one of the hormones that acts on hypothalamus, provides a satiety signal through its action on the CNS receptors, possibly the ventro-medial hypothalamic nucleus (VMN) (Konturek et al., 2004; Meek et al., 2013). However, in DIO, leptin receptors in the brain fail to respond to the leptin signaling, resulting in leptin resistance (Schwartz et al., 1997). Apart of leptin resistance, obesity also causes insulin resistance, which is the primary contributor to obesity-induced dysregulation in macronutrient metabolism, such as carbohydrates, protein, and most importantly lipid (Singla et al., 2010). The well-known hallmarks of obesity are increase plasma triglycerides (TG) and circulating free fatty acids (FFA) levels, which eventually can lead to further comorbidities of obesity, e.g., high blood pressure, non-alcoholic steatohepatitis (NASH), and atherosclerosis.

1.4. DIO impacts organ function which involves alterations of immune cell ratios and functions

In addition, the immune function of the body is affected by DIO, leading to a persistent low grade inflammation (Ellulu et al., 2017). The two organs that are impacted the most are WAT and liver. In DIO, inflammation of AT precedes the hepatic inflammation. In mice, obese AT is characterized by the early, transient infiltration of neutrophils followed by the accumulation of pro-inflammatory CD8⁺ T cells, CD4 Th1 cells and M1 macrophages all of which surround the dying adipocyte forming CLS. Innate immunity is an early and key component in sustaining AT inflammation (Blaszczak et al., 2021). Obesity induces a prominent population of ATMs expressing CD11c, CD9, and Trem2. Adipose tissue eosinophils (ATEs) are important in the control of obesity-associated inflammation and metabolic disease. ATE undergo major age-related changes in distribution and function associated with impaired adipose tissue homeostasis and systemic low-grade inflammation in both humans and mice (Brigger et al., 2020). HFD has been shown to reduce ATE numbers, but such reduction was reversible once the mice were fed with low-calorie diet (Bolus et al., 2018).

The numbers of pro-inflammatory macrophages are increased in AT during obesity. These macrophages produce pro-inflammatory cytokines such as IFN γ , tumor necrosis factor (TNF)- α , IL-6, or IL-1 β , which significantly dampen the proliferation and function of ILC2s. In both mice and humans, the number of adipose tissue resident ILC2s is markedly reduced in response to obesity, and reduced ILC2 function subsequently leads to a decrease in eosinophils and

alternatively activated macrophages in adipose tissue, promoting pathological adipogenesis and insulin resistance. The induced level of pro-inflammatory cytokines such as TNF- α is also partially mediated by leptin, leading to increased proliferation and differentiation of the monocytes (Guzik et al., 2003). Acting on the neutrophils, leptin leads to an increased expression of CD11b, as well as increased neutrophil chemotaxis and oxidative burst (Anderson & Ren, 2002; Knudson et al., 2005). Dysregulated TNF- α release in AT plays a critical role in peripheral insulin resistance in obesity. It has been shown that neutralization of TNF- α in obese and insulin-resistant animals results in significant increases in peripheral insulin sensitivity (Hotamisligil, 1999). Besides myeloid cells, obesity alters the induced Th17 and regulatory T cells in the lamina propria suggesting that mucosal immunity is sensitive to fluctuations in adiposity, and this may exacerbate inflammation leading to type 2 diabetes (Park et al., 2019).

1.5. The properties of the AhR/AhRR signaling pathway

The Aryl hydrocarbon receptor (AhR) is a transcription factor that can be activated by many polyaromatic ligands. AhR is among the first discovered members of the basic helix-loop-helix (bHLH)-PER-ARNT-SIM (PAS) protein family, which comprises heterodimeric transcription factors that act as sensors of environmental signals and are highly conserved (Konopka & Benzer, 1971; Poland et al., 1974). The bHLH domain covers the basic domain at the Nterminus and the HLH domain. The basic domain consists of 15 basic amino acids, and it serves as a DNA-binding motif. This domain is attached to the HLH domain, which allows protein dimerization (Li et al., 2006). Some bHLH proteins bind to sequences containing a consensus hexanucleotide sequence called E-box (5'-CANNTG-3'). The PAS domain contains five antiparallel β -sheets flanked by several α -helices and the domain is made out of 300 amino acid residues (Crews, 1998). The PAS domain is divided into PAS-A and PAS-B sites. The PAS-A domain ensures the specificity of target gene activation by selecting a dimerization partner, whereas the PAS-B domain allows ligand binding (Kewley et al., 2004). AhR and its dimerization partner AhR nuclear translocator (ARNT) consist of both PAS-A and PAS-B domains, and both possess a Q-rich region in the C-terminal domain that is glutamine-rich (Fig. 1.1). Apart from these regions, the C-terminal domain also consists of a subdomain which is enriched with acidic residues (glutamate/aspartate) and another subdomain which is enriched with serine, threonine and proline residues (S/T/P). Coactivators

and co-repressors interact with the AhR via this transactivation domain (Jain et al., 1994). The AhR repressor (AhRR) inhibits AhR activation by competing with AhR for binding Xenobiotics response element (XRE). AhRR contains a PAS-A Domain but no PAS-B domain, making it unable to bind ligands and to induce gene expression (Haarmann-Stemmann et al., 2015). AhRR is also an AhR target gene and negatively regulates AhR function. Unlike AhRR, ARNT has a PAS-B domain, but it also does not bind ligands. The bHLH and the PAS-B domain are involved in binding to the chaperone proteins Hsp90, keeping the AhR stabilized in an inactive form in the cytosol in the absence of ligand (Zhou, 2016).

In human cells, there are two AhRR splice variants; one is the full length AhRR₇₁₉ and the other an AhRR that lacks exon 8 (AhRRΔ8). The latter is the active form in humans, but its expression is not observed in mice (Karchner et al., 2009; MacPherson et al., 2014). The expression of AhRR, on mRNA and protein level can be short-lived due to mRNA decay and ubiquitin-mediated proteasomal degradation, respectively. Tristetraprolin (TTP), an RNAbinding protein, can bind to the two AU-rich elements in the 3'UTR of AhRR mRNA, leading to mRNA decay (Lee et al., 2013). TCDD-mediated AhR activation also leads to the degradation of AhR via the ubiquitin-proteasome pathway (Ma & Baldwin, 2000). An increase in ubiquitination may in turn negatively affect the stability of the AhR and the expression of its target genes. Furthermore, AhRR is not the only suppressor of AhR activity, as TiPARP (TCDD-inducible poly [ADP-ribose] polymeras) can also inhibit AhR transactivation through ADP-ribosylation, leading to degradation of the AhR (Matthews, 2017). Similar to AhRR, the expression of TiPARP is also induced by AhR activation, as it also has multiple XREs in two genomic regions (Grimaldi et al., 2018). Taken together, both AhR and AhRR are regulated tightly, as AhRR mRNA stability is regulated by TTP and AhR can be regulated by its negative regulators such as AhRR, ubiquitination, as well as the three AhR-controlled CYP enzymes (CYP1a1, 1a2, and 1b1) which metabolize AhR lig. Loss of AhRR or TiPARP has been reported to enhance AhR activation and subsequently also modulates the onset of various diseases. For instance, AhRR-deficient mice are more susceptible to DSS-induced colitis (Brandstätter et al., 2016a) and TiPARP-deficient mice also have heightened sensitivity to TCDD-induced steatohepatitis and lethality (Ahmed et al., 2015).

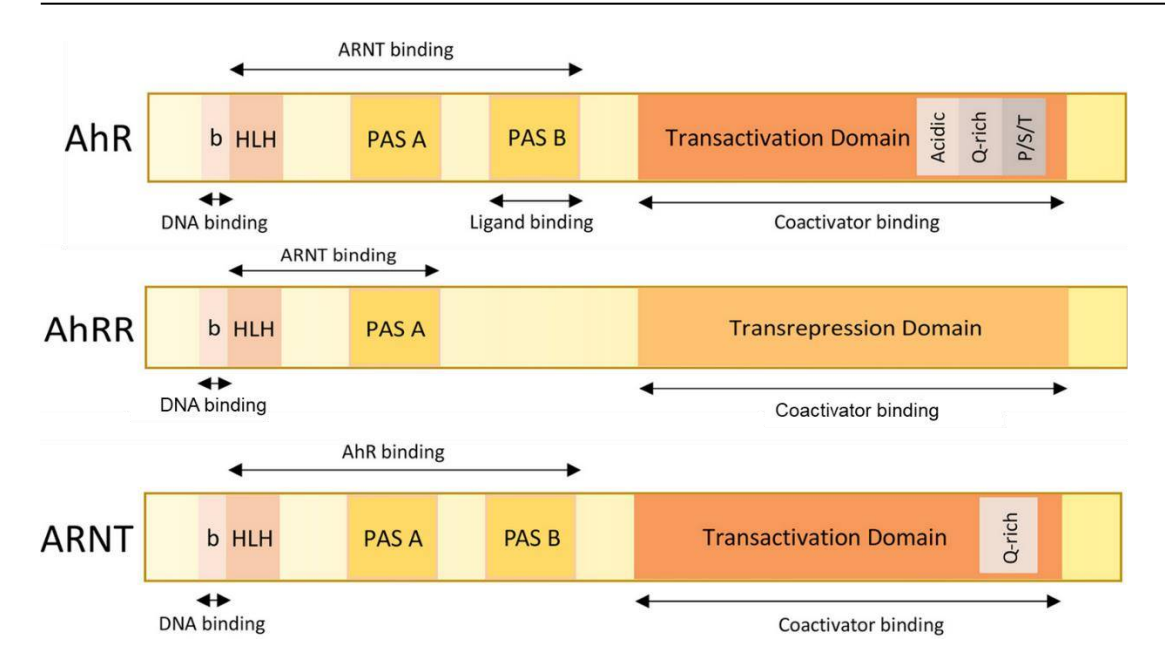


Fig. 1.1 The structure and functional domains of AhR, AhRR, and ARNT. The AhR is a member of the basic helix-loop-helix/Per-Arnt-Sim (bHLH/PAS) family of transcription factors. The N-terminal basic part of the bHLH domain conveys DNA binding, while the HLH region facilitates protein-protein interactions. Two 200-350 amino acid long PAS domains mediate the interaction with other PAS domain containing proteins, like the AhR nuclear translocator (ARNT). PAS-B contains the ligand-binding domain. Regions in the bHLH and PAS domains are involved in Hsp-90 binding. The C-terminal of AhR and ARNT consists of a Q-rich domain, and two additional subdomains can be found only in the AhR; one is enriched with acidic residues and another that is enriched with serine, threonine & proline (S/T/P). The -C terminus is involved in transactivation. Figure was adapted from Larigot et al., (2018).

1.6. The diversity of AhR ligands

AhR can be activated by various ligands that include a variety of environmental toxins like halogenated aromatic hydrocarbons (HAH) and non-halogenated polycyclic aromatic hydrocarbons (PAH). There are multiple ways to classify AhR ligands; they can be categorized either as exogenous versus endogenous ligands, or synthetic versus natural ligands. The best-known exogenous ligand is the highly toxic and metabolically resistant HAH, 2,3,7,8-tetrachlordibenzo- ρ -dioxin (TCDD) that can be found in Agent orange, industrial byproducts, and in some herbicides as toxic contaminants (Denison et al., 2011; Quintana, 2013). Another exogenous AhR ligand is 3-Methylcholanthrene (3MC), which is a carcinogen that can induce estrogenic responses binding to the estrogen receptor (ER) α , hence stimulating a functional interaction between AhR and ER α (Abdelrahim et al., 2006; Cirillo et al., 2019). Another carcinogen, Benzo[a]pyrene (BaP) that is a PAH produced by combustion processes (eg in cigarette smoke) is also a well-studied AhR ligand (Matsunawa et al., 2009). In contrast, there

are also some non-toxic, physiological AhR ligands that are derived from dietary components, particularly flavonoids found in vegetables and fruits (Denison et al., 2002). An example for a naturally occurring AhR ligand precursor is indole-3-carbinol (I3C), which is produced by the enzymatic breakdown of glucobrassicin, a glucosinolate that can be found in cruciferous vegetable such as broccoli and brussels sprouts (Hooper, 2011). By exposure to the stomach acid, I3C is converted into the high affinity AhR ligand indolo[3,2-b]carbazol (ICZ) and diindolylmethane (DIM) (Chen et al., 2001). Apart from exogenous sources, endogenous AhR ligands can be derived from the degradation of tryptophan. L-Kynurenine is formed by catalytic breakdown of tryptophan and has a low affinity for the AhR but nevertheless is of potential physiological relevance (Esser & Rannug, 2015). 6-formylindolo[3,2-b]carbazol (FICZ), also derived from tryptophan, has been shown to strongly induce AhR activity (Wei et al., 1998). There are also molecules that have been termed AhR activators, including hydrogen peroxide and AhR antagonist 3'-methoxy-4'-nitroflavone. They do not bind the AhR directly, but rather inhibit the induction of CYP1A1 enzyme activity by FICZ or TCDD, thus increasing the intracellular level of FICZ or TCDD and thereby promoting AhR activation. This group of mediators includes inflammatory mediators, organic solvents and metals (Wincent et al., 2012).

1.7. Canonical and non-canonical AhR signaling pathways

The AhR signaling pathway is composed of two arms, the canonical and non-canonical signaling pathways, as shown in Fig. 1.2. The canonical pathway has been more extensively studied, yet it cannot explain all of the AhR-mediated effects (Wright et al., 2017). To activate the canonical pathway, AhR ligands bind the cytosolic AhR-Hsp90 complex upon diffusion into the cell cytoplasm. This triggers a conformational change which subsequently leads to the nuclear translocation of AhR, where it dimerizes with ARNT. Following dimerization, AhR is released from the Hsp90 complex and the AhR-ARNT complex binds to XRE that are located in the promoter regions of AhR target genes (reviewed in Lamas et al., 2018; Larigot et al., 2018). AhR target genes range from its own negative feedback regulators like *Ahrr*, *Tiparp*, *Cyp1a1,1a2,1b1*, to genes encoding enzymes involved in the second phase metabolism (UGT1a and GSTa1), or the fatty acid transporter CD36 (Denison & Nagy, 2003; J. H. Lee et al., 2010).

Later, the non-canonical pathway came to light as multiple studies showed that some transcription start sites of AhR-responsive gene do not contain XRE (Boverhof et al., 2005; Frueh et al., 2001; Puga et al., 2000; Tijet et al., 2006). There are several pathways involving AhR with no XRE binding reported (Wright et al., 2017). For instance, direct interaction between AhR and RelB of nuclear factor-κB (NF-κB) has been reported. This leads to the expression of cytokines and chemokines, such as B-cell-activating factor of the TNF family, B-lymphocyte chemoattractant, CCL1, and the transcription factor interferon regulatory factor 3 (IRF 3), and it also decreases the expression of Cyp1a1 (Vogel et al., 2007). Moreover,-AhR expression is also regulated by the NF-κB member RelA in LPS-stimulated DC (U937derived). These results further support a role for NF-κB in AhR-dependent signal transduction as well as in enhancement of LPS responses (Vogel et al., 2014). In the non-canonical pathway, it is speculated that the AhRR-mediated inhibition can still occur by competitively binding to ARNT (Vogel & Haarmann-Stemmann, 2017). Other target genes of the AhR also include cytokines and chemokines, e.g., IL-22, IL-17A, and CCL20. Their expression can be induced by TCDD via the canonical pathway, but they can also be mediated by RelB (Ishihara et al., 2019). RelB/AhR also bind to a yet unrecognized responsive element of the IL-8 promoter and TCDD-mediated IL-8 induction relies on RelB/AhR binding (Vogel et al., 2007).

Lastly, the AhR pathway is known to be regulated by other transcription factors and signaling pathways. For instance, some publications showed a crosstalk between the AhR and other xenobiotic receptors, e.g., Pregnane X Receptor (PXR). The *Cyp1,2,3* genes in zebrafish are under the regulation of both, PXR and AhR (Kubota et al., 2015). Moreover, the activation of AhR also inhibits PXR, leading to a decrease of CYP3A4 in a rifampicin-treated liver cell line and in primary cells (Rasmussen et al., 2017). PXR also protects liver cells from BaP-induced DNA damage by regulating *Ahr* and *Cyp1a1* (Cui et al., 2017). Apart from PXR, NF-E2-related factor 2 (Nrf2) is also reported to be able to modulate AhR expression, by directly binding to Antioxidant Response Element (ARE) on AhR (Shin et al., 2007). AhR can also directly bind to XRE of Nrf2, which in turn regulate Nrf2 and AhR metabolites. This can induce oxidative stress that may also lead to Nrf2 activation (Shin et al., 2007).

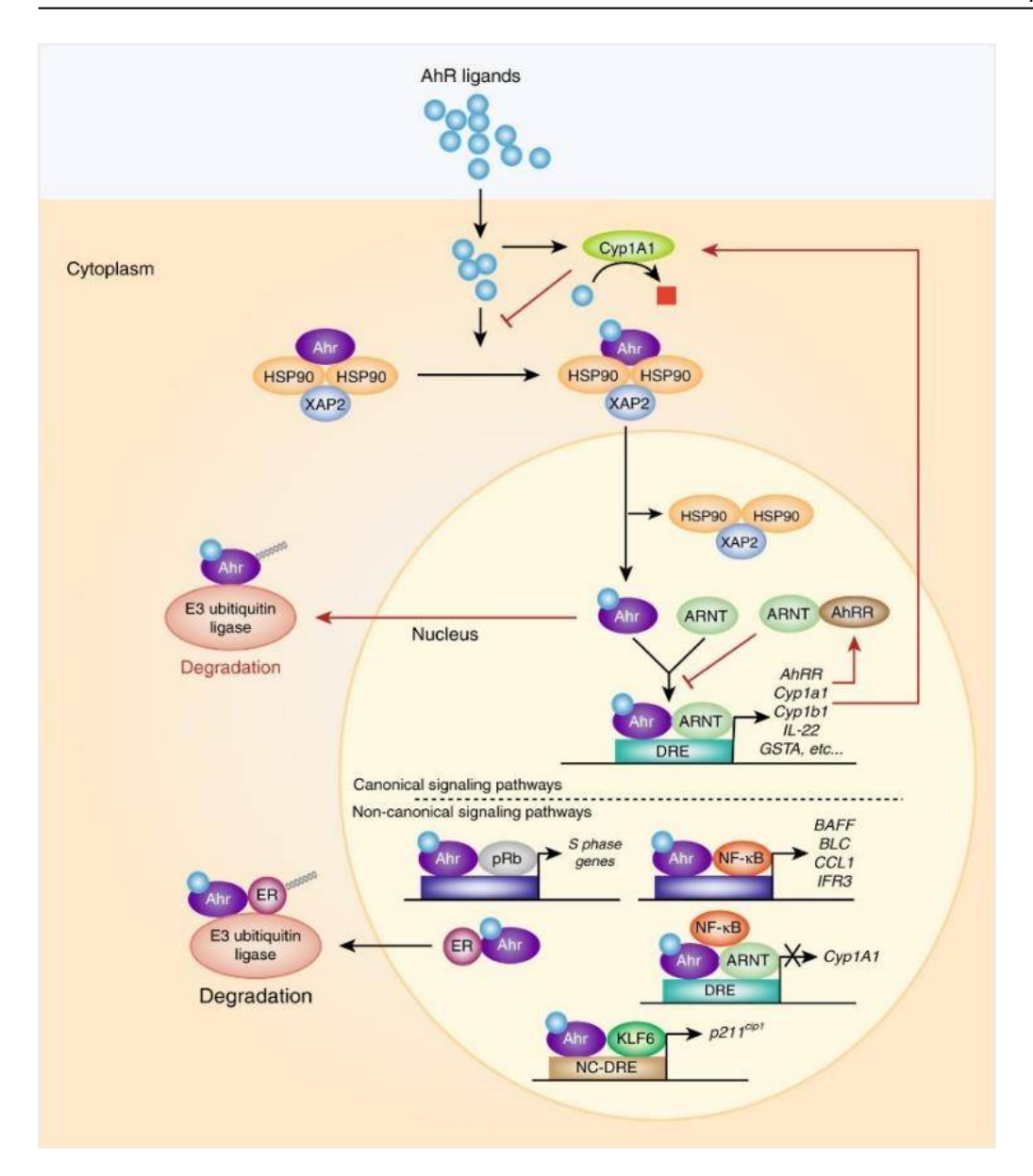


Fig. 1.2 Schematic representation of the canonical and non-canonical AhR signaling pathways. In the absence of ligand, AhR is retained in the cytoplasm in an inactive complex containing chaperone proteins, such as HSP90 and XAP2. After ligand binding, AhR translocates into the nucleus, where it dimerizes with ARNT. The AhR/ARNT dimer binds genomic regions containing XRE that regulate expression of genes encoding several phase I and phase II metabolizing enzymes, such as *Cyp1a1*, *Cyp1b1* as well as several other genes, e.g., *Ahrr*. In the non-canonical pathway, AhR activation by ligands may lead to a direct interaction with pRb. It may also induce the expression of cytokines and chemokines, such as BAFF, BLC, CCL1, and IFR3, AhR through an interaction with NF-κB. The AhR/NF-κB interaction also induces decreased expression of *Cyp1a1*. BAFF, B-cell-activating factor of the tumor necrosis factor family; BLC, B-lymphocyte chemoattractant; CCL1, CC-chemokine ligand 1; IFR3, interferon responsive factor; NF-κB, nuclear factor-κB. Ligand-activated AhR can also bind to ER, promoting the proteolysis of ER by assembling a ubiquitin ligase complex. ER, estrogen receptor. AhR can also dimerize with KLF6 and binds genomic regions containing NC-DRE that regulate the expression of target genes, such as p21cip1, which mediate cell cycle control. KLF6, tumor suppressor Kruppel-like factor 6; NC-XRE, non-consensus XRE. The figure was adapted from Lamas et al. (2018).

1.8. Expression and physiological functions of AhR and its target genes

AhR is highly expressed in liver and barrier organs where high concentrations of AhR ligands from the environment are found, such as intestine, skin, and lung (Bernshausen et al., 2006). AhR and its target genes can be expressed by immune- and non-immune cells. The latter include epithelial, stromal cells, and hepatocytes (Zhou, 2016). There are differences observed between AhR and AhRR in terms of expression; AhR is widely expressed in most cell types, whereas AhRR is mostly expressed in immune cells in different tissues (Brandstätter et al., 2016a). Nevertheless, the physiological functions of both AhR and AhRR highly depend on the organ microenvironment (Yin et al., 2016; Zhou, 2016).

Despite the high expression of AhR in some cells and organs, it does not mean that its target genes are also commensurately expressed. Low expression of AhRR in liver, intestinal epithelial cells (IEC), and keratinocytes has been previously reported using AhRR reporter mice (Brandstätter et al., 2016a). This shows that the expression of AhR and AhRR can be asymmetric. In the myeloid compartment, AhR is expressed by macrophages, DC, monocytes, and monocyte-derived macrophages (Mo-Mac), whereas in the lymphoid compartment, AhR is expressed in some populations of T cells, as well as in NK-cells, and B cells (Zhou, 2016). Due to its broad expression in immune cell subsets, AhR-deficiency has been reported to affect some properties of immune cells, such as proliferation, differentiation, or cytokine profile. For instance, AhR-deficiency significantly reduced the proliferative properties of B cells in adult mice and those of DETC in embryonic and neonatal mice (Kadow et al., 2011; Villa et al., 2017). However, AhR-deficient B cells, did not show alterations in IgG secretion or in the response towards T-independent and T-dependent antigens (Villa et al., 2017). In DETC of neonatal mice, AhR depletion caused a more inflammatory cytokine profile, with enhanced Ifny, Gzmf, and Pdl-1, as well as increased Ccr2, Ccr5, and Ccl1 expressions (Merches et al., 2020). AhR is also essential for development and maintenance of RORγt⁺ ILC, as well as the production of IL-22 by T cells and ILC3 in the gut (Qiu & Zhou, 2013).

In the context of diseases, the net outcome of AhR activation is differentially regulated, i.e., it depends largely on cell type, organ, and the type of ailments. For instance, AhR activation by I3C, DIM, or FICZ could inhibit intestinal inflammatory response, suggesting an important role of AhR activation in regulating intestinal immunity (Chen et al., 2023). In line with this

finding, both systemic and IEC-specific AhR-ablation in mice exacerbated the onset of DSS-induced colitis, alluding to the protective role of AhR against ulcerative colitis (Qazi et al., 2022; Q. Wang et al., 2018). However, overactivation of AhR can also cause deleterious effects, such as formations of cysts and metaplasia-like lesions in the gastric mucosa (Dantsuka et al., 2019). Furthermore, AhR depletion led to reduced metastatic spread of breast cancer cells, suggesting a role of AhR in modulating cell proliferation and expression of MMPs genes (Goode et al., 2014; Parks et al., 2014; Saito et al., 2014). In the liver, AhR signaling can be a double-edged sword. Mice expressing constitutively activated human AhR had a worse hepatic steatosis, but they were protected against other DIO symptoms, such as weight gain and insulin resistance (Lu et al., 2015). Furthermore, AhR activation by kynurenine induced hepatic *Cyp1b1* and *Scd1* expression, leading to hepatosteatosis and body mass gain (Rojas et al., 2021). However, DIM-activated AhR protected against hepatosteatosis and liver inflammation, and promoted Treg dominance (Y. Liu et al., 2014).

Taken together, the net effects of AhR signaling can be favorable or non-favorable, depending on the cell type, the physiological condition of the host, and the local milieu. Nevertheless, the net outcome of AhR signaling in peripheral organs in the context of DIO still needs to be elucidated. Hence, one of the aims of this thesis was to investigate this aspect.

1.8.1. Function of AhR signaling in lipid metabolism and DIO

The possible role of AhR in energy balance has been reported since TCDD, the most potent AhR ligand, was shown to cause wasting syndrome, a condition where weight loss and reduced food intake occur both in mice and human (Girer et al., 2020). Moreover, in addition to the barrier organs, AhR is abundantly expressed in AT and it has also been shown to modulate lipid metabolism and vascular homeostasis. Multiple studies have shown that AhR-deficiency protects against weight gain and other DIO-related symptoms (Girer et al., 2020; Haque et al., 2023; Xu et al., 2015). It has also been reported that AhR confers such protection through sexually dimorphic mechanisms. AhR-deficiency in females led to reduced calorie intake and increased the metabolic rate to protect from HFD-induced weight gain, whereas in male mice no alteration in consumed calories could be observed. Here, DIO induced inflammation was reduced (Haque et al., 2023). Xu et al. (Xu et al., 2015) also reported that the protection against DIO was achieved via increased energy expenditure, as evident by the increased level of *Ucp1*

in BAT and mitochondrial β-oxidation genes in muscle. In addition, AhR negatively regulates adipocyte differentiation and adipogenesis. AhR overexpression leads to reduced differentiation of mature adipocytes and PPARγ expression by inducing its proteasomal degradation, as well as reduced adipogenic gene expression, such as *Cd36*, *Adipsin*, and *Fabp4* (Dou et al., 2019). Previous findings in our lab have also shown that ablating AhRR also protects mice against DIO (unpublished data). Thus, the absence of either AhR or AhRR elicits similar effect in the context of DIO, suggesting that the net effect of their depletion is context-and cell-specific. It can also be that the aforementioned effects of AhR deficiency could have been specifically mediated by AhRR. Nevertheless, the reason why AhR- and AhRR-deficiency have similar effects needs to be further investigated.

Moreover, AhR and its target genes, Cyp1a1, Cyp1b1 are also abundantly expressed in human endothelial cells (Conway et al., 2009). AhR-depletion attenuated HFD-induced endothelial dysfunction by inhibiting lysophosphatidylcholine (a major component of LDL and oxidized LDL), as evident by a greater nitric oxide (NO) reserve that causes vasodilation. Hence, AhR signaling also contributed to HFD-induced vascular dysfunction (da Silva et al., 2022). The three AhR-controlled CYP enzymes are also involved in lipid metabolism, as their ablation resulted in reduced amounts of ω -6 and ω -3 lipid mediators, such as 5-HETE, 14-HDHA, 17-HDHA, 12-HEPE, 15-HEPE and 18R-HEPE (Divanovic et al., 2013). CYP1A1 expression was sufficient to protect against nonalcoholic fatty liver disease (NAFLD) induced by Western diet supplemented with B[a]P by decreasing food intake (Uno et al., 2018). Nevertheless, B[a]P-supplemented Western diet but not Western diet alone induced hepatic steatosis, which is associated with dysregulated bile acid and lipid metabolism, and liver cell damage in CYP1A1-KO but not WT mice. In contrast to CYP1A1, CYP1B1 protects against HFDinduced obesity and glucose intolerance (Liu et al., 2015). Such reduction in weight gain also coincided with increased gene expression involved in fatty acid β-oxidation in WAT, liver and muscle in HFD-fed CYP1B1-KO mice. Taken together, AhR, CYP1A1, and CYP1B1 have been shown to be involved in regulating lipid metabolism and energy balance

2. Aim of the Thesis

AhR is a ligand activated transcription factor that acts as a sensor of endogenous and exogenous polyaromatic chemicals. AhR is activated upon ligand binding and its activation leads to transcription of genes crucial for detoxification of foreign chemicals such as *Cyp1a1*, *Cyp1a2*, and *Cyp1b1*. Besides, AhR signaling is also critically involved in the development and regulation of the immune system. AhR expression is also controlled by its repressor, AhRR, which is mainly expressed in immune cells at barrier organs, as well as by the three AhR-dependent CYP enzymes. However, the roles of AhRR and the AhR-controlled CYP enzymes in health and disease need to be more elucidated. Previously, AhRR/EGFP reporter mice were generated that express eGFP under control of the endogenous Ahrr promoter. These mice are AhRR-deficient and can be used to mirror AhR activation.

Therefore, this thesis aims at elucidating the regulation of AhR signaling by AhRR and the three AhR-controlled Cytochrome P450 enzymes (CYP1A1, CYP1A2, CYP1B1) *in vivo*, especially in small intestine, liver, and adipose tissue. Therefore, AhRR/EGFP reporter mice and mice that lack *Cyp1a1*, *Cyp1a2*, and *Cyp1b1* were crossed and the activation of AhR will be assessed in immune and non-immune cells under physiological and pathological conditions, such as overnutrition.

There are three aims of this thesis:

First, to analyze if the enhanced ligand availability in the absence of *Cyp1a1*, *Cyp1a2*, and *Cyp1b1* will subsequently enhance AhR activation and therefore AhRR/EGFP expression. Second, if the absence of the three CYP enzymes and/or AhRR will be sufficient to alter the composition of immune and non-immune cell subsets in different organs *in vivo*. For both aims, we investigate the different mouse lines in a naïve state, under treatment with the AhR ligand 3MC, and under diet-induced obesity (DIO). The third aim of the thesis is to elucidate whether the absence of the three CYP enzymes and/or AhRR will affect the physiological response to high-fat diet. Specifically, we want to analyze DIO-induced weight gain, glucose tolerance levels and liver damage.

3. Materials

3.1. Equipments

Table 3.1. Equipments

Equipment	Article (company)
Automatic tissue processor for paraffin	Leica TP1020 (Leica Microsystems,
embedding	Wetzlar,
	Germany)
Agarose gel electrophoresis	PerfectBlue Gel System (Peqlab, Erlangen,
D 1	Deutschland)
Balances	440-35A (Kern & Sohn, Balingen,
	Germany) ABJ-NM (Kern & Sohn, Balingen,
	Germany)
	EW-N (Kern & Sohn, Balingen, Germany)
Beaker glass	100ml (Simax Bohemia Cristal, Selb,
0	Germany)
Blood glucose monitor	M400 (Omron, Kyoto, Japan)
Blotting Device	V20-SDB Fisherbrand™ Semi-Dry
	Blotters (Fisher Scientific, Waltham, USA)
Cell counting chamber	Neubauer improved (La Fontaine via
	Labotec,
G . 10	Göttingen, Germany)
Centrifuges	5415R (Eppendorf, Hamburg, Germany)
	Allegra X-15R (Beckman Coulter, Pasadena, USA)
Centrifugal Devices for biomolecular	Pall Life Science, Port Washington, USA
separation Microsep with Omega	Tan Ene Science, Fort Washington, OSA
membrane	
Chemistry analyzer	Picollo Xpress (Abaxis, Union City, USA)
Cryostat	CM3050S (Leica, Wetzlar,
	Germany)
Flow Cytometer	BD LSR II Flow (BD Biosciences,
	Heidelberg, Germany)
	BD Symphony A5 (BD Biosciences,
Freezer (-20°C)	Heidelberg) Bosch GSD12A20 (Bosch, Gerlingen,
11cc2c1 (-20 C)	Germany)
	Profi Line GG4310 (Liebherr, Biberach,
	Germany)

Freezer (-80°C)	New Brunswick Ultra-Low Temperature	
	Freezer	
	(Eppendorf, Hamburg, Germany)	
Fridge (+4°C)	KTR16A21/02 (Bosch, Gerlingen,	
	Germany)	
Heating devices	TS1 ThermoShaker (Biometra, Göttingen,	
	Germany)	
	Heatingblock Thermostat TH21 (HLC BioTech,	
	Bovenden, Germany)	
	Waterbath WNB 22 (Memmert,	
	Schwabach,	
	Germany)	
Homogenizer	Precellys®24 (Peqlab, Erlangen, Germany)	
	Handmixer	
Ice machine	Scotsman Flockeneisbereiter AF200	
	(Hubbard	
	Systems, Birmingham, USA)	
Incubator (cell culture)	CB 150 (Binder, Tuttlingen, Germany)	
Incubator with shaking function	Innova 44 (Eppendorf, Hamburg,	
	Germany)	
Luminometer	Centro LB960 (Berthold, Bad Wildbad,	
	Germany)	
Measuring cylinder	250ml, 500ml, 1000ml, 2000ml (VWR,	
Microscopes	Wayne, USA) BZ-9000 (Keyence, Montabaur, Germany)	
Meroscopes	LSM800 Airyscan (Zeiss, Oberkochen,	
	Germany)	
Microtome	Leica RM2255 (Leica Microsystems,	
	Wetzlar, Germany)	
Peristaltic pumo	Pumpdrive 5001(Schwabach, Germany)	
Pipettes	10μl, 20μl, 200μl, 1000μl (Eppendorf,	
	Hamburg, Germany)	
	2,5µl ErgoOne (StarLab, Hamburg, Germany) Multichannel DV8-10, DV12-	
	50, DV8-300 (HTL Lab Solutions,	
	Warszawa, Poland)	
Real-Time PCR Detection System	CFX96 TouchReal-Time PCR Detection	
	(Bio-Rad, Munich, Germany)	
Spectrophotometer	NanoDropTM ND-1000 (NanoDrop	
CDC DA CE L 4	Products, Wilmington, USA)	
SDS-PAGE electrophoresis	Mini-PROTEAN tetra cell (Biorad, USA)	
Transilluminator	Transilluminator UST-30M-8R (BioView, Rehovot,	
	Israel)	
	151 (101)	

Vortex shaker	Vortex Genie 2 (Scientific Industries, New	
	York, USA)	
Western blot imaging	Odyssey 92120 Infrared imaging system	
	(LiCor, USA)	

3.2. Consumables

Table 3.2 Consumables

Product	Article (Company)
Blood glucose test strips	Accu-Check instant (Roche Diabetes Care,
	Inc., Indianapolis, USA)
Cell culture plates (6-,12-,24-,48-,96-	Greiner, Frickenhausen, Germany
well)	
Cell strainer (100 μm, 70 μm)	Corning, Glendale, USA
	PluriSelect, Leipzig, Germany
Cover slips	Carl Roth, Karlsruhe, Germany
Cryomold	Sakura Finetek, Torrance, USA
Cryotubes	Sarstedt, Nümbrecht, Germany
Disposal Bags	Carl Roth, Karlsruhe, Germany
Embedding cassette	Carl Roth, Karlsruhe, Germany
Falcon tubes (15 and 50 mL)	Greiner, Frickenhausen, Germany
Flow cytometry tubes	Sarstedt, Nümbrecht, Germany
Glass beads	Carl Roth, Karlsruhe, Germany
Glass slides	Thermo Fisher, Waltham, USA
Gloves	Sentina Ambidextrous Nitrile
Microtubes (2 ml, 1,5 ml, 0,5 ml)	Sarstedt, Nümbrecht, Germany
Omnican ® 50 Syringes	B. Braun, Melsungen, Germany
Parafilm®	Bemis, Neenah, USA
Petri dishes	Greiner, Frickenhausen, Germany
Reagent reservoirs	VWR, Darmstadt, Germany
Screw cap microtube	Sarstedt, Nümbrecht, Germany
Serological pipette (5 ml, 10 ml, 25 ml)	Greiner, Frickenhausen, Germany

Sterican® needles	B. Braun, Melsungen, Germany
Surgical Scalpel	B. Braun, Melsungen, Germany
Syringes (1 ml, 5 ml, 10 ml)	B. Braun, Melsungen, Germany

3.3. Chemicals

Table 3.3. Chemicals		
Chemical	Company	
100bp DNA Ladder	New England BioLabs, Ipswich, USA	
10x TAE buffer	Invitrogen, Carlsbad, USA	
2-Propanol >99.5%	Roth, Karlsruhe, Germany	
3-Methylcholanthrene	Sigma-Aldrich, St. Louis, USA	
6-Formylindolo(3,2-b)carbazole	Enzo Life Science, New York, USA	
Acetone	VWR, Darmstadt, Germany	
Albumin Bovine Fraction V, pH=7.0	SERVA Electrophoresis GmBH, Heidelberg, Germany	
Ampicillin-ratiopharm 1g/l	Ratiopharm, Ulm, Germany	
Collagenase IV	Sigma-Aldrich, St. Louis, USA	
Dithiothreitol (DTT) Molecular Grade	Promega, Fitchburg, USA	
DNase/RNase-Free Water	Zymo Research, Irvine, USA Invitrogen, Carlsbad, USA	
Dulbecco's PBS	Sigma-Aldrich, Steinheim, Germany	
Entellan	Merck, Darmstadt, Germany	
Ethanol 70% (methylated)	Roth, Karlsruhe, Germany	
Ethanol absolute for molecular biology	ApliChem, Darmstadt, Germany	
Ethanol Rotipuran >99.8%	Roth, Karlsruhe, Germany	
Ethylenediaminetetraacetic acid (EDTA)	Sigma-Aldrich, St. Louis, USA	
FACS Clean Solution	BD Bioscience, Franklin Lakes, USA	

FACS Rinse Solution	BD Bioscience, Franklin Lakes, USA	
Fetal Bovine Serum	ThermoFischer, Waltham, USA	
FFA-free BSA (A7030)	Sigma-Aldrich, St. Louis, USA	
Fixable Viability Dye eFluor 780	eBioscience, San Diego, USA	
Gelatin from porcine skin	Sigma-Aldrich, St. Louis, USA	
Gey's Balanced Salt Solution (GBSS)	Sigma-Aldrich, St. Louis, USA	
Hank's Balanced Salt Solution (HBSS) with / without Ca ²⁺ (10x)	Gibco (Life Technologies), Carlsbad, USA	
HEPES	Sigma-Aldrich, St. Louis, USA	
Kaiser's glycerol gelatine phenol-free	Carl Roth, Karlsruhe, Germany	
Oil-Red-O powder	Sigma-Aldrich, St. Louis, USA	
OneComp/ UltraComp ebeads	eBioscience, San Diego, USA	
Paraformaldehyde (PFA)	Merck, Darmstadt, Germany	
Penicillin-Streptomycin	Gibco (Life Technologies), Carlsbad, USA	
peqGOLD Universal Agarose	peqlab, Erlangen, Germany	
Phosphate Buffered Saline	Dulbecco Merck, Darmstadt, German	
Precision Count Beads TM	Biolegend, San Diego, USA	
Protease Inhibitor cOmplete tablets mini	Roche, Indianapolis, USA	
Protein G Sepharose®	Sigma-Aldrich, St. Louis, USA	
RIPA lysis and extraction buffer	ThermoFisher, Waltham, USA	
RPMI 1640	ThermoFisher, Waltham, USA	
Tissue-Tek® O.C.T.™ Compound	Sakura Finetech, Torrance, USA	
Triton X-100	Sigma-Aldrich, St. Louis, USA	
Trypan Blue	Sigma-Aldrich, St. Louis, USA	
Tween-20	Roth, Karlsruhe, Germany	
Xylol	Roth, Karlsruhe, Germany	

3.4. Solutions

Table 3.4. Solutions

Solution Content Adipose tissue digestion buffer 0.3% (3 mg/mL)	
Adipose tissue digestion buffer 0.3% (3 mg/mL)	
-	
2 mg/mL Collagenase II	
in plain DMEM	
Complete RPMI 1640 RPMI Medium 10% FCS	
1% L-Glutamine	
1% Penicillin-Streptomycin	
50μM β-Mercaptoethanol	
Histology blocking buffer PBS	
2,5% BSA	
5% Goat Serum	
Intestinal digestion solution #1 5mM DTT in HBSS	
2% FCS	
Penicillin: 100U/ml	
Streptomycin: 100µg/ml	
Intestinal digestion solution #2 5mM EDTA in HBSS	
2% FCS	
Penicillin: 100U/ml	
Streptomycin: 100µg/ml	
Intestinal digestion solution #3 HBSS	
10mM HEPES	
Penicillin: 100U/ml	
Streptomycin: 100µg/ml	
iver collagenase solution for perfusion HBSS without Ca ²⁺	
50mg/mL Collagenase IV (1:100)	
Liver digestion buffer GBSS	
Collagenase D 80µL/10mL	
Lysis buffer (tail lysis) Aqua dest.	
5 mM EDTA, pH 8,0	
0,2 % SDS	
200 mM NaCl	
0,1 mg/ml Proteinase K	
PFA (4%) 4g PFA 100ml PBS	
Skin digestion buffer PBS	
DNase I (200 U/ml)	
Liberase TM (0.8 U/ml)	
Skin (neonatal) digestion buffer for complete RPMI1640	
dermis Dispase II (2,4 U/mL)	
Skin (neonatal) digestion buffer for complete RPMI 1640 (3mL)	
epidermis DNAse I (130U/ml)	
Stop Buffer for FACS PBS	
20% FCS	

3.5. Enzymes

Table 3.5. Enzymes

Enzyme	Company
Collagenase II	PAN-Biotech, Aidenbach, Germany
Collagenase IV	Sigma-Aldrich, St. Louis, USA
Dispase II	
DNase I	Roche, Basel, Switzerland
Liberase TM	Roche, Basel, Switzerland
Proteinase K	Sigma-Aldrich, St. Louis, USA

3.6. Kits *Table 3.6. Kits*

1000 5.0. 1105	
Name	Company
ABsolute qPCR SYBR Green ROX	Thermo Scientific, Waltham, USA
Direct-zol Miniprep RNA Purification Kits	Zymo Research, Irvine, USA
Dual-Luciferase reporter assay system	Promega, Mannheim, Germany
Foxp3 / Transcription Factor Staining	Thermo Scientific, Waltham, USA
Buffer Set	
MyTaq HS Red DNA Polymerase	Bioline, London, UK
Picrosirius Red staining kit	ScyTek Laboratories, Logan, USA
Quick-RNA Miniprep RNA purification	Zymo Research, Irvine, USA
kit	

3.7. Antibodies

3.7.1. Antibodies for FACS

Table 3.7 FACS antibody list

Target	Clone	Dilution	Company
B220	RA3-6B2	1:200	Biolegend
CCR2		1:200	R&D systems
CD3E	145-2C11	1:200	Biolegend
CD4	RM4-5	1:200	Biolegend
	GK1.5	1:200	BD

CD8b YTS156.7.7 1:100 Biolegend CD11b M1/70 1:200 Biolegend / BD CD11c N418 1:200 Biolegend CD19 6D5 1:200 Biolegend CD24 M1/69 1:200 Biolegend CD25 PC61 1:200 BD CD31 MEC13.3 1:200 Biolegend CD44 IM7 1:200 Biolegend CD45 30-F11 1:400 (liver, S.I), Biolegend
CD11c N418 1:200 Biolegend CD19 6D5 1:200 Biolegend CD24 M1/69 1:200 Biolegend CD25 PC61 1:200 BD CD31 MEC13.3 1:200 Biolegend CD44 IM7 1:200 Biolegend CD45 30-F11 1:400 (liver, S.I), Biolegend
CD19 6D5 1:200 Biolegend CD24 M1/69 1:200 Biolegend CD25 PC61 1:200 BD CD31 MEC13.3 1:200 Biolegend CD44 IM7 1:200 Biolegend CD45 30-F11 1:400 (liver, S.I), Biolegend
CD24 M1/69 1:200 Biolegend CD25 PC61 1:200 BD CD31 MEC13.3 1:200 Biolegend CD44 IM7 1:200 Biolegend CD45 30-F11 1:400 (liver, S.I), Biolegend
CD25 PC61 1:200 BD CD31 MEC13.3 1:200 Biolegend CD44 IM7 1:200 Biolegend CD45 30-F11 1:400 (liver, S.I), Biolegend
CD31 MEC13.3 1:200 Biolegend CD44 IM7 1:200 Biolegend CD45 30-F11 1:400 (liver, S.I), Biolegend
CD44 IM7 1:200 Biolegend CD45 30-F11 1:400 (liver, S.I), Biolegend
CD45 30-F11 1:400 (liver, S.I), Biolegend
1:200 for all other tissues and cells
CD62L MEL-14 1:200 Biolegend
CD64 X54-5/7.1 1:200 Biolegend
CD69 H1.2F3 1:200 Biolegend
CD103 2E7 1:200 Biolegend
CD115 AFS98 1:200 Biolegend
CD135 A2F10 1:200 Biolegend
CD172a P84 1:200 Biolegend
CD206 C068C2 1:200 Biolegend
c-Kit 2B8 1:200 BD
EpCAM G8.8 1:200 Biolegend
F4/80 BM8 1:200 Biolegend
Ki67 SolA15 1:200 eBioscience
Ly6C HK1.4 1:200 Biolegend
Ly6G 1A8 1:200 Biolegend
MerTK 2B10C42 1:200 Biolegend
MHCII M5/114.15.2 1:200 Biolegend
NK1.1 PK136 1:200 Biolegend
NKp46 29A1.4 1:200 Biolegend
Siglec-F E50-2440 1:200 Biolegend
TCRβ H57-597 1:200 Biolegend
TCR γδ GL3 1:200 Biolegend
Ter119 TER-119 1:200 Biolegend
Tim4 21H12 1:200 Biolegend

3.7.2. Antibodies for Histology *Table 3.8 Histology antibody list*

Table 3.8 Histology antibody l	ıst		
Target	Clone	Dilution	Company
B220	RA3-6B2	1:50	Biolegend
CD31	2H8	1:100	Invitrogen
CD34	RAM34	1:200	Invitrogen
CD45	30-F11	1:100	Biolegend
CD90.2	30-H12	1:100	Biolegend
EpCAM	G8.8	1:200	Biolegend
F4/80	BM8	1:50	Biolegend
Ki67	SolA15	1:50	eBioscience
LYVE-1	polyclonal	1:100	Cell Signaling
PDGFRα	D1E1E	1:100	Cell Signaling
Podoplanin (gp38)	8.1.1	1:200	Biolegend
SIGNR1	2C7B27	1:50	Biolegend
SiglecF	E50-2440	1:50	Biolegend
TCRβ	H57-597	1:100	BD
IgG Alexa Flour 594 (goat anti-rat, anti-rabbit, and anti-hamster)	Polyclonal	1.:200	Life Technologies
IgG Alexa Fluor 647 (goat anti-rat and anti-rabbit)	Polyclonal	1:200	Life Technologies
IgG Texas Rat (goat anti-rat)	Polyclonal	1:200	Life Technologies

3.7.3. Antibodies for Western Blot

Table 3.9 Western blot antibodies list

Target	Clone	Dilution	Company
GAPDH	6C5	1:200	Acris
V5-epitope tag	E10	1:100	Santa Cruz Biotech
IRDye 680RD	polyclonal	1:200	Licor Biosciences
IRDye 800CW	polyclonal	1:200	Licor Biosciences

3.8. PCR Primers

Table 3.10 PCR primers list

Table 3.10 PCR primers list			
Target	Species		Sequence
Ahr	murine	fwd	5′-TGC ACA AGG AGT GGA CGA-3′
		rev	5'-AGG AAG CTG GTC TGG GGT AT-3'
Ahrr	murine	fwd	5′-GGG TAA AGA GCT TCT TCC AAG C-3′
		rev	5'-ACG GGG AAC CCT CTG TAT G-3'
Cd36	murine	Fwd	5'-AGATGACGTGGCAAAGAACAG-3'
		rev	5'-CCTTGGCTAGATAACGAATCTG-3'
Cyp1a1	murine	fwd	5'-CCTCATGTACCTGGTAACCA-3'
		rev	5'-AAGGATGAATGCCGGAAGGT-3'
Fabp4	murine	Fwd	5′-GCGTGGAATTCGATGAAATCA-3′
		rev	5'-CCCGCCATCTAGGGTTATGA-3'
Gapdh	murine	fwd	5'-GAGCCAAACGGGTCATCA-3'
		rev	5'-CATATTTCTCGTGGTTCACACC-3'
Ppary	murine	fwd	5'- ACAAGACTACCCTTTACTGAAATTACCAT- 3'
		rev	5'-TGCGAGTGGTCTTCCATCAC-3'
Rps6	murine	fwd	5'-ATTCCTGGACTGACAGACAC-3'
		rev	5'-GTTCTTAGTGCGTTGCT-3
Tristetraprolin	murine	fwd	5'-TCTCTTCACCAAGCCCATTC-3'
		rev	5'-ATCGACTGGAGGCTCTCG-3'
Ahr	human	fwd	5'-TGG TCT CCC CCA GAC AGT AG-3'
		rev	5′-TTC ATT GCC AGA AAA CCA GA-3′
Ahrr	human	fwd	5′-TGT CCT CTT GCA GGG TCT G-3′

		rev	5'-AAA TAT CGTCCC TTC TGC ACT C-3'
Ahrr∆8	human	fwd	5'-AGT ACT CGG CCT TCC TGA CC-3'
		rev	5'-CGC CTT CTT CTT CTG TCC AA-3'
Cyp1a1	human	fwd	5'-CAG GTA TGT GGT GGT ATC AG-3'
		rev	5′-GGT AGG TAG CGA AGA ATA GG-3′

3.9. qPCR reagents

Table 3.11 qPCR reagents

Reagents	Producer
OligoDt	Thermo scientific, Waltham, USA
Absolute qPCR mix SYBRgreen TM	Thermo scientific, Waltham, USA
RevertAid transcriptase	Thermo scientific, Waltham, USA
dNTP	Thermo scientific, Waltham, USA
Ribolock	Thermo scientific, Waltham, USA

3.10. Mouse Diets

Table 3.12 Mouse diets list

Mouse Diet	Producer
High-fat diet (ssniff® EF acc. D12492 (I) mod.)	ssniff Spezialdiäten GmbH, Soest, Germany
Control diet (ssniff® EF acc. D12450B (I) mod.)	ssniff Spezialdiäten GmbH, Soest, Germany

3.11. Software

Table 3.13 Software used for data analysis

Software used for data analysis Software	Company
Affinity Designer	Serif (Europe) Ltd., Nottingham, England
BZ-II Analyzer	Keyence, Montabaur, Germany
CFX ManagerTM	Bio-Rad, Munich, Germany
FACS Diva	BD, Franklin Lakes, USA
Fiji (Image J)	Open source scientific analysis program
FlowJo v.10	BD, Franklin Lakes, USA

GraphPad Prism 6	GraphPad, La Jolla, USA
Microsoft Office 2011 for Windows	Microsoft, Redmond, USA
NanoDropTM ND-1000	NanoDrop Products, Wilmington, USA

3.12. Animals

These following genetically modified mice were used for experiments.

Table 3.14 A list of genetically engineered mice used in experiments

Mouse line	Strain	Description
AhRR ^{E/E}	C57BL/6	Mouse line expressing EGFP instead of AhRR, under the control of the <i>Ahrr</i> promoter (Brandstätter et al., 2016a)
Triple CYP-/- AhRR+/+	C57BL/6	Mouse line expressing AhRR but lacking CYP1A1, CYP1A2, and CYP1B1 (Dragin et al., 2008)
Triple CYP-/- AhRR ^{E/E}	C57BL/6	Mouse line expressing EGFP under the control of the <i>Ahrr</i> promoter and lacking CYP1A1, CYP1A2, and CYP1B1 (unpublished)

3.13. Generation of AhRRE/E and Triple CYP-deficient mice

Homozygous AhRR^{E/E} mice were generated in our group (Brandstätter et al., 2016a). Mice were originally generated on a mixed C57BL/6J/129Ola genetic background and backcrossed to C57BL/6J for 11 generations. Mice were also screened for expression of the high affinity C57BL/6 allele by PCR as described (Hosoya et al., 2008). In all experiments, only mice with the high affinity allele of the AhR were used. CYP1A1/1B1^{-/-} and CYP1A2/1B1-/- double-knockout lines have been described (Uno et al., 2006). The CYP1A1/1A2^{-/-} double-knockout was generated via Cre-mediated interchromosomal excision (Dragin et al., 2007). These mouse lines have been backcrossed into the C57BL/6J background for eight generations, so that the knockout genotypes reside in a genetic background that is >99.8% C57BL/6J (Nebert et al., 2000). Breeding of the CYP1A1/1A2^{-/-} with the CYP1B1^{-/-} mice produced the CYP1A1/1A2/1B1 triple-knockout line (Triple CYP^{-/-} mice) in the C57BL/6J background (Dragin et al., 2008). To generate Triple CYP^{-/-}AhRR^{E/E} mice, Triple CYP^{-/-} mice were intercrossed with AhRR^{E/E} mice at the LIMES Institute animal facility.

4. Methods

4.1. Animal Experiments

All mice were maintained and bred at the Life and Medical Science Institute (LIMES) Genetic Resources Center (GRC) at the University of Bonn. The animals were kept in individual ventilated cages with up to five mice per cage under specific-pathogen-free (SPF) condition and had unlimited access to food and water. All animal experiments were approved by the regional authorities of North Rhine-Westphalia (Germany), project number was AZ: 81-02.04.2019.A262. Mice were sacrificed by cervical dislocation.

4.1.1. Genomic DNA isolation and gel electrophoresis

In order to determine the genotype of mice, genomic DNA was isolated, and the genetically modified locus was amplified via PCR and visualized on an agarose gel. For this, ear punch biopsies were lysed O/N. at 56°C with 500μl lysis buffer and Proteinase K (100 μg/ml). The next day, tubes were inverted and centrifuged at 16,000g for 10 min at 4 °C. The DNA containing supernatant was transferred to a fresh tube and the DNA was precipitated by addition of 500μl isopropanol, followed by inversion of the tube and centrifugation at 16,000 g for 10 min. Then, the precipitated DNA pellet was washed with 500μl 70 % Ethanol, centrifuged at 16,000g for 5 min and the pellet was air-dried. Then, the DNA was dissolved in 100 μl TE-buffer and stored at 4 °C until the PCR was performed. The master mix for each strain-specific genotyping PCR was added to the DNA and the PCR was run in a thermocycler (the program is shown in the table below). Afterwards, the PCR products were applied together with a 100 bp DNA standard on a 1.5 % agarose gel with SYBRTM Safe (1:20000) to identify mouse genotypes.

Table 4.1 PCR protocol for genotyping

Reagent	Volume (per reaction)
H2O	13,5 μL
4x MyTaq Buffer	4 μL
Primer 1	0,7 μL
Primer 2	0,7 μL
MyTaq Polymerase	0,1 μL

Genomic DNA 1,5 μL

4.1.2. In vivo Ligand Stimulation with 3MC

Mice were treated per gavage with 3MC (10mg /kg body weight) in DMSO/olive oil (1:4 v/v) for 16 hours. Control mice received 200μL PBS in DMSO / olive oil with the same ratio. After being treated, all animals were observed for 15 minutes. They were sacrificed after 16 hours of treatment by cervical dislocation and the respective organs were analyzed.

4.1.3. High-fat diet experiment

8-week old mice were fed for 14 weeks with either HFD (ssniff® EF acc. D12492 (I) mod.) or matching control diet Control diet (ssniff® EF acc. D12450B (I) mod.). Diet was refilled every week. Mice were scored and weighed once a week. Two weeks prior to the end of experiment, fasting glucose level was measured, and an in vivo glucose tolerance test was conducted. The mice were sacrificed after 14 weeks by cervical dislocation and organs were analyzed.

4.1.4. Glucose-tolerance test

Mice were fasted for 6 hours prior to the test and then weighed. The tails of the mice were incised with a scalpel to obtain blood from the tail vein. Then, their basal blood glucose level was measured by a blood glucose meter. Following basal measurement, 2g/kg Glucose was injected i.p. into every mouse. The dose and volume were estimated as follows: 8 x body weight from a 0.25 g/mL glucose solution in 0.9% NaCl. Measurement of the blood glucose concentration was repeated after 15, 30, 60, 90,120, and 180 min.

4.1.5. Generation of bone-marrow-derived DC

BMDC were generated by flushing the femur and tibia of mice with PBS. Cells were cultured in RMPI 1640 medium PAA, Coelbe, Germany) containing 10 % FCS, 1% L-glutamine, and 1% penicillin/streptomycin mixture. Culture medium was supplemented with 2% GM-CSF on day 0 and day 3. After 6 days, cells were seeded onto 6-well-plates ($5x10^6$ cells/well) and 2 hours later they were treated with either LPS (100 ng/µl), 3MC (10 µM), or DMSO as control (0.1%) for 16 hours. Cells were cultured in an incubator with 5% CO2 at 37°C.

4.2. HepG2 and HEK293T cell culture

HepG2 and HEK293T cells were cultured in RPMI1640 and DMEM medium, respectively. All media had been supplemented with 10% FCS, 1% L-glutamine, 1% penicillin/streptomycin, and 50μM β-mercaptoethanol. Then, the cells were cultured in an incubator with 5% CO2 at 37°C. For cell passaging, cells were detached with 0.25 % trypsin/EDTA (Gibco) for 5 minutes and the trypsin was then deactivated with complete medium. Following centrifugation, cells were resuspended in medium and their number was counted using a hemocytometer and a light microscope. Cells were then passaged with 1:3-1:5 ratio.

4.3. Cell stimulations with LPS and AhR ligands

Unless otherwise specified, 3MC (stock concentration 10 mM) was diluted to 10 μ M working concentration unless otherwise specified, while LPS (stock concentration 2 mg/ml) was diluted to 100 ng/ml. All compounds were diluted in complete RPMI 1640 medium. For the concentration kinetics, FICZ, DIM, and ICZ were used at six different concentrations (100 μ M, 10 μ M, 1 μ M, 100 nM, 10 nM, 1nM).

4.4. mRNA decay

Bone marrow was flushed from the tibia and femur and was differentiated with GM-CSF for 6 days. Then, BMDC from one 10 cm petri dish were re-seeded into four 6 cm dishes (1,5 million cells /well) two hours prior to adding either 5 μ g/ml ActD or ActD and 10 μ M 3MC.

4.5. Histology

4.5.1. Tissue preparation for cryosections

All tissues were fixed in 4% PFA and dehydrated in a sucrose gradient (5%, 10%, 20%) until they sunk. Then, they were embedded in OCT tissue freezing medium and were subsequently stored at -80°C. The cryoblocks were cut in 10 µm thick sections using a cryostat. For gonadal WAT (WATg), the tissue was embedded with porcine gelatin instead of OCT.

4.5.2. Tissue preparation for paraffin sections

PFA-fixed tissue samples were transferred into plastic cassettes and further processed with the Leica Benchtop Tissue Processor that incubates tissue samples in a series of ascending alcohol concentrations for dehydration. Then, tissue samples were embedded into paraffin, cooled down and stored at room temperature. Paraffin embedded tissue samples were subsequently processed with a rotary microtome to obtain 5µm sections. These sections were transferred to a warm water bath (40°C) and afterwards dragged onto microscope slides. After drying in a heating cabinet (2 hours), slides were stored at room temperature until further processing.

4.5.3. Immunofluorescence staining

Cryosections were air-dried for 10 min and re-hydrated with PBS for another 10 min prior to staining. They were then permeabilized and blocked using 2% BSA, 1% goat serum, and 0.01%Triton-X in PBS. Sections were stained with conjugated antibodies or purified primary antibodies combined with secondary antibodies. Then, DAPI (1µg/ml) was used to counterstain the nuclei of the cells. Subsequently, the sections were washed twice with 0.05% Tween-20 in PBS and then submerged in deionized VE water. Finally, they were dried and mounted with Mowiol/Dabco solution. After O/N drying at room temperature, the sections were kept at 4°C.

4.5.4. Hematoxylin and Eosin (H&E) staining

H&E staining was performed to analyze gross tissue morphology. Briefly, paraffin sections were treated with xylol (100%), alcohol (70-100%), and water to deparaffinize the tissues. Then, the cell's nuclei were counterstained with hemalaun, which is a basic dye that reacts with the negatively charged cell components (e.g. nucleic acids in the nucleus). This reaction gives rise to the blue colored stain. In contrast, eosin is an acidic dye that reacts with the positively charged components, such as the amino groups of proteins found in the cytoplasm, resulting in a pink colored stain. The exact protocol is delineated in the table below.

Table 4.2 Deparaffinization and H&E staining steps

Treatment	Time
Xylol	10 (min)
Xylol	10 (min)
100% ethanol	5 (min)
100% ethanol	5 (min)
95% ethanol	2 (min)
70% ethanol	2 (min)

Aqua dest.	1 (min)
Mayer's hemalaun solution	3 (min)
0,1% Hydrochloric acid	2 (sec)
VE water	3 (min)
Eosin Y solution	3(min)
VE water	30 (sec)
95% ethanol	10 (sec)
95% ethanol	10 (sec)
100% ethanol	10 (sec)
100% ethanol	10 (sec)
Xylol	5 (min)
Xylol	5 (min)

4.5.5. Picrosirius red staining

Picrosirius red staining is used to detect and visualize collagen fibers type I and III, as well as muscles in paraffin tissue sections. Following deparaffinization and hydration with water, paraffin sections were submerged in picrosirius red solution from the picrosirius red staining kit (ScyTek) for 1 hour. The sections were then washed with the acetic acid solution contained in the staining kit and subsequently with 100% ethanol. Sections were directly mounted with Euparal mounting medium.

4.5.6. Oil-Red-O staining

Oil-red-O staining was used to visualize the fat cells and neutral fat, as it stains the triglycerides contained in lipid droplets of adipocytes red and the hemalaun will stain the nuclei in blue. Cryosections were thawed for 10 minutes at room temperature and Oil-Red O staining stock solution was prepared by dissolving the powder in 100% isopropanol (3 mg/mL). Then, the working solution was prepared by diluting the stock solution in water at a 3:2 ratio. The solution was then filtered and preheated to 60°C. Slides were first covered with 100% propylene glycol for 2 minutes, then with Oil-red-O solution for 10 minutes. Sections were counterstained with hemalaun for 1 minute and were washed with distilled water twice. Finally, they were mounted using Kaiser's glycerol gelatine.

4.5.7. Microscopy

Imaging of sections that were stained with immunofluorescent antibodies or chromogenic solutions was performed using the Keyence BZ-9000 microscope. For the immunofluorescently stained sections, the imaging mode was set to monochrome and four dyes were used, DAPI, GFP, Cy5, and either TRITC or TexasRed. For the chromogenically stained sections, the imaging mode was set to color. Images were taken at various magnifications (4x, 10x, 20x, and 40x). Afterwards, images were analyzed with the BZII Analyzer and contrast / color adjustment was done with Fiji (ImageJ) software. For the 40x magnification images of gallbladder and small intestine, a Zeiss LSM880 Airyscan confocal microscope was also used.

4.5.8. Spatial Phenotyping

Spatial phenotyping was done by Dr. David Bejerano (from the group of Prof. Andreas Schlitzer) on liver tissue that had been fixed with 4% paraffin. Tissue staining using CODEX/PhenoCyclerTM (Akoya Bioscience) and images were taken with Zeiss Axio Observer (Bayerl et al., 2023).

4.6. Single cell suspensions from various tissue for FACS analysis

In general, mice were sacrificed by cervical dislocation and the organs of interest were transferred to PBS-filled multiwell plates. Different digestion protocols were used for each of the organs and as delineated in the following sub-sections. Following the digestion process, cells were resuspended in 200 uL PBS and transferred to 96-well plates for staining.

4.6.1. Small Intestine (Lamina Propria and IEL)

SI were flushed with cold PBS and the surrounding fat tissue, as well as Peyer's Patches were removed. SI was cut longitudinally and cut into 1-2 cm-long pieces. The pieces were transferred into 50 ml Falcon tubes containing 20 ml digestion solution 1 and incubated in a shaking incubator at 37°C for 20 min. Then, the tissues were transferred into another 50 ml Falcon tube containing 20 ml digestion solution 2 and incubated in a shaking incubator for 15 min. This step was repeated twice and in both steps the waste was collected and centrifuged at 400xg for 5 min to obtain the IEL fraction. In the last digestion step, tissues (excluding IEL) were incubated in a shaking incubator in 10 mL digestion solution 3 for 10 min at 37°C. Following digestion, tissues were transferred into a 6 well-plate and minced

into small pieces and the digestion solution 3 supplied with DNaseI and LiberaseTM was applied. The tissue was further incubated in a shaking incubator (60 rpm) at 37° C for 45 min. The tissues were subsequently homogenized by pipetting with a serological pipette. The cell suspension was filtered through either a $100~\mu m$ (for myeloid cells) or a $70~\mu m$ (for lymphocytes) cell strainer to obtain a single-cell suspension. Cells were washed twice with PBS and centrifuged.

4.6.2. WATg (stromal vascular fraction)

After WATg was harvested from the peri-gonadal area, the surrounding muscle tissues and ductus epididymis were removed. Tissue was stored in cold PBS and minced in a petri dish and then transferred into a 15 ml Falcon tube that contained 2 ml of Collagenase II digestion mix. The tissue was digested at 37°C in an incubator for 30 min and shaken vigorously every 5 min until it dissolved. Stop buffer was added and the tissue was passed through a 100 µm cell strainer. Tissue was centrifuged at 200xg for 5 min and incubated for 10 min at RT. The floating fraction was removed with a pipette. Cells were resuspended in 1 ml 1x RBC lysis buffer incubated for 5 min at 37°C and afterwards washed with 4 ml FACS-buffer, centrifuged, and resuspended in FACS-buffer.

4.6.3. Adult murine ear skin

The harvested ears were stored in PBS at 4°C until processing. The dorsal side of the ear was separated from the ventral side and ear cartilage was removed. The skin from both the dorsal and ventral sides was minced in a 12-well plate and 500 µl digestion buffer containing Liberase and DNAseI was applied. Tissues were incubated in a shaking incubator (100 rpm) at 37°C for 90 min. Tissues were then dissociated by pipetting with blunted tips and by filtering through either 100 µm (for myeloid) or 70 µm (for lymphocytes) cell strainers. Lastly, the cell suspension was centrifuged at 400xg 10 min at 4°C and the cell pellets were resuspended in 200 µl PBS.

4.6.4. Neonatal murine epidermis

After decapitation, the tails and limbs of neonates were cut. Then, the whole-body skin was peeled off as intact as possible and was stored in cold, sterile PBS. Skin was incubated in 1 ml digestion mix containing Dispase II (2,4 U/mL) in RPMI1640 medium, for 1.5 hours at 37°C. The epidermis was then separated from the dermis and was incubated in 3 ml DNAse I-containing RPMI1640 solution for 30 min at 37°C. The epidermal tissue was pipetted vigorously, passed through a 70 μm strainer and washed with PBS, before it was

finally centrifuged at 300xg for 8min at 4°C. The washing step was repeated twice. The cell pellets were resuspended in 200 ul PBS.

4.6.5. Isolation of immune cells from Liver

Following cervical dislocation, hepatic perfusion was immediately conducted via the vena cava using a Gr.20 Sterican needle (Braun) and the portal vein was cut. The perfusion was first performed with cold PBS until the liver was pale, then with 5 ml Collagenase D solution (10 mg/ml in HBSS without Ca²⁺). Following perfusion, the liver was extracted and the gallbladder, as well as the surrounding connective tissues were removed. The liver was kept in PBS until further processing. It was then minced in a 5 cm petri dish and the tissue was transferred into a 50 ml Falcon tube containing digestion solution (5 mg/ml Collagenase D in HBSS with Ca²⁺). The tissue was then incubated in a shaking incubator (250 rpm) at 37°C for 17 min and was then passed through a 100 µm filter and flushed with 40 ml GBSS. Cells were centrifuged at 50xg for 2 min to remove hepatocytes. The supernatant was collected and transferred into another 50 ml Falcon tube and centrifuged at 800xg for 10 min. A Percoll gradient was prepared by layering the 20 ml 25% Percoll on top of the 15 ml 50% Percoll solution, the latter was stained with 200 µl Phenol Red to make it easier to detect the interphase. Following centrifugation, cells were resuspended in 10 ml PBS and were slowly pipetted onto the Percoll gradient and then centrifuged at 1200xg (acceleration = 7 and deceleration = 0) for 30 min. The interphase was collected with a 1000 µl pipette tip, washed with 30 ml PBS, and centrifuged at 800xg for 10 min at 4°C. This process was repeated twice before cells were finally resuspended in 200 µl PBS.

4.6.6. Isolation of immune cells from Spleen

Spleens were mashed using the back of a syringe and passed through a $100 \,\mu m$ cell strainer to obtain single-cell suspensions. RBC lysis was performed for 5 min to remove the remaining erythrocytes. RBC lysis buffer (BioLegend) was diluted 1:10 in VE water. Cells were washed with PBS and centrifuged at $400 \,\mathrm{xg}$ for 5 min at $4^{\circ}\mathrm{C}$, before being finally resuspended in $200 \,\mu l$ PBS.

4.7. FACS staining

Cells were stained in 96-well V-bottom plates with 50 ul of diluted antibodies (see FACS panel for each organ) and Fc block that had been diluted in PBS (1:100) for 30 minutes in the dark at 4°C. For panels where anti-CD64 was included, the cells were first stained with

anti-CD64 for 30 min without Fc block prior to staining with the rest of the antibodies. Cells were then kept at 4°C until measurement.

4.7.1. LIVE/DEAD® Fixable Dead Cell Staining

The LIVE/DEAD® fixable dead cell stain kit was used to discriminate between living and dead cells. Cells were incubated in 100 or 200 µl PBS containing the fixable dye at a dilution of 1:1000 for 30 min on ice. The staining was typically performed in combination with the surface antibody staining. Afterwards, cells were washed with 300 to 500 µl PBS (1400 rpm, 5 min) and were then further processed.

4.7.2. Fixation of cells for flow cytometric analysis or intracellular staining

After surface staining and optional LIVE/DEAD® staining, cells were fixed with 2% PFA for 20 min at room temperature. Afterwards, cells were washed with 300 to 500 µl PBS (1400 rpm, 5min) and resuspended in 300 µl MACS buffer. The intracellular staining was conducted with Foxp3/transcription Factor Staining Buffer Set according to the protocol provided by the manufacturer (Thermo Scientific).

4.8. Western Blot

For Western blot analysis of BMDC, total protein was extracted using 200 µl of RIPA buffer. Cell lysates were resuspended in beta-mercaptoethanol-containing SDS-PAGE sample buffer prior to loading. Proteins were then separated by SDS-polyacrylamide gel electrophoresis (PAGE), transferred to a nitrocellulose membrane (unless otherwise specified) by means of semi-dry Western blot. Membranes were blocked by 5% milk in TBST for 1 hour at RT and then incubated with primary antibody diluted with 2.5% milk in TBST O/N at 4°C. After that, membranes were treated with secondary antibodies diluted with 2.5% milk in TBST (LiCor IRDye 800CW and 680RD) for 2 hours at RT to allow two-color detection. The fluorescence signal was then detected by an Odyssey® Imaging System (LiCor).

4.9. Real Time Quantitative PCR (qPCR)

4.9.1. RNA isolation

To isolate whole RNA from SI, colon or any other tissues, tissue samples were explanted, cleaned from intestinal content or fat and transferred into glass bead tubes. These tubes

were snap frozen in liquid nitrogen and subsequently stored at -80°C until further usage. 600 μ l of QIAzol Lysis Reagent were added to the tissue samples immediately before thawing. Tissue lysis and homogenization were performed with the Precellys®24 homogenizer at 6000 rpm (3x20 seconds). RNA was isolated using the Zymo Research Direct-zol MiniPrepkit according to the manufacturer's instructions. RNA was eluted with 30 μ l of DNase/RNase-free water and the RNA concentration was determined using a NanoDrop1000 photospectrometer. The RNA was stored at -80°C for further procedures.

4.9.2. cDNA synthesis

Isolated whole RNA was transcribed into complementary DNA (cDNA) by the enzyme reverse transcriptase. The employment of Oligo(dT) primers ensures the reverse transcription of messenger RNA (mRNA), which is protected against degradation by exonucleases by modification with a 3' poly(A) tail. For all experiments between 0.5 and 1µg of RNA was used for the reverse transcription. The RNA was diluted to the desired concentration in DNase/RNase free water. A maximum volume of 10 µl RNA was used. RNA was mixed with 3µl Oligo(dT) primer, which hybridizes to the poly(A) tail of mRNA. The mixture was incubated for 10 min at 70°C to unfold and denature the RNA and allow the primers to anneal to the RNA. Afterwards the samples were cooled down on ice. Then, a master mix consisting of other reagents needed (**Table 3.11**) was added and the cDNA reaction mix was incubated for 1 hour at 40°C. A final 5-min incubation at 95°C inactivated the reverse transcriptase and stopped the reaction.

4.9.3. qPCR

A real-time polymerase chain reaction (qPCR) was used to quantify the amount of DNA molecules, which has been previously transcribed from mRNA, based the amplification of targeted DNA in real-time. After conversion of RNA in cDNA the cDNA was used as a template for amplification via PCR. The 2x Absolute qPCR SYBR Green Mix contains all components for the quantitative PCR reaction, except primer and template. The mix contains appropriate amounts of SYBR Green I dye and Thermo-Start DNA Polymerase. SYBR Green preferentially intercalates into newly synthesized double-stranded DNA and subsequently emits green light at a wavelength of 520nm. The CFX96 TouchTM Real-Time PCR detection system detects the signal that increases with advancing DNA amplification. One PCR reaction had a volume of 15 μl and included 7.5μl 2x Absolute qPCR SYBR Green Mix, 0.3μl forward primer, 0.3μl reverse primer, 1.9μl water and 5 μl cDNA. The

cDNA, synthesized as described in section 4.9.2, was diluted 1:5 with water prior to the qPCR reaction. The CFX96 thermocycler program is listed in the table below.

Table 4.3 qPCR program

	Incubation Time	Temperature
1x	15 (min)	95°C
	20 (min)	95°C
44x	40 (min)	60°C
	60 (min)	40°C

Following the amplification, a melting curve analysis of the synthesized double stranded DNA fragments was performed to check if the PCR primers used produce one specific PCR product or potential unwanted unspecific products or primer dimers. For this purpose, the thermo cycler raises the temperature in steps of 0.5°C from 65 to 95°C. The melting temperature was determined by a strong reduction of SYBR Green fluorescence signal as a consequence of its dissociation from the DNA.

4.9.4. Comparative Ct Method Quantification

The comparative Ct method of quantification is a relative quantification method based on an internal reference gene (e.g. GAPDH) that is used to determine fold-difference expression of a target gene. The quality of this method largely depends on the selection of a good reference or housekeeping gene that is stably expressed and largely independent of any experimental conditions. A housekeeping gene corrects for differences in the quality and quantity of the RNA that was initially utilized, which can affect the whole PCR process. During the PCR the accumulation of the SYBR Green fluorescence signal was measured. A threshold cycle (Ct) was determined at the time point where the amount of SYBR green fluorescence exceeds the background fluorescence. Ct values are inversely correlated to the amount of nucleic acid within the sample. Ct values of the target gene were corrected for the Ct values of the reference gene forming the Δ Ct value in treated and control samples (Δ Ct1=Ct_{Target} treated-Ct_{Reference} treated, Δ Ct2=Ct_{Target} control-Ct_{Reference} control). In a second step control Ct values were subtracted from the Ct values of treated samples (Δ \DeltaCt= Δ Ct1- Δ Ct2). Normalized target gene expression as fold change of treated over control samples was finally determined by the formula 2- Δ Ct.

4.10. Luciferase assay

For reporter gene analyses, 300,000 HepG2-DRE cells/well were seeded in 12-well plates, treated with various ligands, and cultured for 16 hours. Then, cell lysates were prepared and luciferase activitiy was determined using the luciferase assay system (Promega, Mannheim, Germany) in a Luminometer (Berthold, Germany). Luciferase activities were not normalized against protein concentration.

4.11. FAT scoring for WATg fibrosis

The FAT score was determined for WATg sections as shown in the publication of Bel Lassen et al. (Bel Lassen et al., 2017). On a histological level, fibrosis is characterized by pericellular and/or perilobular collagen deposition (PCF and PLF), lobular inflammation, and ballooning of adipocytes, the latter being the driving force of fibrosis. The severity of PCF and PLF was scored with ratings ranging from 0 (mild) to 2 (severe). At level 0, the fibrosis is mild; no or limited PCF/PLF observed, for PLF the fibrosis thickness is similar to the diameter of less than 1 adipocytes. For level 1, moderate PCF/PLF is observed, for PLF the fibrosis thickness is similar to the diameter of 1 adipocyte. In level 2, severe PCF/PLF is observed, for PLF the fibrosis thickness is similar to the diameters of 2 adipocytes, whereas for PCF adipocytes trapping is also apparent. The PCF and PLF scores are then combined to determine the final FAT score, which ranges from 0 to 3. A FAT score of 0 means neither PCF nor PLF is observed. FAT 1 means moderate PCF and/or PLF is observed. FAT 2 means either severe PCF or PLF is observed. FAT 3 means both severe PCF and PLF are present.

4.12. Statistical analysis

Statistical analysis was performed using the unpaired Students t-test, if just two independent groups or two conditions for one experimental group were compared. For the determination of statistical difference between three or more independent experimental groups, the one-way ANOVA was used. The two-way ANOVA was used when analyzing the mean differences between groups that have been split on two independent variables. All data are presented as mean plus standard error of the mean (SEM) if not stated otherwise in the figure legend. Significance was defined by reaching certain p-values in the statistical tests (* p<0.05, ** p<0.01, *** p<0.001). All statistical analysis was conducted with the software GraphPad Prism.

5. Results

5.1. Validation of AhRR-V5 protein expression in mice

The initial goal of my PhD work was to elucidate the protein-protein interaction between AhRR and its binding partners in myeloid cells, as the AhRR may carry out other functions apart from being an AhR repressor. For this purpose, a ChIP-seq experiment would be useful, as it could help not only to identify the DNA binding sites of the AhRR under physiological conditions in an unbiased manner, but also shed light on the AhRR function in general. Before a ChIP-seq could be performed, AhRR expression on the protein level needed to be proven. For this, BMDC were treated with 3MC, as a previous study using AhRR/EGFP reporter mice showed that BMDC from AhRR^{E/+} mice showed 15 times higher AhRR/EGFP expression in lymph-node-derived DC following a 16-hour 3MC treatment compared to control cells (Brandstaetter et al., 2016).

As no suitable antibodies to detect AhRR expression are commercially available, our group generated AhRR-V5 tagged mice using the CRISPR/Cas technology (P. Hatzfeld, I. Förster and H. Weighardt, unpublished). The targeting strategy used for epitope tagging is shown in Fig. 5.1 A. A V5-epitope tag was inserted into the C-terminus of the AhRR protein. This epitope tag was chosen because high affinity antibodies against it are commercially available. Besides, it has been reported that it can be used for ChIP-seq experiments in murine models (Burg et al.,2016). To generate the V5-tagged AhRR mice, ribonucleoprotein complexes of Cas9 and sgRNAs together with a DNA oligo containing the V5-tag sequence flanked by homology arms were electroporated in fertilized oocytes of C57B6J/RCC mice. Correct insertion of the DNA oligo encoding the epitope tag was verified by sequencing. The resulting mice were viable and fertile. A representative genotyping result of this mouse line is shown in Fig. 5.1 B.

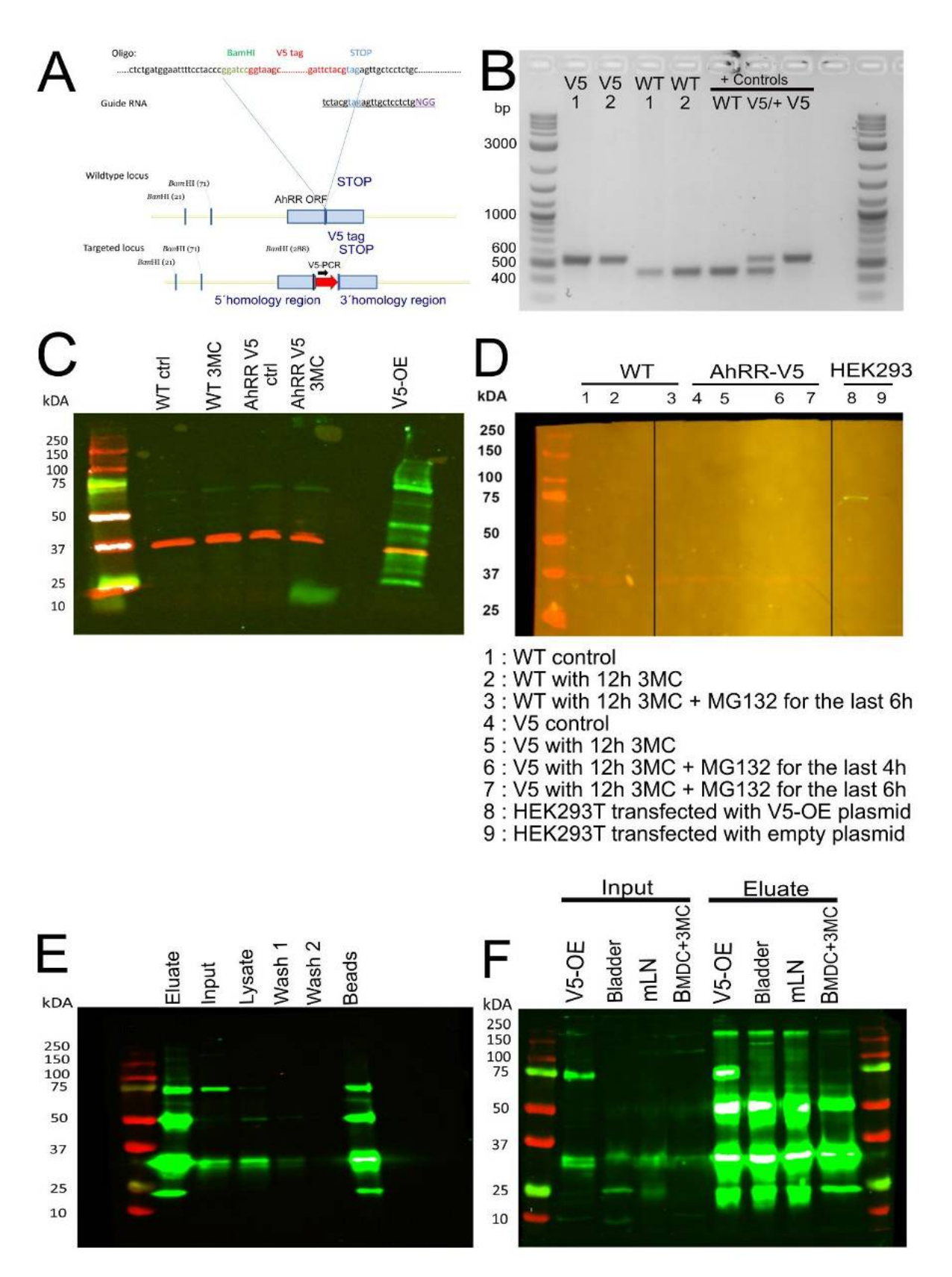


Fig. 5.1 AhRR expression in BMDC is not detectable by Western blot. A) Schematic representation of the strategy used to generate epitope tagged mice. The black arrow indicates where the AhRR-V5 primers hybridize for genotyping B) Genotyping of two WT and AhRR-V5 mice and controls showed a 512 bp fragment for AhRR-V5 and 470 bp Fragment for the WT allele. C) A representative Western blot result of BMDC from WT and AHRR-V5 expressing mice, which were treated either with 0.1% DMSO (ctrl) or 10μM 3MC for 20 hours, is shown. Lysates from HEK293T cells transfected with an AhRR-V5 construct (V5-OE) was used as positive control. The AhRR-V5 band is detected at 76 kDA and GAPDH is at 37 kDA. D) Western

blot from whole lysates of BMDC from WT and AhRR-V5 mice. WT and AhRR-V5 samples were treated either only with 3-MC for 12 hours or additionally with MG132 in the last 4- or 6-hour. E) Immunoprecipitation (IP) of AhRR-V5 in HEK293T cells overexpressing AhRR-V5. The input sample is the precleared protein lysate before the IP process. The lysate control was taken from the antibody/coupled lysate and should represent proteins that were not bound to the beads. The eluate sample is antibody-coupled protein that has been released from the beads. F) IP of AhRR-V5 in HEK293T cells overexpressing AhRR-V5, bladder, mLN, and 20-hour 3MC-treated BMDC from AhRR_V5 mice. All blotting steps were performed on nitrocellulose membrane except for D, which was done on a PVDF membrane.

For the analysis of AhRR-V5 protein expression, BMDCs from both WT and AhRR-V5expressing mice were harvested ($\pm 5 \times 10^6$ cells) and Western blot analyses were conducted to determine AhRR-V5 protein expression following a 20-hour treatment with 3MC (a representative image is shown in Fig. 5.1 C). A specific AhRR-V5 signal should be detected at 75 kDA in the 800nm (green) channel, whereas GAPDH as a loading control was detected at 37 kDA in the 360nm (red) channel. Whole-cell lysates from BMDCs were used and the protein concentration was neither measured nor adjusted, as the goal of the experiment was to see if the AhRR in BMDC was expressed at all. The positive control for the experiment was generated by transfecting HEK293T cells with an expression plasmid coding for AhRR-V5, resulting in cells that overexpressed AhRR-V5. So far, only the positive control yielded a specific AhRR-V5 signal at 75kDA, whereas there were unspecific signals at 73-74 kDA in all BMDC samples (both WT and AhRR-V5). However, in the positive control there were also unspecific bands at around 50 and 20 kDA, which could have been caused by AhRR degradation. Nevertheless, GAPDH expression could be detected in all samples, which indicated that the blotting process per se had been successful. However, the concentration of AhRR protein in primary cells from AhRR-V5 mice appeared to be too low to be detected by means of Western blot. There are multiple factors that could have led to this result, such as a low expression level per se, high protein turnover rate or insufficient amount of BMDC used for the Western blot. Also, an increased expression of UbCM4 (the mouse ortholog of E2 ligase UbcH7) caused by TCDD-mediated-AhR-activation, can lead to an overall increase of proteasomal degradation of proteins (Mejía-García et al., 2015). However, it is not proven if 3MC-mediated activation can also elicit such an effect.

To analyze if proteasomal degradation caused a reduced nuclear translocation of AhR, hence also reduced expression of AhRR, or reduced expression of AhRR itself, another experiment was conducted, in which a proteasome inhibitor, MG132 was used. BMDC cultures were either treated only with 3MC for 16 hours without MG132 or were first treated with 3MC for 10 or 12 hours, and then co-treated with MG132 for 6 or 4 hours. MG132 is a peptide

aldehyde that covalently binds to the beta-subunits of the 20S proteasome, which leads to an overall inhibition of the proteolytic activity of the 26S proteasome complex (Guo & Peng, 2013). In this experiment, a PVDF membrane instead of a nitrocellulose one was used (Fig. **5.1 D**), as it is postulated to have a greater binding capacity for proteins. Thus, it is considered more suitable to detect low abundant proteins. The 3MC stimulation time was reduced in this experiment to 16 hours to see if the AhRR protein expression would be better visible at this time point compared to the 20-hour time point that was used in the previous experiment. The reason was because on mRNA level the expression of Ahrr post 3MC stimulation peaked at around the 12-hour time point before it dropped at the 24-hour time point, as shown in the next chapter (Fig. 5.5). In this experiment, also complete lysates of BMDCs were used. However, the modifications of the timing of the experiments still did not give better results, as a high background fluorescence was detected. Nevertheless, similar to the previous experiment, only the positive control showed a specific band, indicating that MG132 at this dose and time point could not increase AhRR protein expression. Moreover, the GAPDH bands at 37 kDA were still visible, although they appeared really faint, so the possibility of AhRR degradation can still not be excluded.

Since the AhRR protein level is probably too low to be detected by Western blot alone, we tried to enrich it by means of immunoprecipitation (IP) (performed by Philip Hatzfeld), in which the AhRR-V5 protein was 'pulled' by anti-V5-protein A/G complexes and V5antibody was also used to detect the expression of V5-tagged-AhRR. In order to determine if the IP protocol worked properly, we precipitated the AhRR-V5 protein from the positive control (Fig. 5.1 E), which was generated by transfecting HEK293T cells with an expression plasmid coding for AhRR-V5 similar to the one used for the previous Western blot experiments. The eluate yielded a clear band at 75kDA, signifying that the AhRR-V5 protein was successfully precipitated. Once it was determined that the IP protocol worked, multiple IP experiments were performed to compare the expression of AhRR in several organs, e.g. bladder, mLN, and 20-hour-3MC-treated BMDC with AhRR-V5-overexpressing HEK293T cells used before. Whole protein lysates from bladder and mLN were used, as AhRR is moderately expressed on mRNA level in these two organs (Tsutchiya et al., 2013; Brandstaetter et al., 2016). BMDCs were cultured in ten 10 cm petri dishes ($\pm 50 \times 10^6$ cells) for this experiment and their protein content was then concentrated using a membrane with a 50k molecular weight cut-off. Here, the amount of BMDC was 10x higher than the previous Western blot experiment. The purpose of using a higher BMDC amount was to see if increasing the amount of cells helped to circumvent the low expression level of the AhRR.

The IP experiments also worked in principle, as a clearly visible band at 75 kDA could be detected both in the input and eluate of the V5-overexpressing sample used as positive control (a representative blot is shown in **Fig. 5.1 F**). However, again no AhRR-V5 signal could be detected neither in the organ samples, nor in the BMDC samples as there was no clearly visible band seen at 75kDA, both in the input and the eluate sample. This means that after 20 hours of 3MC stimulation, the AhRR protein level in 20x10⁶ BMDC is still lower than the detection threshold of the IP followed by Western blot. Also, no AhRR-V5 protein could be detected in the input sample of bladder and MLN tissue. Therefore, it might be possible that the AhRR is expressed at extremely low levels *in vivo* or was already degraded either on mRNA or protein level before the IP was carried out.

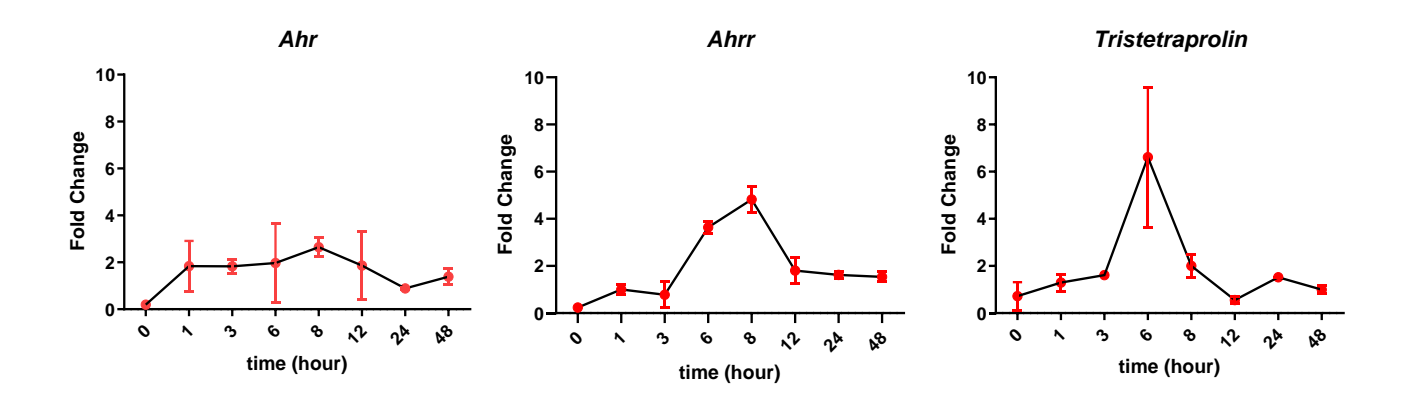


Fig. 5.2 The peak of *Ttp* expression coincides with the peak of Ahrr expression. qPCR results of BMDC that were treated with 10 μ M 3MC. Data was normalized to 0.1% DMSO-treated control. The qPCR results show the gene expression of *Ahr*, *Ahrr*, and Tristetraprolin (TTP) as fold change (2^{- $\Delta\Delta$ Ct}). Error bars represent mean \pm SEM. n=2.

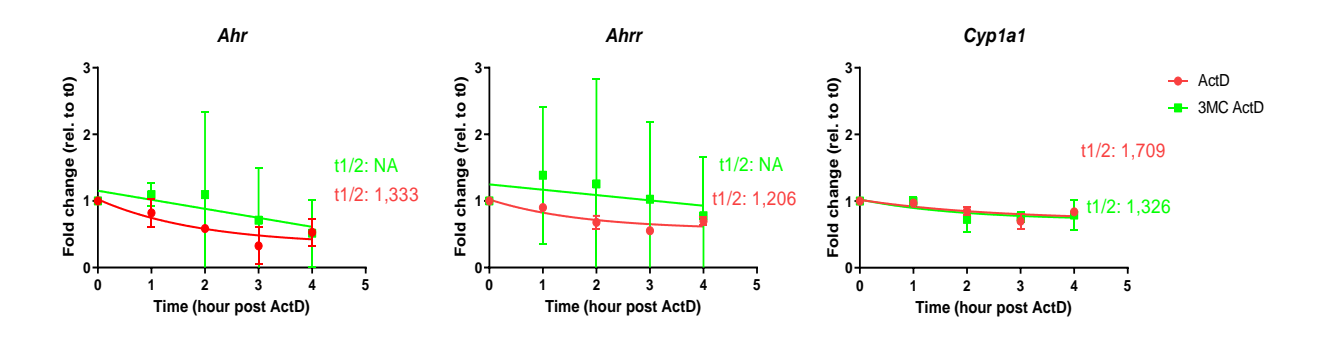


Fig. 5.3 The mRNA decay rates of *Ahr* and its target genes. HepG2 cells were treated with actinomycin D only or co-treated with 3MC and Actinomycin D for 4 hours. Then, the expression of *Ahr* and its target genes were analyzed by qPCR. Data was normalized to the expression of reference gene and samples treated with the respective treatments for 0 hour. The qRT-PCR results show the gene expression of *Ahr*, *Ahrr*, and *Cyp1a1* as fold change $(2^{-\Delta\Delta Ct})$. Error bars represent mean \pm SEM.

Another reason for the low expression of AhRR-V5 *in vivo* could be that the *Ahrr* expression might be regulated on a post-transcriptional level. A study by Lee et al. (Lee et al., 2013)

showed that tristetraprolin (TTP) binds to 3' AU-rich elements (ARE) at the 3-prime terminus of the Ahrr mRNA and leads to destabilization and thereby reduction of the Ahrr transcripts. In addition, FICZ administration in mice during DSS colitis led to upregulation of TTP (Wang et al., 2017). Thus, a time kinetics experiment was conducted in BMDC in order to analyze Ttp expression after stimulation with 3MC. The result showed that 3MC treatment did not significantly alter Ahr expression over the 48-hour time course (Fig. 5.2 A), whereas Ahrr expression started to increase at 6 hours and peaked 8 hours after stimulation before it dropped at the 12-hour time point (Fig. 5.2 B). This increase in Ahrr was preceded by an increase in Ttp mRNA that peaked 6-hour after stimulation (Fig. 5.2 C). The earlier increase of Ttp mRNA and therefore protein might account for the decrease in Ahrr expression after the 8hour time point, as a previous study showed that mRNA decay could be caused by the binding of TTP to the AU-rich element (ARE), which occurs post-transcriptionally. It is also important to mention that Ahrr mRNA contains two AREs in its 3'UTR (Lee et al., 2013). Hence, the very low AhRR expression on protein level might have been caused by a degradation of Ahrr mRNA. Subsequently, an mRNA decay experiment has also been conducted on HepG2 cells, by treating the cells either with 10 mg/ml Actinomycin D (ActD) only or with a 3MC and ActD combination for 4 hours (Fig. 5.3). ActD is a DNA intercalator that inhibits transcription elongation by all three polymerases (I, II,III) (Nguyen et al., 1996). The result showed that in ActD-treated cells the half-lives of Ahrr and Ahr mRNA were comparable, around 1,2-1,3 hours, whereas the half-life of Cyp1a1 was a bit longer (1,7 hours). As 3MC and ActD cotreatment did not induce a linear mRNA decay for Ahr and Ahrr, the half-lives of both genes could not be calculated. For Cyplal, the co-treatment resulted in a slightly shorter mRNA half-life than the ActD treatment alone.

All in all, our attempts to detect AhRR-V5 protein expression in BMDCs by Western blot and IP/Western blot failed despite multiple attempts to find the optimal 3MC stimulation time, harvesting time point, MG132 administration, and the use of different blotting membranes. It seemed that the AhRR expression was very low in vivo. Hence, we concluded that it would not be reasonable to continue with the ChIP-seq experiment, since this procedure requires ca. 10^6 - 10^7 cells and it involves more modification steps (e.g. cross-linking, fragmentation, freezing) that may reduce the availability of AhRR protein even more.

5.2. Determination of the optimal concentration and activation time point of different AhR ligands

Since the regulation of AhR gene induction is complex, the net outcome depends on many factors, e.g. the nature of the ligand, duration of AhR activation, physiological condition of the cells, the cell type activated and which target genes get up or downregulated. For instance, TCDD and DIM are both AhR agonists but the elicited effects from both ligands are different; TCDD is highly toxic and can lead to liver toxicity and other deleterious effects, e.g. an impaired immune response (Kerkvliet et al., 1990), and DIM can suppress carcinogenesis (Lubet et al., 2011). One reason that accounts for the TCDD-mediated toxicity is that it cannot be metabolized by the CYP1A1, CYP1A2, and CYP1B1 enzymes, which metabolize the majority of AhR ligands, leading to a constitutive activation of AhR (Navrátilová et al., 2017). These three CYP enzymes are encoded by target genes of the AhR. Among other target genes generated following ligand mediated AhR activation, Ahrr and Tiparp encode two proteins that act as repressors of AhR. However, the mechanism used by these two repressors differs, as AhRR acts as direct negative feedback regulator, whereas TiPARP regulates AhR activity by ADP-ribosylation (MacPherson et al., 2014). Hence, the outcome of AhR signaling is hard to predict. To get more insight into AhR signaling, we collaborated with the group of Prof. Jan Hassenauer, LIMES Institute, to perform mathematical modelling of the AhR signaling pathway. This model consists of parameters, which are Michaelis-Menten-derived reactions describing the dynamics of each protein and metabolite in the system. The reactants in the aforementioned reactions are called species. The data was formatted in PEtab format that enables the specification of parameter estimation problems (Schmiester et al., 2021) and the model simulation was performed using AMICI (Fröhlich et al., 2021). The growth of every species over time is described by a set of ordinary differential equations (ODEs), which consist of the rate laws and stoichiometry matrices of the reactions. To fit the model, experimental data were needed to estimate the parameters of the ODEs to minimize the negative loglikelihood function (Schmiester et al., 2020). Therefore, we performed experiments which show dose and time kinetics of Ahr activation and expression of its target genes, e.g., Ahrr, Cyp1a1, and Tiparp on mRNA level. Here, we used HepG2 cells to analyze this.

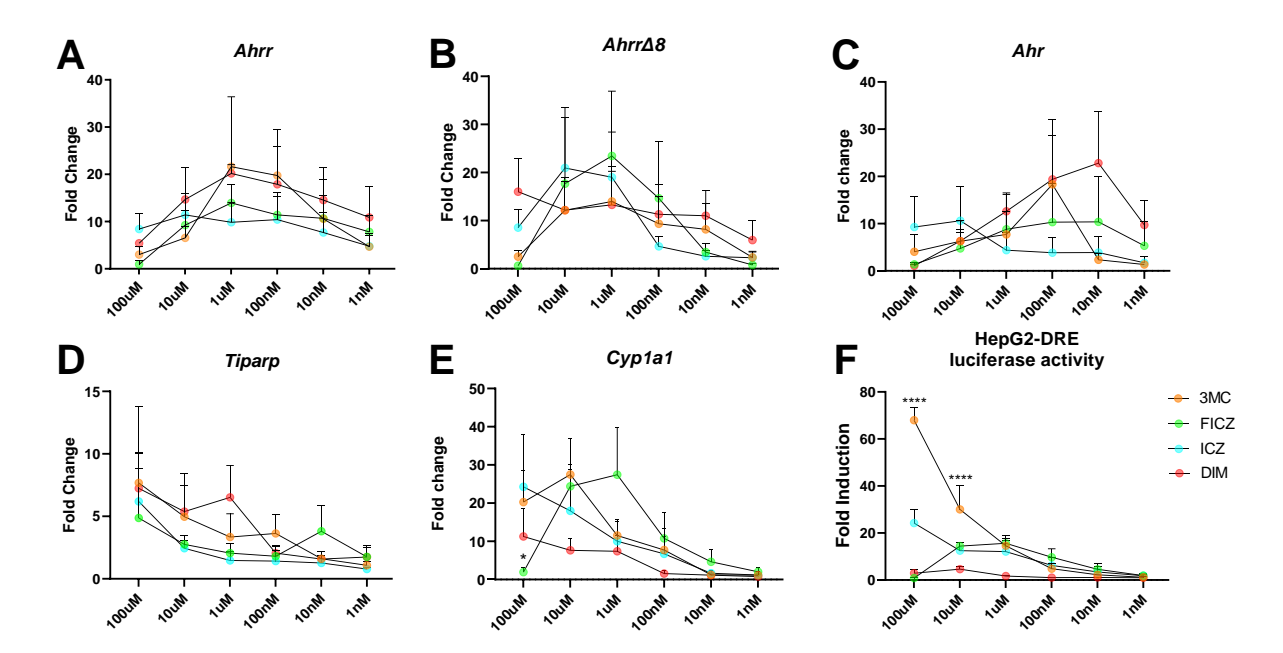


Fig. 5.4 3MC is the most potent stimulus to induce the expression of most AhR target genes. The expression of AhR target genes and transcriptional activation of Ahr in HepG2 and HepG2-DRE cells were measured by (A-E) qPCR and F) Luciferase assay after stimulating the cells with different concentrations of AhR ligands for 16 hours. For the qPCR experiment, the fold change was calculated by $2^{-\Delta\Delta CT}$ and for the luciferase experiment the fold induction was calculated by normalizing the Relative Light Units of the firefly signal induced by the 3MC-treated samples to the DMSO-treated controls. In E) *, p < 0.05, between FICZ and ICZ. In F) **** p < 0.0001 between 3MC and the other three ligands, at the same concentration. Results are shown as mean \pm standard error of the mean (SEM) and significance was analyzed by two-way ANOVA corrected for multiple comparisons by the Bonferroni's test * p<0,5, *** p<0,01, **** p<0,001. N = 3.

The HepG2 cell line was used because it is a hepatoma-derived cell line that expresses AhR target genes, particularly *Cyp1a1*. Second, a cell line can be passaged indefinitely, making it more easy to use for kinetics experiments. It is also important to mention that since HepG2 is a human cell line, it expresses two variants of *Ahrr*, the full length *Ahrr*₇₁₅ and the spliced *Ahrr*Δ8 that lacks exon 8 of the full-length variant. The latter is the predominantly active AhRR variant in human cells (Karchner *et al.*, 2009). In addition, I also used a HepG2-DRE cell line, which stably expresses a luciferase gene under the control of 5 DRE regions of the murine *Cyp1a1* promoter (a gift from Thomas Haarmann Stemmann, IUF Düsseldorf). Using this stably transfected cell line, *Cyp1a1* promoter activity can be compared to the induction of *Cyp1a1* transcripts, which can be measured by qPCR after treatments with various ligands.

For the concentration kinetics, the optimal concentrations of the four AhR ligands that have been routinely used in our lab had to be determined. They were 3-methylcholanthrene (3MC), 6-formylindolo[3,2-b]carbazole (FICZ), indolo [3,2-b] carbazole (ICZ), and 3,3-diidolylmethane (DIM). The optimal concentration was defined as a concentration, at which the expression level of all target genes in the cells treated with all ligands were clearly higher than after control treatment with DMSO. The 16- hour time point was chosen, as previous

experiments in our lab had shown that target genes of AhR were highly expressed at this time point in this cell line, but it was still not known if this was the most optimal time point. Thus, three independent qPCR and luciferase assays were conducted (**Fig. 5.4**). At first glance, the variation in between experiments is quite large. Interestingly, the four ligands chosen showed different potencies, as the expression of the AhR and its target genes peaked at different concentrations and at different magnitude, depending on which ligands were used.

Overall, 3MC was the most potent ligand, followed by FICZ, ICZ, and DIM, although there were some differences in potency across the four target genes. Most of the ligands also reached their optimum concentration at 1 µM, hence the concentration curves were mostly bellshaped, except for *Tiparp* expression. For *AhRR* expression, 3MC was the most potent ligand (Fig. 5.4 A), as it could induce Ahrr expression 22 times higher as compared to control at 1 μM, followed by DIM, which could induce Ahrr 18-fold at the same concentration (Fig. 5.4 A). Meanwhile, for induction of Ahrr 18 expression, FICZ and ICZ were the most potent ligands, with a similar potency (Fig. 5.4 B); FICZ was the most potent inductor for Ahrr∆8, as it could upregulate it 23-fold at a concentration of 1 µM. In addition, ICZ-treated cells also expressed Ahrr Δ8 at a similar level (20 fold) but at a higher concentration (10 μM). Expression of Ahrr Δ8 peaked after stimulation with 3MC at a concentration of 1 μM, but the magnitude of induction was almost 50% lower (14-fold) compared to the FICZ-treated group. Unlike in the case of Ahrr, where DIM could induce Ahrr expression up to 22-fold already at 1 μ M (Fig. 5.4 A). Ahrr∆8 was induced by DIM ~15-fold at 100 µM and the induction declined from 10 μM to 1 nM (Fig. 5.4 B). In terms of Ahr expression, DIM was the most potent stimulus, as it could induce Ahr expression 22-fold at only 10 nM, followed by 3MC, which could induce Ahr expression to 18-fold at 100 nM (Fig. 5.4 C). Furthermore, DIM also induced Tiparp expression by a factor of 7 at 1 μM and increasing DIM concentration to 100 μM only increased the expression of *Tiparp* expression to around 8 times (Fig. 5.4 D). Meanwhile, 3MC increased *Tiparp* expression 3.5-fold starting at 100 nM and further increased its expression to around 7.5-fold at 100 μM. Here, the concentration of 3MC was 10x higher than the concentration needed to induce Ahrr and Ahrr $\Delta 8$ to their peak expression. Furthermore, for Cyp1a1, 3MC, ICZ and FICZ induced Cyp1a1 to a comparable level (25-30-fold) (Fig. **5.4** E). For *Cyp1a1*, FICZ and ICZ were the most potent stimuli, as they both induced *Cyp1a1* expression to a comparable level, but FICZ could induce it at a lower concentration; Cyp1a1 was induced by FICZ at 1 µM to 30-fold, whereas 3MC and ICZ induced it to 28-fold at 10 μM and 24-fold at 100 μM, respectively. The results also showed that Cyp1a1 induction by DIM was the lowest among the four stimuli, and stimulation of the cells with 1-100 μ M of DIM resulted in a similar level of *Cyp1a1* expression (8-10-fold), but concentrations smaller than 1 μ M failed to induce *Cyp1a1* expression.

HepG2-DRE cells were used to determine the Cyplal promoter activity (Fig. 5.4 F). Here, except for FICZ-treated cells, the promoter activity of Cyp1a1 was directly proportional to the ligands' concentration. The cells that were treated with 100 µM 3MC had a significantly higher induction of Cyp1a1 promotor activity (up to 60-fold), followed by ICZ (23-fold) at the same concentration. Promotor activity was rather low in FICZ and DIM treated cells, whereas 3MC induced Cyp1a1 slightly more at a concentration of 10 μM compared to 100 μM. In DIM-treated cells, Cyp1a1 promoter activity was only minimally induced to 2.5 and 4 times at 100 µM and 10 µM, respectively, and no induction was observed at concentrations of 1 μM or lower. Interestingly both, promotor activity and Cyp1a1 mRNA levels, were induced by 100 μM FICZ to a lower level compared to 10 μM. Similarly, the expression levels of Ahrr, $Ahrr \Delta 8$, and Ahr were low (< 10-fold) when treated with the four ligands at a concentration of 100 µM. It is possible that these ligands are toxic for the cells at a high concentration, therefore a cell viability assay, such as an MTT assay should be conducted to prove this. In conclusion, 3MC at the concentration of 1 µM was chosen as the most appropriate stimulus for the next experiment, a time kinetic experiment. In summary, these data show that 3MC can elicit the highest expression of all AhR target genes, except Ahrr∆8, whereas DIM was the most potent stimulus to induce Ahrr and Ahr.

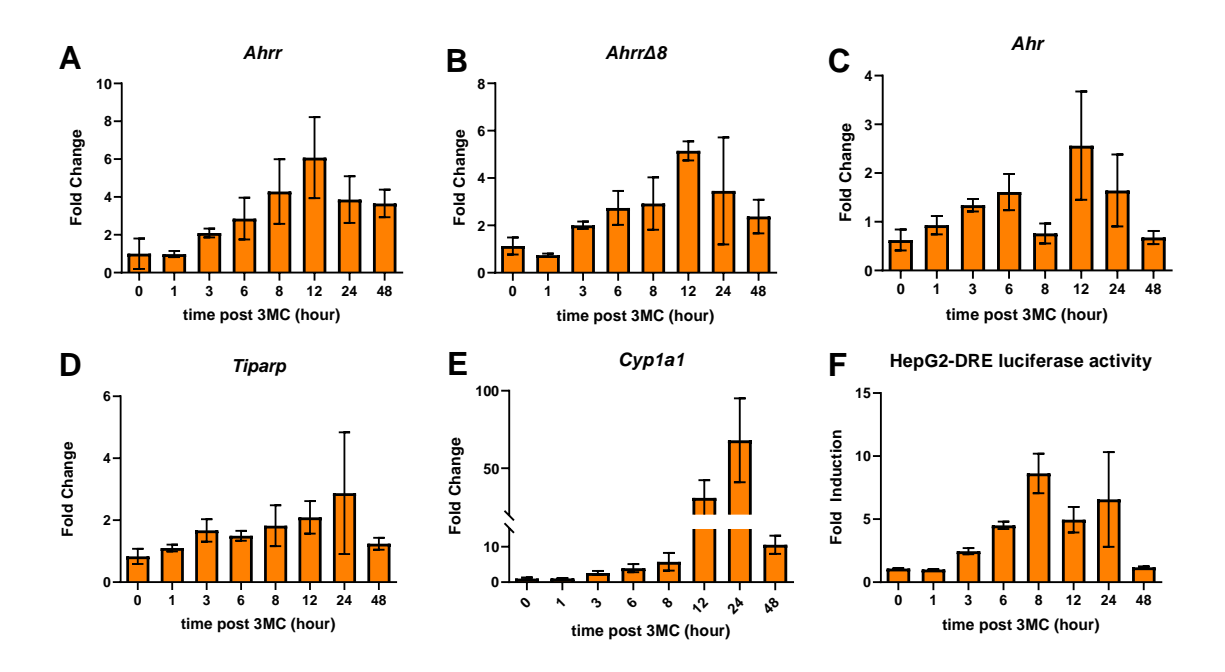


Fig. 5.5 *Cyp1a1* expression was highest among all target genes following 3MC stimulation. The expression of AhR target genes and transcriptional activation of *Ahr* in HepG2 and HepG2-DRE cells were measured by (A-E) qPCR and F) luciferase assays, respectively. Cells were stimulated with 3MC at a concentration of 1 μM and at multiple time points. Results are shown as mean \pm standard error of the mean (SEM). For the qPCR experiment fold changes were calculated by $2^{-\Delta\Delta CT}$, whereas for the luciferase experiment the fold induction was calculated by normalizing the Relative Light Units (RLU) of the firefly signal induced by the 3MC-treated samples to the DMSO-treated controls. n =3 for qPCR and n =2 for luciferase assay.

After choosing 3MC as the most suitable ligand and determining its optimal concentration at 1 µM, three independent time kinetic experiments were conducted. The experimental setup for the time kinetic experiment was similar to the one of the concentration kinetics, HepG2 and HepG2-DRE cells were used for qPCR and luciferase assay, respectively. This time 3MC-treated cells were harvested at 8 different time points (0, 1, 3, 6, 8, 12, 24, and 48 hours post stimulation). Here, Ahrr expression peaked up to 6-fold after 12-hour stimulation (Fig. 5.5 A), but it then returned to its base level at the 24- and 48-hour time points. A similar result was observed for Ahrr 18 expression, which also reached its peak at an 5.5-fold induction at the 12-hour time point, whereas it was reduced from 24 hours onwards (Fig. 5.5) **B**). In general, the expression level of Ahr did not increase much overtime; its expression reached the highest point at the 12-hour time point, where it only increased by 2.5-fold. This time point was the same at which Ahrr expression was highest (Fig. 5.5 C). Like Ahr, Tiparp expression levels were not highly induced by 3MC throughout the 48-hour time course, its expression increased to only around ~ 2.8 -fold at the 24-hour time point (Fig. 5.5 D). This showed that the expression dynamics of *Tiparp* differed from those of *Ahrr* and *Ahrr* $\Delta 8$. The expression level of the last AhR target gene analyzed here, Cyplal, was induced to 45-fold by 3MC at 12 hours, but the highest expression was observed at the 24-hour time point with

a 65-fold induction over the control, followed by a decline at the 48-hour time point (**Fig.** 5.5 E).

As for the concentration kinetics experiment described above, a luciferase assay using HepG2-DRE was also conducted to analyze the promoter activity of Cyplal over time (Fig. **5.5** F). In this case, however, a discrepancy between the Cyp1a1 promoter activity and the Cyplal expression levels measured by qPCR was obvious, indicating that the two methods led to distinct results. In the luciferase assay, the Cyp1a1 promoter activity peaked at the 8hour and not at the 24-hour time point as seen for the Cyp1a1 transcripts. Furthermore, when comparing this result to the one that was conducted for the concentration kinetics samples (Fig. 5.4 F), it is evident that the overall RLU levels were lower. The highest induction of luciferase activity in the previous experiment was around 18 times higher than the control after 16 hours of treatment with 1µM 3MC, whereas here the highest induction was around 8 times higher than control at 8-hour time point. Therefore, it could either be that the 16hour time point was optimal for Cyp1a1 promotor activation, but unfortunately it was not included in this experiment. Alternatively, the cells used for the time kinetic experiment gave overall lower signals and thus the experiment should be interpreted with caution. Therefore, the results of the qPCR of the time kinetics experiment, but not the luciferase data have been used to fit and optimize the values of the parameters used in the mathematical model to make it more reliable, i.e., to have a higher estimation accuracy. The mathematical modelling is performed in the group of Prof. Jan Hasenauer at the IRU Mathematics and life science.

5.3. Visualization of AhRR-Expressing Cell Subsets in Different Organs Under Steady-State Conditions

The AhR signaling pathway plays a role in various organs in the body, but AhRR expression is the highest in barrier organs in both healthy and diseased states. Therefore, its expression appears to be tightly controlled. It was once thought that AhRR solely represses AhR, but the literature showed that AhRR can also directly regulate cellular functions, e.g., immune responses (Vogel *et al.*, 2017). The cytochrome P450 (CYP) 1a1, CYP1a2, and CYP1b metabolize AhR ligands, thus curtailing the duration of AhR activation. In line with this notion, mice lacking all three CYP enzymes showed enhanced AhR activation (Nebert et al., 2004). Here we used mice lacking all AhR-dependent CYP-enzymes, to analyze the influence of enhanced AhR-activation on AhRR expression and the composition of immune cells in mice. We used naïve Triple CYP-KO AhRR^{E/E}

mice. The latter was generated from Triple-CYP KO mice (Dragin et al., 2008) which were crossed to AhRR^{E/E} mice that express EGFP under the control of the *Ahrr* promoter/enhancer elements and thus are AhRR-deficient. There were two aims of this study; first, to analyze if the enhanced ligand availability in the absence of *Cyp1a1*, *Cyp1a2*, and *Cyp1b1* would subsequently enhance AhR activation and therefore AhRR expression. Second, it was tested whether the absence of the three CYP enzymes or the additional deficiency of AhRR is sufficient to alter the composition of immune and non-immune cell subsets in different organs *in vivo*.

Peripheral organs of Triple CYP-KO AhRR^{+/+} and Triple CYP-KO AhRR^{E/E} were characterized by immunohistology and FACS analysis and compared to AhRR^{E/E} and WT mice. The organs used for this purpose were small intestine, gallbladder, gonadal fat (gWAT) stromal vascular fraction, liver, skin, and spleen. The AhRR expression and the frequencies of different cell subsets in each organ were examined and will be discussed separately in the following sub-sections.

5.3.1. AhRR expression and analysis of cell subsets in the small intestine

AhRR is expressed in the small intestines' lamina propria of both Triple CYP-KO AhRR^{E/E} and AhRR^{E/E} mice, albeit with a different expression level; AhRR expression is expressed in more cell types in Triple CYP-KO AhRR^{E/E} mice compared to AhRR^{E/E} mice. In AhRR^{E/E} mice, AhRR is expressed in the lamina propria of the intestinal villi as shown in Fig. 5.6. A, whereas in the Triple CYP-KO AhRR^{E/E} mice, AhRR is expressed additionally in the area surrounding the crypts and it extends to the muscularis mucosa (Fig. 5.6. B). The identity of these additional AhRR-expressing cells found in Triple CYP-KO AhRR^{E/E} mice were yet to be elucidated. However, based on their large size and appearance, they look more like stromal cells than immune cells. To identify these cells by means of immunofluorescence staining stromal cell markers were chosen for counterstaining the EGFP signal to differentiate e.g. endothelial cells, fibroblasts or intestinal stem cells. Among the first markers that were tested, stainings with a marker for vascular endothelial cells (CD31/PECAM) and a marker for lymphatic endothelial cells (LYVE-1) were carried out (Fig. 5.6). We could show that both, vascular and lymphatic endothelial cells are among the EGFP+ cells. Furthermore, the attempt to elucidate if the AhRR-expressing cells are fibroblasts was challenging, as fibroblasts are a highly heterogeneous population of cells. There are many combinations of markers that can help identifying fibroblasts, such as CD34, PDGFRα, and gp38 (podoplanin). On its own, each of these markers is also expressed on

multiple other cell types; CD34 is usually expressed on stem cells, fibroblasts, and telocytes. Telocytes are perceived as supporting cells that regulate the activity of tissue-resident stem cells. They play a role in shaping the microenvironment of stem cells and contribute to tissue renewal and repair (Rosa et al., 2021).

Also, the marker distribution of the latter cell population is still debatable, as two papers showed different definitions of telocytes; McCarthy et al. (McCarthy et al., 2020) showed that telocytes are CD34- PDGFRahi, but Kondo et al. (Kondo et al., 2019) showed that telocytes are CD34⁺ PDGFRα⁺ cells. Apart from being expressed by telocytes, PDGFRα is also expressed by intestinal fibroblasts (Muhl et al., 2022). It also plays a role in vessel formation (Santini et al., 2020) and intestinal epithelial growth during early development (Maimets et al., 2022). Lastly, gp38 can be expressed on lymphatic endothelial cells, myofibroblasts, and cells of the intestinal lamina propria. To identify the AhRR-expressing cells, a CD34/PDGFRα co-staining was used to identify fibroblasts (Fig. 5.6. E), whereas the combination of CD34/gp38 was used to identify intestinal stem cells (Fig. 5.6. F). Fig. **5.6**. E shows that AhRR expression mostly overlapped with either PDGFR α^+ or CD34⁺ cells but AhRR/EGFP⁺ cells did not co-express PDGFRα and CD34. These cells are probably CD34- telocytes, as they localized at the tip of the villi. Meanwhile, Fig. 5.6. F shows that AhRR/EGFP expression also mostly overlapped with gp38 expression, but not with CD34 expression, indicating that these AhRR/EGFP⁺ cells could also be fibroblasts or myofibroblasts. Further staining with α-SMA and PDGFRβ or other pericytes marker is necessary to properly identify myofibroblasts, as they are supposed to be α-SMA⁺ but PDGFRβ-. Besides, cells that co-express gp38 and CD34, but not AhRR could be identified. They are localized around the crypt areas, the niche of intestinal stem cells. Hence, it might be possible, that these gp38⁺ CD34⁺ cells are stem cells, but further staining with Lgr5 should be done to conclude this.

Based on these findings, however, there were still EGFP⁺ cells that were negative for all of these markers, which might be either immune cells (Brandstätter et al., 2016) or other stromal cell types. To identify AhRR-expressing immune cells, FACS analysis should be carried out, as AhRR is expressed by multiple cell subsets, e.g. intraepithelial lymphocytes (IELs) and type 3 innate lymphoid cells (ILC3) among others. It is also important to note that the only AhRR/EGFP signal found in the epithelial layer came from IEL and not from the epithelial cells themselves (Brandstätter et al., 2016). This is intriguing, as epithelial cells as the first layer are highly exposed to AhR ligands in the intestinal lumen, particularly in

the proximal SI, and AhR expression is also highest in this area (Ireland et al., 2004; Stockinger et al., 2021).

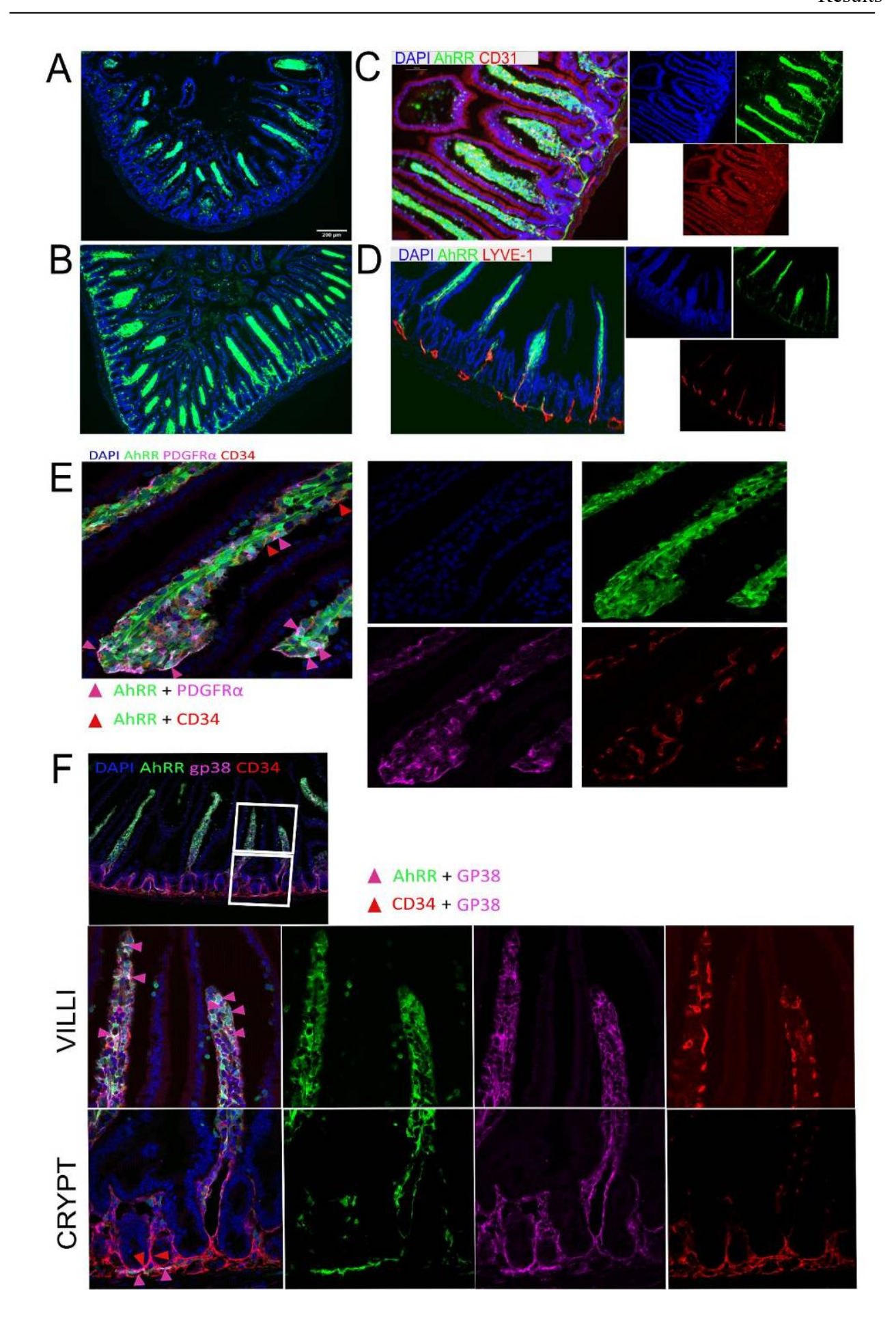


Fig. 5.6. Enhanced AhRR/EGFP Expression in the Small Intestine of Triple CYP-KO AhRR^{E/E} mice. Expression of AhRR/EGFP in cryosections of the small intestine of A) AHRR^{E/E} and B) Triple CYP-KO AhRR^{E/E} under physiological conditions. Images C-F) are taken from the small intestine of Triple CYP-KO AhRR^{E/E} mice. C) and D) depict co-localization of AhRR/EGFP with markers of vascular endothelial cells (CD31) and lymphatic endothelial cells (LYVE-1). E) depicts co-localization of AhRR with CD34 and PDGFRα, whereas F) depicts co-localization of AhRR with CD34 and gp38 (podoplanin). Images A and B are taken at 10x magnification, whereas C and D were taken at 20x magnification. Images A-D were taken with a Keyence 9000 epifluorescent microscope. E and F were taken at 40x magnification with a Zeiss LSM Airyscan 800 confocal microscope. Scale bar = 200 μm.

5.3.2. AhRR expression and analysis of cell subsets in the skin

Similar to the small intestine, AhRR is expressed in the skin of both Triple CYP-KO AhRR^{E/E} and AhRR^{E/E} mice. Also here, AhRR/EGFP expression was found in additional cell types in Triple CYP-KO AhRR^{E/E} mice compared to AhRR^{E/E} mice. As for the intestine, the identity of these cells was further elucidated by means of flow cytometry and immunohistology. Based on the histological analysis, AhRR/EGFP expression in the epidermis was not as strong as in the dermis. In the dermis, AhRR was expressed mostly in the papillary dermis in AhRR^{E/E} mice (Fig. 5.7. A), whereas in Triple CYP-KO AhRR^{E/E} mice, AhRR expression was not only stronger in both epidermis and papillary dermis, but even extended to the reticular dermis (Fig. 5.7. B). At this point, it was not clear if these EGFP⁺ cells were primarily immune cells or a mixture of immune and stromal cells and/or vascular cells. Further histologic analyses with more markers were conducted to determine the identity of the cells. Furthermore, flow cytometry analysis was conducted to investigate which immune cell populations express AhRR/EGFP. Skin myeloid and lymphocyte subsets were gated based on the strategy depicted in Fig. 5.8. For the myeloid subsets, cDC and monocyte-derived cells were gated with separate gating strategies. Following the exclusion of debris, dead cells, and doublets, cDC1 and cDC2 cells were gated by their expression of CD24 and CD11b; cDC1 cells were identified as CD24⁺ CD11b⁻, whereas cDC2 cells were identified as CD24⁻ CD11b⁺ Ly6C⁻ CD64⁻ cells. Langerhans cells were identified as CD24⁺ CD11b⁺ cells (Fig. 5.8 A). Monocyte-derived cells were identified as CD24⁻ CD11b⁺ Ly6C^{hi/int} CD64^{int/-} and the CD64int cells and were further divided based on the expression of CCR2 (Fig. 5.8 B). Skin lymphocytes could be divided into three main subsets, which were the TCRβ⁺ conventional T cells, TCRγδ^{int} dermal γδ T cells, and TCR $\gamma\delta^{hi}$ DETC (**Fig. 5.8 C**).

There were no significant differences between the genotypes in the frequencies of total Langerhans, cDC1, monocyte-derived cells (both CCR2⁺ and CCR2⁻) (**Fig. 5.9 A**). In these subsets, large variations in the single data sets were observed and this was particularly

observed in the frequencies of the CCR2⁺ and CCR2⁻ monocyte subsets. In contrast, significant differences were observed in the proportions of cDC2. The frequency of cDC2 (**Fig. 5.9 A**) was significantly higher in Triple CYP AhRR^{E/E} mice compared to WT mice but cDC2 were not altered either in AhRR^{E/E} mice nor in Triple CYP AhRR^{+/+} mice. This suggests that the increase in cDC2 frequency occurred only when both, AhRR and Triple CYP enzymes were missing and that the absence of either AhRR or the Triple CYP enzymes alone did not increase the cDC2 frequencies.

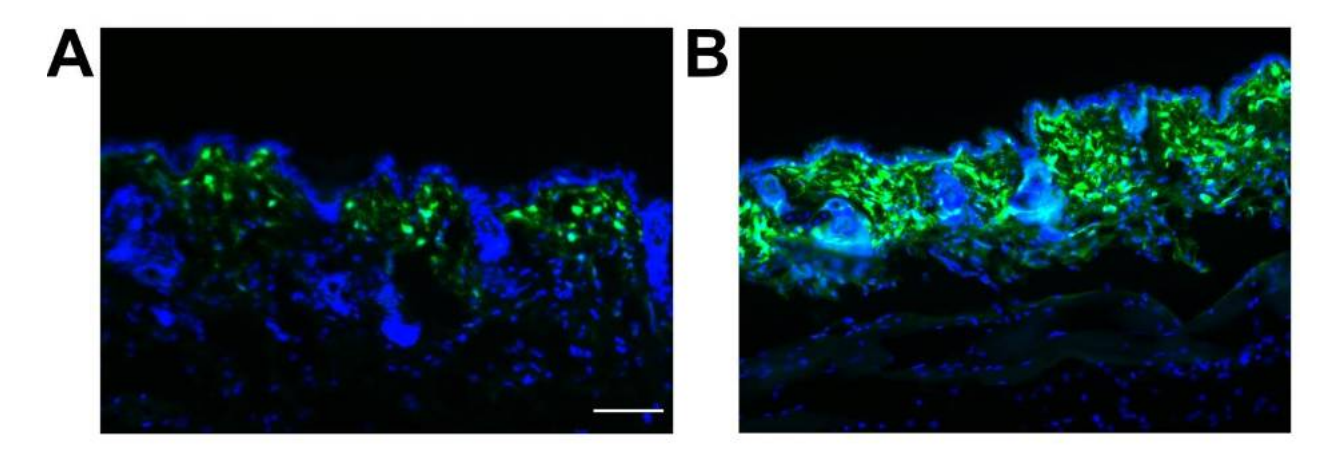


Fig. 5.7. Enhanced AhRR/EGFP expression in the back skin of Triple CYP-KO AhRR^{E/E} mice on a histological level. EGFP-expressing cells mark AhRR expression in the back skin A) of AhRR^{E/E} and B) Triple CYP-KO AhRR^{E/E} mice. Exemplary sections were shown. Images were taken at 20x magnification. Scale bar = 100μ m.

Overall, the histology and FACS analyses were in line, as the latter also showed a higher expression of AhRR in the total living cells of Triple CYP-KO AhRR^{E/E} mice compared to AhRR^{E/E} mice (**Fig. 5.9 B**), with approximately 9 times more AhRR/EGFP⁺ cells per total living cells. In the myeloid cell compartment, around 60% of Langerhans cells expressed AhRR in Triple CYP AhRR^{E/E} mice, whereas only 42% of them expressed AhRR in AhRR^{E/E} mice (**Fig. 5.9 C**). In the two DC subsets, AhRR was more predominantly expressed by cDC2 than by the cDC1 subset. Around 60% of cDC2 cells expressed AhRR in Triple CYP AhRR^{E/E} mice, whereas only 20% of them expressed it in AhRR^{E/E} mice. In the cDC1 subset, AhRR expression was only observed in Triple CYP AhRR^{E/E} mice, but not in AhRR^{E/E} mice; about 20% of cDC1 expressed AhRR in the Triple CYP AhRR^{E/E} mice (**Fig. 5.9 C**). Moreover, the frequency of AhRR-expressing cells in the total monocyte-derived cells was similar to that of the cDC2 subset; around 60% and 18% of monocyte-derived cells expressed AhRR in the Triple CYP AhRR^{E/E} mice, respectively. Consequently, the frequency of AhRR-expressing cells in the two monocyte-derived subsets (CCR2⁺ and CCR2⁻) was also mirrored to the one of the parent populations.

A. SKIN - DC & LANGERHANS GATING

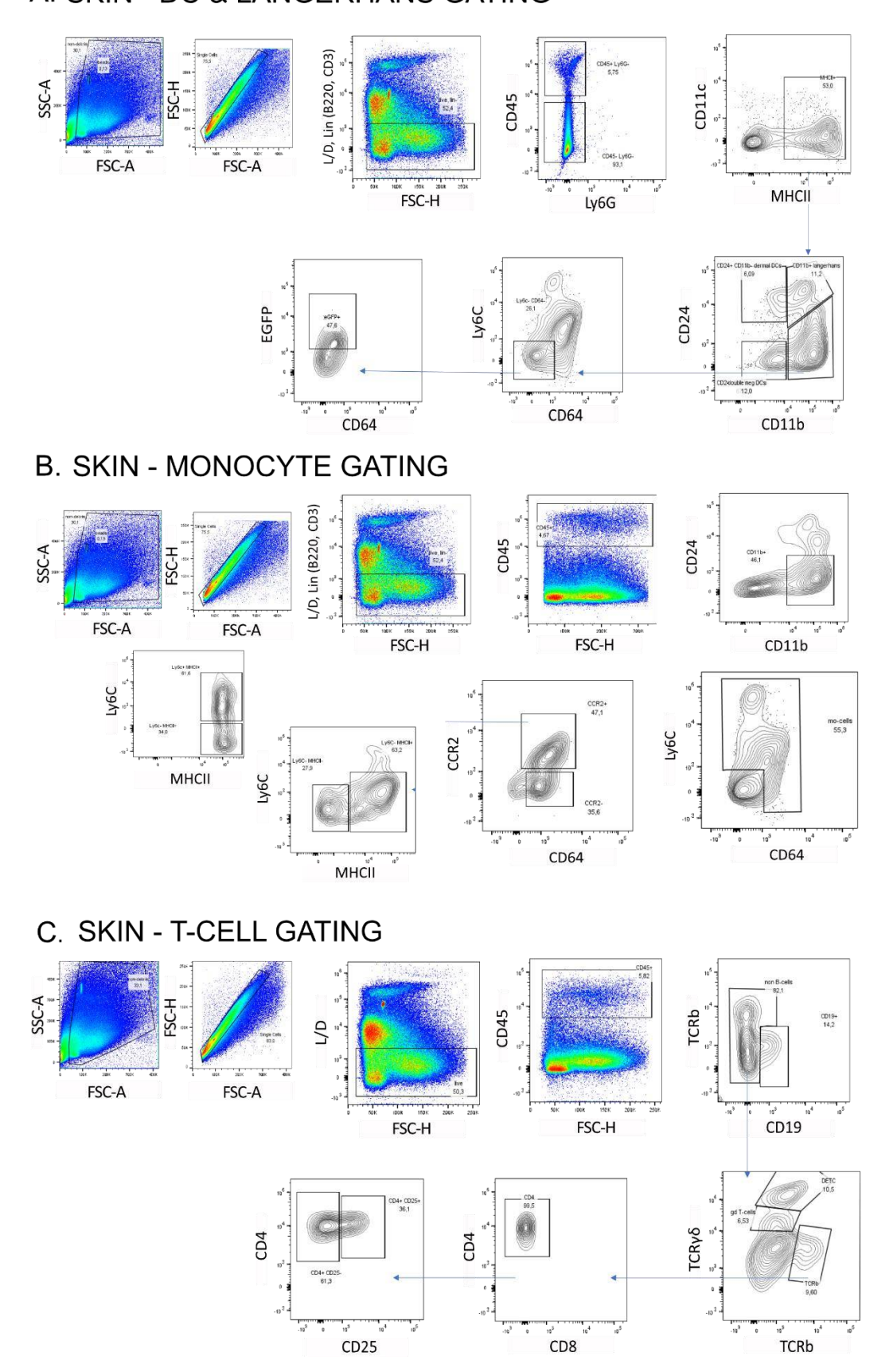


Fig. 5.8. Gating strategies for myeloid and lymphocytes subsets in the ear skin. Cells were gated for living single CD45⁺ cells. A) cDC1 cells were identified as CD24⁺ CD11b-, whereas cDC2 cells were identified as CD24⁻ CD11b⁺ Ly6C⁻ CD64- cells. Langerhans cells were identified as CD24⁺ CD11b⁺ cells. B) Monocyte-

derived cells were identified as CD24- CD11b⁺ Ly6C^{hi/int} CD64^{int/-} and the CD64^{int} cells were further divided based on the expression of CCR2. C) T cell subsets were divided into $TCR\beta^+$ conventional T cells, $TCR\gamma\delta^{int}$ dermal $TCR\gamma\delta^+$ cells, and $TCR\gamma\delta^{hi}$ DETC.

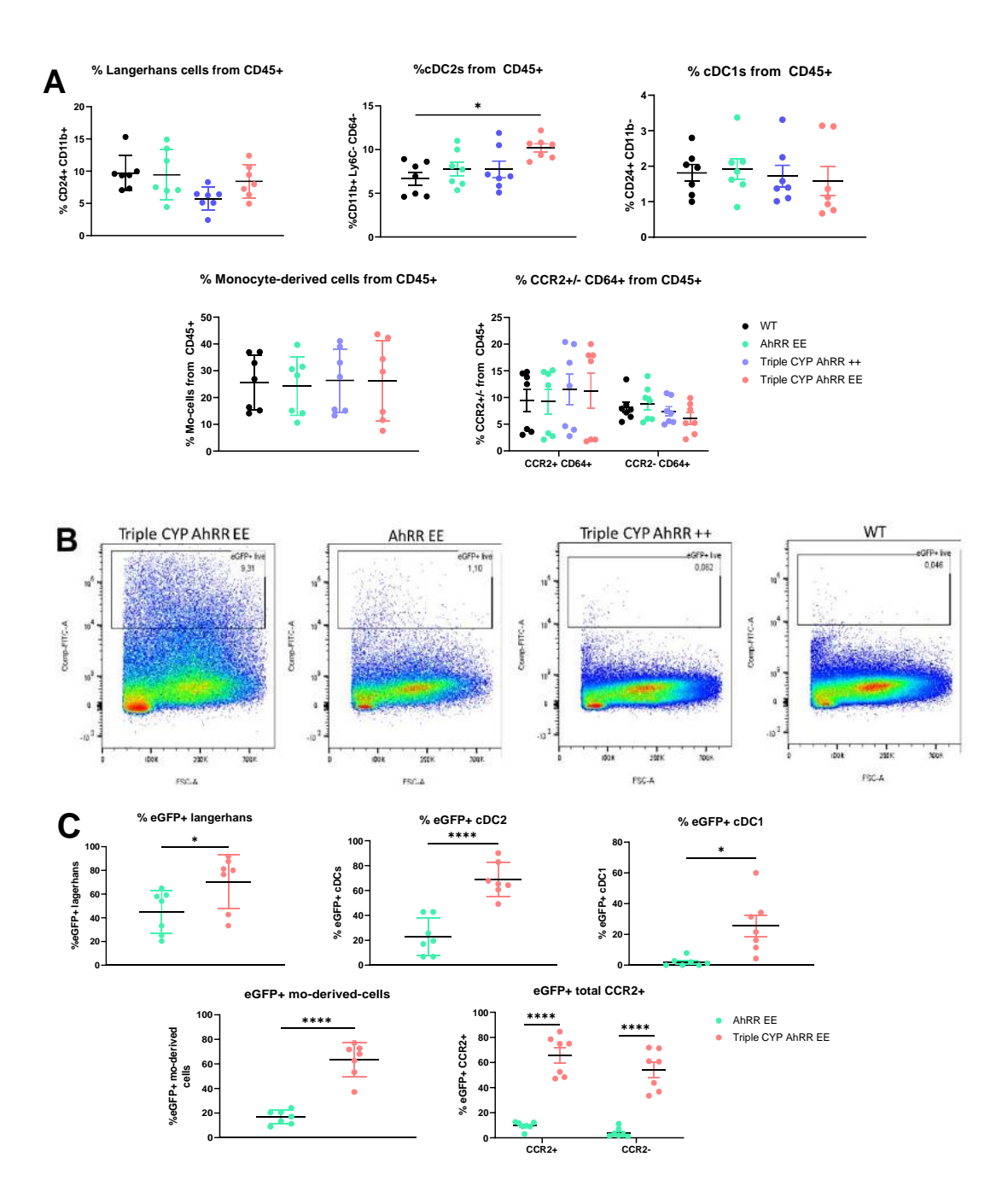


Fig. 5.9. Elevated cDC2 frequency and AhRR/EGFP expression in all myeloid subsets in the skin of Triple CYP AhRR^{E/E} mice. Skin cells were isolated from the ear skin of 8-week old naïve mice. They were stained for Langerhans cells, cDC2, cDC1, total monocyte-derived cells, and CCR2^{+/-} CD64⁺ cells and analyzed by flow cytometry. A) The frequencies of myeloid cells, B) AhRR/EGFP expression in total living cells and C) AhRR/EGFP expression in each of the cell subsets were quantified. Percentages of EGFP⁺ cells were calculated from the total cell number of each subset. Results are shown as mean ± SEM and significance was analyzed by either one-way ANOVA corrected for multiple comparisons by the Bonferroni's method (frequencies of cell subsets) or simple paired t-test (frequencies of EGFP⁺ cells). * p<0,05, ** p<0,01, **** p<0,0001. Data was pooled from three independent experiments (n = 7) of ear skin of Triple CYP AhRR^{E/E}, AhRR^{E/E}, Triple CYP AhRR^{+/+}, and WT mice.

Regarding the frequencies of the lymphocytes, CD4⁺ T cells (**Fig. 5.10 A**) were significantly increased in Triple CYP AhRR^{E/E} mice by ~4% compared to WT mice, while AhRR^{E/E} and Triple CYP AhRR^{+/+} mice showed unaltered frequencies. It is also important to mention that in the skin most of the TCR β ⁺ cells were CD4⁺ T cells. AhRR^{E/E} mice, however, had a significantly higher frequency (~2% of total CD45⁺ cells) of dermal TCR γ δ cells compared to WT mice. Moreover, a slight decrease, instead of an increase was observed in Triple CYP-KO AhRR^{E/E} mice. In contrast to the aforementioned cell subsets, epidermal γ δ T cells (DETC) were reduced roughly from 6% to 2% in Triple CYP AhRR^{E/E} and AhRR^{E/E} mice (**Fig. 5.10 A**), suggesting that this effect was mediated by the deficiency of AhRR and not by the CYP enzymes. Nevertheless, it has yet to be elucidated if this is caused by impaired proliferation or impaired seeding of DETC precursors in the skin that takes place during day 14-18 of gestation (Havran & Allison, 1990).

In general, AhRR/EGFP expression was more pronounced in myeloid cells than in lymphocytes. In the lymphocyte subsets, AhRR/EGFP was barely expressed in CD4⁺ T- cells in AhRR^{E/E} mice, but almost 25% of CD4⁺ T cells in Triple CYP AhRR^{E/E} mice expressed AhRR (**Fig. 5.10 B**). Compared to conventional CD4⁺ T cells, the AhRR expression in the two $\gamma\delta$ T cells subsets (epidermal TCR $\gamma\delta^{hi}$ DETC and dermal TCR $\gamma\delta^{int}$ cells) was higher in both AhRR^{E/E} and Triple CYP AhRR^{E/E} mice. AhRR was expressed by 17% and 30% of dermal TCR $\gamma\delta^{+}$ cells in AhRR^{E/E} and Triple CYP AhRR^{E/E} mice, respectively (**Fig. 5.10 B**). Interestingly, the frequencies of AhRR-expressing DETC in AhRR^{E/E} and Triple CYP AhRR^{E/E} mice were comparable, around 60% and 65%, respectively.

In line with the FACS data, immunofluorescent staining also showed that most of the AhRR-expressing cells, both in the epidermis and dermis are CD45⁺ immune cells (**Fig. 5.11 A**). In **Fig. 5.11 B** it was shown that some of the epidermal immune cells express TCR $\gamma\delta$, thus they were DETC. To determine, if the proliferation of DETC is affected by AhRR and/or the deficiency of the three AhR-dependent CYP enzymes, cryosections of back skin obtained from 8-week mice were co-stained with Ki67 and TCR $\gamma\delta$ antibodies. Initially it was planned to quantify the total TCR $\gamma\delta$ cells and the double positive cells in the epidermis, but only very few Ki67⁺ TCR $\gamma\delta$ ⁺ cells (around 0-3 cells/image) could be detected (**Fig. 5.11 C**). This might be due to the fact that in mice older than 4 weeks, the DETC frequency is maintained at ~5–8% of all epidermal cells (Kadow et al., 2011) and these cells might not be proliferative in adult mice. Next, proliferating DETC from mice were quantified at post-natal day 2, a time point where DETCs are still actively proliferating. Here, epidermal cell suspensions were analyzed by flow cytometry.

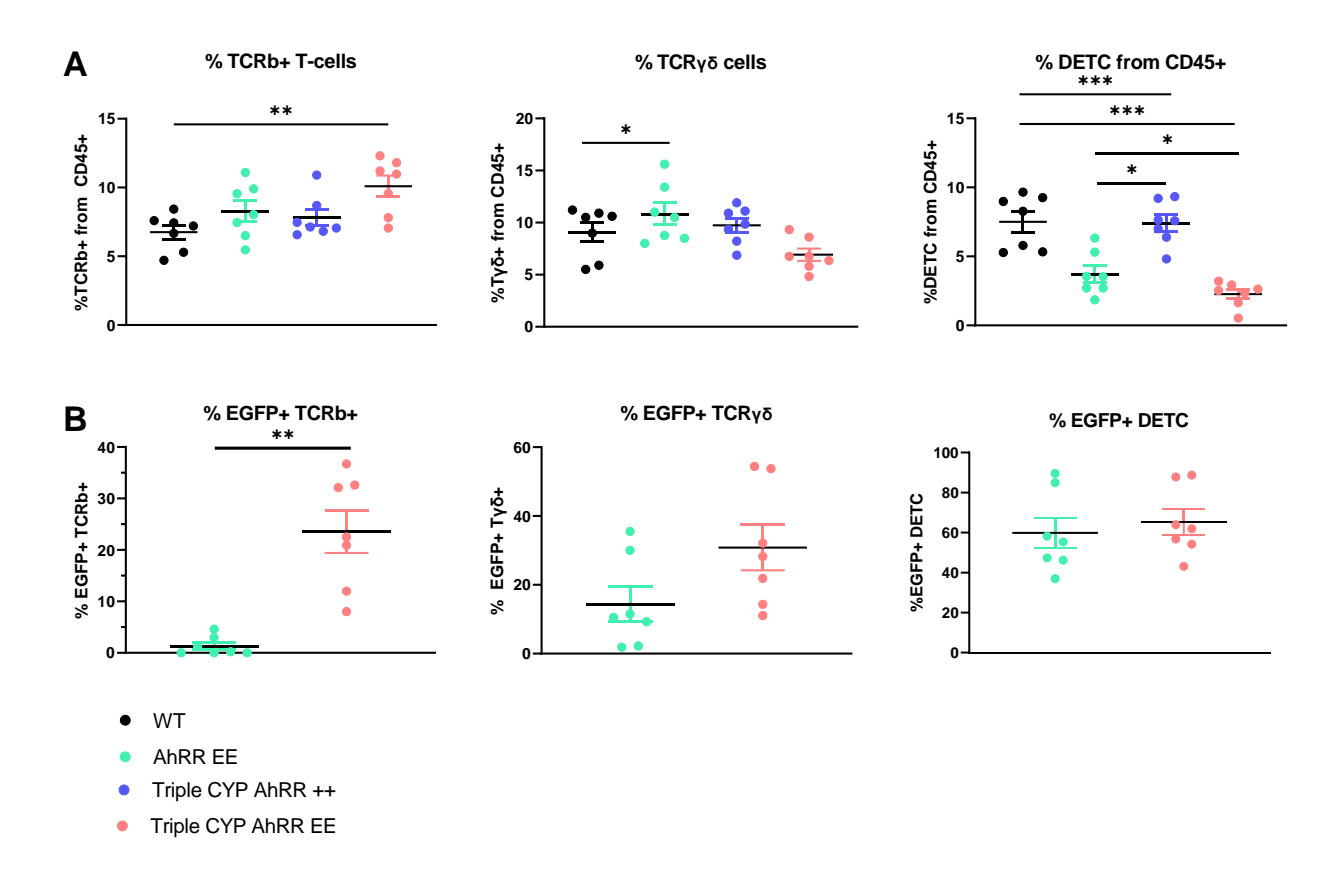


Fig. 5.10 Ablation of AhRR reduces the frequency of DETC. T cell subsets from 8-week naïve mice and the AhRR/EGFP⁺ expression in each subset was analyzed by flow cytometry. The frequencies of A) $TCR\beta^+$ T cells, dermal $TCR\gamma\delta$, and DETC, as well as B) the AhRR/EGFP⁺ were quantified. Percentages of EGFP⁺ cells were calculated from the total of each myeloid subset. Results are shown as mean ± SEM and significance was analyzed by either one-way ANOVA corrected for multiple comparisons by the Bonferroni's method (for the cell subset frequencies) or simple paired t-test (for the EGFP⁺ cells frequencies). * p<0,05, ** p<0,01, *** p<0,001. Data was pooled from three independent experiments (n = 7).

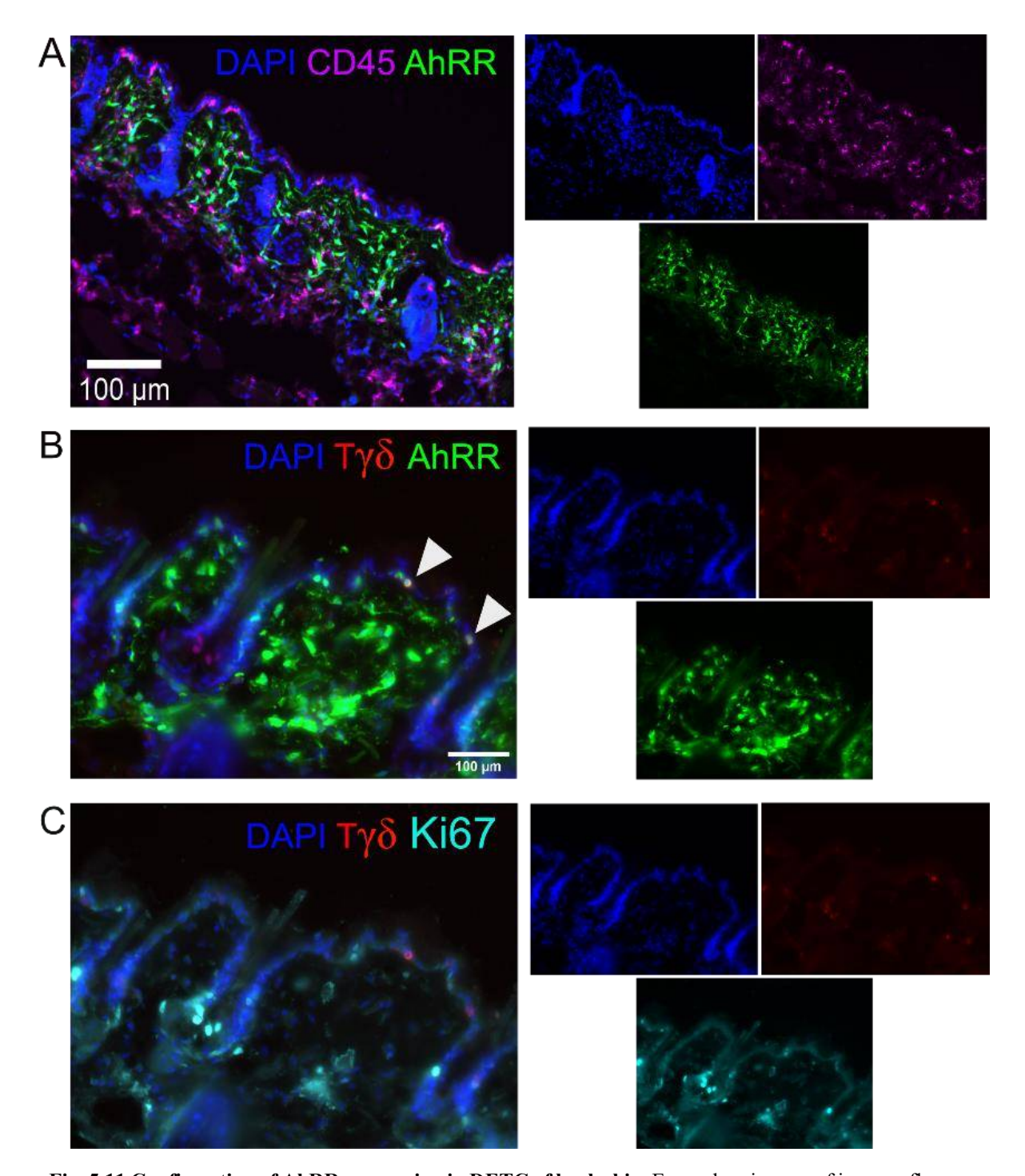


Fig. 5.11 Confirmation of AhRR-expression in DETC of back skin. Exemplary images of immunofluorescence stainings of A) anti-CD45, white arrows show co-localization of AhRR and CD45. B) anti-TCR $\gamma\delta$, white arrows show co-localization of AhRR and TCR $\gamma\delta$, C) no co-localization between Ki67 and TCR $\gamma\delta$ was observed. Image A) and C) were taken at 20x and B) was taken at 40x.Scale bar = 100 μ m.

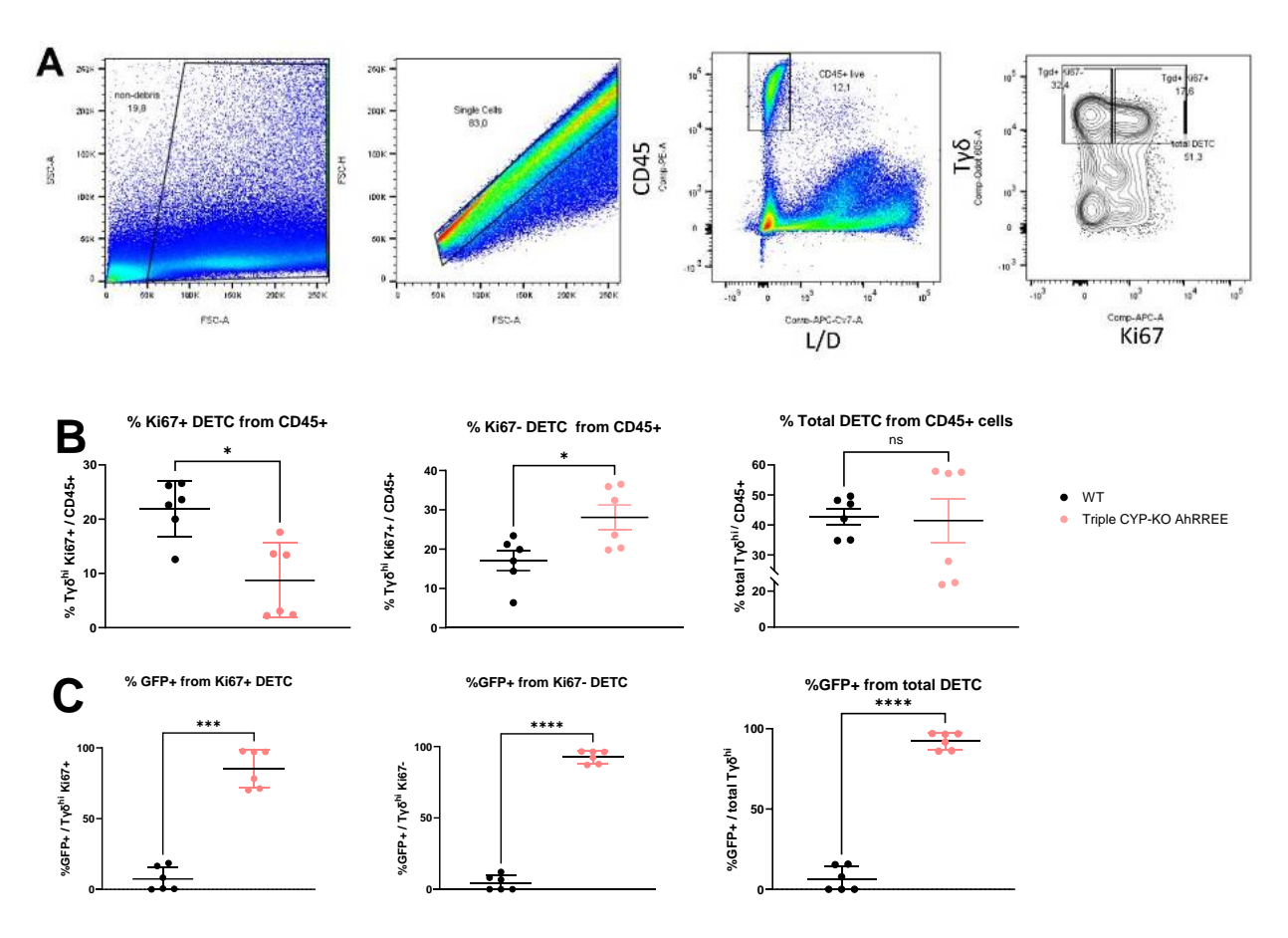


Fig. 5.12 Ablation of the three AhR-dependent CYP enzymes and AhRR reduced the frequency of proliferating DETC in mice on post-natal day 2. A) Gating strategy of Ki67⁺ proliferating and Ki67⁻ non-proliferating $T\gamma\delta^{hi}$ DETC in the whole-body-skin of post-natal day 2 mice. B) Frequencies of proliferating, non-proliferating, and total DETC were determined by flow cytometry. Results are shown as mean ± SEM and significance was analyzed by simple paired t-test. C) AhRR/EGFP⁺ expression in the proliferating, non-proliferating, and total DETC, respectively. * p<0,5*, **** p<0,001. ***** P ≤ 0,0001. N= 5. Data was pooled from two independent experiments (n = 6).

Prior to quantifying the proliferating DETC in neonatal mice, a suitable time point needed to be determined. According to Kadow et al. (Kadow et al., 2011), the most ideal time point to analyze proliferating DETC is at post-natal day 14 (p14), the time point where DETC proliferation peaked in WT mice, and proliferation was already declining in AhR-KO mice. However, the hair-growth cycle at p14 is at the late anagen, in which the morphogenesis of hair follicles is highly active (Lin et al., 2004). This made it difficult to efficiently remove the epidermis from the dermis. Therefore, I chose post-natal day 2 (p2) mice instead, since the hair-growth cycle is still at early anagen phase, which led to an easy and reproducible isolation of epidermal tissue from the whole body (except limbs and tails) of the mice. For this experiment, only WT and Triple CYP AhRR^{E/E} mice were used, as the mice from the other two genotypes did not yield progeny in a timely manner. FACS analysis was conducted to quantify the proliferating DETC and the gating strategy is shown in Fig. 5.12 A. Significantly more proliferating DETC could be detected at p2 compared to adult mice. Of note, a lower number of non-proliferating DETC were detected in WT mice

compared to Triple CYP AhRR^{E/E} mice (**Fig. 5.12** B), although the frequencies of total DETC between the two genotypes were comparable. Moreover, the AhRR expression in DETC in Triple CYP AhRR^{E/E} mice at p2 was higher than the one in adult 8-week mice (**Fig. 5.12** C) since almost 100% of DETC, both proliferating and non-proliferating, expressed AhRR in p2 mice.

In conclusion, deficiency of both, the AhRR and the three AhR-dependent CYP enzymes caused an increase in the frequencies of cDC2 and CD4⁺ T cells, but the absence of AhRR alone was enough to reduce the frequency of epidermal TCR $\gamma\delta^{hi}$ DETC. In contrast, for dermal TCR $\gamma\delta^{int}$ cells, the absence of AhRR led to different outcomes; AhRR deficiency alone increased the cell frequency but the deficiencies of both AhRR and the three CYP enzymes decreased the cell frequency. Moreover, the ablation of both AhRR and the three AhR-dependent CYP enzymes significantly reduced the frequency of proliferating DETC in p2 mice.

5.3.3. AhRR expression and analysis of cell subsets in the liver

Interestingly, an AhRR/EGFP signal has not been detected in the liver of AhRR^{E/E} mice (Brandstätter et al., 2016), despite the high level of AhR expression in this organ (Esser and Rannug, 2015). This finding also holds true when cryosections of the liver of AhRR^{E/E} mice were analyzed in this thesis (Fig. 5.13 A). Remarkably, AhRR/EGFP expressing cells could be detected in Triple CYP AhRR^{E/E} mice (Fig. 5.13 B). In liver, CYP1A1 and CYP1A2 are constitutively expressed, but the former is more highly expressed than the latter (Klomp et al., 2020), whereas the constitutive expression of CYP1B1 is more limited (Falero-Perez et al., 2018). Hence, the lack of the three AhR-dependent CYP enzymes combined with the lack of the AhRR probably increased the ligands bioavailability to a certain level that was sufficient to prolong or enhance the activation of AhR thus enabling hepatic AhRR expression. Additional histological analysis (Fig. 5.13 B, D, and E) showed, however, that the AhRR was not localized in hepatocytes, but rather in the vicinity of the surrounding vessels. Therefore, immunofluorescent staining with the markers of blood and lymph vessels, CD31 and LYVE-1, respectively, was conducted. Nevertheless, there was only a minimal colocalization between AhRR and these two vessel markers (Fig. 5.13 D), since some of the EGFP⁺ cells overlapped with CD31⁺ cells, but not with LYVE-1⁺ cells.

To identify the cells that were neither CD31⁺ nor LYVE1⁺, liver cryosections were also stained with F4/80 and Tim4 antibodies to assess if AhRR/EGFP expression colocalized with perivascular macrophages and/or Kupffer cells (KC). Because the AhRR is highly expressed in myeloid cells and due to the presence of AhRR/EGFP⁺ cells surrounding the vessels, these

AhRR-expressing cells could be perivascular macrophages. As KC are the most predominant myeloid cell type in the liver under physiological conditions, it also could not be excluded that the AhRR-expressing cells were KC. Sections were stained with antibodies against F4/80 and Tim4. Perivascular macrophages are F4/80⁺ Tim4⁻, whereas KC are F4/80⁺ Tim4⁺. However, the immunostaining showed no overlap of F4/80 and Tim4 staining with AhRR/EGFP, indicating that the AhRR-expressing cells were neither KC nor perivascular macrophages. Furthermore, an overlapping expression of F4/80 and Tim4 was observed in most of the F4/80⁺ cells (**Fig. 5.13 D**). To elucidate the identity of the EGFP⁺ cells in liver, we collaborated with Prof. Andreas Schlitzer and Dr. David Bejarano, who performed spatial proteomics using the PhenocyclerTM system on liver tissues (Bayerl et al., 2023). The results demonstrated that most of the EGFP⁺ signals derived from the CD45- compartment (**Fig. 5.13 E**). Out of the CD45⁻ subset, the EGFP⁺ cells co-localized with CD73 (ecto-5'-nucleotidase) in both central veins (CV) and portal veins (PV) and not with CD31/PECAM, SMA, or EPCAM (**Fig. 5.13 F**). These EGFP+ cells predominantly localized near the central, rather than the portal veins and they are likely to be hepatic stellate cells.

For the quantification of hepatic immune cell subsets, flow cytometry analysis was conducted, and the gating strategy is shown in Fig. 5.14. FACS analysis of the liver turned out to be challenging, due to high autofluorescence signals in several channels, including the live/dead channel, which made it hard to strictly exclude the dead cells. This could be attributed either to autofluorescence that might arise from erythrocytes or LSEC, or by phagocytosis of the live/dead marker by macrophages or to cell death during the processing of the samples. Nevertheless, the myeloid subset was first gated as cells lacking CD19 and NK1.1 expression. Then, KC were identified as CD11bint F4/80hi Tim4+ cells and cDCs were identified as Ly6lo MHCII+ CD11chi cells. The two cDC subsets were distinguished by the expression of either XCR1 (cDC1) or CD172a (cDC2). For the lymphocyte subset, T cells were identified as TCRβ⁺ NK1.1⁻ cells, whereas NKT cells were TCR β^+ NK1.1⁺. In **Fig. 5.14**, it can also be seen that most of the F4/80^{hi} cells were also Tim4⁺, which supported the histology result shown in Fig. 5.13 D. In addition, there was a tendency that both Triple CYP-KO $AhRR^{+\!/\!+}$ and Triple CYP-KO $AhRR^{E\!/\!E}$ mice had less Tim4⁺ F4/80⁺ KC than AhRR^{E/E} and WT mice (Fig. 5.15 A). This effect was therefore mediated by the absence of the three AhR-dependent CYP enzymes, rather than absence of AhRR. Frequencies of both cDC1 and cDC2 subsets appeared to be very low (Fig. 5.15 B) and were comparable in WT, Triple CYP-KO AhRR+/+ and Triple CYP-KO AhRRE/E mice. Although the frequencies were very low, AhRR^{E/E} mice had the highest cDC2 percentage compared to the

other mouse lines analyzed. Here, the difference was significantly higher compared to WT mice. For $TCR\beta^+$ T cells, NK-, and NKT cells subsets, there were no differences in their frequencies across all genotypes (**Fig. 5.15** C).

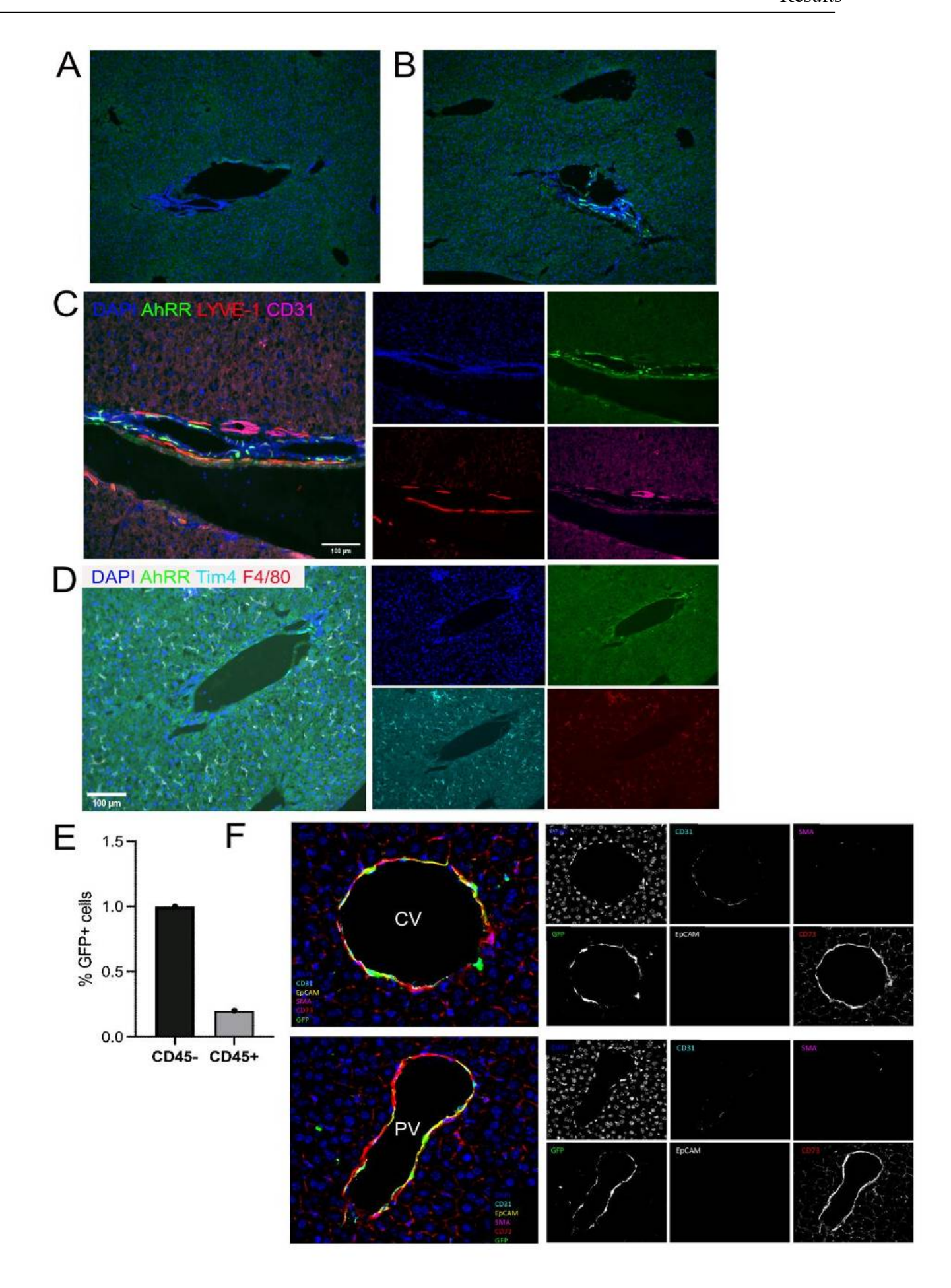


Fig. 5.13 AhRR/EGFP expression in the liver is observed in Triple CYP-KO AhRR^{E/E} but not AhRR^{E/E} mice in histological sections. Expression of AhRR/EGFP in. A) AhRR^{E/E} and B) Triple CYP-KO AhRR^{E/E} mice. Immunofluorescence staining of liver cryosections counterstained for C) CD31 and LYVE-1, D) Tim4 and F4/80. E) Percentage of EGFP+ CD45- and CD45+ cells quantified by spatial proteomics. F) EGFP+ cells co-localized with CD73 in central veins (CV) and portal veins (PV), but not with CD31, EpCAM, and SMA. All Images were taken at 20x magnification and scale bar = $100\mu m$.Images in A-D were taken with Keyence BZ-9000 and Images in F were taken with Zeiss Axio Observer.

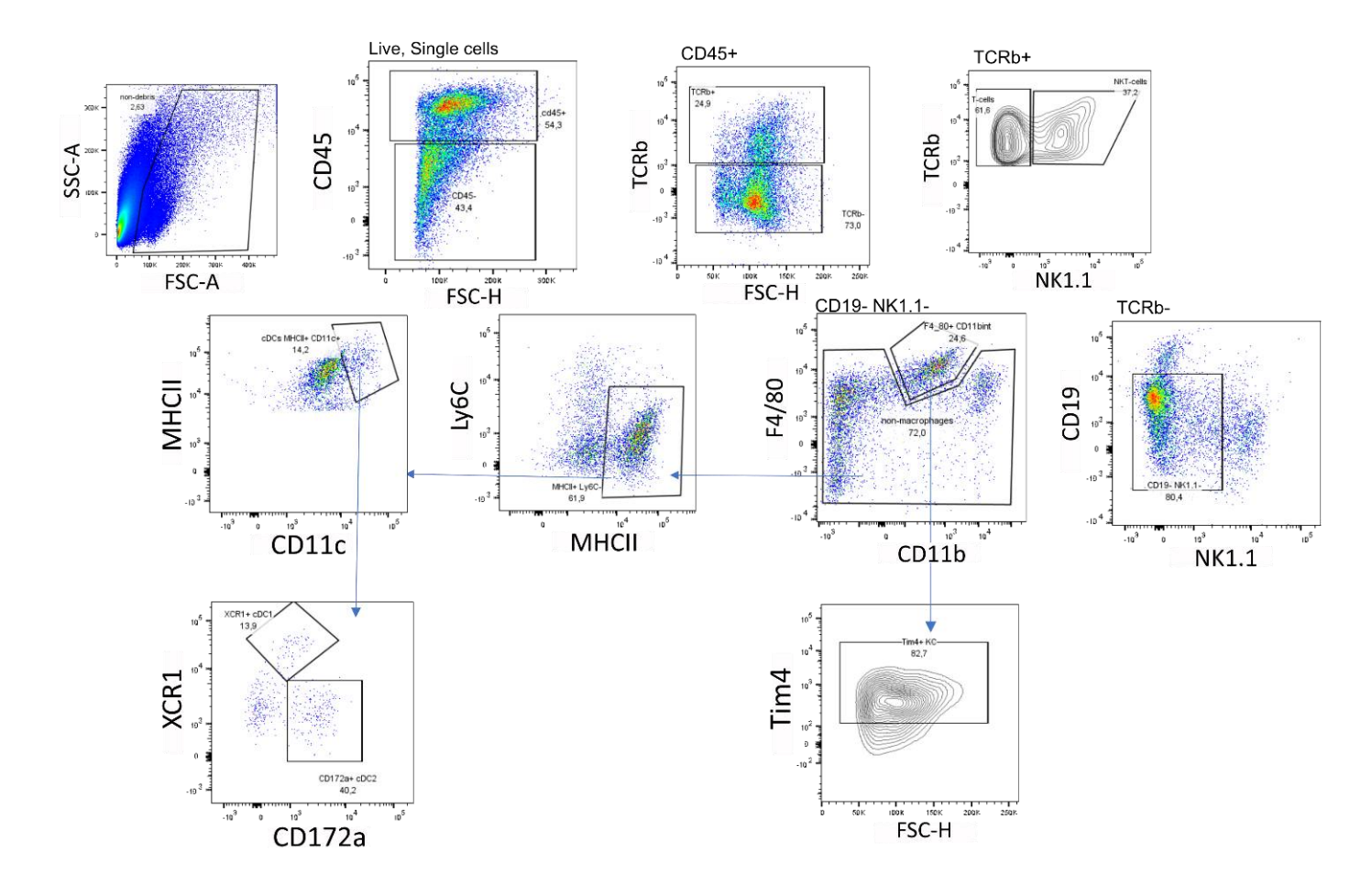


Fig. 5.14 Gating strategies for myeloid and lymphocyte subsets in the liver. Cells were gated for living single CD45⁺ cells. T cells were identified as $TCR\beta^+$ NK1.1⁻ cells, whereas NKT cells were $TCR\beta^+$ NK1.1⁺ cells. KC were identified as $CD11b^{int}$ F4/80^{hi} Tim4⁺ and cDCs were identified as $Ly6^{lo}$ MHCII⁺ CD11chi. The two cDC subsets were distinguished by the expression of XCR1 (cDC1) or CD172a (cDC2).

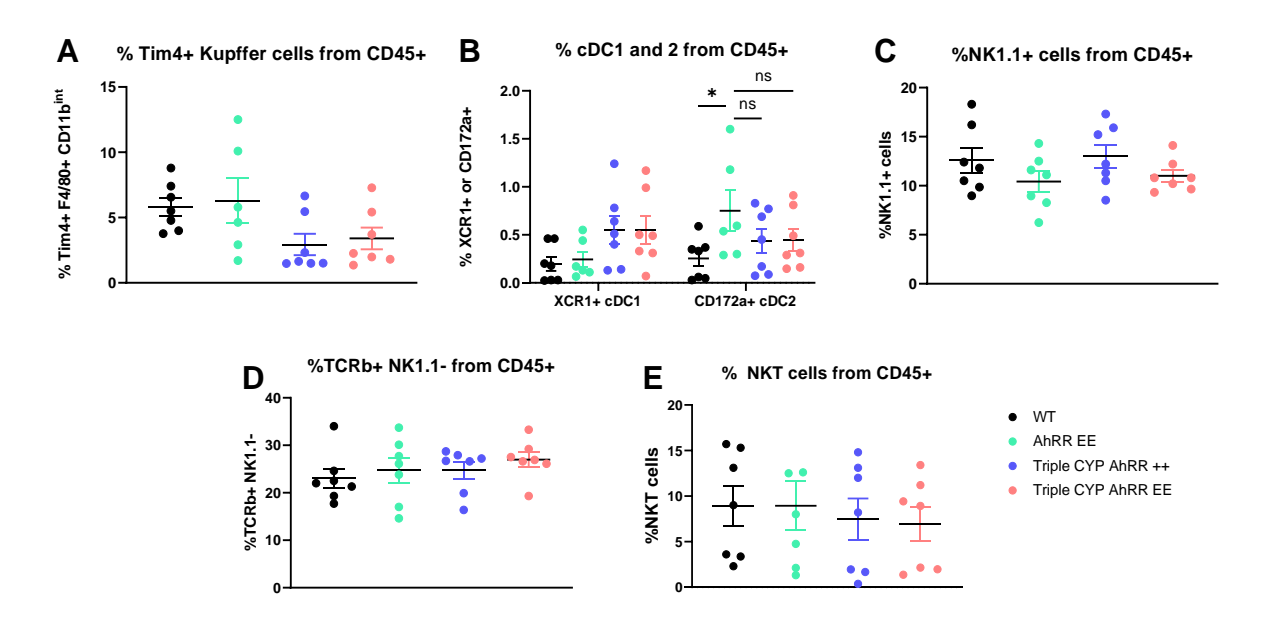


Fig. 5.15 Ablation of AhRR or the three AhR-dependent CYP enzymes did not cause significant differences in lymphocyte and myeloid subsets. KC, cDC1 & cDC2, NK, T cells, and NK1 cells were isolated from 8-week naïve mice and were analyzed by means of flow cytometry. The frequencies of myeloid cells were quantified. Results are shown as mean \pm SEM and significance was analyzed by one-way ANOVA corrected for multiple comparisons by the Bonferroni's method. * p<0,5. Data was pooled from three independent experiments (N = 7).

AhRR/EGFP expression was also monitored by flow cytometry and was only detected in the Triple CYP-KO AhRR^{E/E} mice and even in these mice, only ~2% of total living cells expressed the AhRR (Fig. 5.16 A), which is in line with the histology result shown in Fig. 5.13 A and B. The results obtained by FACS analysis did not fully correspond to the histology results, as CD45 stromal cells did not express AhRR/EGFP in either Triple CYP-KO AhRR^{E/E} or AhRR^{E/E} mice (Fig. 5.16 B). This could be due to a loss of certain CD45⁻ cells during organ processing and digestion. Surprisingly, a small fraction of CD45⁺ cells expressed AhRR and these were TCRβ⁺ and NK1.1⁺ cells rather than DC or macrophages in Triple CYP-KO AhRR^{E/E} mice (Fig. 5.16 C and D). Based on the literature, these TCRβ⁺ cells could be conventional T cells or natural killer T cells (NKT cells) that express semi-invariant TCRαβ chains and NK1.1 (Hua et al., 2011). Only 2% of the TCRβ⁺ NK1.1⁻ subset and around 12% of NK1.1⁺ in the Triple CYP-KO AhRR^{E/E} mice expressed AhRR (Fig. 5.16 C and D). Interestingly, even though in the histologic evaluation no EGFP expression in AhRR^{E/E} mice could be detected, the FACS analysis showed that there were some EGFP⁺ expressing cells present, as ~1% of TCRβ⁺ NK1.1⁻ cells and 6% of NK1.1+ NK cells expressed AhRR/EGFP. One reason that may account for this discrepancy might be that all five lobes were used for FACS analysis and only one liver lobe was analyzed for histology. But also technical reasons may have caused the

discrepancy as FACS is a more sensitive method to detect the EGFP signal, or the cytoplasmic EGFP signal might have been lost during fixation for histology.

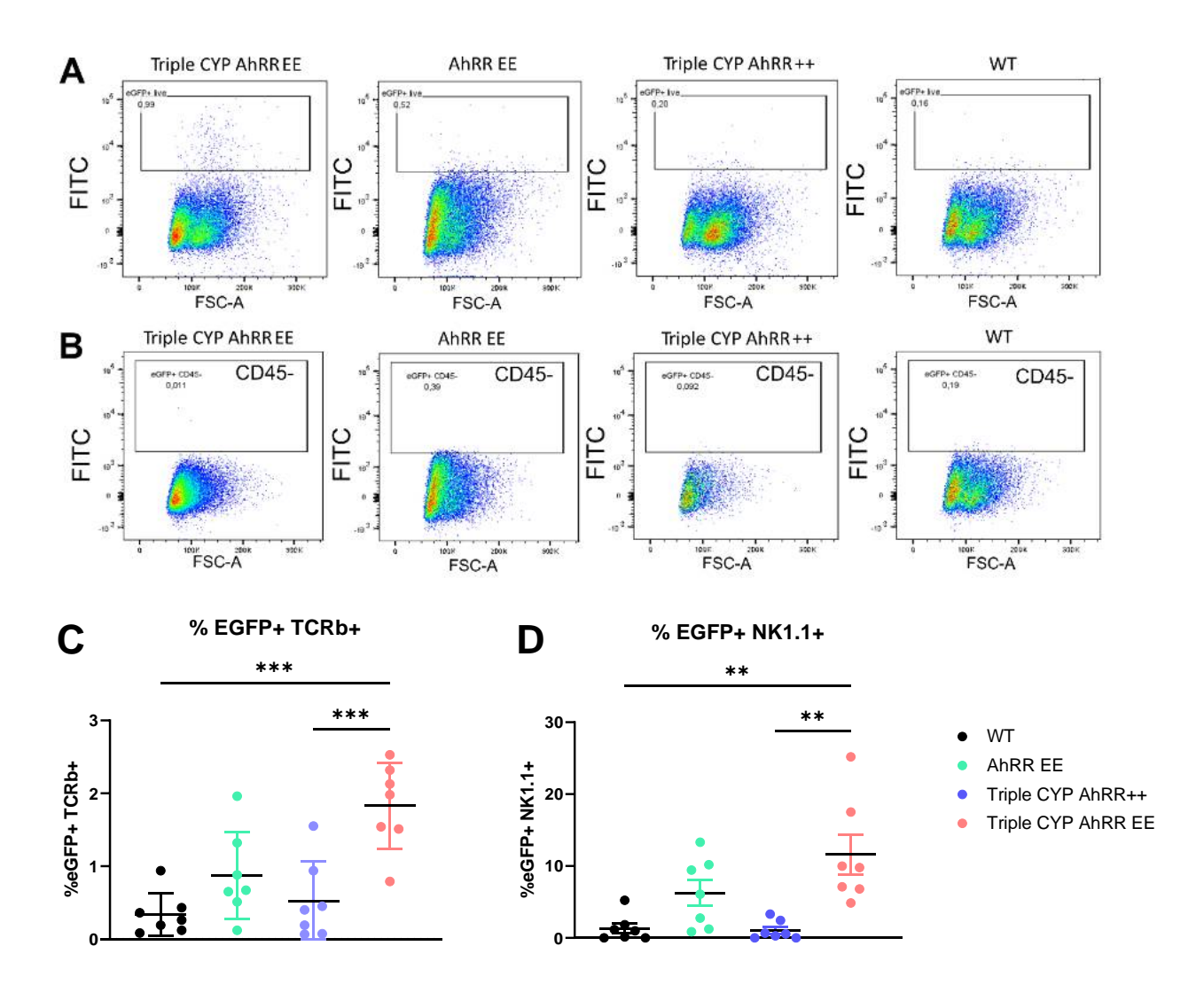
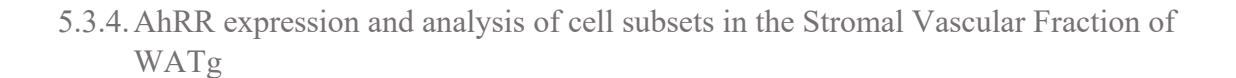


Fig. 5.16 AhRR/EGFP is expressed in hepatic immune cell subsets. AhRR/EGFP $^+$ cells from A) total living cells, B) CD45 $^-$ cells, C) T- and D) NK cells were analyzed by flow cytometry. Debris and doublets were excluded prior to gating of the hepatic AhRR/EGFP $^+$ cells. Results are shown as mean \pm SEM and significance was analyzed by either one-way ANOVA corrected for multiple comparisons by the Bonferroni's method. * p<0,5, *** p<0,01, **** p<0,001. N= 5 (data was pooled from two experiments).



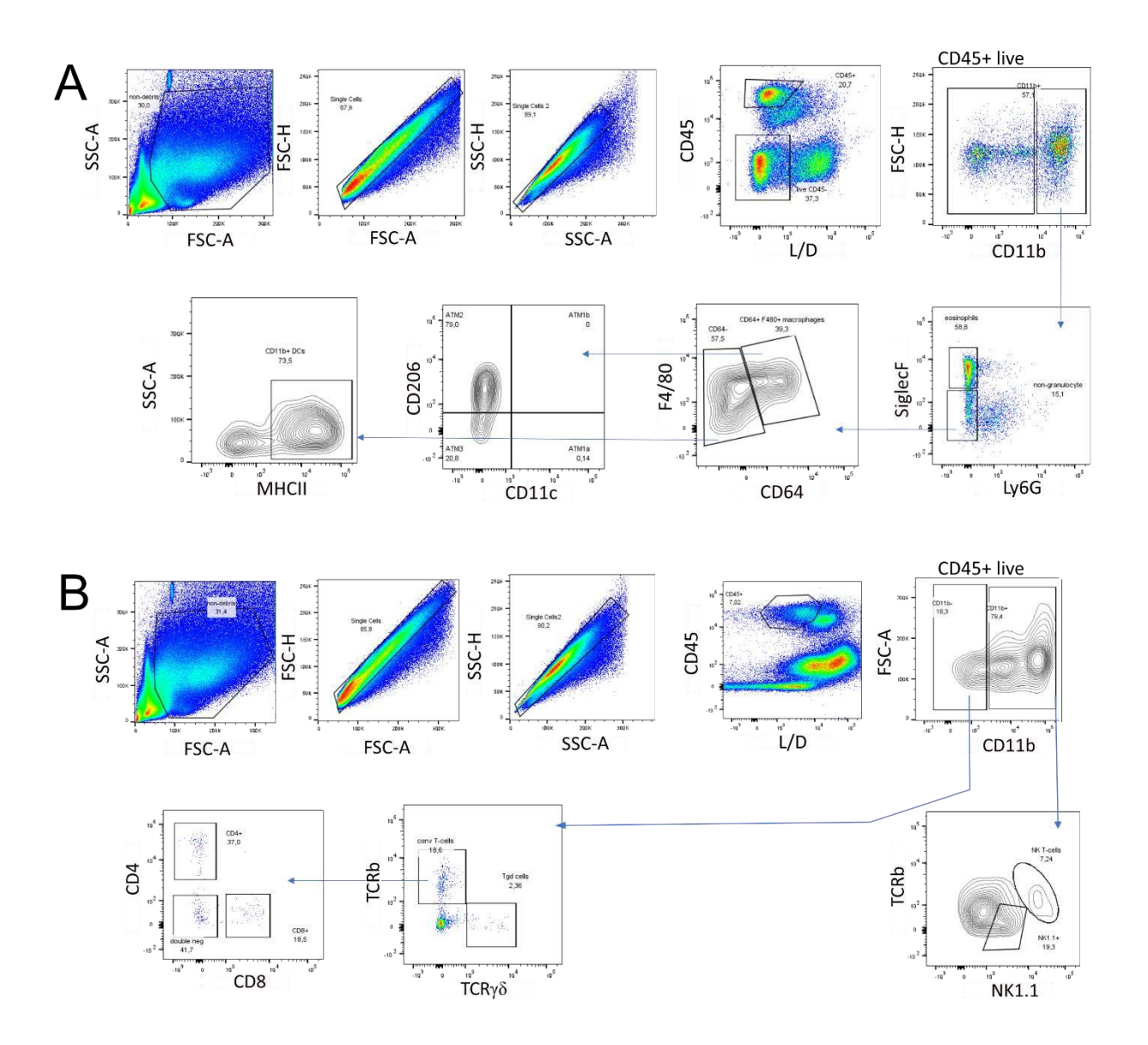


Fig. 5.17 Gating strategies for myeloid and lymphocyte subsets in the SVF of WATg. Cells were gated for living single CD45⁺ cells. A) eosinophils were identified as CD11b⁺ SiglecF⁺ Ly6G- cells, macrophages were identified as F4/80⁺ CD64⁺ cells and were further divided into 4 subsets: ATM 1a, b, 2, and 3. ATM 1a and 1b were identified as CD11c⁺ CD206- and CD206⁺, respectively. ATM2 were defined as CD206⁺ CD11c- cells, whereas ATM3 were defined as CD206- CD11c- cells. cDCs were identified as CD11b^{+/-} F4/80^{lo} CD64⁺ MHCII⁺ cells. B) In the lymphocyte subset, conventional T cells were identified as TCRβ⁺ CD11b-, which could be further divided into CD4⁺ and CD8⁺ cells. Tγδ cells expressed TCRγδ and were CD11b-. In the CD11b⁺ fraction, NK cells and NKT cells were identified as TCRβ- NK1.1⁺ and TCRβ⁺ NK1.1⁺, respectively.

For the analysis of adipose tissue, gonadal white adipose tissue (WATg) was pooled from 2-3 mice/genotype in each experiment, as the mice were young female mice that did not have a large amount of adipose tissue. The SVF was isolated and FACS analysis was

conducted. The gating strategies for both, myeloid cells and T cells are shown in **Fig. 5.17 A and B**, respectively. Following the exclusion of debris, doublets, and lymphocytes, the CD11b^{+/-} cDC subset was gated based on the expression of MHCII and lack of F4/80 as well as CD64. Macrophages were identified as CD11b⁺ SiglecF⁻ Ly6G⁻F4/80⁺ CD64⁻ cells, whereas eosinophils were identified as CD11b⁺ SiglecF⁺. For the lymphocyte subsets, B cells were identified as CD19⁺ MHCII⁺ cells. Conventional T cells were identified as TCR β ⁺ cells, which could be further divided into CD4⁺ and CD8⁺ T cells, whereas T γ 8 cells were identified as TCR γ 8 cells. Lastly, the NK cells and NKT cells were identified by their expression of CD11b, as well as TCR β ⁻ NK1.1⁺ and TCR β ⁺ NK1.1⁺, respectively.

The FACS results showed that there were no significant differences in the frequencies of eosinophils, macrophages, and CD11b⁺ DCs across all genotypes, although Triple CYP-KO AhRR^{E/E} and Triple CYP-KO AhRR^{+/+} mice had a slightly higher frequencies of cDCs compared to WT and AhRR^{E/E} mice (Fig. 5.18 A). More experiments are required to see if it is just a mere variation, or an effect mediated by the deficiency of the three AhRdependent CYP-enzymes. Furthermore, all of the mice predominantly harboured CD206⁺ CD11c⁻ non-inflammatory adipose-tissue macrophages (ATM2) as shown in Fig. 5.17 A. This is in line with the literature, since all mice were fed a normal chow and no high-fat diet that can lead to metaflammation and to the accumulation of CD206- ATM 3, as well as CD11c⁺ ATM1a and 1b macrophage subsets (Morris et al., 2015). In terms of AhRR/EGFP expression, macrophages, SiglecF⁺ eosinophils, and CD45⁻ cells were positive in Triple CYP-KO AhRR^{E/E} mice, (Fig. 5.18 B and C), whereas only background signals were detected in AhRR^{E/E}, Triple CYP-KO AhRR^{+/+} and WT mice. AhRR expression in macrophages was expected, as Brandstaetter et al. (Brandstaetter et al., 2016) showed high expression of the AhRR in macrophages, but it was a new finding to observe AhRR/EGFP expression in CD45⁻ cells and eosinophils in WATg. In liver, AhRRexpression in the CD45 fraction in the liver was barely detected by FACS, and AhRRexpression was also not detectable in eosinophils in the other organs analyzed here. However, AhRR is also expressed in intestinal eosinophils (Diny et al., 2022). Lastly, the frequencies of NK-, NKT, conventional- and Tyδ cells (Fig. 5.19 A-C) were highly variable between the samples, therefore it is hard to conclude if there was a difference between the genotypes. In addition, none of these cell subsets expressed AhRR/EGFP in WATg.

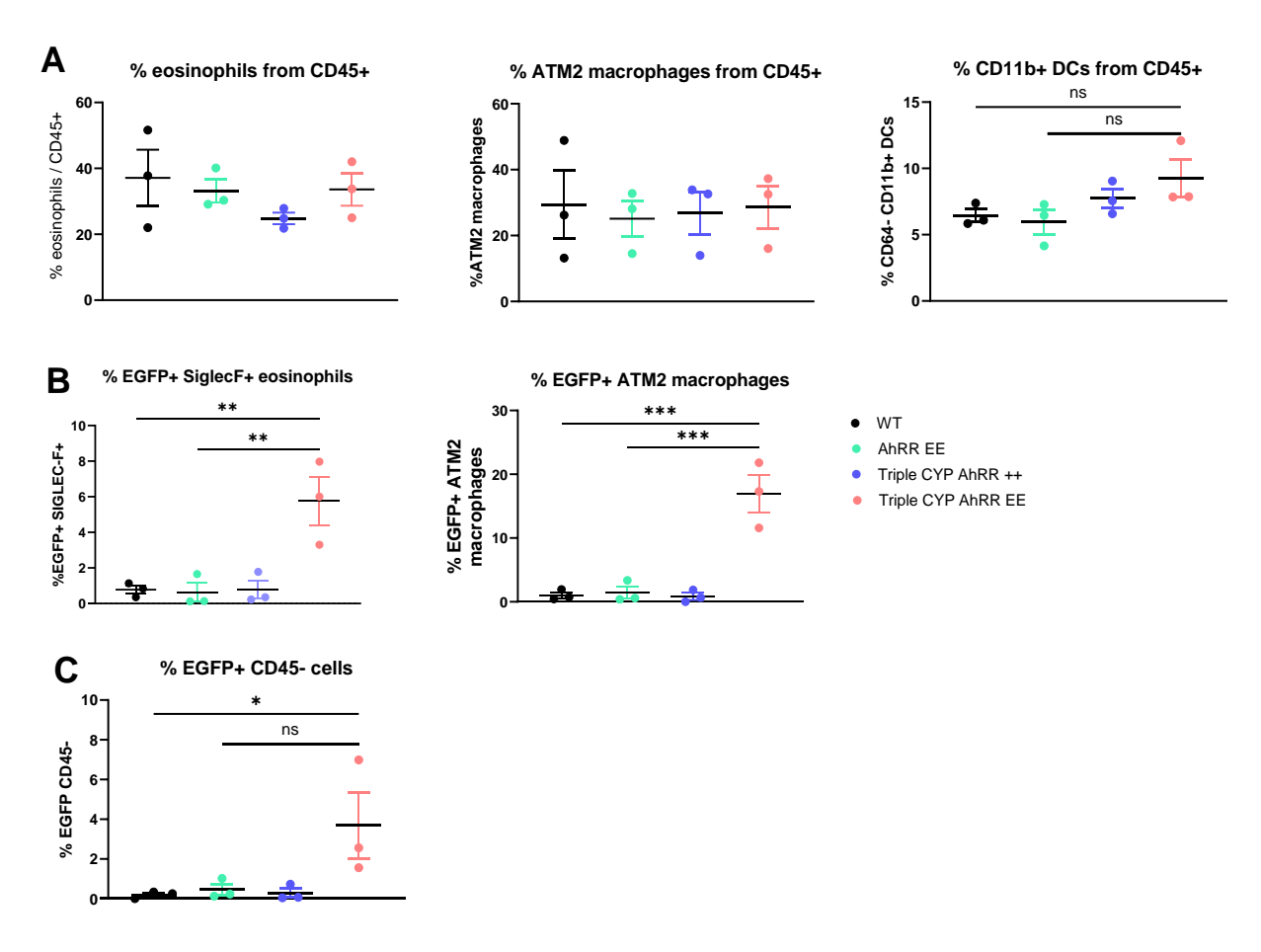


Fig. 5.18 Enhanced expression of AhRR/EGFP in Triple CYP EE mice did not lead to significant changes in the frequencies of myeloid cells in WATg. SVF cells were isolated from the WATg of 8-week naïve mice and the frequencies of A) myeloid cell subsets, as well as EGFP⁺ B) eosinophils and ATM 2 macrophages and C) $CD45^-$ cells across all genotypes were quantified. Results are shown as mean \pm SEM. Data was pooled from 2-3 mice / experiment. * p<0,5, ** p<0,01, *** p<0,001. N = 3 independent experiments.

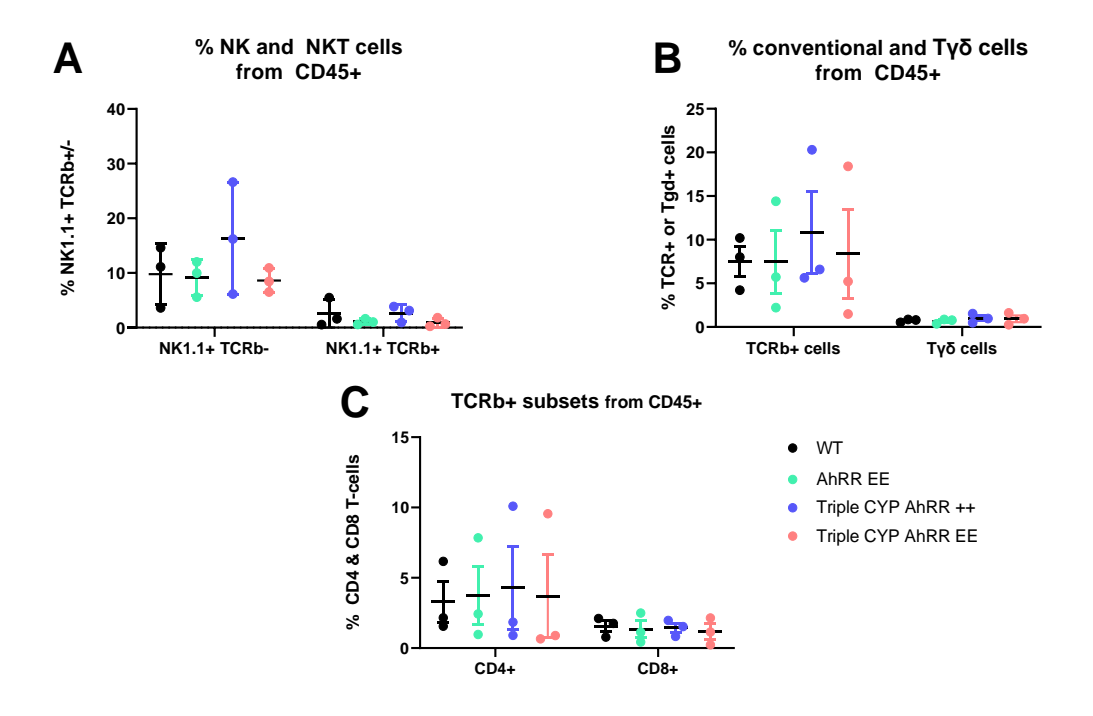


Fig. 5.19 Neither deficiency of AhRR- nor AhR-dependent CYP enzymes led to significant changes in lymphocyte subsets in WATg. SVF cells were isolated from the WATg of 8-week naïve mice. Then, the frequencies of A) NK and NKT cells, B) T cells expressing $\alpha\beta$ (conventional) and $\gamma\delta$ TCR receptor, C) CD4 and CD8⁺ conventional T cells were quantified. Results are shown as mean \pm SEM. N = 3 independent experiments.

5.3.5. AhRR expression and analysis of cell subsets in the gallbladder

Out of all other organs analyzed in this experiment, the gallbladder is the least wellinvestigated organ and the function of the three AhR-dependent CYP enzymes, as well as AhR or AhRR in gallbladder has not been analyzed well, although all molecules should be expressed there, especially in the biliary epithelium (Lakehal et al., 1999, Volz et al., 2008). Surprisingly, when analyzing the liver sections from Triple CYP-KO AhRR^{E/E} mice, AhRR/EGFP expression was found in the extrahepatic bile duct (Fig.5.20 A). Therefore, we asked, which cell type might express the AhRR in the bile duct and gallbladder. Analysis of gallbladder sections showed that similar to the liver, AhRR/EGFP is only expressed in Triple CYP-KO AhRR^{E/E} mice and not in AhRR^{E/E} mice (Fig.5.20 B). These AhRR/EGFP⁺ cells localized in the subepithelial area in the lamina propria and they were found parallel to the mucosal folds. Looking at the morphology of these AhRR/EGFPexpressing cells, they might be too big for being immune cells and some of them also seemed to have processes, making them look like fibroblasts. To confirm this notion, gallbladder cryosections were stained with a pan-immune cell marker, CD45 (Fig.5.20 C and D), as well as a fibroblast marker, CD90.2 (Fig. 5.20 E). From the CD45 staining (Fig.5.20 C and D), it is apparent that most of the EGFP⁺ cells are not CD45⁺ immune cells, although a smaller proportion of the cells do express CD45 (**Fig.5.20 C**, white arrow). Also, in some of the sections of Triple CYP-KO AhRR^{E/E} mice, there were CD45⁺ cell clusters detectable (**Fig.5.20 C**, white circle). However, such clusters of immune cells were not always found in the cryosections from the other three genotypes, but more sections need to be analyzed, as only five sections/genotype were analyzed so far. Due to this low number of analyzed sections, it is not yet clear if the deletion of AhRR and/or the three CYP enzymes causes the accumulation of immune cells in clusters. In addition, flow cytometry analysis would be necessary to quantify the total number of CD45⁺ cells to determine if AhRR- or Triple CYP-deficiency can cause an increase of immune cells in the gallbladder. Unfortunately, CD90.2 staining did not seem to work for gallbladder (**Fig.5.20 D**), as most of the CD90.2 signals did not colocalize with the DAPI signal and therefore are most likely unspecific. Thus, a possible co-localization of the AhRR/EGFP signal with CD90.2 could not be assessed.

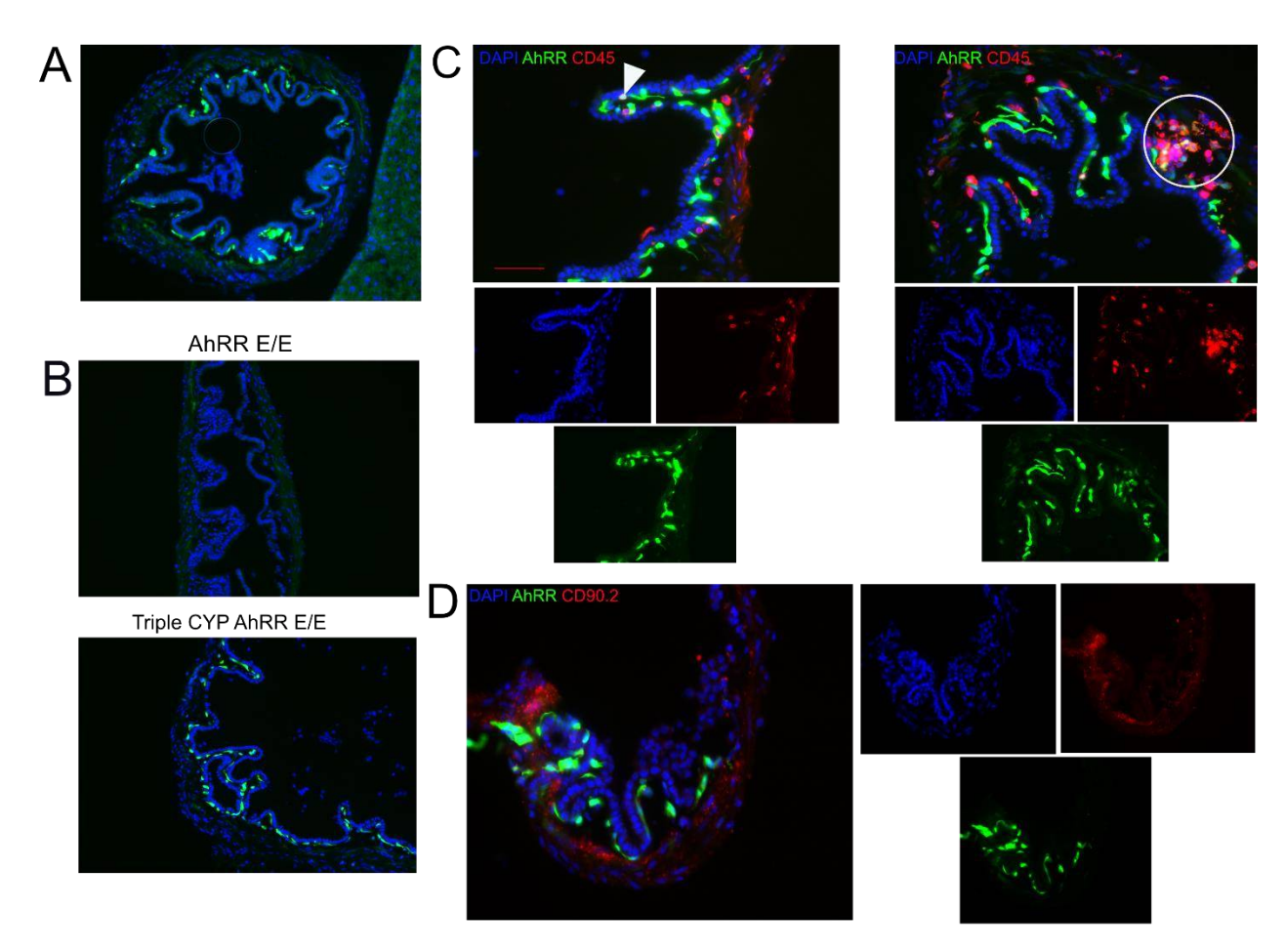


Fig.5.20 AhRR/EGFP is expressed in the gallbladder of Triple CYP AhRR^{E/E} mice. A) AhRR/EGFP expression in extrahepatic bile duct in Triple CYP-KO AhRR^{E/E} mice. B) AhRR/EGFP-expressing cells in the gallbladder of AhRR^{E/E} and Triple CYP-KO AhRR^{E/E} mice. Immunofluorescence staining of gallbladder cryosections with C) anti-CD45 and D) anti- CD90.2. Images A was taken at 20x, B was taken at 10x, and C-E were taken at 40x magnification. Scale bar = $100\mu m$.

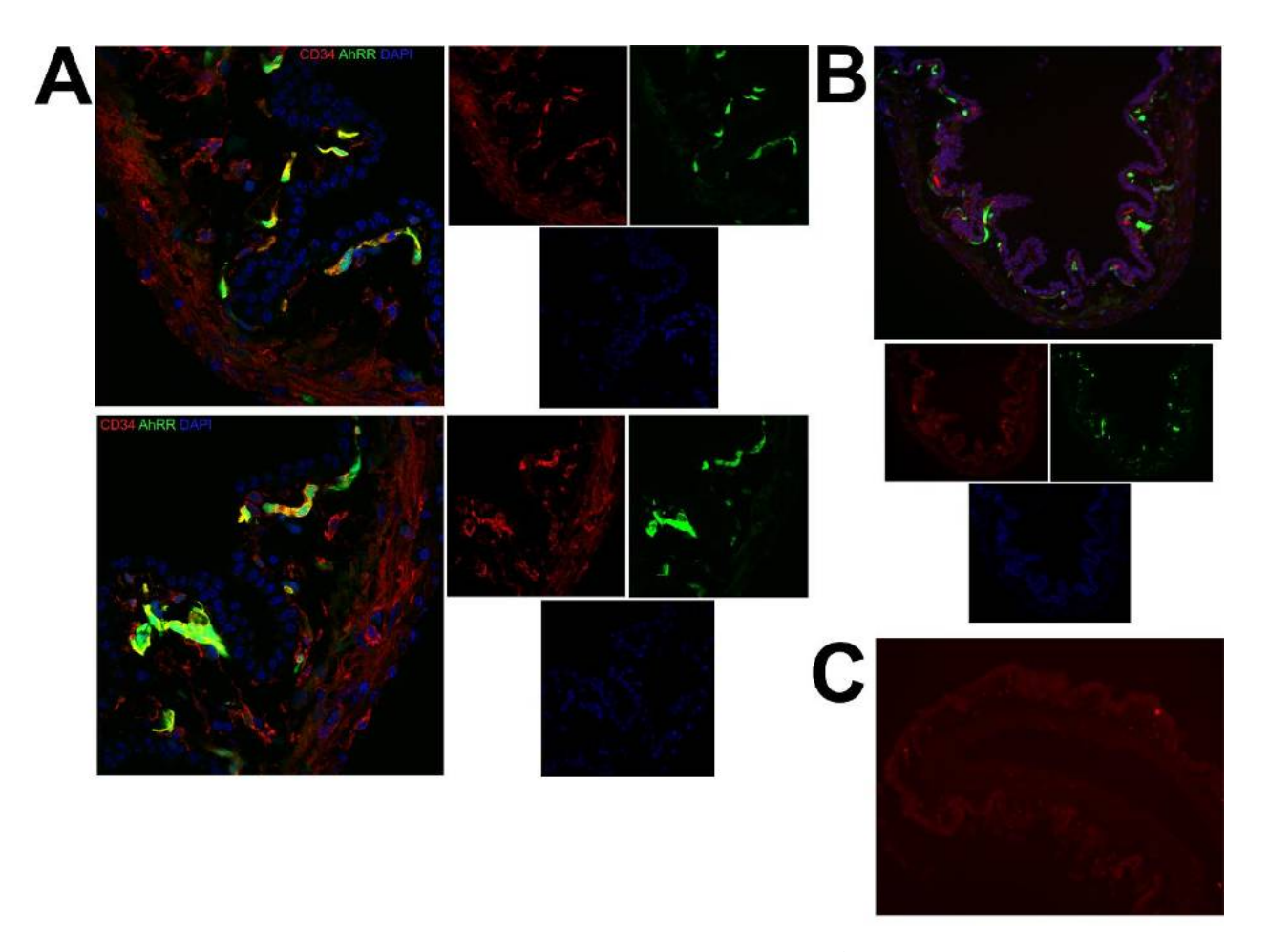


Fig. 5.21 The AhRR/EGFP-expressing cells in the gallbladder are CD34 $^+$ stromal cells. Cryosections of gallbladders from Triple CYP-KO AhRR^{E/E} mice were stained with antibodies against A) CD34 and B) PDGFR α . C) A cryosection was stained only with a secondary antibody as a control for the PDGFR α staining. Images in (A) were taken at 40x magnification, whereas images (B and C) were taken at 20x magnification. These images were taken from two different mice.

According to a paper by Liang *et al.* (Liang et al., 2021) who published a scRNAseq data set of gallbladder cells during gallstone formation, there are four main cell subsets in the gallbladder, EpCAM⁺ epithelial cells, endothelial cells, fibroblasts, and smooth muscle cells. They also describe a small subset of macrophages, which might be the AhRR-expressing CD45⁺ cells in the cluster seen here (depicted in **Fig.5.20** C). The EGFP-expressing cells localize in the sub-epithelial space, thus, they can either be endothelial cells, fibroblasts, or smooth muscle cells. Moreover, based on literature, various stromal cells other than fibroblasts or endothelial cells exist in the gallbladder, such as pericytes, and telocytes/interstitial cells of Cajal (Diaz-Flores et al., 2020). However, after staining and visualizing both blood and lymphatic vessels in the intestine, the volume of these AhRR-expressing cells appeared to be bigger than both types of endothelial cells. Besides,

the pattern of AhRR expression in the gallbladder did not resemble the localization patterns of both blood and lymphatic vessels. They also did not localize adjacent to blood vessels, since the blood vessels in gallbladder are localized beneath the mucosal layer (Damor et al., 2013). Therefore, these cells might be either fibroblasts or telocytes. In order to determine which markers were expressed by telocytes, a literature search was conducted, and it showed that telocytes expressed CD34 (Diaz-flores et al, 2020) or co-express both CD34 and PDGFRα (Ding et al., 2023). The CD34 staining worked well and it showed that the AhRR-expressing cells in the subepithelial space largely colocalize with CD34 expression, indicating that these cells could be telocytes, but the CD34⁺ cells in the muscularis layer did not express AhRR (Fig. 5.21 A). Thus, it might be that the CD34⁺ cells in the mucosal and muscularis layers are different cell types, and only the cells in the subepithelial space express AhRR. Further, PDGFRα expression did not seem to overlap with AhRR (Fig. 5.21 B) but the PDGFRα signal was largely unspecific, as the section stained only with the secondary antibody also showed some signals (Fig. 5.21 C). Nevertheless, AhRR expression in the stromal cells of the gallbladder has not been reported before and the role of AhRR in the gallbladder should be analyzed in more detail.

5.3.6. AhRR expression and analysis of cell subsets in the spleen

In general, AhRR/EGFP was expressed in the spleen of both Triple CYP-KO AhRR^{E/E} mice and AhRR^{E/E} mice, but with a much lower intensity in AhRR^{E/E} mice, as expected from the expression analysis of the other organs analyzed here. This was shown by both histological (**Fig. 5.22 A**) and FACS analysis (**Fig. 5.22 B**). AhRR/EGFP expression in the spleen of AhRR^{E/E} mice was barely seen, unlike in Triple CYP-KO AhRR^{E/E} mice, where AhRR/EGFP was expressed in vessels and to a lesser extent in cells in either red pulp or marginal zone (**Fig. 5.22 A**). A similar result was also obtained by FACS analysis (**Fig. 5.22 B**). AhRR/EGFP expression in AhRR^{E/E} mice was only 0.05% of total living cells, while it was around 1% (20x higher) in the Triple CYP-KO AhRR^{E/E} mice. The identity of these AhRR/EGFP-expressing cells was further elucidated by flow cytometry and immunohistology.

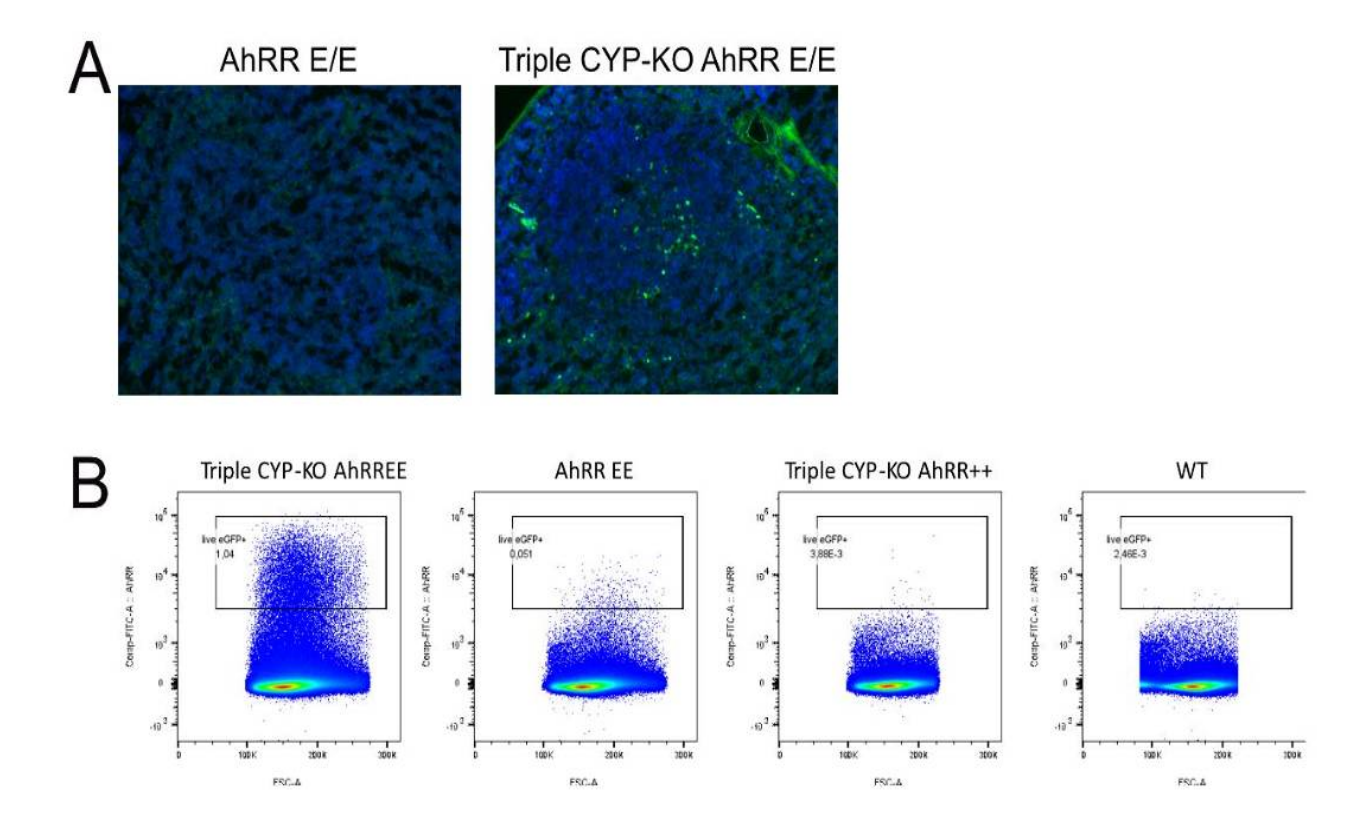


Fig. 5.22 Enhanced AhRR expression is observed in the spleen of Triple CYP-KO AhRR^{E/E} mice on histological level. A) AhRR/EGFP-expressing cells in spleen cryosections from AhRR^{E/E} and Triple CYP-KO AhRR^{E/E} mice. Images were taken at 20x magnification. B) FACS analysis of AhRR/EGFP expression in all living cells in all genotypes.

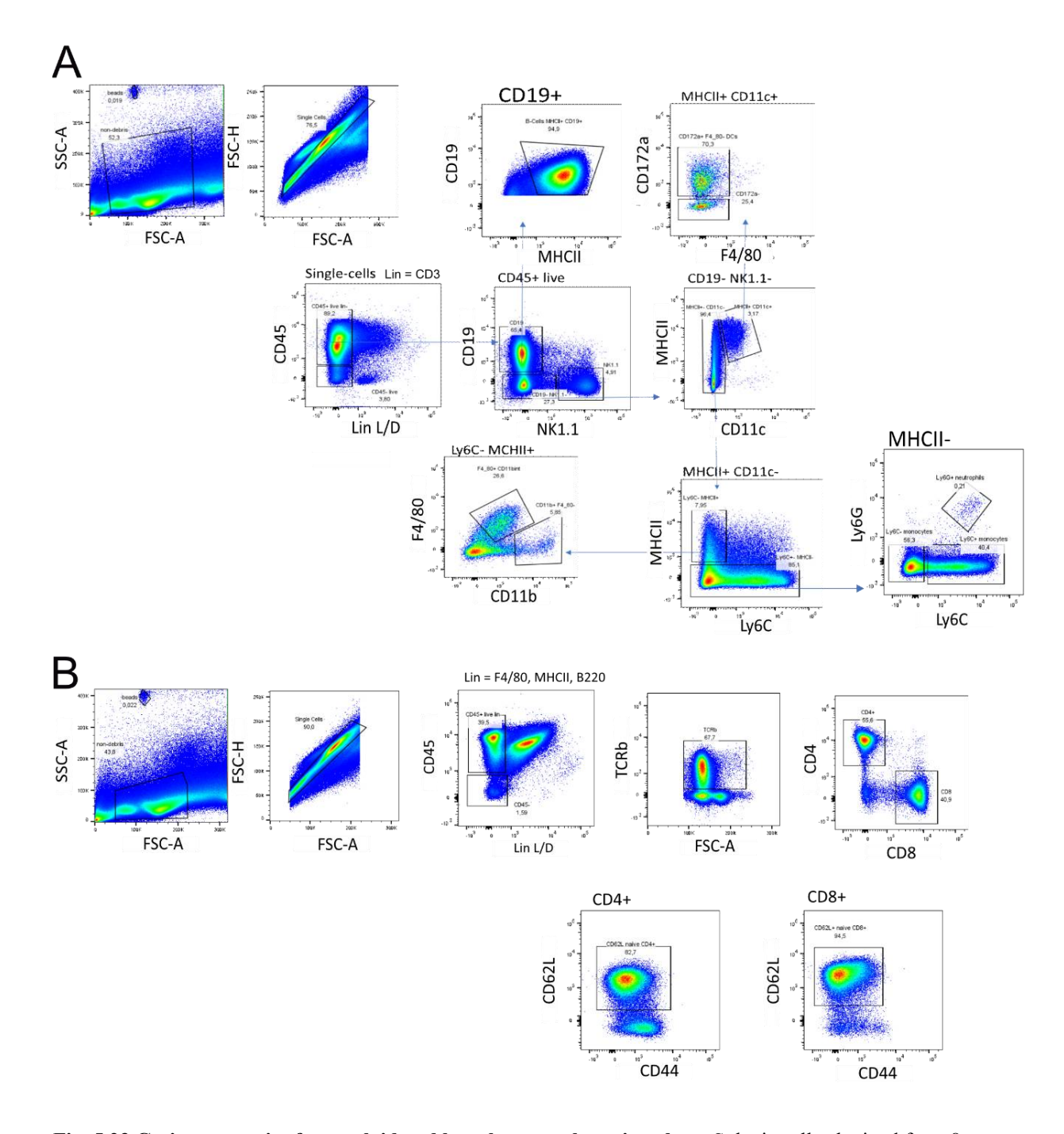


Fig. 5.23 Gating strategies for myeloid and lymphocyte subsets in spleen. Splenic cells obtained from 8-week naïve mice were first gated for living single CD45 $^+$ cells. A) Gating for B cells and myeloid cells. B cells were identified as CD19 $^+$ MHCII $^+$ cells. In the myeloid subset, cDCs were identified as MHCII $^+$ CD11c $^+$. Macrophages were identified as Ly6C $^-$ MHCII $^+$ F4/80 $^+$ CD11bint cells, whereas monocytes were identified as MHCII $^-$ Ly6G $^-$ Ly6C $^+$. B) T cell subsets were divided into TCR β^+ conventional T cells, which were further divided into CD4 $^+$ and CD8 $^+$ T cells. The naïve T cells from both subsets expressed CD62L $^+$ in addition to either CD4 $^+$ or CD8 $^+$.

Splenic myeloid and lymphocyte subsets were gated based on the strategies depicted in **Fig. 5.23 A and B**, respectively. Following the exclusion of debris, doublets, and lymphocytes, cDC were gated by their expression of MHCII and CD11c. Macrophages were identified as Ly6C⁻ MHCII⁺ F4/80⁺ CD11b^{int} cells, whereas monocytes were identified as MHCII- Ly6G⁻ Ly6C^{+/-}. B cells were identified as CD19⁺ MHCII⁺ cells and conventional T cells as $TCR\beta^+$ cells, which could be further divided into CD4⁺ and CD8⁺ T cells. Naïve T cells from both subsets were detected by the expression of CD62L.

In terms of frequency, B cells are among the highly represented cells in the spleen as expected and no differences in frequencies were observed across all genotypes Fig. 5.24 A. In the myeloid cell subset, monocytes had the highest frequency, especially the Ly6Cmonocyte subset with 10-14% of the total CD45⁺ immune cells, followed by the Ly6C⁺ monocyte subset with ~6% of CD45⁺ cells (**Fig. 5.24 B**). Interestingly, the frequency of NK cells was significantly higher in the AhRR^{E/E}, Triple CYP-KO AhRR^{+/+}, and Triple CYP-KO AhRR^{E/E} mice compared to WT mice (Fig. 5.24 C). In addition, the frequencies of macrophages and total cDCs were quite low (0,5-1%) and no significant differences across all genotypes were observed (Fig. 5.24 D and E). Mice deficient in the three AhRdependent CYP enzymes showed a tendency to have a higher frequency of macrophages compared to the other genotypes analyzed (Fig. 5.24 D), but the variation between the samples was rather high. Initially, it was planned to also analyze the MHCII CD11c Ly6C+ Ly6G⁺ neutrophils, but neutrophils could not be detected in most samples (data not shown). Furthermore, in the T cell subset, there was also no significant difference across all genotypes, neither in terms of total T cells nor in the individual CD4⁺ or CD8⁺ T-cell subset (Fig. 5.25 A-E).

Only 0.5% of B cells expressed AhRR in Triple CYP-KO AhRR^{E/E} mice, in the other genotypes no AhRR/EGFP expression could be detected (**Fig. 5.26 A**). Also, only 2-3% of monocytes and NK cells expressed AhRR (**Fig. 5.26 B and C**), whereas in macrophages only 1% expressed AhRR. Again, AhRR/EGFP expression could only be detected in Triple CYP-KO AhRR^{E/E} mice (**Fig. 5.26 D**). In the cDC subset, ~50% of cDC expressed AhRR and they only made up around 0.7% of total CD45⁺ cells (**Fig. 5.26 E**). In addition, approximately 10% of cDC expressed AhRR/EGFP in AhRR^{E/E} mice. In this mouse line, AhRR/EGFP was also expressed by 0.6% of total macrophages. In the T cell subsets, AhRR/EGFP expression was also observed mostly in CD4⁺ T cells rather than in CD8⁺ T cells, as around 2-3% of CD4⁺ were AhRR/EGFP⁺, whereas only 0.13% of CD8⁺ T cells

expressed AhRR (**Fig. 5.27**). Here, AhRR/EGFP expression was mainly restricted to T cells of Triple CYP-KO AhRR^{E/E} mice.

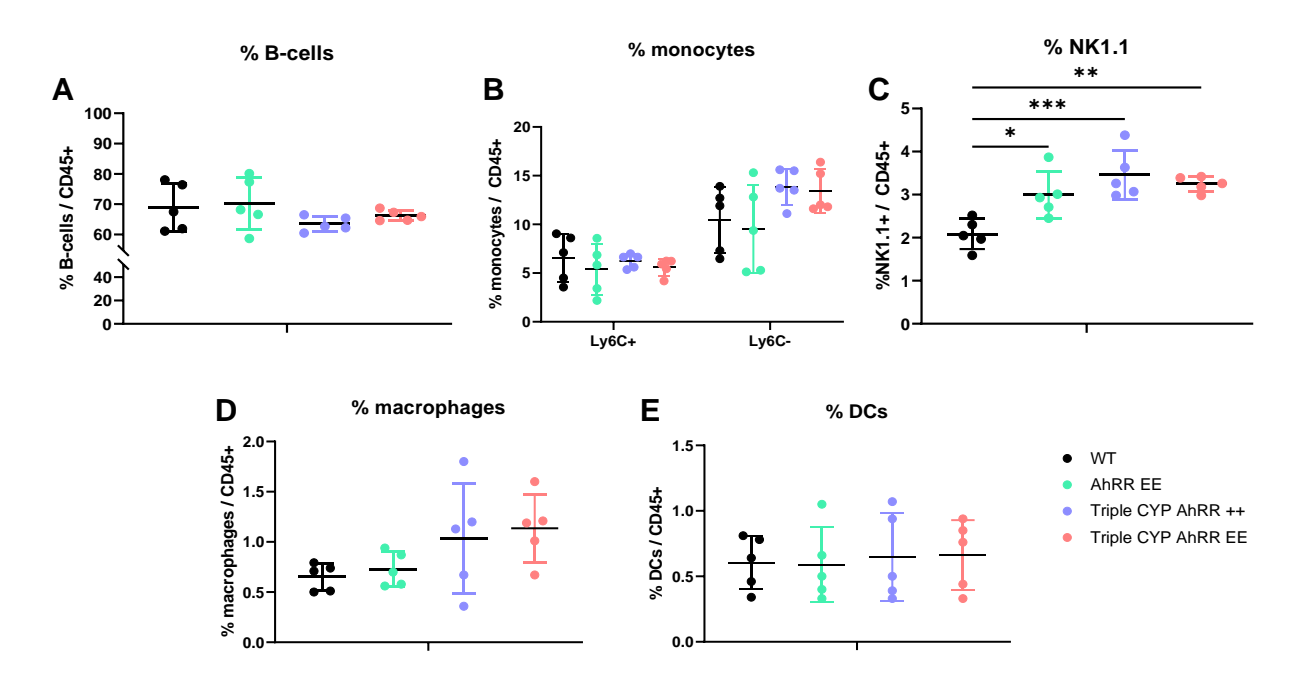


Fig. 5.24 Deficiency in either AhRR or the three AhR-dependent CYP enzymes can elevate the frequency of NK cells. Immune cells were isolated from the ear skin of 8-week naïve mice. The frequencies of distinct cell populations of total CD45⁺ cells are depicted. A) CD19⁺ B cells, B) NK1.1⁺ NK cells, C) CD11b⁺ DCs, D) CD4⁺ T cells, E) CD8⁺ T cells across all genotypes. Results are shown as mean ± SEM and significance was analyzed by one-way ANOVA corrected for multiple comparisons by the Bonferroni's method. * p<0,5, *** p<0,01, *** p<0,001. Data was pooled from two experiments. n=5.

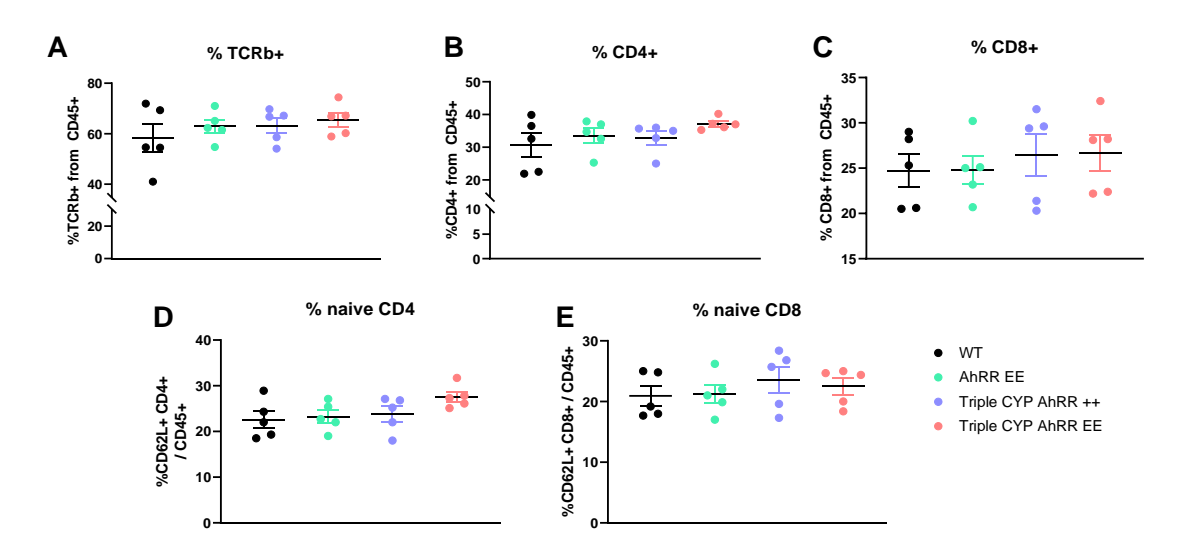


Fig. 5.25 Deficiency in neither AhRR nor Triple CYP alters the frequency of T cells in the spleen. The frequencies of total $TCR\beta^+$ T cells, as well as $CD4^+$ and $CD8^+$ T cells were calculated from all $CD45^+$ cells. Results are shown as mean \pm SEM. Data was pooled from two experiments. n=5.

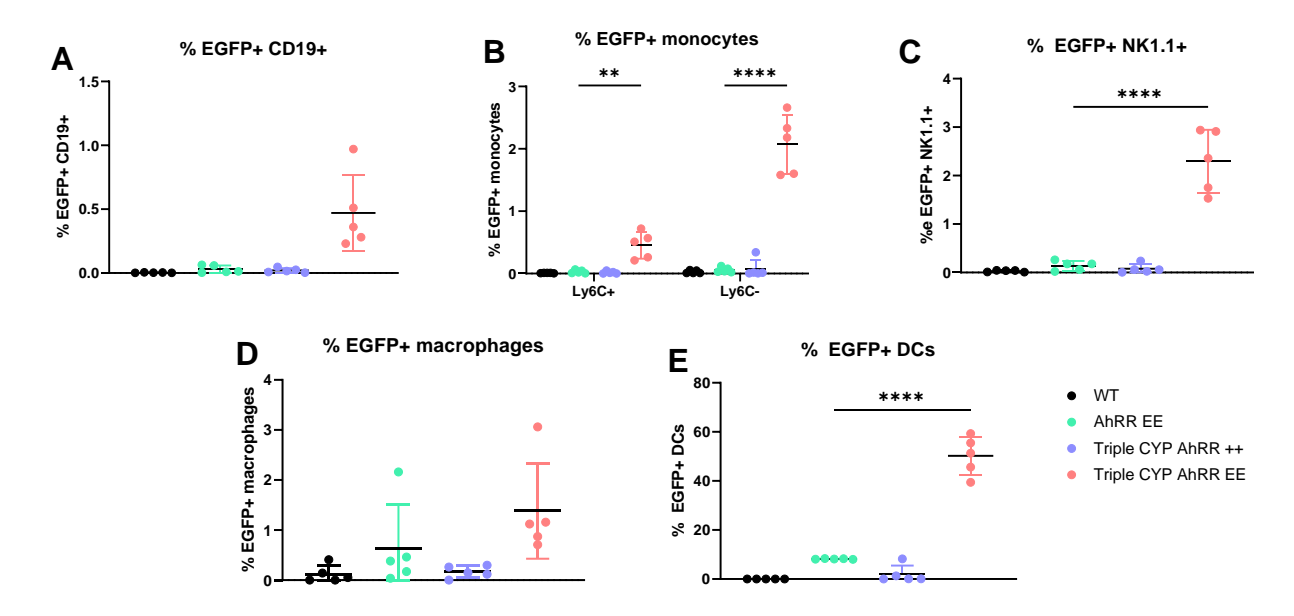


Fig. 5.26 . Triple CYP deficiency enhances AhRR/EGFP expression in the splenic myeloid cell subsets in Triple CYP AhRR^{E/E} mice. AhRR/EGFP $^+$ expression of A) CD19 $^+$ B cells, B) monocytes C) NK cells D) macrophages E) DCs were analyzed and quantified by means of flow cytometry. Results are shown as mean \pm SEM and significance was analyzed by one-way ANOVA (A,C,D,E) or two-way ANOVA (B) corrected for multiple comparisons by the Bonferroni's method. ** p<0,01, **** p<0,0001. Data was pooled from two experiments. n=5.

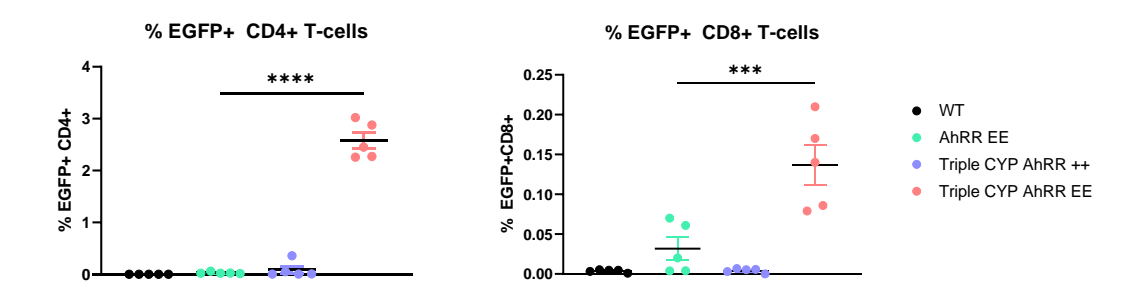


Fig. 5.27 AhRR/EGFP expression in splenic T lymphocyte subsets was detected in Triple CYP AhRR^{E/E} but not in AhRR^{E/E} mice. Frequencies of CD4 $^+$ T cells and CD8 $^+$ T cells across all genotypes are depicted. Results are shown as mean \pm SEM and significance was analyzed by one-way ANOVA (A,C,D,E) or two-way ANOVA (B) corrected for multiple comparisons by the Bonferroni's method. * p<0,05, **** p<0,0001. Data was pooled from two experiments. n=5.

AhRR/EGFP expression in Triple CYP-KO AhRR^{E/E} mice in a small number of T- and B lymphocytes was also observed in histology (**Fig. 5.28 A**), where a co-localization of the AhRR/EGFP signal with some TCR β^+ - or B220⁺cells was visible. The AhRR/EGFP expression was relatively low compared to other organs analyzed, like intestine or skin. Nevertheless, the histology result was in line with the FACS result, where only ~2.5% of T cells and 0.5% of B cells expressed AhRR (**Fig. 5.27**). Furthermore, AhRR expression could be observed in or near the marginal sinus (**Fig. 5.28 B**). Since the FACS analysis showed

that ~1.2% of splenic macrophages expressed AhRR (**Fig. 5.26 D**), it was interesting to analyze if these AhRR-expressing cells were marginal zone macrophages. Hence, the cryosections of the spleen of Triple CYP-KO AhRR^{E/E} mice were co-stained with B220 and SIGNR1 to visualize the B cells and the marginal zone macrophages, respectively. However, there was no co-localization of AhRR/EGFP and SIGNR1. These cells could be marginal metallophilic macrophages (MMMΦs), as they were localized in the marginal sinus (Borges da Silva et al., 2015) or endothelial cells of the sinus. Further immunofluorescent stainings with F4/80, Siglec1, MOMA1 and CD31 are required to see if these AhRR-expressing cells are indeed MMMΦs.

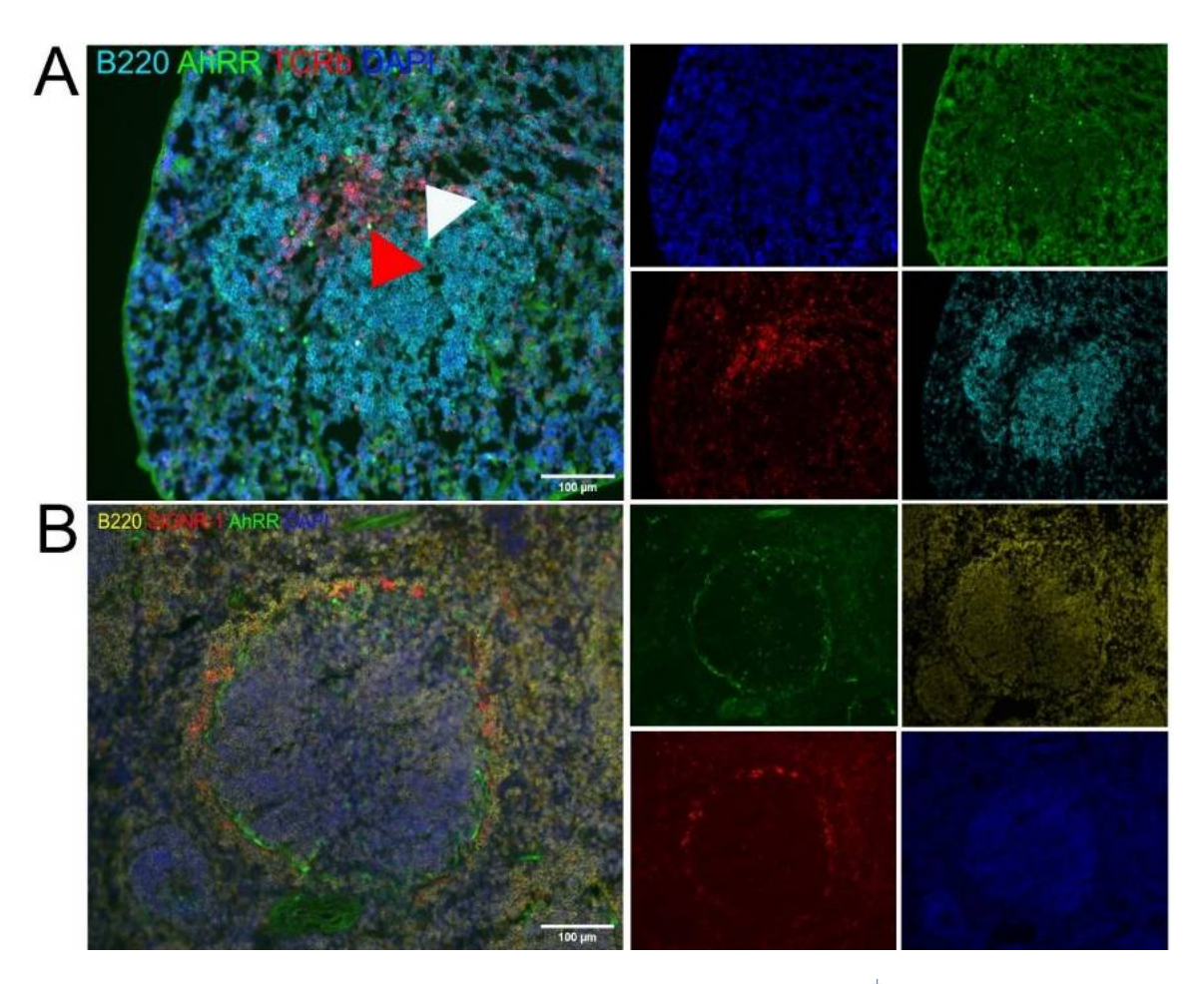
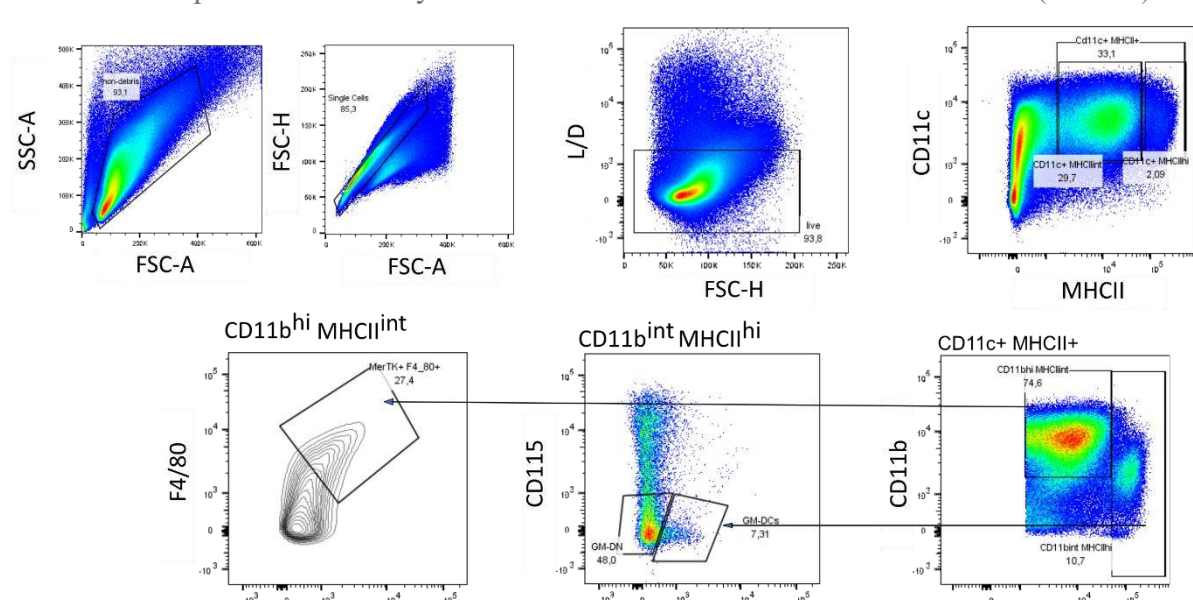


Fig. 5.28 AhRR/EGFP is expressed in T- and B cells, but not in SIGNR1⁺ marginal zone macrophages. A) Exemplary samples of cryosections of Triple CYP-KO AhRR^{E/E} mice stained with anti-TCR β and anti-B220, respectively. The Red arrow indicates co-localization of AhRR/EGFP with TCR β , whereas the white arrow co-localization of AhRR/EGFP in B220⁺ cells. B) Staining of cryosections of Triple CYP-KO AhRR^{E/E} mice with anti-B220 and anti-SIGNR1, which are the markers of B cells and marginal zone macrophages, respectively. Scale bar = 100 μ m, images were taken at 20x magnification.

MHCII



5.3.7. AhRR expression and analysis of cell subsets in bone-marrow-derived DC (BMDC)

Fig. 5.29 Gating strategy for myeloid subsets in BMDC. BMDC obtained from 8-week old naïve mice were first gated for living single cells. GM-DCs were first identified as CD11c⁺ MHCII⁺. The level of MHCII expression was directly proportional to the activation state of the GM-DCs. GM-DCs were separated from the monocytes-derived cells by their CD11b^{int} MHCII^{hi} expression, then were further characterized by the CD135 expression; The double negative DCs (GM-DN) did not express CD135 and CD115, while the bona fide GM-DCs expressed CD135. The macrophages (GM-macs) were identified by their expression of both F4/80 and MerTK.

MerTK

CD135

BM cells were obtained from 8-week-old mice differentiated with GM-CSF for 6 days. Then, the different myeloid subsets contained in BMDC were gated based on the strategy depicted in Fig. **5.29** (Helft et al., 2015). In general, there was a high variance of the CD11b⁺ MHCII⁺ subset between the experiments (Fig. 5.30). The lower datapoints were derived from BMDCs generated in the first experiment, in which the BMDCs might not have been differentiated properly, as there were only 30-45% total DC (CD11c⁺ MHCII⁺) detectable (**Fig. 5.30 A**). Nevertheless, the LPS treatment worked in all experiments, since there was a shift in MHCII expression in the LPStreated BMDCs to a higher level, regardless of the genotype, signifying an increase in maturation of the BMDCs subset (Fig. 5.30 B and C). Treatment with 3MC, however, did not lead to any alterations in cell frequencies. This was expected, as acute 3MC treatment did not affect the differentiation/maturation of DCs in previous experiments (data not shown). Moreover, there was no significant difference in frequency of the CD115- CD135- double negative (GM-DN) population across all genotypes and treatments, although the LPS-treated samples tended to have a higher GM-DN frequency compared to control and 3MC-treated cells (Fig. 5.30 D). The GM-DC population was the smallest subset, with $\sim 1.3\%$ of total living cells (Fig. 5.30 E), whereas the macrophage subset in the cultures (GM-Macs, MerTK⁺, F4/80⁺, and CD115⁺) was more abundant, with 3-8% of total live cells (Fig. 5.30 E and F). This is in agreement with the findings of Helft *et al.* (Helft et al., 2015), who showed that GM-CSF-generated BMDCs consisted mostly of GM-Macs instead of GM-DC. Interestingly, the frequency of MerTK⁺ F4/80⁺ GM-Macs of Triple CYP-KO AhRR^{E/E} mice was significantly reduced (**Fig. 5.30 F**) compared to the other genotypes, implying that deficiencies in both, AhRR and the three AhR-dependent CYP enzymes might diminish GM-Mac differentiation. Interestingly, LPS-treatment also downregulated CD115 expression in GM-Macs *in vitro*, not only in WT but also in the other three genotypes (**Fig. 5.31**). This result is in line with previous findings published by O'dea *et al.*, where also downregulation of CD115 in WT mice post-LPS treatment was also observed (O'Dea et al., 2009). Another study also demonstrated that LPS decreased cell-surface MerTK in WT macrophages, but increased soluble MerTK (Cai et al., 2016). Such a phenomenon may account for the decrease in the frequency MerTK⁺ F4/80⁺ GM-Macs following LPS treatment.

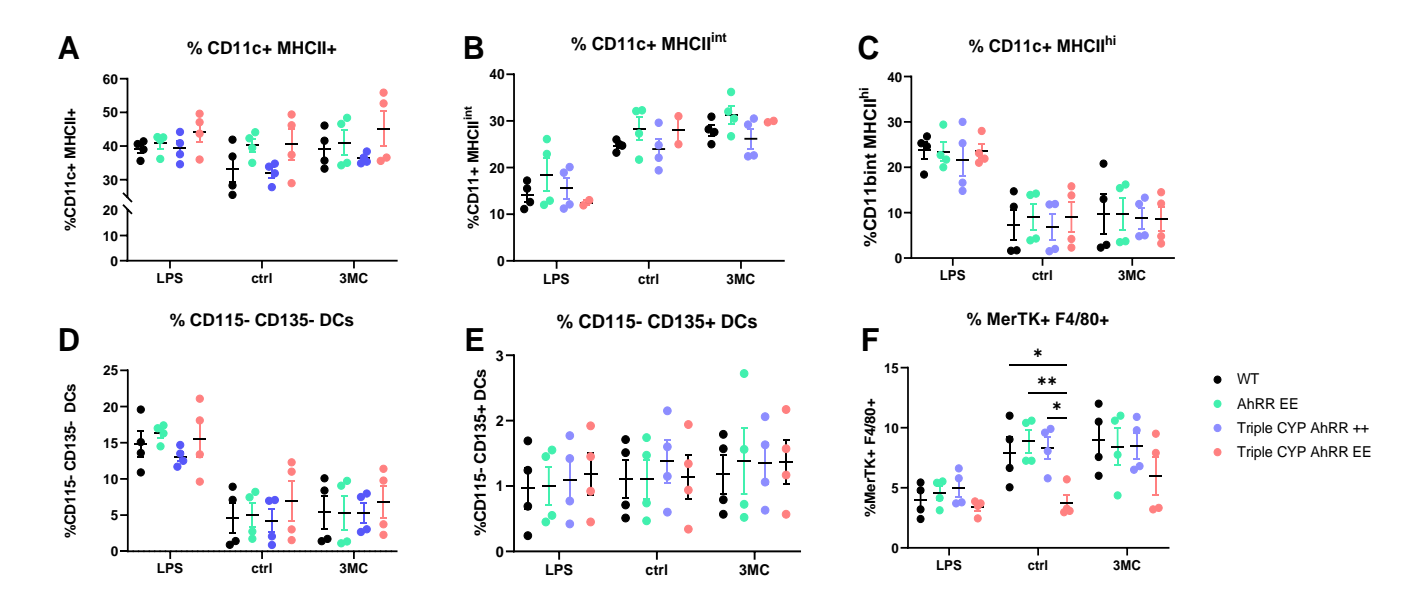


Fig. 5.30 The absence of both AhRR and Triple CYP reduces GM-Mac frequency. The frequencies of A) total mature BMDCs, B) $CD11c^+$ MHCI^{lint} BMDCs, C) activated $CD11c^+$ MHCII^{hi} BMDCs D) $CD115^-$ CD135- DN DCs, E) $CD115^+$ DCs, and F) MerTK $^+$ F4/80 $^+$ GM-MAC were quantified from total live single cells. Results are shown as mean \pm SEM and significance was analyzed by two-way ANOVA corrected for multiple comparisons by the Bonferroni's method. * p<0,05; ** p<0,01. Data was pooled from two experiments. n=4.

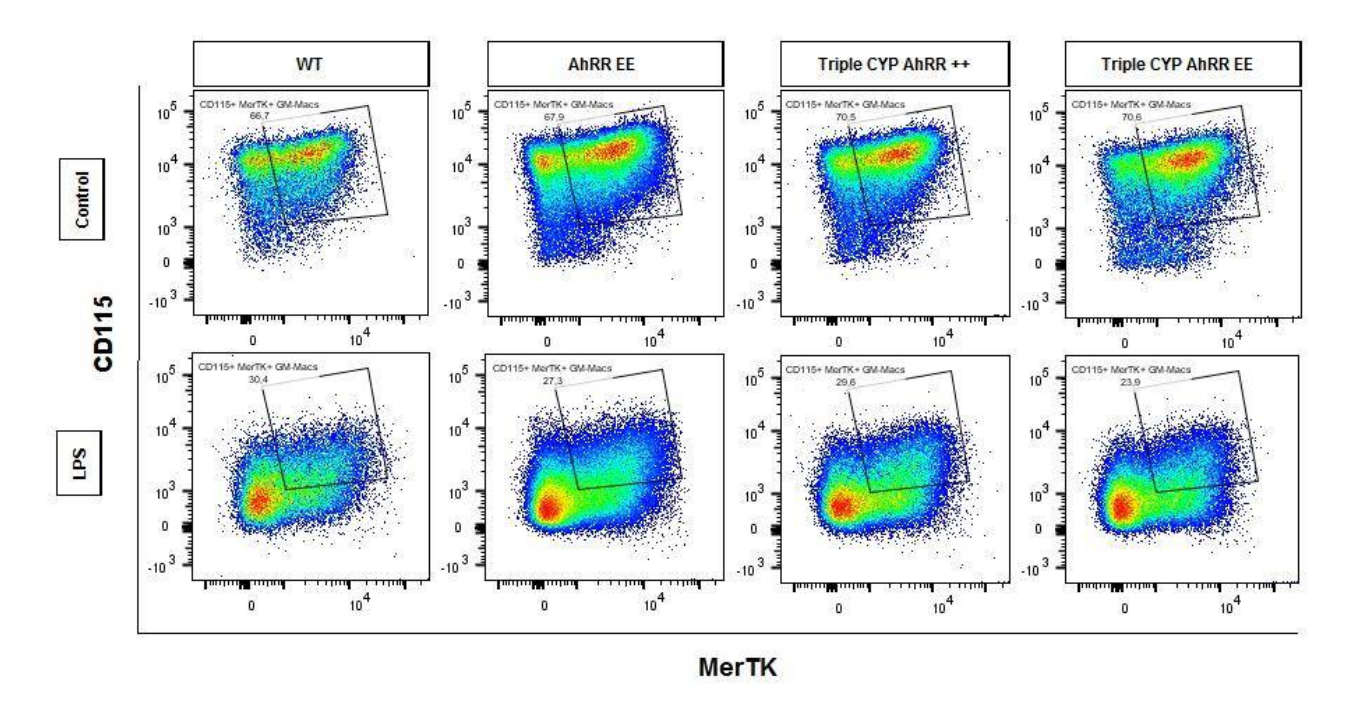


Fig. 5.31 LPS-mediated downregulation of CD115 in BMDCs of WT mice. BMDCs that were differentiated by GM-CSF were treated with LPS aor DMSO only as control and were analyzed by flow cytometry. After gating the F4/80⁺ MerTK⁺ GM-Macs, the expression of CD115 on GM-Macs was analyzed.

AhRR/EGFP was highly expressed in both Triple CYP AhRR^{E/E} and AhRR ^{E/E} mice with comparable frequencies in CD11c⁺ MHCII⁺, GM-DN, and GM-Mac subsets in both control and 3MC-treated samples (**Fig. 5.32 A-C**). The 3MC treatment did not further increase the AhRR expression in all subsets in both Triple CYP AhRR^{E/E} and AhRR ^{E/E} mice, as ~95% cells in all cell subsets in the control samples already expressed AhRR. However, AhRR expression in the MerTK⁺ F4/80⁺ GM-Macs subset of AhRR^{E/E} mice was significantly reduced after LPS-treatment, compared to the control and the 3MC-treated samples (**Fig. 5.32 C**), but this did not occur in the GM-Mac of Triple CYP-KO AhRR^{E/E} mice. The bonafide GM-DC subset consisted of only few cells (**Fig. 5.30 E**) and none of them expressed AhRR (data not shown).

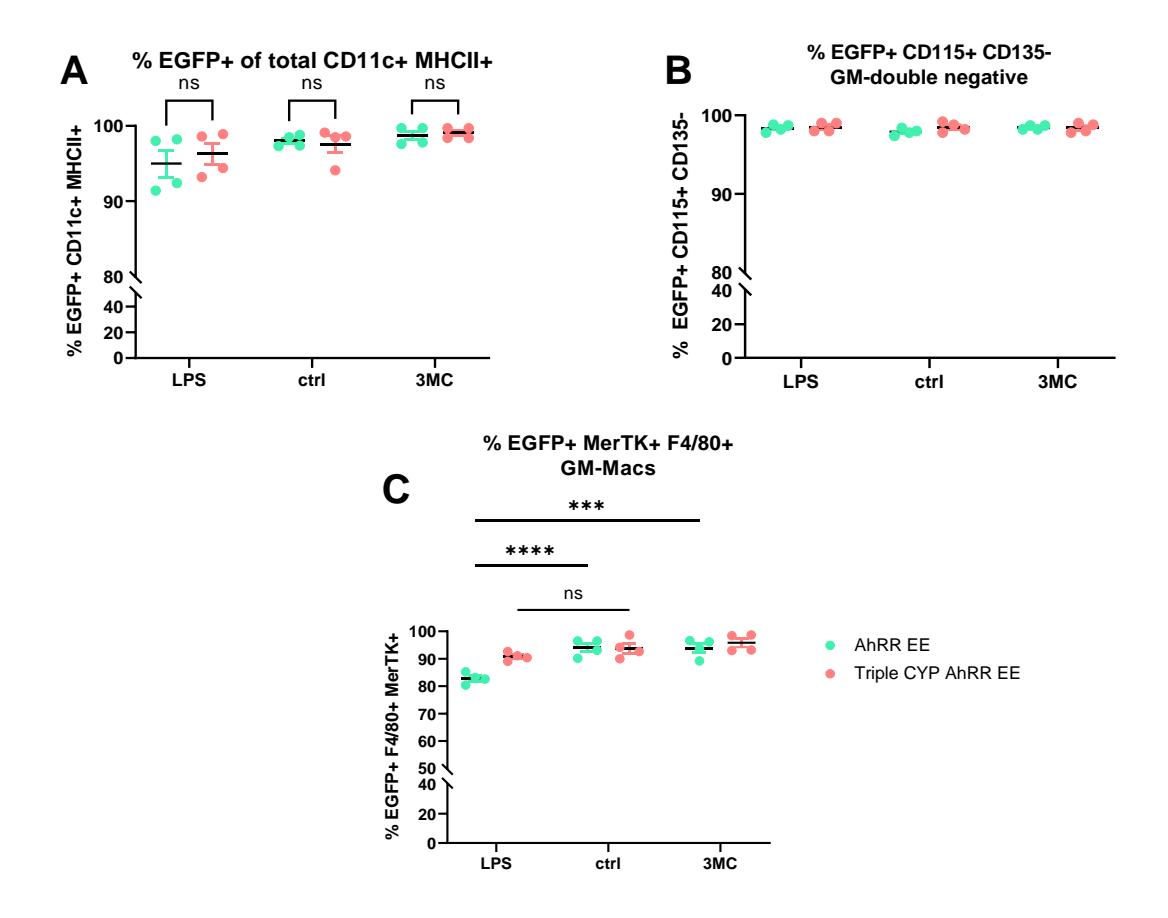


Fig. 5.32 Comparable AhRR/EGFP expression was detected in the BMDC subsets of Triple CYP AhRRE/E and AhRRE/E mice regardless of the treatments. Frequency of EGFP⁺ cells in A) total mature CD11c⁺ MHCII⁺ BMDCs B) GM-double negative cells C) MerTK⁺ F4/80⁺ GM-Macs* p<0,5, *** p<0,001, **** p<0,0001. Data was pooled from two experiments. n=5.

5.4. AhR ligand application enhances AhRR expression in multiple cell subsets of peripheral organs under physiological conditions

AhRR, CYP1A1, CYP1A2, and CYP1B1 are negative regulators of the AhR signaling pathway and their expression is induced by the activation of AhR. The activation of AhR is induced by many polyaromatic ligands. The source of potential AhR ligands is ranging from endogenous metabolites to dietary constituents (e.g, I3C) and environmental toxins (e.g, TCDD, BPA, 3MC). As already discussed above, in this thesis, 3MC was used as a prototypic ligand to activate the AhR. Injecting mice interperitoneally with 3MC has also been shown to be effective in inducing AhRR expression in myeloid cells in secondary lymphoid organs and small intestine (Brandstätter et al., 2016b). Another study showed that supplementing a diet that had a reduced AhR ligand content with I3C, a dietary AhR ligand, could rescue AhRR expression in murine immune cell subsets in secondary lymphoid organs and small intestine (Schanz et al., 2020). Therefore, it was of interest to investigate if acute treatment with 3MC for 16 hours can also

induce or upregulate the expression of AhRR *in vivo*. 3MC was administered by oral gavage, as it is a non-invasive administration method and ensures direct intestinal absorption of the ligand.

5.4.1. AhRR expression in small intestine

AhRR expression in the SI has been well documented in previous publications, both in IEL and immune cells of the lamina propria (Brandstätter et al., 2016b; Schanz et al., 2020a). In these studies, AhRR expression has been shown to be strongly regulated by the high availability of AhR ligands in SI, which also influenced barrier integrity of the intestine during DSS-induced colitis (Schanz et al., 2020). Hence, it was interesting if the combination of ablation of the AhRR and/or the three AhR-dependent CYP enzymes with an acute 3MC treatment would lead to a further enhanced AhRR/EGFP expression in both IEL and immune cells in lamina propria. For this purpose, intestinal epithelial cells and IEL were isolated together with the SI lamina propria to generate single cell suspensions for flow cytometry. Small samples from the proximal and distal small intestine were also taken for histology and qRT-PCR, respectively.

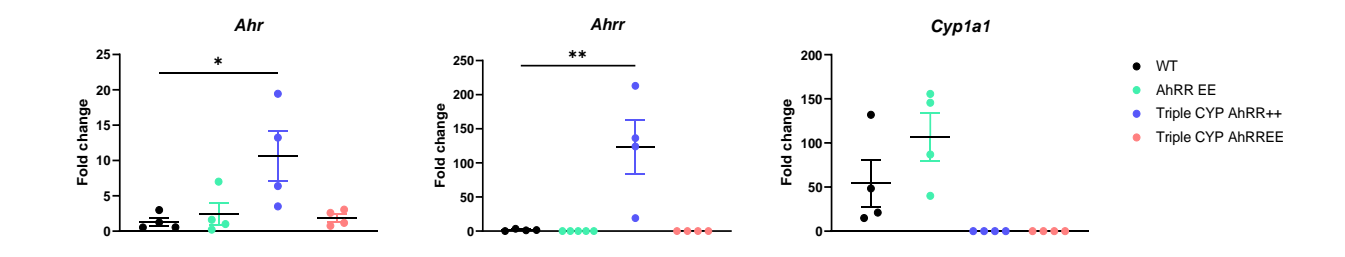


Fig. 5.33 AhR and its target genes in SI 16 hours post in vivo 3MC treatment. WT, AhRR^{E/E}, Triple CYP-KO AhRR^{E/E} mice were treated with 3MC by oral gavage for 16 hours and the expression of AhR and its target genes were analyzed by qPCR. Data was normalized to the expression of a reference gene and the DMSO-treated control. The qRT-PCR results show the gene expression of *Ahr*, *Ahrr*, and *Cyp1a1* in terms of fold change ($2^{-\Delta\Delta Ct}$). Error bars represent mean \pm SEM. Significance was analyzed by one-way ANOVA corrected for multiple comparisons by the Bonferroni's method, * p<0,05, *** p<0,001. Data was pooled from two independent experiments (n=4).

The gene expression of AhR and its target genes was also examined in the SI by qRT-PCR prior to analyzing the AhRR/EGFP expression to validate if the 3MC treatment for 16 hours efficiently induced AhR activation. Interestingly, 3MC-mediated AhR activation increased Ahr expression in the Triple CYP-KO AhRR^{+/+} but not Triple CYP-KO AhRR^{E/E} mice (**Fig. 5.33**, left figure) and Ahrr expression was also upregulated in Triple CYP-KO AhRR^{+/+} mice, but not in WT mice. This is intriguing, as Ahr expression might be upregulated as a result of the enhanced Ahr activation, but such an increase in Ahr was not observed in the liver of Triple CYP-KO AhRR^{+/+} mice, where a ~30-fold upregulation of Ahrr was observed post 3MC treatment (**Fig. 5.44** in the

next sub-chapter). The underlying cause of this increased *Ahr* expression was unclear. Nevertheless, the 3MC treatment was sufficient to induce the expression of *Ahrr* in Triple CYP-KO AhRR^{+/+} mice but not in WT mice (**Fig. 5.33**, middle figure) and the expression of *Cyp1a1* in both WT and AhRR^{E/E} mice also slightly increased (**Fig. 5.33**, right figure).

5.4.1.1. AhRR expression in IEL

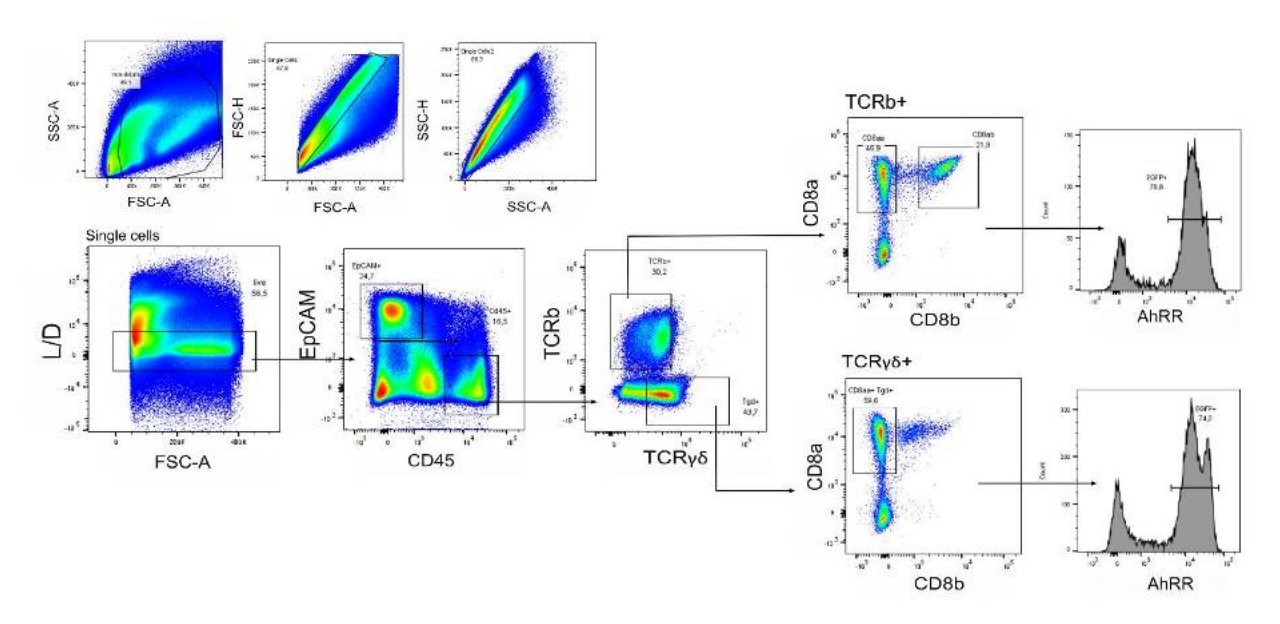


Fig. 5.36 Gating strategy for IEL of SI. SI was isolated from 8-week-old mice and single cell suspensions were generated prior to gating IEL and epithelial cells. Epithelial cells (IEC) were identified as $CD45^-$ EpCAM⁺ cells, whereas IEL were divided into TCRβ⁺ and TCRγδ⁺ cells. For the TCRβ⁺ cells, they were further identified as either CD8αα or CD8αβ IEL. For the TCRγδ⁺ cells, they were identified as CD8αα expressing IEL.

IEL reside in between the intestinal epithelial cells, hence they are the first immune cells that encounter pathogens or dietary/chemical by-products, including AhR ligands. AhR activity has been proven to be necessary to maintain the IEL and IEC cell turnover (Li et al., 2011) and it was shown that AhRR deficiency led to reduced colonic CD8 α ⁺TCR γ δ ⁺ IEL. However, this reduced IEL number was notobserved in the SI (Brandstätter et al., 2016b). Another AhR target gene, *Cyp1a1* is also expressed in IEC (Schiering et al., 2017a) Hence, it was of our interest to see if there would be inherent differences in IEC and IEL frequencies in the mice that are deficient in AhRR and/or the three AhR-dependent CYP enzymes. Moreover, it is also important to know if 3MC would further enhance AhR activation, hence AhRR expression in the intestinal IEL and if this would translate to altered cell frequencies. Following the 16-hour treatment of mice with 3MC or PBS, cells in intestinal epithelia and lamina propria were isolated and analyzed by flow cytometry. The frequencies of the total immune cells and the AhRR/EGFP-expressing immune cells in each subset, as well as the Median Fluorescence Intesity (MFI) of the

AhRR/EGFP signal were quantified. The gating strategy used is shown in **Fig. 5.36**. Here, epithelial cells were identified as CD45⁻ EpCAM⁺ cells, whereas IEL were divided into TCR β ⁺ and TCR γ δ ⁺ cells. For the TCR β ⁺ cells, they were further identified as either CD8 α α ⁺ or CD8 α β ⁺. For the TCR γ δ ⁺ cells, they were identified as TCR γ δ ⁺ CD8 α α ⁺ cells.

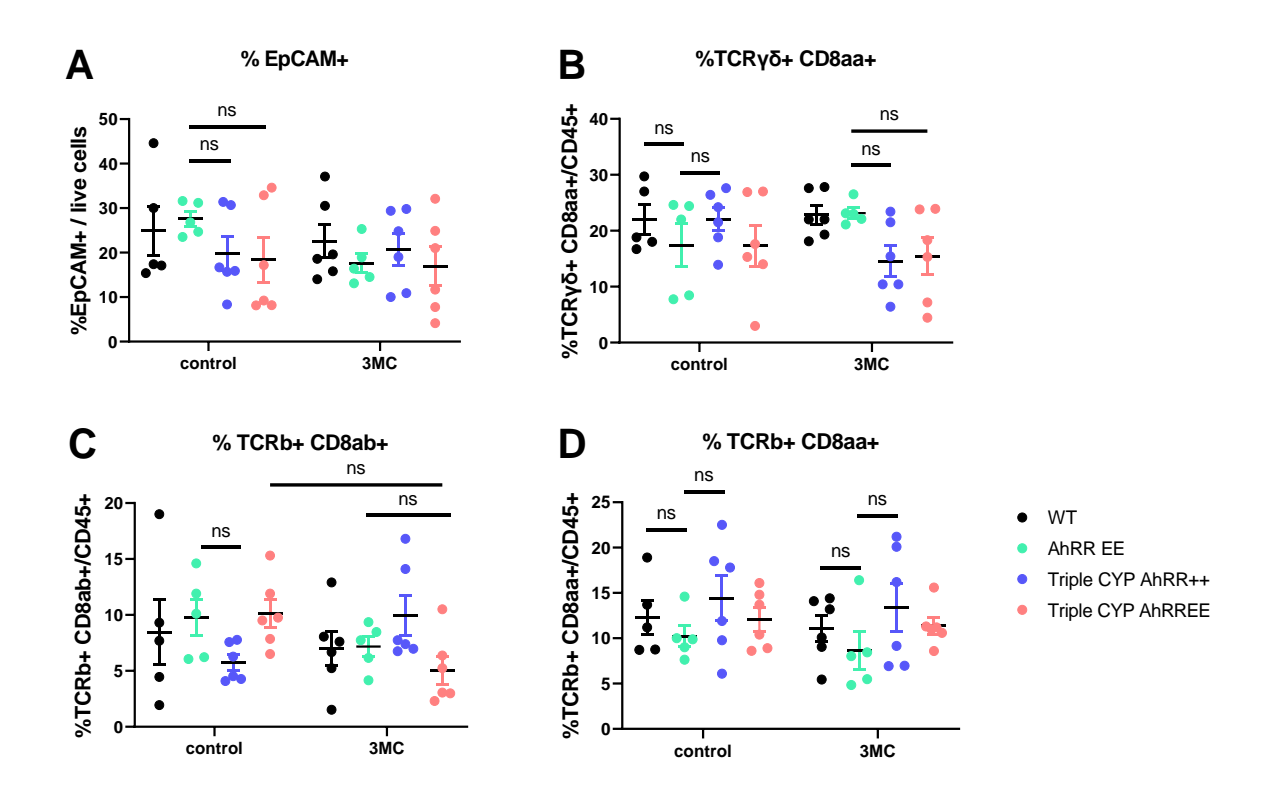


Fig. 5.37 3MC does not alter the frequencies of epithelial cells and T cell subsets in SI. SI was isolated from mice that were treated with DMSO control or 3MC (10mg/kg) by oral gavage for 16 hours. The cells in the epithelial layer were then gated for EpCAM^+ , $\text{TCR}\gamma\delta^+$ $\text{CD8}\alpha\alpha^+$, $\text{TCR}\beta^+$ $\text{CD8}\alpha\beta^+$, and $\text{TCR}\beta^+$ $\text{CD8}\alpha\alpha^+$. The frequencies of the cell subsets were analyzed by means of flow cytometry and were quantified out of the total CD45 cells. Results are shown as mean \pm SEM and significance was analyzed by two-way ANOVA corrected for multiple comparisons by the Bonferroni's method. * p<0,5. Data was pooled from two independent experiments (n=5 for AhRR^{E/E} and WT in control group, n=6 for the other genotypes).

In terms of the frequencies of EpCAM⁺ epithelial cells and immune cell subsets, there were minor but no significant differences across all four genotypes and treatment groups. (**Fig. 5.37 A-D**). The IEC frequency of AhRR^{E/E} mice was comparable to the one the WT in both control and 3MC groups, but in the 3MC group, this frequency was slightly reduced by ~10% in AhRR^{E/E} mice (**Fig. 5.37 A**). Moreover, no significant differences were observed in the frequencies of the three IEL subsets in both control and 3MC groups (**Fig. 5.37 B-D**). The frequency of TCR $\gamma\delta^+$ CD8 $\alpha\alpha^+$ IEL in Triple CYP-KO AhRR^{+/+} mice was reduced by ~9% in the 3MC group compared to control (**Fig. 5.37 B**). On the contrary, the TCR β^+ CD8 $\alpha\beta^+$ cell frequency was reduced by ~3% in the 3MC-treated Triple CYP-KO AhRR^{E/E} mice (**Fig. 5.37 C**). On the contrary, the frequency of TCR β^+ CD8 $\alpha\beta^+$ cell in the 3MC-treated Triple CYP-KO AhRR^{E/E} mice (**Fig. 5.37 C**). On the contrary, the frequency

by ~5% compared to the control group. In the $TCR\beta^+$ $CD8\alpha\alpha^+$ subset, there was no apparent tendency in cell frequency in both control- and 3MC-groups (**Fig. 5.37 D**).

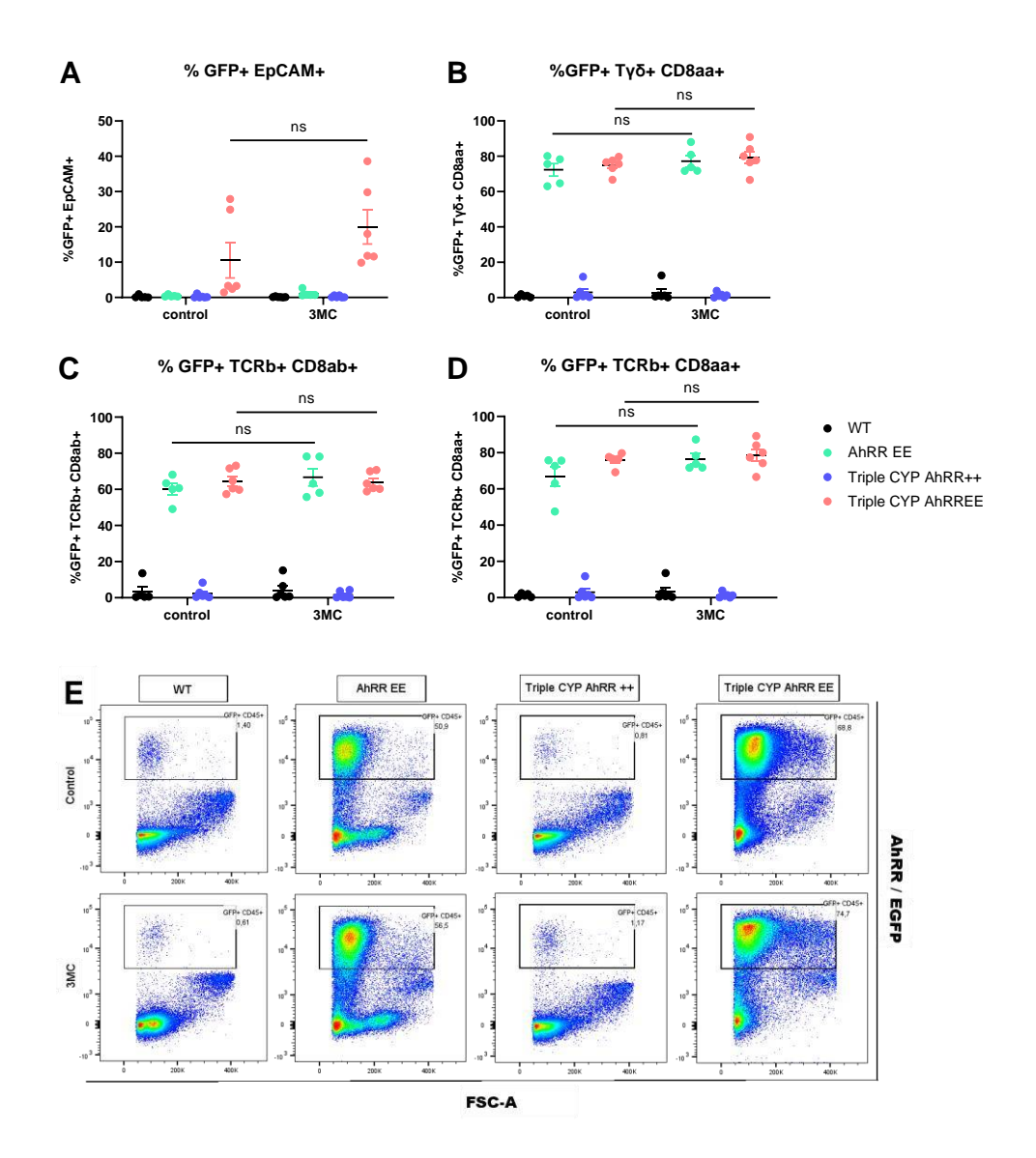


Fig. 5.38 3MC treatment does not increase the frequencies of AhRR-expressing IEL. The EGFP⁺ IEL subsets were analyzed by flow cytometry (A-D) and their frequencies were quantified. Results are shown as mean ± SEM and significance was analyzed by two-way ANOVA corrected for multiple comparisons by the Bonferroni's method, ns = not significant. E) Representative figures of EGFP-expressing CD45⁺ IEL from both control and 3MC groups of all genotypes. Data was pooled from two independent experiments (n=5 for AhRR^{E/E} and WT in control group, n=6 for the other genotypes).

Overall, AhRR was highly expressed in all IEL subsets analyzed (60-80% AhRR-expressing IEL) in both AhRR^{E/E} and Triple CYP-KO AhRR^{E/E} mice, and to a much lesser extent in IEC (**Fig. 5.38 A-D**). In IEC, AhRR was solely detected in Triple CYP-KO AhRR^{E/E} mice. In the control group, AhRR was barely expressed, despite the abundant AhR expression in IEC (Esser and Rannug, 2015) but it was further enhanced (by about 10 times) by 3MC treatment (**Fig. 5.38 A**). In the three IEL subsets, AhRR was already highly expressed in AhRR^{E/E} mice but was not further enhanced in Triple CYP-KO AhRR^{E/E} mice (**Fig. 5.38 B-D**). However, a background

EGFP signal was also detected in the WT and Triple CYP-KO AhRR^{+/+}mice (**Fig. 5.38 E**), as ~0.5-1.5% CD45⁺ cells were captured in the EGFP⁺ gate. Furthermore, 3MC treatment did not upregulate AhRR expression in either AhRR^{E/E} or Triple CYP-KO AhRR^{E/E} mice. This result is in line with the study by Brandstaetter et al. (Brandstaetter et al., 2016), where AhRR was also not detected in the IEC of AhRR^{E/E} mice but was highly expressed in the IEL subsets. The histological analysis of 3MC-treated Triple CYP-KO AhRR^{E/E} mice also revealed barely any AhRR-expressing cells in intestinal epithelial cells co-localized with EpCAM (**Fig. 5.39**). Most of the AhRR-expressing cells in the epithelial layer could be IEL (**Fig. 5.39**, white arrows), but co-staining with lymphoid markers, e.g., $TCR\beta$ or $TCR\gamma\delta$ would be necessary to determine their identities. In terms of MFI, consistent with the EGFP expression analysis, a high background signal was also detected in WT and Triple CYP-KO AhRR^{+/+} mice in IEC and in all IEL subsets (**Fig. 5.40 A-D**). This made analyzing the true EGFP expressions in AhRR^{E/E} and Triple CYP-KO AhRR^{E/E} difficult.

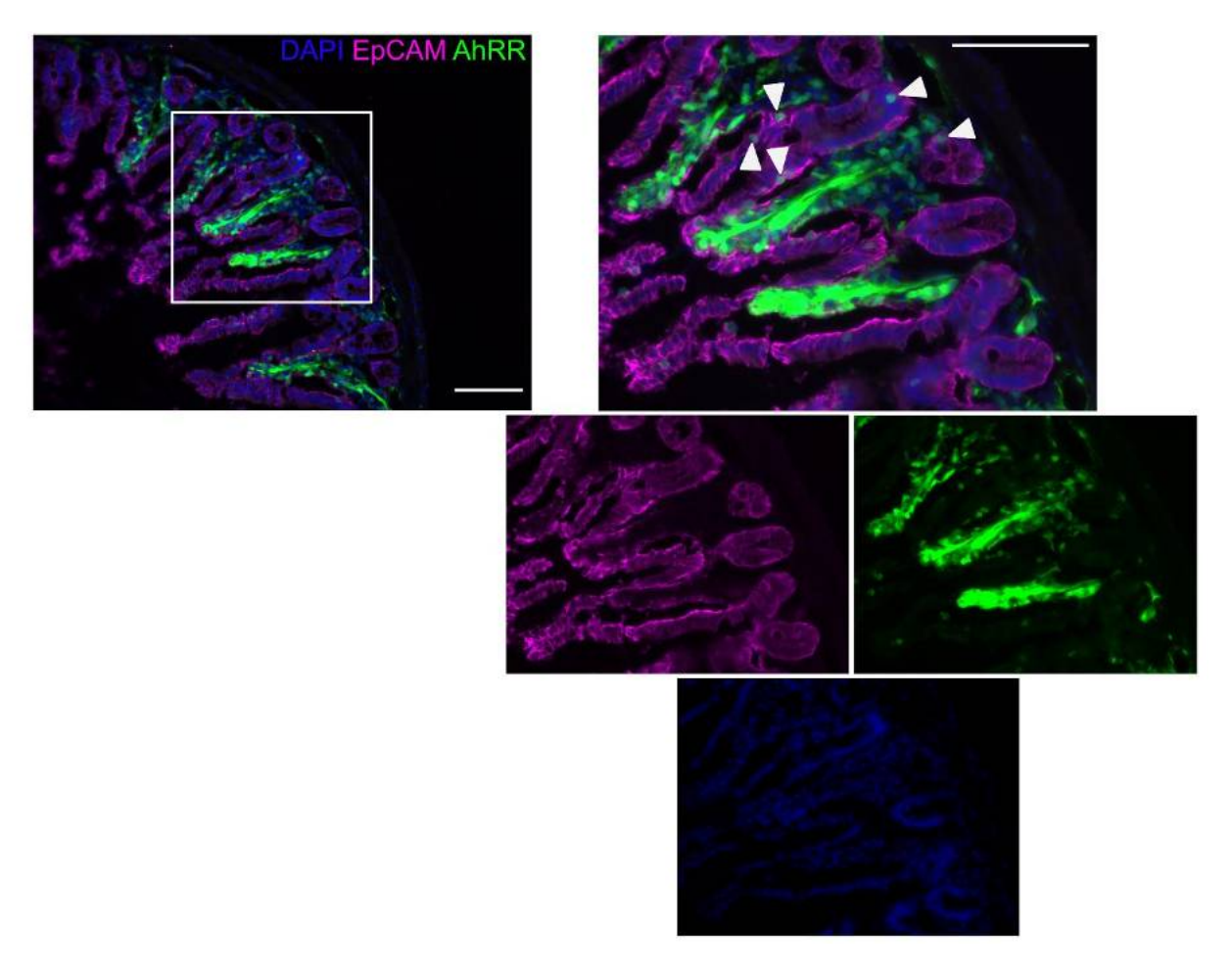


Fig. 5.39 Minimal expression of AhRR in IEC was observed in intestinal epithelia of 3MC-treated Triple CYP-KO AhRR^{E/E} mouse. Cryosections of the SI of Triple CYP-KO AhRR^{E/E} that had been treated with 3MC was stained with EpCAM to visualize the IEC. The AhRR/EGFP expression was also visualized to observe if there was co-localization of AhRR and EpCAM. White arrows depict AhRR-expressing cells in the epithelial layer of the SI. The left image was taken at 20x magnification, whereas the right image was taken at 40x magnification. Scale bar = $100 \ \mu m$.

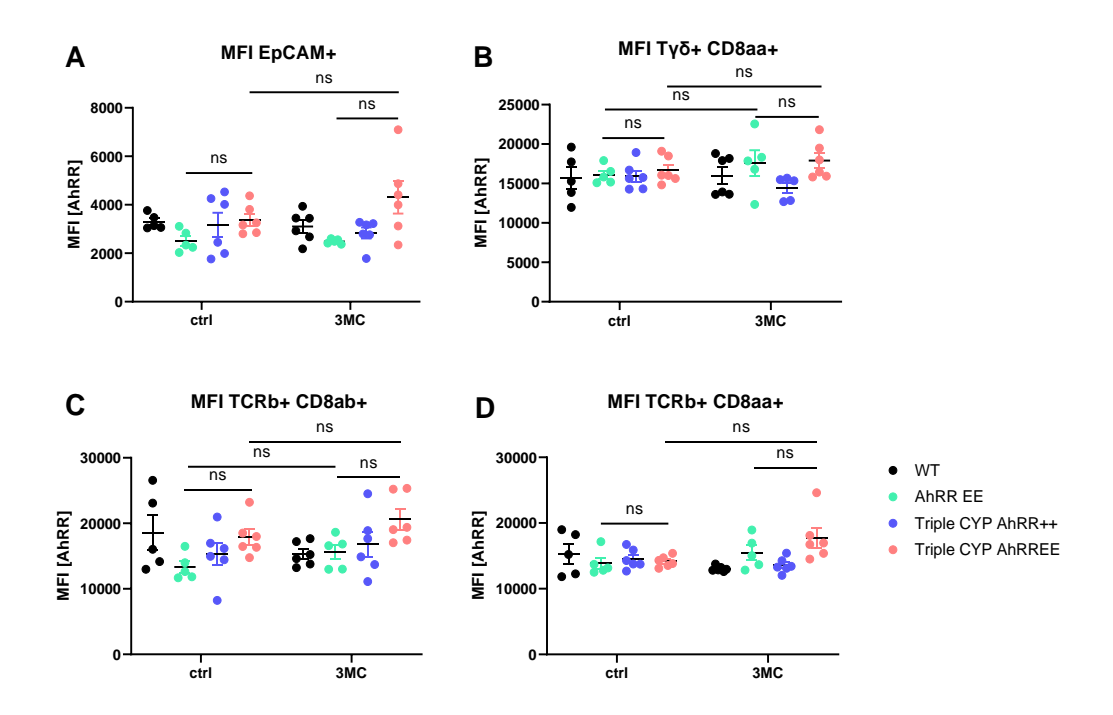


Fig. 5.40 There is no difference in MFI of AhRR/EGFP between genotypes and treatment groups. The MFI of AhRR/EGFP in the IEL subsets were analyzed by flow cytometry (A-D) and their frequencies were quantified. Results are shown as mean \pm SEM and significance was analyzed by two-way ANOVA corrected for multiple comparisons by the Bonferroni's method, ns = not significant. Data was pooled from two independent experiments (n=5 for AhRR^{E/E} and WT in control group, n=6 for the other genotypes).

5.4.1.2. AhRR expression in the lamina propria of SI

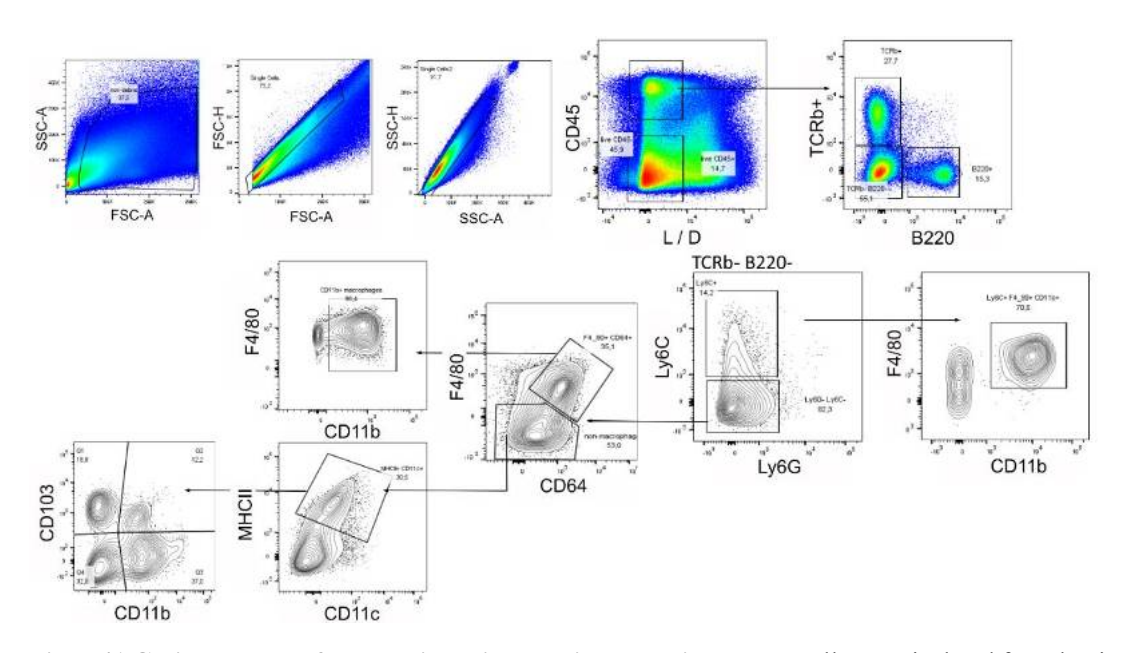


Fig. 5.41 Gating strategy for small intestinal lamina propria cells. SI cells were isolated from lamina propria and gated for living single CD45⁺ cells prior to further gating for B- and T cells, macrophages, Mo-Mac, and cDC. B- and T cells were identified by their expression of B220⁺ and $TCR\beta^+$, respectively. Mo-Mac were identified as Ly6C⁺ Lc6G- F4/80⁺ cells, whereas macrophages were identified as F4/80⁺ CD64⁺ Ly6C- cells, and cDC were identified as MHCII⁺ CD11c⁺ cells. cDC was further divided into three subsets, CD103⁺ CD11b⁺, CD103⁺ CD11b-, and CD103- CD11b⁺ cDC.

Next we focused on the analysis of AhRR expression in the lamina propria by flow cytometry, as AhRR is expressed in the lymphoid and myeloid cell subsets in the lamina propria of AhRR E/E mice (Brandstätter et al., 2016b). It was unknown, however, if the ablation of the three AhR-dependent CYP enzymes and 3MC treatment would further upregulate the AhRR expression in these subsets. The gating strategy is outlined in **Fig. 5.41 Gating strategy for small intestinal lamina propria cells**. The flow cytometry analysis revealed that there was a big variance between the samples and that there were no significant differences in the frequency of cell subsets between PBS- and 3MC-treated mice across all genotypes (**Fig. 5.42 A-E**). Only in the T-cell subset, ablation of either AhRR or the three CYP enzymes appeared to slightly reduce the T-cell frequency.

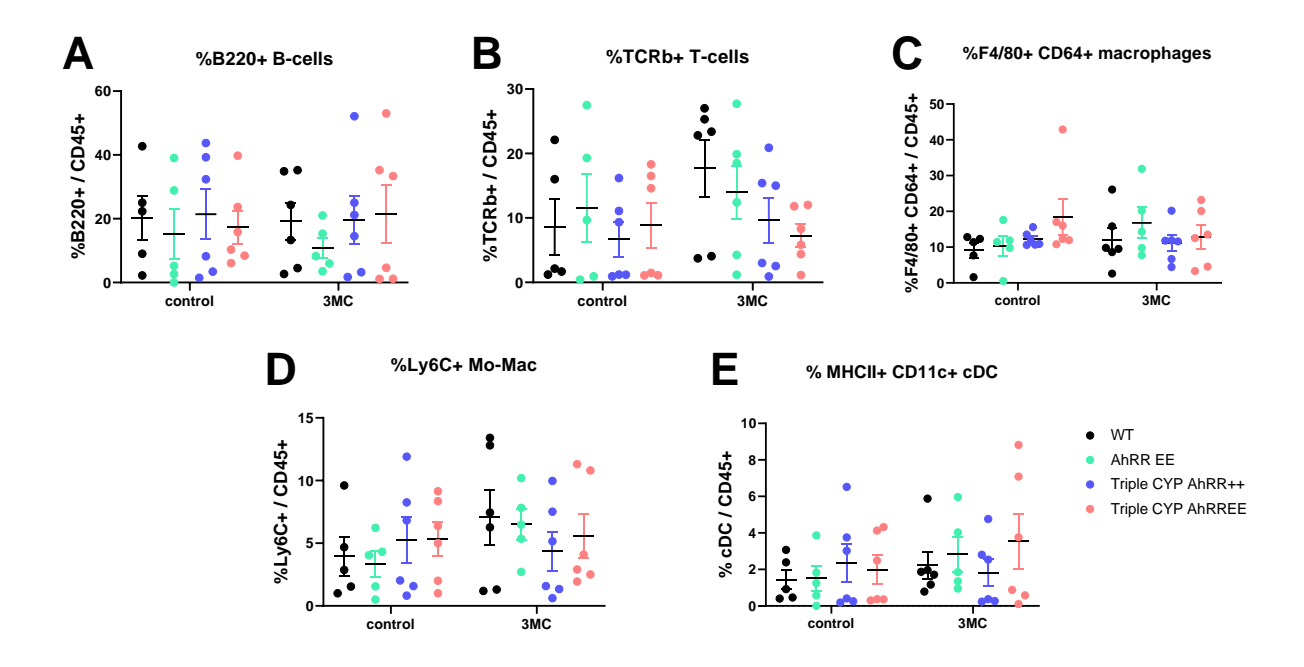


Fig. 5.42 3MC does not alter myeloid and lymphoid cell subsets in SI lamina propria. SI lamina propria cells were isolated from mice that were treated with DMSO as control or 3MC (10mg/kg) by oral gavage for 16 hours. The cells were then gated for B- and T cells, macrophages, Mo-Mac, and cDC. The frequencies of the immune cell subsets were analyzed by flow cytometry. The frequencies of myeloid cells were quantified in relation to the total CD45⁺ cells. Results are shown as mean \pm SEM and significance was analyzed by two-way ANOVA corrected for multiple comparisons by the Bonferroni's method. Data was pooled from two independent experiments (n=5 for AhRR^{E/E} and WT in control group, n=6 for the other genotypes).

In general, AhRR expression was similar comparing the AhRR^{E/E} and Triple CYP-KO AhRR^{E/E} mice in each treatment group across almost all immune cell subsets. In B- and T cells of both AhRR^{E/E} and Triple CYP-KO AhRR^{E/E} mice, 3MC slightly increased the AhRR/EGFP expression (**Fig. 5.43 A & B**), with a higher increase in the latter subset in AhRR^{E/E} mice. In macrophages 3MC significantly increased the AhRR expression in the Triple CYP-KO AhRR^{E/E} mice, whereas in AhRR^{E/E} mice, 3MC only slightly increased the AhRR expression (**Fig. 5.43**

C). In Mo-Mac, the AhRR expression was also significantly increased in Triple CYP-KO AhRR^{E/E} mice, but it remained constant in AhRR^{E/E} mice (**Fig. 5.43 D**). In cDC, the overall frequency of AhRR-expressing cells was low (**Fig. 5.43 E**), and the total cDC frequency was also low (**Fig. 5.42 E**). In terms of AhRR/EGFP fluorescence intensity, there was no difference in MFI across the genotypes and treatment groups in the lymphoid subsets (**Fig. 5.44 A-B**). In macrophages, AhRR MFI was slightly increased in the 3MC-treated Triple CYP-KO AhRR^{E/E}, but not in AhRR^{E/E} mice (**Fig. 5.44 C**). In the Mo-Mac, 3MC caused an increased MFI both in WT and Triple CYP-KO AhRR^{+/+} mice (**Fig. 5.44 D**). This might suggest that 3MC *per se* can cause autofluorescence, as described before (Qin et al., 2002). Lastly, in the cDC subset, 3MC slightly increased the AhRR/EGFP MFI, particularly in AhRR^{E/E} mice (**Fig. 5.44 E**).

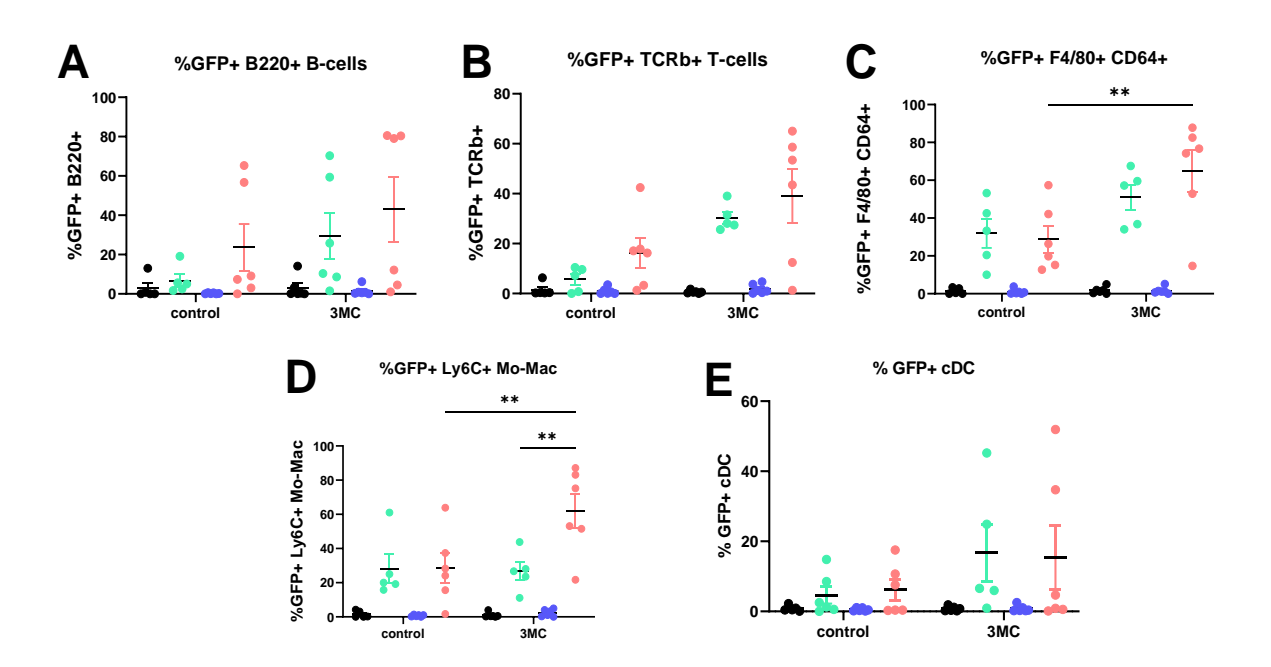


Fig. 5.43 The frequencies of AhRR-expressing macrophages and Mo-Mac were increased by 3MC. The frequencies of AhRR/EGFP-expressing immune cell subsets were analyzed by flow cytometry. Results are shown as mean \pm SEM and significance was analyzed by two-way ANOVA corrected for multiple comparisons by the Bonferroni's method. Data was pooled from two independent experiments (n=5 for AhRR^{E/E} and WT in control group, n=6 for the other genotypes).

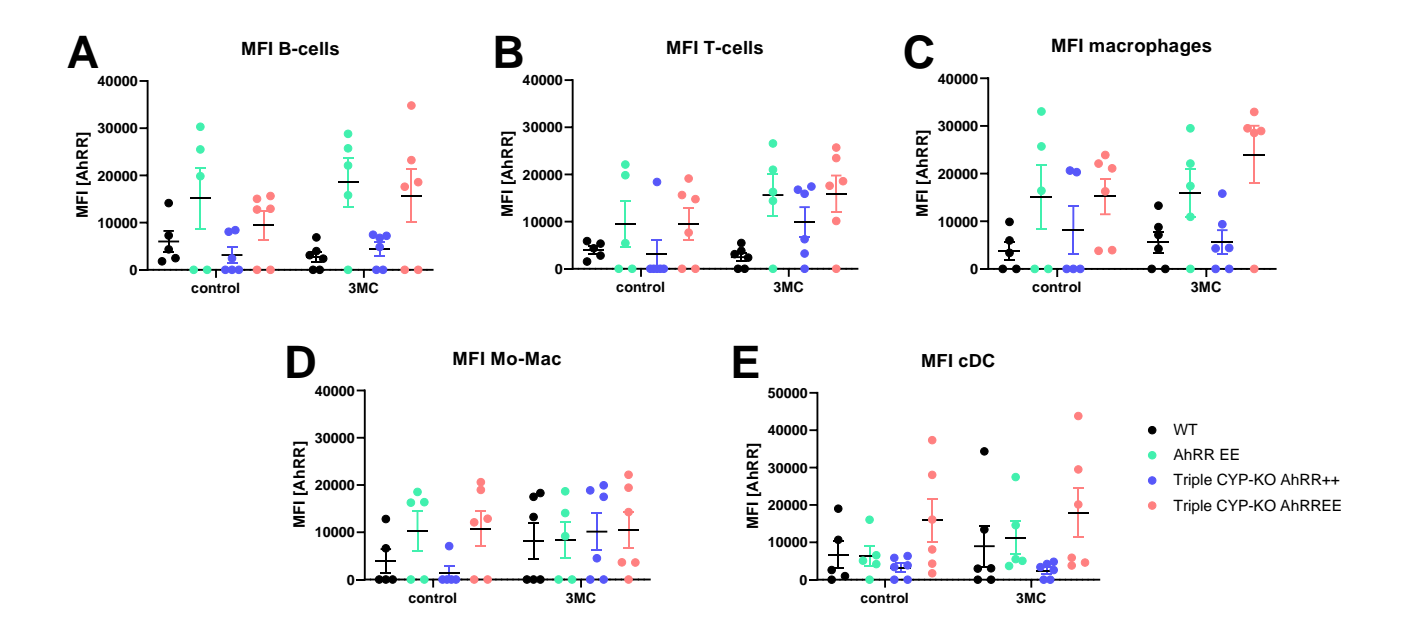


Fig. 5.44 Fluorescence intensity of AhRR-expressing immune cells was not significantly increased by 3MC. The median fluorescence intensity (MFI) of AhRR/EGFP-expressing immune cell subsets were analyzed by flow cytometry. Results are shown as mean \pm SEM and significance was analyzed by two-way ANOVA corrected for multiple comparisons by the Bonferroni's method. Data was pooled from two independent experiments (n=5 for AhRR^{E/E} and WT in control group, n=6 for the other genotypes).

Histological analysis showed that there was an increase in AhRR-expressing cells in 3MC-treated AhRR^{E/E} mice compared to control, as there were more AhRR/EGFP signals at the base of the villi (**Fig. 5.45**). In Triple CYP-KO AhRR^{E/E} mice, 3MC-treatment induced more AhRR/EGFP expression at the pericryptal area, and the intensity appeared higher. However, this observation was based on three sections/animal, hence more sections need to be analyzed and quantified to reach a definitve conclusion. It is also not clear if there are more stromal cells (e.g., fibroblast, telocytes, trophoblasts, and endothelial cells) which upregulated AhRR after 3MC treatment, as it has been shown in the previous chapter that AhRR was also expressed in stromal cells in Triple CYP-KO AhRR^{E/E} mice. In the future, flow cytometry or spatial proteomics would be helpful to quantify and visualize the localization of these AhRR-expressing stromal cell subsets.

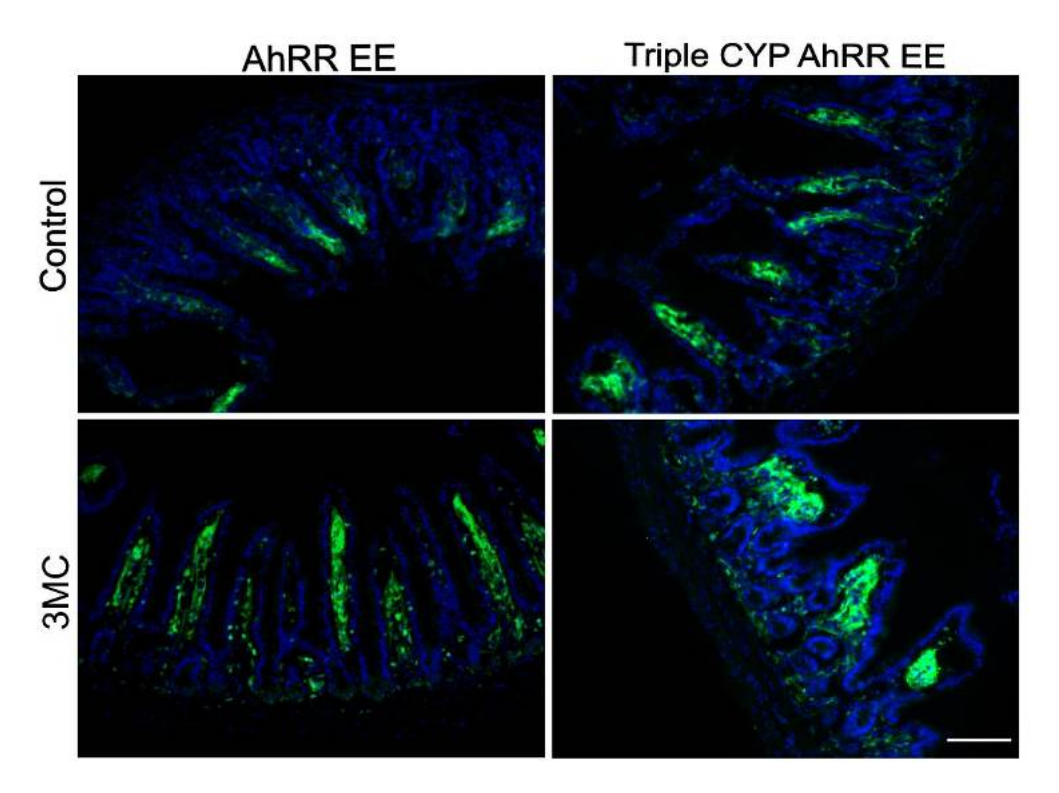


Fig. 5.45 AhRR expression in SI in control and 3MC-treated mice. SI cryosections were retrieved from AhRR^{E/E}, and Triple CYP-KO AhRR^{E/E} mice that had been treated by DMSO (control) or 3MC for 16 hours. Images were taken at 20x magnification with similar exposure time. Scale bar = $100 \mu m$.

5.4.2. AhRR expression in Liver

The liver is the main organ responsible for metabolism of various xenobiotics, due to the strong presence of enzymes of the CYP superfamily (Renaud et al., 2011). Previous findings showed that hepatic AhR activation by a low dose of TCDD is associated with the upregulated expression of genes involved in lipid, glucose, and cholesterol metabolism (Sato et al., 2008). Another possible reason why AhR is thought to be involved in the energy and lipid metabolism of the liver is that its ablation led to spontaneous lipid accumulation and fibrosis in liver (Schmidt et al., 1996; Wada et al., 2016). In contrast, the expression and possible roles of AhRR in liver still remains elusive.

In the previous chapter, it was shown that hepatic expression of AhRR is only observed in the Triple CYP-KO AhRR^{E/E} mice, and it was detected mostly in lymphocytes and also in endothelial cells. This result suggests that the four negative regulators of AhR had to be ablated simultaneously in order to induce AhRR/EGFP expression in some cells of the liver. Therefore, we wondered whether further upregulation of AhR activation by administration of 3MC would be able to enhance AhRR/EGFP expression in the hepatic immune cells or even hepatocytes of Triple CYP-KO AhRR^{E/E} mice, and whether it would also result in a detectable AhRR/EGFP expression in AhRR^{E/E} mice. In addition, expression of AhR and its target genes in liver samples

was examined by qRT-PCR in parallel to ensure that the oral gavage of 3MC (10mg/kg body weight) was able to activate the *Ahr*, hence also increasing the expression of its target genes. AhR activation did not significantly affect *Ahr* transcription level regardless of genotypes, whereas the ablation of the three CYP enzymes and AhRR significantly upregulated the transcription of the *Ahrr* and *Cyp1a1* genes, respectively (**Fig. 5.44**). This result suggests that the oral 3MC treatment was sufficient to induce the expression of AhR target genes. It also showed that in WT mice, *Ahrr* was not upregulated after 16-hour 3MC treatment. Only in Triple-CYP-deficient mice *Ahrr* expression was induced by ~30-fold. *Cyp1a1* expression was already induced in WT mice by 20-fold, and in AhRR^{E/E} mice a ~50-fold upregulation was observed post 3MC-treatment. Moreover, neither the increase of *Ahrr* in Triple CYP-KO AhRR^{+/+} mice nor the increase of *Cyp1a1* in AhRR^{E/E} mice affected the AhR expression levels following the 16-hour 3MC treatment.

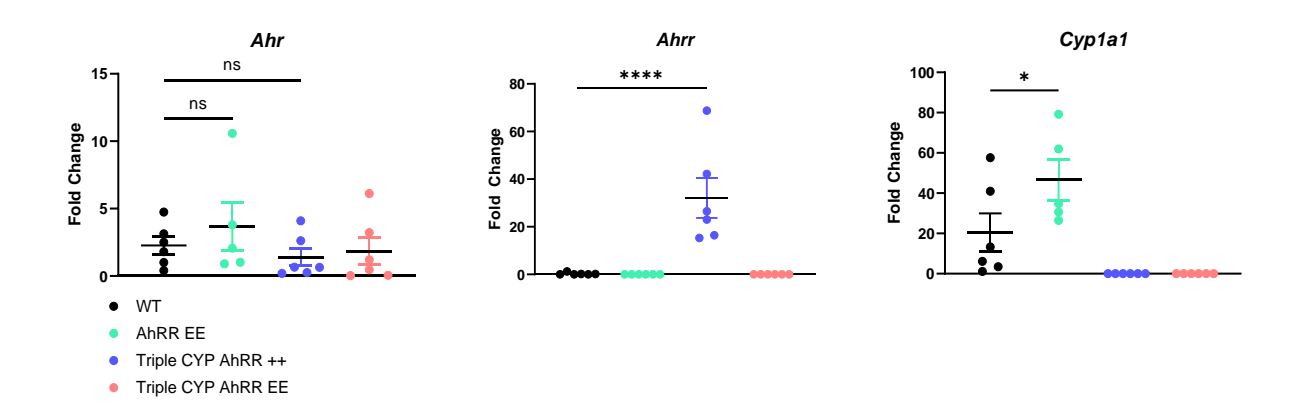


Fig. 5.44. The expression of AhR and its target genes in liver 16 hours post in vivo 3MC treatment. WT, AhRR^{E/E}, Triple CYP-KO AhRR^{+/+}, and Triple CYP-KO AhRR^{E/E} mice were treated with 3MC (10mg/kg) by oral gavage for 16 hours and the expression of AhR and its target genes was analyzed by qPCR. Data was normalized to the expression of the reference gene and to the DMSO-treated control. Gene expression of *Ahr*, *Ahrr*, and *Cyp1a1* is depicted as fold change ($2^{-\Delta\Delta Ct}$). Error bars represent mean \pm SEM. Significance was analyzed by one-way ANOVA corrected for multiple comparisons by the Bonferroni's method, ns = not significant, * p<0,05, **** p<0,0001. Data was pooled from two independent experiments (n=5 for AhRR^{E/E}, n=6 for the other genotypes).

Following the validation of the expression of AhR and its target genes, the AhRR/EGFP expression in the hepatic immune cell subsets and their cell frequencies were also analyzed by flow cytometry after 3MC treatment. For the flow cytometric analysis, livers of 8-week-old naïve mice treated with PBS or 3MC for 16 hours were isolated to generate single cell suspensions. Then, the frequencies of NKT-, T cells, NK cells, as well as KC, cDC1 & cDC2 were analyzed. The gating strategy is shown in **Fig. 5.47**. The myeloid subset was first gated by the lack of CD19 and NK1.1 expression. Then, KC were identified as CD11b^{int} F4/80^{hi} Tim4⁺ CD31- and cDCs were identified as Ly6^{lo} MHCII⁺ CD11c^{hi}. Mo-Mac subsets were divided into two subpopulations, based on the expression of F4/80 and Ly6C; either as F4/80⁺ Ly6C⁺ CD11b⁺ or

F4/80⁺ Ly6C- CD11b⁺. Moreover, Mo-Mac can lose their Ly6C expression as they get settled in an organ (Zhang *et al.*, 2018). Monocytes were identified as Ly6C⁺ MHCII⁺/-. Lastly, cDC were identified as Ly6C- MHCII⁺ CD11c^{hi}. The cDC subsets were distinguished by the expression of either CD11c or CD11b, but their frequencies were low (< 0.5 %) (data not shown), hence they were not included in this analysis.

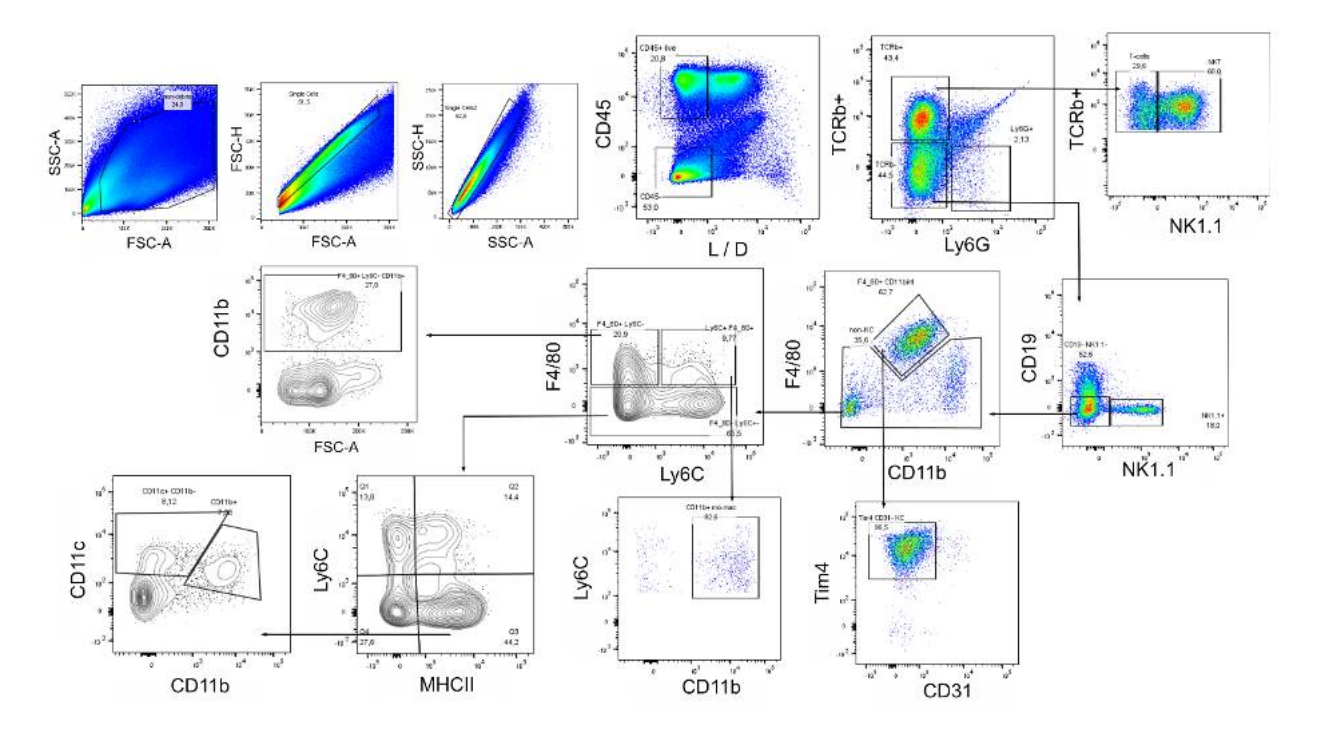


Fig. 5.47 Gating strategies for myeloid and lymphocyte subsets in the liver. Liver cells were isolated from 8-week-old mice treated with either DMSO as control or 3MC. Cells were then gated for living single CD45⁺ cells. T cells were identified as $TCRβ^+$ NK1.1- cells, whereas NKT cells were $TCRβ^+$ NK1.1⁺ cells. KC were identified as $CD11b^{int}$ F4/80^{hi} Tim4⁺ CD31-, whereas monocyte-derived macrophages (Mo-Mac) were defined either as F4/80⁺ Ly6C⁺ CD11b⁺ or F4/80⁺ Ly6C- CD11b⁺. The monocyte population was identified as Ly6C⁺ MHCII⁺/-. cDC were identified as Ly6C⁻ MHCII⁺ CD11c^{hi}. The two cDC subsets were distinguished by the expression of CD11c and CD11b.

Regarding the frequencies of various cell subsets in the liver, there was no significant difference across all genotypes in general in both the control- and 3MC-treated group. However, there were tendencies that the deletion of the three AhR-dependent CYP enzymes mediated a decrease in NKT cells, one of the most predominantly expressed immune cell subsets in the liver (Fig. 5.48 A). The ablation of AhRR alone also seemed to slightly decrease the T-cell subset in both treatment groups (Fig. 5.48 B), whereas the ablation of either AhRR or the three CYP enzymes tended to increase the NK cells in the control, but not in the 3MC group (Fig. 5.48 C). In the myeloid subsets, the cell frequencies were much lower than that of lymphocytes (Fig. 5.48 D-G) and there was also no difference in frequencies across all genotypes. An increase in neither monocytes nor Mo-Mac was observed post 3MC treatment, which makes sense as the mice did not undergo chronic inflammation that can lead to monocyte recruitment from the blood and to

an increase in Mo-Mac in the liver (Shi & Pamer, 2011). Hence, there was no inherent difference caused by the ablation of AhRR and/or the three CYP enzymes and the 16-hour 3MC treatment also did not alter the frequencies of immune cell subsets regardless of genotypes. Moreover, this result also differed from the one shown in Chapter 3 (**Fig.5.15** in Chapter 3), as there was a significant increase in the cDC2 frequency in AhRR^{E/E} mice compared to WT mice. However, caution needs to be exercised when comparing the immune cell frequencies from these two experiments, as the liver processing method for this experiment differs from the one used in Chapter 3.

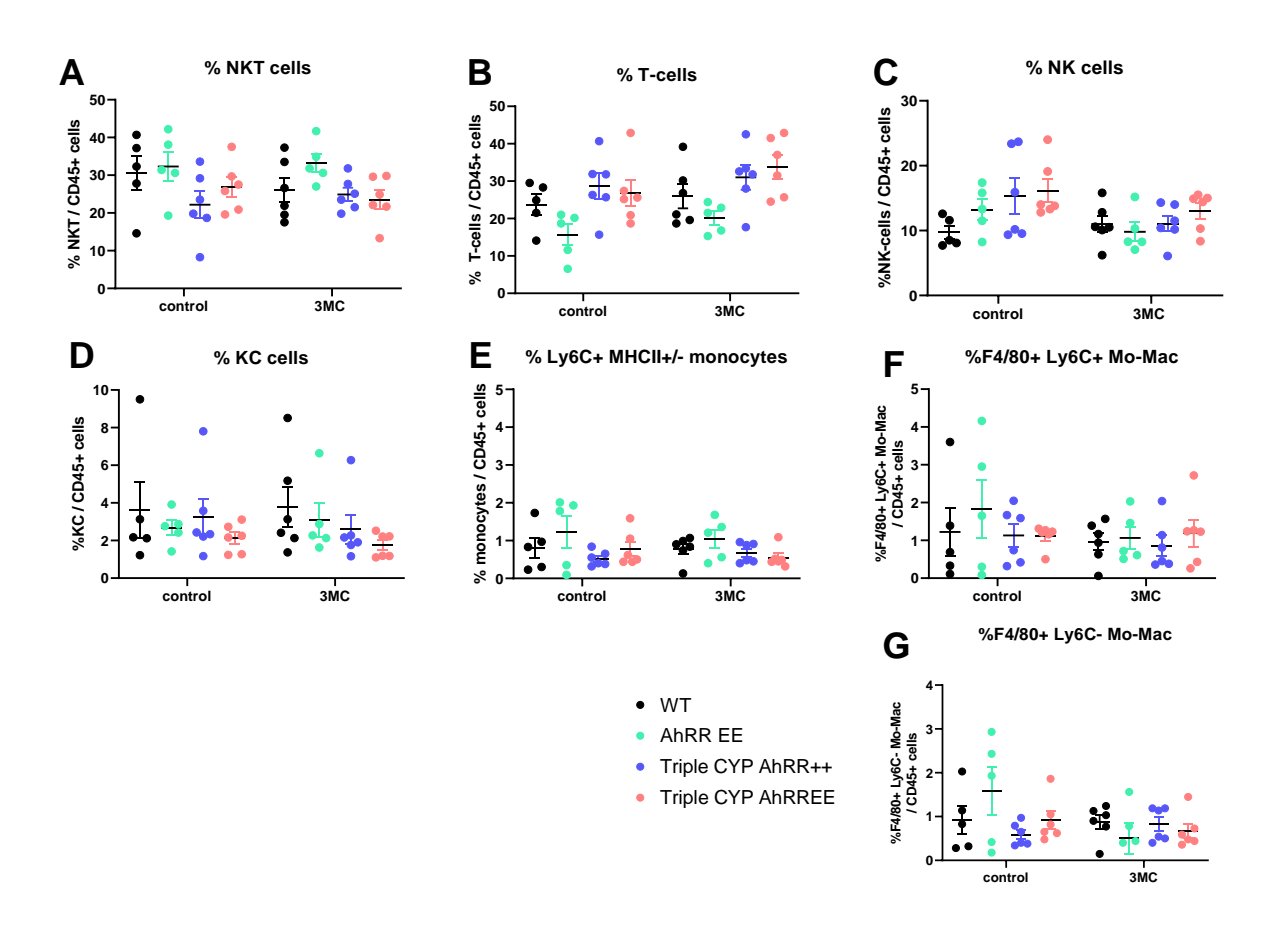


Fig. 5.48 Acute 3MC treatment did not cause significant differences in frequencies of lymphocytes and myeloid subsets in the liver. NKT-, T cells, NK cells, as well as KC, cDC1 & cDC2 were isolated from 8-week old naïve mice that were treated with control and 3MC (10 mg/kg) by oral gavage for 16 hours. The frequencies of the immune cell subsets were analyzed by means of flow cytometry. The frequencies of myeloid cells were quantified out of the total CD45⁺ cells. Results are shown as mean \pm SEM and significance was analyzed by two-way ANOVA corrected for multiple comparisons by the Bonferroni's method. * p<0,5. Data was pooled from two independent experiments (n=5 for AhRR^{E/E} and WT in control group, n=6 for the other genotypes).

Regarding AhRR/EGFP expression, the result for the untreated control group was consistent with the previous experiment shown in chapter 3 in which AhRR/EGFP was expressed only in cell subsets of Triple CYP-KO AhRR^{E/E} mice. Furthermore, in line with the qRT-PCR result (**Fig. 5.44**), the ablation of the three CYP enzymes could significantly upregulate AhRR also on the protein level. The-3MC treatment significantly increased the AhRR/EGFP expression in Triple

CYP-KO AhRR^{E/E} mice in almost all immune cell subsets (Fig. 5.49 A-G). Nevertheless, the magnitude of this increase differed from one subset to the others. For instance, the EGFP expression in NKT cells was 15 times higher in the 3MC-treated Triple CYP-KO AhRR^{E/E} mice (Fig. 5.49 A), whereas in T cells the increase was ~6 times higher (Fig. 5.49 B). In NK cells, the AhRR/EGFP expression was already high in the control group and 3MC further induced it ~20 times (Fig. 5.49 C). In KC, there was also a ~6 times higher upregulation, but again, a high variance was observed in the 3MC group, therefore, the difference was not significant (Fig. 5.49 **D)**. In monocytes, as well as Ly6C⁺ and Ly6C⁻ Mo-Mac, a 30-50-fold upregulation was observed (Fig. 5.49 E-G). This strong increase should, however, be put into perspective considering the overall low cell numbers of these cell subsets as they only made up < 2% of the total immune cells in the liver as shown in Fig. 5.48 E-G. In AhRR^{E/E} mice, in some immune cell subsets such as T cells, Ly6C⁺ monocytes, as well as Ly6C⁺ and Ly6C- Mo-Mac (**Fig. 5.49 B,E,F, and G**), a slight increase of AhRR/EGFP expression was observed. In T cells, there were 2 times more AhRR-expressing cells in the 3MC group (Fig. 5.49 B), whereas in the monocyte and the two Mo-Mac subsets, a 10-20-fold upregulation was observed (Fig. 5.49 E-G). Furthermore, the MFI of the AhRR/EGFP-expressing cells was measured (Fig. 5.49 G-I). Interestingly, in NKT- and T cells, 3MC could enhance the MFI of the AhRR/EGFP reporter in AhRR^{E/E} mice to a level that was comparable with the one of Triple CYP-KO AhRR^{E/E} mice (Fig. 5.49 G and H), but such an increase was not observed in NK cells (Fig. 5.49 I). Taken together, the FACS analysis further proved that the 3MC treatment increased AhR activation, hence also AhRR expression.

The histological analysis in the previous chapter showed that there AhRR/EGFP expression occurs in endothelial cells that partially expressed PECAM/CD31 or LYVE1 (blood and lymph vessel markers) in some of the intrahepatic vessels of Triple CYP-KO AhRR^{E/E} mice but not in AhRR^{E/E} mice. Thus, it was interesting to assess if 3MC treatment would also increase the AhRR/EGFP expression in these endothelial cells in both Triple CYP-KO AhRR^{E/E} mice and in AhRR^{E/E} mice. In contrast to the enhanced AhRR/EGFP expression in the immune cell subsets, there appeared to be no AhRR/EGFP expression in liver endothelial cells in either AhRR^{E/E} mice or Triple CYP-KO AhRR^{E/E} mice after 3MC treatment (**Fig. 5.50**). However, it is important to note that only 5 sections were analyzed qualitatively, and quantitative analysis of the CD45⁻ cells from at least one liver lobe needs to be conducted. Lastly, 3MC treatment did not induce AhRR expression in hepatocytes (**Fig. 5.50**).

Results

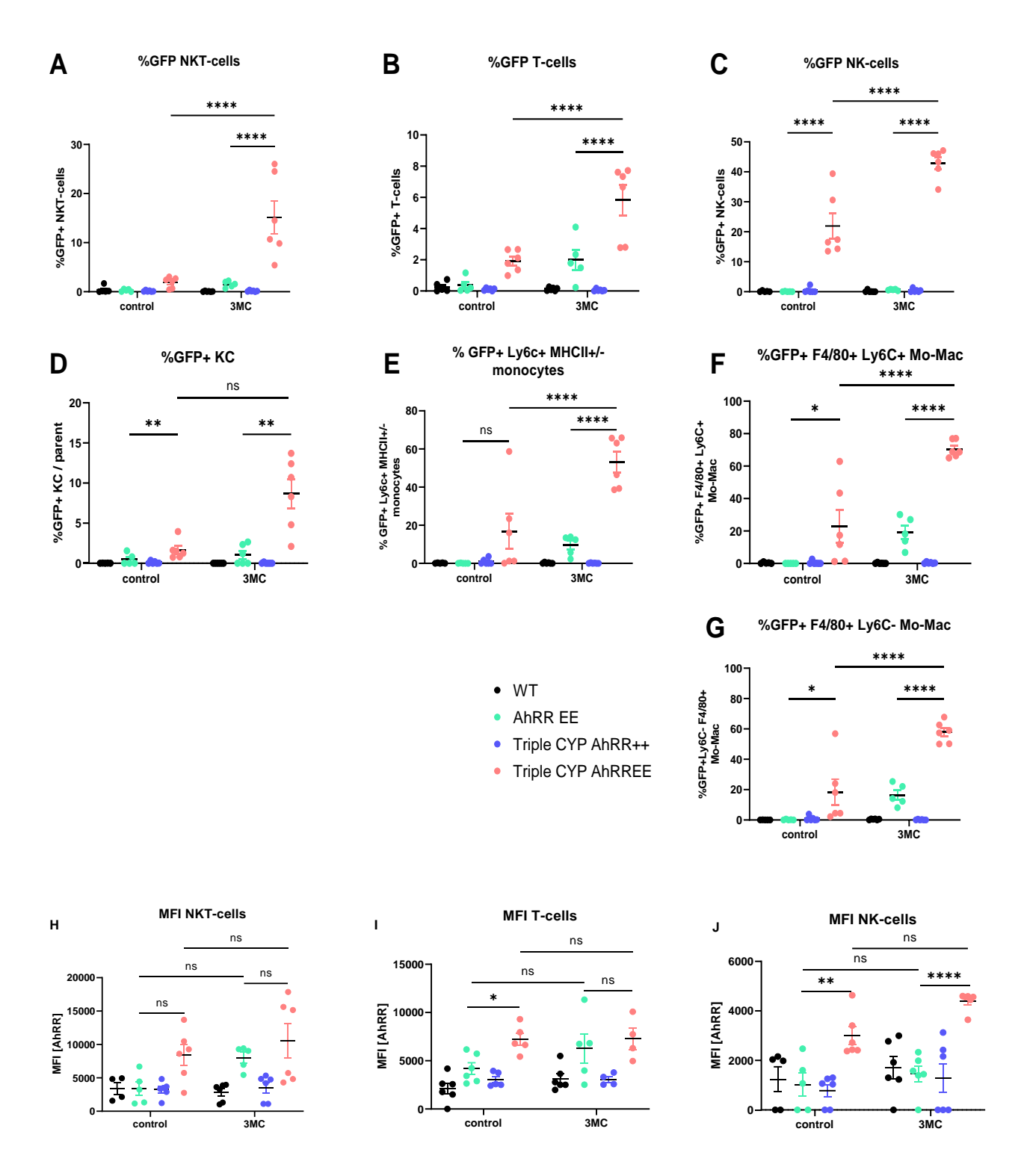


Fig. 5.49 Acute 3MC-treatment increased the frequencies and the MFI of AhRR-expressing immune cells in the liver. The frequencies of EGFP⁺ cells from lymphocytes and myeloid subsets (A-F), as well as the median fluorescence intensity (MFI) of the AhRR/EGFP expression were analyzed by flow cytometry. Results are shown as mean \pm SEM and significance was analyzed by two-way ANOVA corrected for multiple comparisons by the Bonferroni's method. ** p<0,01, *** p<0,001, **** p<0,0001. Data was pooled from two independent experiments (n=5 for AhRR^{E/E} and WT in control group, n=6 for the other genotypes).

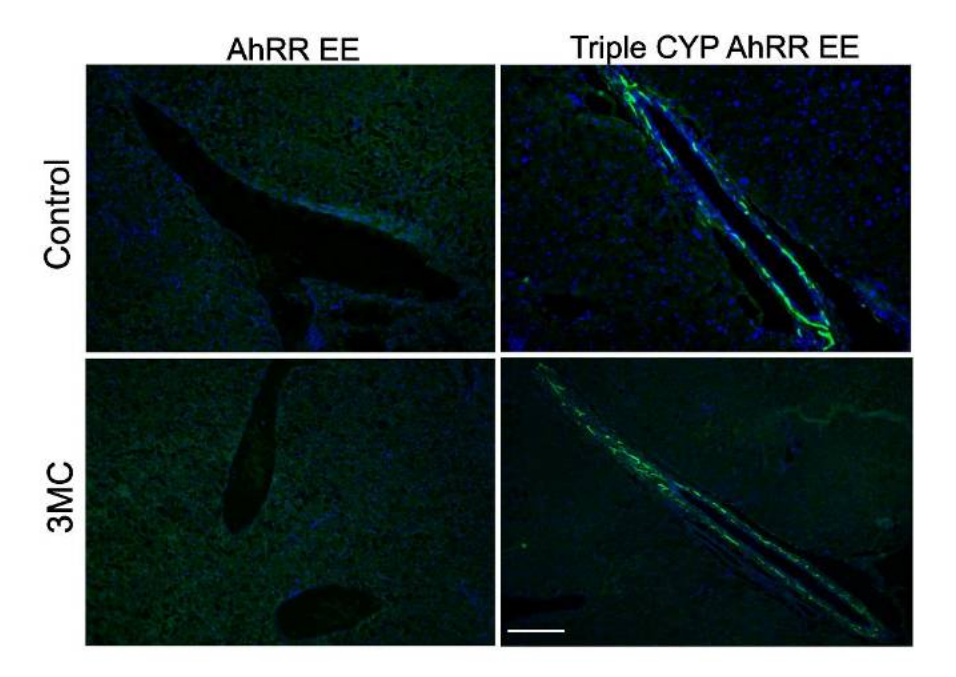


Fig. 5.50 3MC does not enhance AhRR expression or its intensity in intrahepatic vessels. One lobe of the liver of the DMSO- and 3MC-treated mice was embedded and cryosections were prepared. Images were taken at 20x magnification with similar exposure time Scale bar = $100\mu m$.

5.4.3. AhRR expression in gonadal white adipose tissue (WATg)

Apart from xenobiotic metabolism, the AhR is thought to play a role in modulating energy metabolism, as it is highly expressed in metabolically active tissues, e.g. liver or adipose tissue. It has been shown that AhR activation mediated by a 28-day-TCDD-stimulation led to reduced glucose uptake by pancreatic and adipose tissue, possible due to a reduction in glucose transport proteins (Enan et al., 1992, Sayed et al., 2022). As the localization of AhRR expression in adipose immune cells and its function in this tissue is still unknown, we investigated the influence of 3MC on AhR signaling in immune cells in WATg, by quantifying AhRR expression and immune cell frequencies in this tissue.

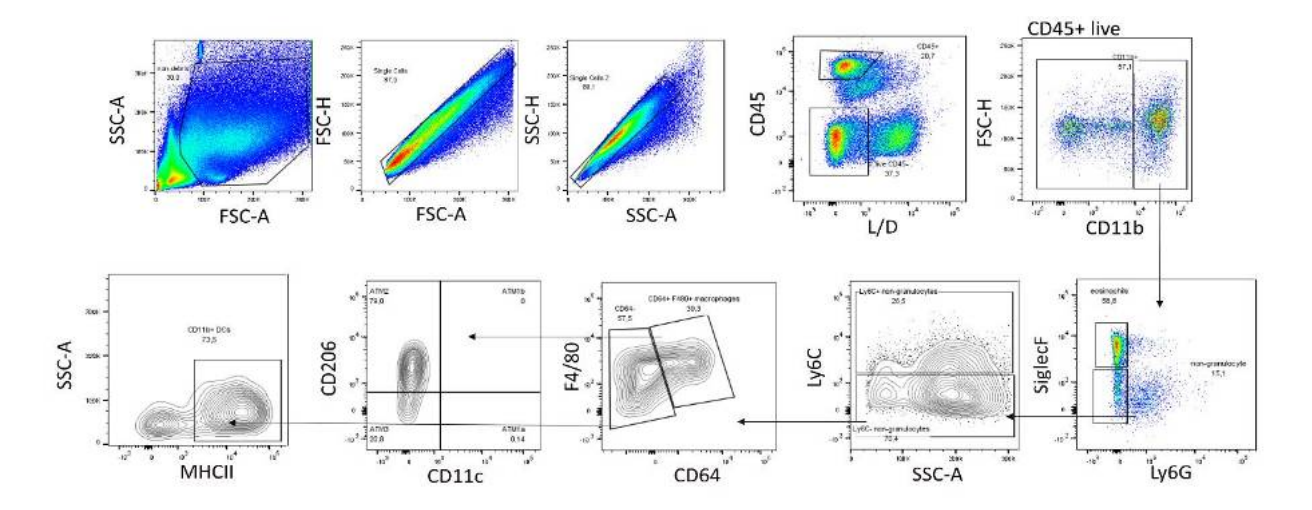


Fig. 5.51 Gating strategy of myeloid subsets in the SVF of WATg. The stromal vascular fraction (SVF) was isolated from WATg of 8-week-old mice treated with either DMSO only or 3MC and the samples were gated for living single CD45⁺ cells. Then, eosinophils were identified as CD11b⁺ SiglecF⁺ Ly6G- cells, monocytes were identified as Ly6C⁺ cells, whereas macrophages were identified as F4/80⁺ CD64⁺ cells. They were further divided into 4 subsets: ATM 1a, b, 2, and 3. ATM 1a and 1b were identified as CD11c⁺ CD206- and CD206⁺ cells, respectively. ATM 2 were defined as CD206⁺ CD11c- cells, whereas ATM 3 were defined as CD206- CD11c- cells. cDCs were identified as CD11b^{+/-} F4/80^{lo} CD64- MHCII⁺ cells.

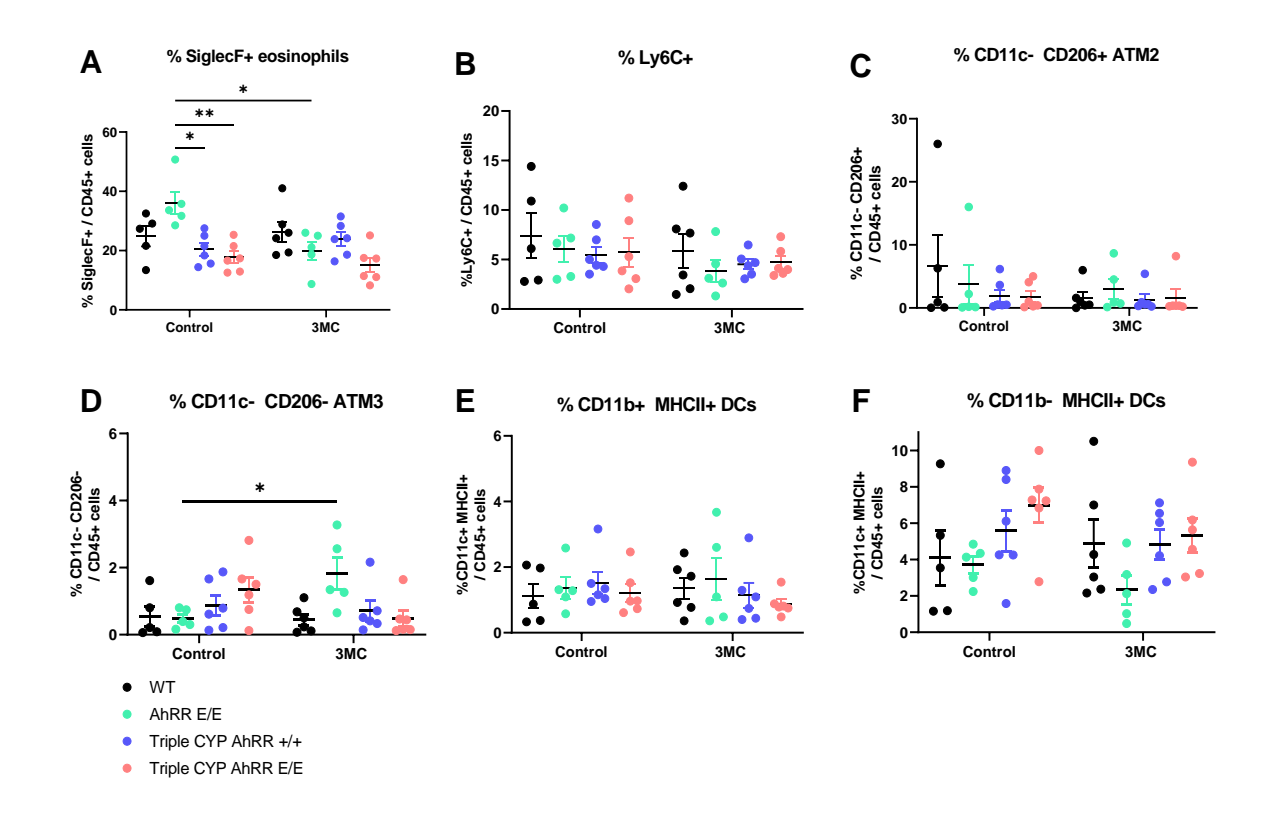


Fig. 5.52 3MC increased the frequency of ATM3 in AhRR^{E/E} mice in WATg. The stromal vascular fraction (SVF) was isolated from WATg of 8-week old mice treated with either DMSO only as control or with 3MC. Then, cells were stained for A) eosinophils, B) monocytes, C-D) ATMs, and E-F) DC and were analyzed by flow cytometry. Results are shown as mean \pm SEM and significance was analyzed by two-way ANOVA corrected for multiple comparisons by the Bonferroni's method. * p<0,05, ** p<0,01. Data was pooled from two independent experiments (n=5 for AhRR^{E/E} and control WT, n=6 for the other genotypes).

As shown in the immune cells of liver and SI, AhRR expression in the mice following 16-hour 3MC- or DMSO treatment was investigated. To test the effect of 3MC on AhRR expression in WATg, the SVF of WATg was isolated and the resulting cell suspension was analyzed by flow cytometry. As the mice used were lean 8-week-old female mice, the availability of WATg was limited, hence only analysis of the myeloid cell subset was conducted. The gating strategy used for this experiment is shown in **Fig. 5.51**. Following the exclusion of debris, dead, and CD45-cells, the immune cells were identified. Eosinophils were identified as CD11b⁺ SiglecF⁺ Ly6G-cells, monocytes were identified as Ly6C⁺ cells, and Adipose Tissue Macrophages (ATM) were identified as F4/80⁺ CD64⁺ cells. They were further divided into 4 subsets: ATM1a, b, 2, and 3. ATM 1a and 1b were identified as CD11c⁺ CD206- and CD206⁺, respectively. ATM2 were defined as CD206⁺ CD11c- cells, whereas ATM3 were defined as CD206- CD11c- cells. cDCs were identified as CD11b^{+/-} F4/80^{lo} CD64⁻ MHCII⁺ cells.

Analysis of immune cells in WATg revealed that the frequency of eosinophils was markedly decreased in the 3MC-treated AhRR^{E/E} mice; whereas in the untreated control group, the eosinophil frequency in AhRR^{E/E} mice was significantly higher compared to the Triple CYP-KO AhRR^{E/E} mice (**Fig. 5.52**). In contrast, there was no alteration in the frequencies of Ly6C⁺ monocytes and CD206 ATM (**Fig. 5.52 B and C**). The frequency of CD206⁻ ATM was upregulated in 3MC-treated AhRR^{E/E} mice (**Fig. 5.52 D**). For the two cDC subsets, no significant difference in terms of cell frequency was observed, both between genotypes and treatment groups (**Fig. 5.52 E and F**). Nevertheless, in the CD11b⁻ cDC subset, the frequencies in the control-treated Triple CYP-KO AhRR^{E/E} mice were slightly increased compared to WT, but such an increase was not observed in the 3MC-treated group. In this group, the cell frequency in the AhRR^{E/E} mice was also slightly reduced compared to WT mice (**Fig. 5.52 F**).

The AhRR/EGFP reporter was expressed with varying frequencies in DMSO-treated Triple CYP-KO AhRR^{E/E} control mice, whereas it was barely expressed in DMSO-treated AhRR^{E/E} control mice (**Fig. 5.53** A-F). Overall, 3MC could significantly increase the AhRR/EGFP⁺ cells in both Triple CYP-KO AhRR^{E/E} and AhRR^{E/E} mice. The 3MC treatment could significantly increase the AhRR-expressing eosinophil subset by ~10% in Triple CYP-KO AhRR^{E/E} mice, but no significant upregulation was observed in AhRR^{E/E} mice (**Fig. 5.53** A). In the rest of the myeloid subsets, 3MC significantly increased the AhRR/EGFP expression in both AhRR^{E/E} and Triple CYP-KO AhRR^{E/E} mice. In the monocyte subset, the frequencies of EGFP-expressing cells in AhRR^{E/E} and Triple CYP-KO AhRR^{E/E} mice markedly increased by ~60% and 50%,

respectively (**Fig. 5.53 B**). In the ATM2 and ATM3 macrophage subsets, 3MC increased the frequency of AhRR-expressing macrophages in AhRR^{E/E} and Triple CYP-KO AhRR^{E/E} mice by ~60% and ~30%, respectively (**Fig. 5.53 C and D**). Similarly, in the CD11b⁺ DC subset, the AhRR/EGFP⁺ cells frequencies increased by ~50% in the AhRR^{E/E} and Triple CYP-KO AhRR^{E/E} mice (**Fig. 5.53 E**). In the CD11b⁻ subset, the AhRR/EGFP⁺ cell frequencies increased by 30% in the AhRR^{E/E} and 50% in Triple CYP-KO AhRR^{E/E} mice (**Fig. 5.53 F**).

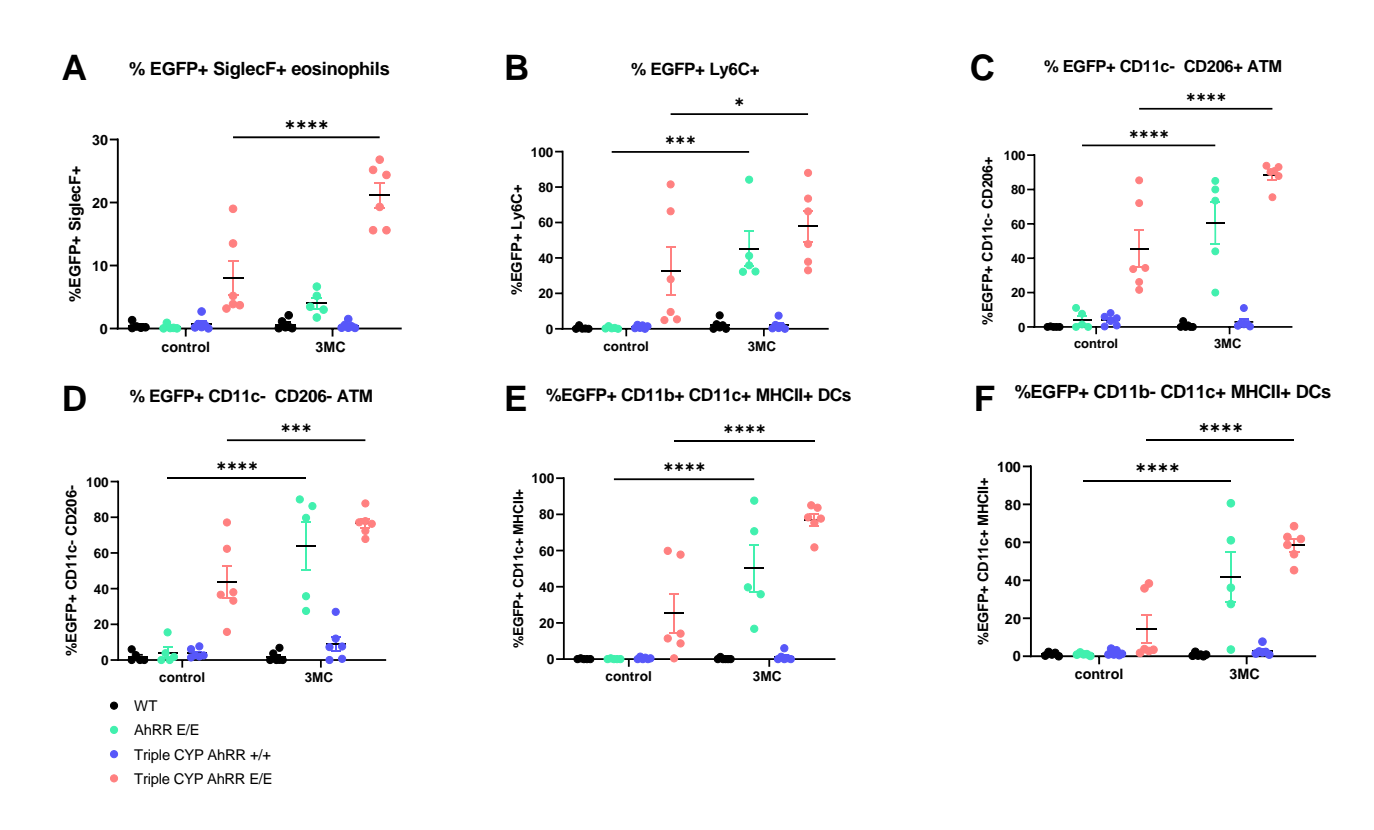


Fig. 5.53 3MC significantly increases the frequency of AhRR-expressing eosinophils in Triple CYP-KO AhRR^{E/E} mice in WATg. The frequencies of AhRR/EGFP-expressing myeloid cells from each subset were quantified. Percentages of EGFP⁺ cells were calculated from the total cell number of each subset. Results are shown as mean \pm SEM and significance was analyzed by two-way ANOVA corrected for multiple comparisons by the Bonferroni's method. **** p<0,0001. Data was pooled from two independent experiments (n=5 for AhRR^{E/E} and WT in control group, n=6 for the other genotypes).

Apart from increasing the frequencies of the AhRR/EGFP-expressing cells, 3MC treatment also increased the MFI of AhRR in some of the myeloid cell subsets in both Triple CYP-KO AhRR^{E/E} and AhRR^{E/E} mice (**Fig. 5.54 A-F**). For instance, the MFI of AhRR/EGFP was markedly increased in the eosinophil subset in the 3MC group, but not in Triple CYP-KO AhRR^{E/E} mice (**Fig. 5.54 A**). In monocytes, the MFI was only slightly increased in 3MC-treated AhRR^{E/E} and Triple CYP-KO AhRR^{E/E} mice (**Fig. 5.54 B**). In the ATM2 subset, the AhRR MFI significantly increased in the 3MC- treated Triple CYP-KO AhRR^{E/E} mice, and to a lesser extent also in AhRR^{E/E} mice (**Fig. 5.54 C**). Here, the MFI between the two aforementioned genotypes in the

3MC group also differed significantly. In the ATM3 subset, the difference in the MFI of AhRR/EGFP between control- and 3MC-treated Triple CYP-KO AhRR^{E/E} and AhRR^{E/E} mice was not significant (**Fig. 5.54 D**), but the MFI between the Triple CYP-KO AhRR^{E/E} and AhRR^{E/E} mice in the 3MC group was. In CD11b⁺ DC, 3MC significantly increased the AhRR MFI in both Triple CYP-KO AhRR^{E/E} and AhRR^{E/E} mice (**Fig. 5.54 E**). In CD11b⁻ DC, high variances in AhRR/EGFP MFI across all genotypes and treatment groups were observed and there was also a high background noise in WT and Triple CYP-KO AhRR^{+/+} mice in both treatment groups (**Fig. 5.54 F**).

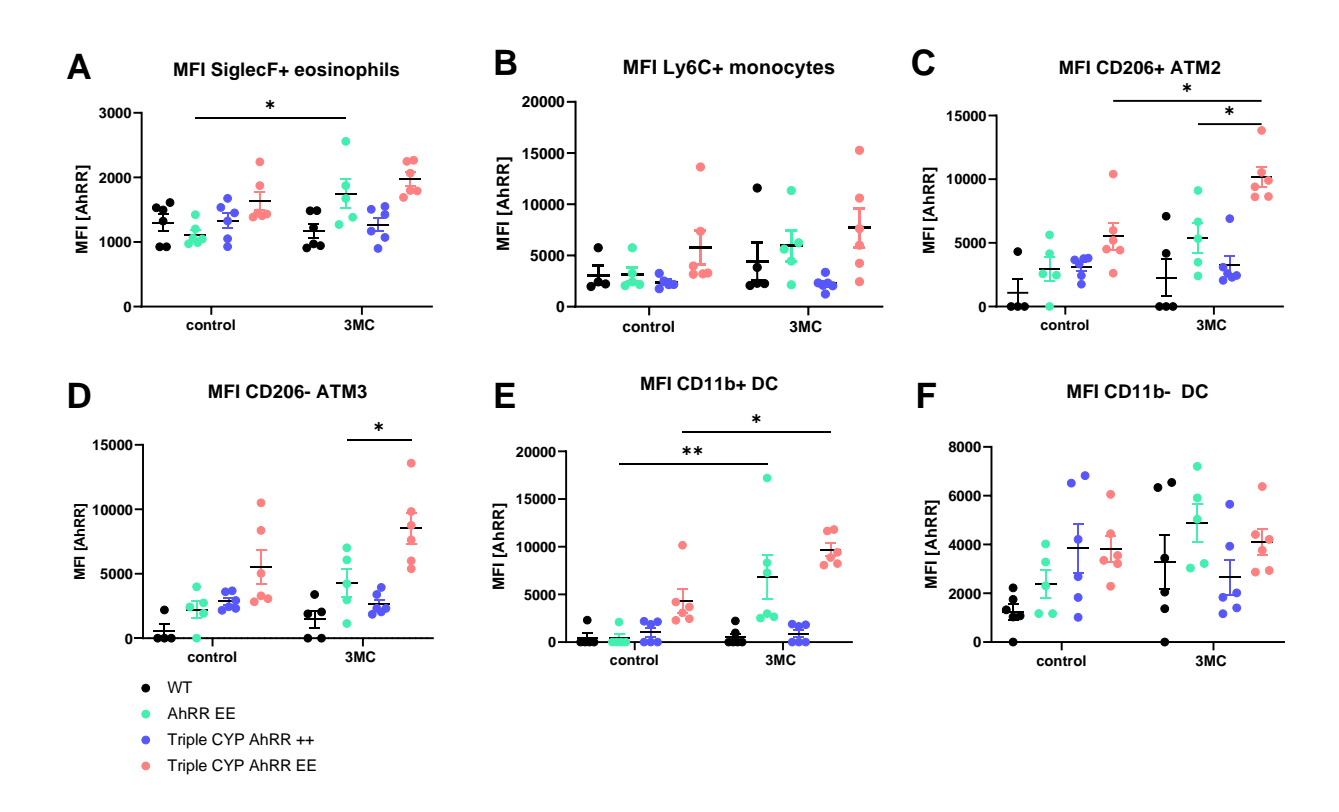


Fig. 5.54 3MC enhances the MFI of AhRR/EGFP expression of some of the myeloid cell subsets in WATg. Median Fluorescence Intensity (MFI) of AhRR/EGFP from each myeloid subset were quantified. Results are shown as mean \pm SEM and significance was analyzed by two-way ANOVA corrected for multiple comparisons by the Bonferroni's method. **** p<0,0001. Data was pooled from two independent experiments (n=5 for AhRR^{E/E} and WT in control group, n=6 for the other genotypes).

Aside from analyzing the AhRR/EGFP expression by means of flow cytometry, histologic analysis was conducted. Cryosections generated from gelatin embedded WATg samples were mounted and visualized using an epifluorescence microscope. However, the attempt to perform this analysis was challenging, as the tissue was delicate and there was a high autofluorescence observed in the WATg of mice from all genotypes. Hence, determining the true EGFP signal was hard. Nevertheless, 3MC treatment did not appear to increase the EGFP signal and a real EGFP signal appears to only be found in the Triple CYP-KO AhRR^{E/E} mice (**Fig. 5.55**). Nevertheless,

since AhRR is mostly expressed in immune cells, it could also be that the presence of adipocytes on tissue level made the increase of AhRR expression in immune cells less noticeable, due to their bigger size. Previous imaging analyses of WATg and WATi cryosections in our lab using a confocal microscope have also shown that the AhRR/EGFP signal was only found in Triple CYP-KO AhRR^{E/E} mice (data not shown). Thus, visualizing the tissues with a confocal microscope would be advantageous in the future to minimize the high autofluorescence and to determine if 3MC treatment increases EGFP expression in Triple CYP-KO AhRR^{E/E} and AhRR^{E/E} mice. It would also be interesting to stain for stromal cell and pre-adipocytes markers, to see if EGFP expression is also enhanced in these subsets following 3MC treatment.

Taken together, 16-hour in vivo 3MC treatment was sufficient to increase the frequencies and MFI of AhRR/EGFP-expressing myeloid cells in WATg, as well as to modify the frequency of eosinophils and ATM3 in AhRR^{E/E} mice. This result now raised the question whether enhanced AhR signaling would also alter immune cell subsets and function in a metabolically altered state.

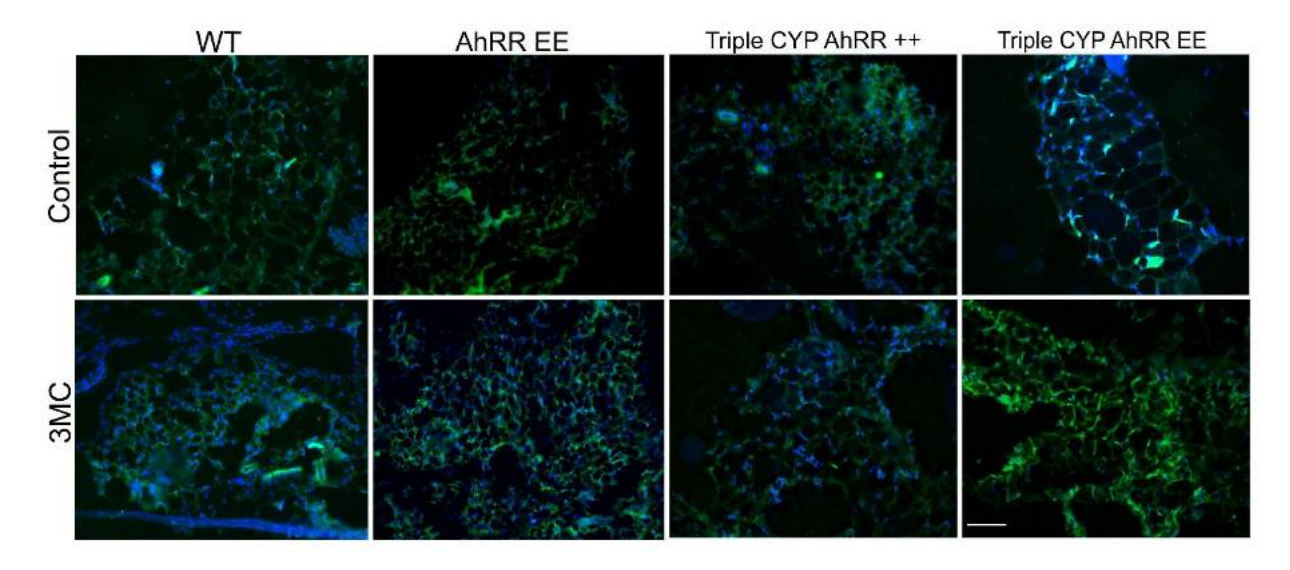


Fig. 5.55 Tissue autofluorescence was observed in the cryosections of WATg. Expression of AhRR/EGFP in WT, AhRR^{E/E}, Triple CYP-KO AhRR^{+/+}, and Triple CYP-KO AhRR^{E/E} mice treated with DMSO (control) or 3MC. Immunofluorescence stainings of WATg cryosections counterstained for C) CD31 and LYVE-1, D) Tim4 and F4/80. All Images were taken at 20x magnification and scale bar = $100\mu m$.

5.5. Modulation of AhR signaling and immune cell frequencies in diet-induced obesity

Several publications already showed that AhR signaling mediates diet-induced obesity (DIO) in rodents, as complete ablation of AhR prevented weight gain and also protected against liver fibrosis and insulin resistance (da Silva et al., 2022; Kerley-Hamilton et al., 2012; Moyer et al., 2016; Rojas et al., 2021; C. Wang et al., 2011). In line with these findings, mice carrying the high-affinity AhR allele had higher weight gain and more gonadal fat mass, following 28-week

WWestern diet feeding than mice carrying the low-affinity allele (Kerley-Hamilton et al., 2012). Exposure to AhR ligands such as TCDD and dioxin-like PCBs also correlated with an increased risk for diabetes (Alonso-Magdalena et al., 2011). Findings from our lab have shown that similar to AhR, loss of AhRR was also sufficient to protect from weight gain and glucose intolerance (unpublished data). To further elucidate the involvement of AhR signaling in DIO, other AhR target genes, such as those encoding the three AhR-dependent CYP enzymes were also ablated. Mice lacking AhRR and/or the three CYP enzymes were fed for 14 weeks with either high-fat diet (HFD) with 60 kJ% lard content or the matching control diet (CD), an isocaloric diet with only 10 kJ% fat content. Both, HFD and CD are purified diets that contain less AhR-activating phytochemicals comparable to the ligand-reduced diet used by Schanz et al., 2020 (Schanz et al., 2020b). Furthermore, the three CYP enzymes are also involved in lipid metabolism by mediating lipid mediator biosynthesis and their ablation also reduced neutrophil numbers in the peritoneal cavity following zymosan treatment (Divanovic et al., 2013), which may also help resolving adipose tissue inflammation in DIO (Lopategi et al., 2016). Thus, it would be interesting to know if dysregulation in lipid mediator synthesis by the absence of the CYP-enzymes would influence the course of DIO.

The aims of this experiment were to investigate if the ablation of the three AhR-dependent CYP enzymes and/or AhRR would alter the physiology, cellularity of the tissue, and gene expression levels in the context of DIO. In addition, we analyzed whether the deficiency of the CYP-enzymes would enhance AhR signaling in the presence of limited supply of AhR ligands. Hence, body and organ weights, blood glucose as well as liver enzymes and cholesterol markers in the serum were measured. Apart from that, the frequencies of the immune subsets, as well as the AhRR expression in these subsets in SI, liver, and WATg were also analyzed.

5.5.1. Physiological alterations induced by high fat diet

Mice aged 8-10 weeks old were fed with either HFD or CD for 14 weeks. The mice were weighed and scored every week. At the 12-week-mark, a glucose tolerance test was performed, in which mice were injected with 250mg/mL glucose i.p (8μL/g bodyweight) and their blood glucose levels were measured first within 15-minute-, then within 30-minute intervals up to 150 minutes post glucose challenge (**Fig. 5.56 A**).

Ablation of AhRR and/or the three AhR-dependent CYP enzymes led to systemic physiological alterations. The body weight measurements indicated that the HFD feeding worked, as HFD-fed mice gained anywhere from 10-18g more weight, compared to the CD-fed mice at the end of week 14. The result also confirmed previous experiments done in our lab, in which AhRR

depletion protected against weight gain following 14-week HFD feeding. However, only a slight change was observed in the weight curve over the course of 14 weeks between the genotypes in both HFD and CD groups (Fig. 5.56 B), but at the end of experiment, HFD-fed AhRR^{E/E} mice gained significantly less weight (~5g) compared to WT mice (Fig. 5.56 C). A similar tendency was also seen in Triple CYP-KO AhRR^{E/E} mice although their body weight was not significantly lower than the WT and Triple CYP-KO AhRR+/+ mice. Further, Triple CYP-KO AhRR+/+ mice had a slightly higher weight gain compared to WT mice (~2g more). Similar tendencies in the distribution of the weight gain of AhRR^{E/E} and Triple CYP-KO AhRR^{E/E} mice were also observed in CD-fed mice. Moreover, the glucose tolerance test (GTT) showed that the glucose challenge worked, as the blood glucose peaked at the 30 minutes time point in both HFD and CD groups. The maximum blood glucose levels in the HFD groups were about 5-10 mmol/L higher compared to the CD group, depending on the genotype (Fig. 5.56 D). The blood glucose level of CD-fed mice started to decrease from 60 minutes onwards. The reduced weight gain in the AhRRdeficient mice in the HFD group was accompanied by better glucose tolerance, particularly in AhRR^{E/E} mice compared to WT mice, as the blood glucose in AhRR^{E/E} mice was 6 and 8 mmol/L less than WT at the 60- and 90-minute time points (Fig. 5.56 D). Interestingly, a similar reduction in blood glucose concentration in AhRR^{E/E} mice compared to WT was also observed in the CD group. In the HFD group, it was also apparent that the peak blood glucose level of WT mice was sustained up to 90 minutes, whereas in AhRR^{E/E} mice, it already declined at the 60-minute time point. The ablation of the three CYP enzymes also reduced the glucose tolerance, as the blood glucose level of Triple CYP-KO AhRR+/+ mice in the HFD group failed to return to the baseline level even at the 150-minute endpoint. Nevertheless, AhRR-deficiency slightly overturned the reduced glucose tolerance caused by the ablation of the triple CYP enzymes, since the blood glucose level of the Triple CYP-KO AhRR^{E/E} mice tended to be lower than in the Triple CYP-KO AhRR^{+/+} mice, and it already started to decrease at 90 minutes. This suggests that the loss of AhRR led to inherently leaner mice and higher glucose tolerance, as it was observed in both HFD and CD groups, whereas the ablation of the three CYP enzymes led to opposite effects, but such effects were only apparent in HFD-fed mice. The results regarding AhRR-deficient mice are in line with the previous results obtained in our group, where loss of AhRR was protective against DIO (unpublished data). Interestingly, deficiency of the three CYP enzymes led to higher weight gain, which might be related to the dysregulated lipid metabolism in these mice.

To assess if HFD inflicted liver damage, serum ALT and AST were measured. AhRR^{E/E} and Triple CYP-KO AhRR^{E/E} mice fed with HFD had slightly lower ALT and AST levels compared to WT and Triple CYP-KO AhRR^{+/+} mice (**Fig. 5.56**, left and middle figures). The AST and

ALT serum results were reflected in the calculated AST/ALT ratio, as the Triple CYP-KO AhRR^{+/+} mice also had the highest ratio in the HFD group. However, HFD feeding did not increase the ratio in the other three genotypes; the ratio in WT mice was comparable to AhRR^{E/E} and Triple CYP-KO AhRR^{E/E} mice in both CD and HFD group. Moreover, serum triglyceride levels, which indicate increased free fatty acids in the circulation were increased in the HFD group compared to CD group regardless of the genotypes (**Fig. 5.56 E**, right figure).

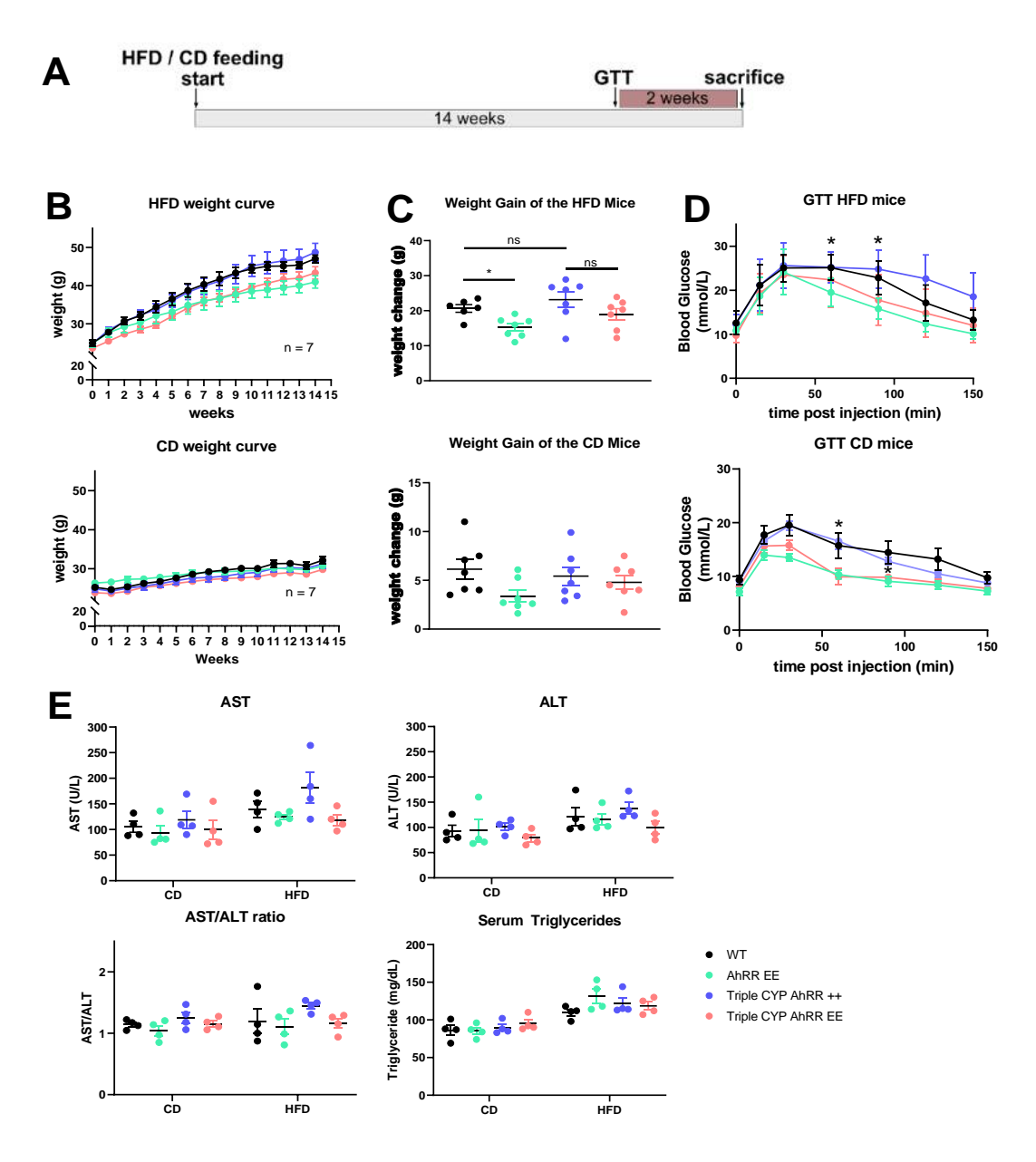


Fig. 5.56 Lack of AhRR reduced weight gain and increased glucose tolerance in the presence and absence of CYP enzymes. A) WT, AhRR^{E/E}, as well as Triple CYP-KO AhRR^{+/+} and AhRR^{E/E} were fed with either a HFD or CD for 14 weeks. An in vivo glucose tolerance test was conducted 2 weeks prior to sacrificing the mice. B) The mice were weighed and scored every week throughout the experiment and C) the weight difference between the beginning and the end of experiment was calculated. D) During the glucose tolerance test, mice were challenged with glucose and blood glucose levels were measured within 15- and 30-minute intervals. E) the serum AST, ALT, AST/ALT ratio, and Triglycerides obtained at the end of experiment were measured. Results are shown as mean ± SEM and significance was analyzed by one-way (B-D) or two-way ANOVA corrected for multiple comparisons by the Bonferroni's method. * p<0,5. In Figure D, * refers to the significance between WT and AhRR^{E/E} mice. For Figures B-D, data was pooled from two independent experiments (n=7), whereas for Figure E, data was from one experiment only (n=4).

5.5.2. Cellular composition of the small intestinal intraepithelial lymphocytes and lamina propria after HFD challenge

Obesity has been shown to alter the intestinal milieu and immune compartments therein (Khan et al., 2021). Simultaneously, AhR activation by β-naphthoflavone plays a role in immune cell maintenance at mucosal barrier sites, as it protected junctional complexes in the murine intestinal epithelium via PKC and p38MAPK signaling pathway (Postal et al., 2020). Another study also showed that AhR activation via indigo also protected against HFD-induced insulin resistance by enhancing IL-22 production (Lin et al., 2019). The ablation of AhRR and/or the three AhR-dependent CYP enzymes was supposed to enhance AhR signaling, as shown in Chapter 4. Here, it was interesting to determine if the frequencies of immune cells would be altered in the absence of AhRR and/or the three CYP enzymes in DIO and in the limited presence of AhR ligands when fed a HFD and CD.

5.5.2.1. Cellular compositions of IEL

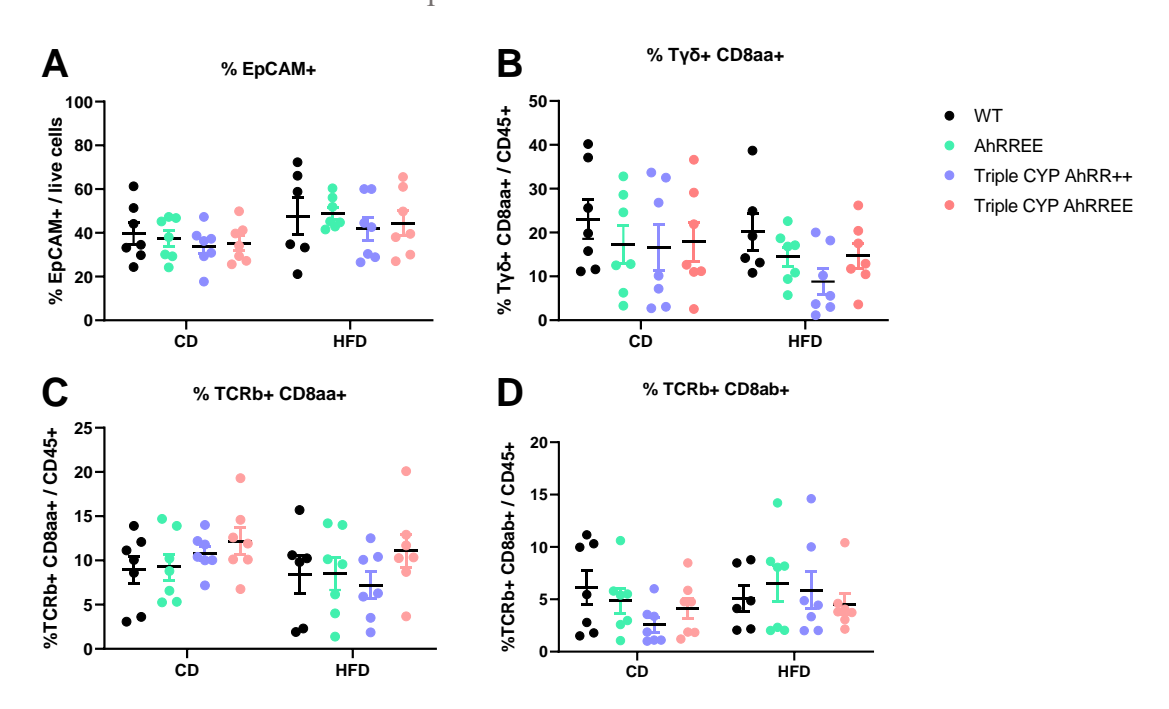


Fig. 5.57 HFD does not alter the frequencies of cell subsets in intestinal epithelium. SI was isolated from mice that were fed with either a CD or HFD for 14 weeks. The cells from the epithelial layer were then gated for EpCAM⁺, $TCR\gamma\delta^+$ $CD8\alpha\alpha^+$, $TCR\beta^+$ $CD8\alpha\beta^+$, and $TCR\beta^+$ $CD8\alpha\alpha^+$. The frequencies of the cell subsets were analyzed by flow cytometry and were quantified out of the total $CD45^+$ cells. Results are shown as mean \pm SEM and significance was analyzed by two-way ANOVA corrected for multiple comparisons by the Bonferroni's method. Data was pooled from two independent experiments (n=7).

Following isolation of SI cells from the epithelial layer, the cells were gated for EpCAM⁺ IEC, $TCR\gamma\delta^+ CD8\alpha\alpha^+$, $TCR\beta^+ CD8\alpha\beta^+$, and $TCR\beta^+ CD8\alpha\alpha^+$ IELs. The gating strategy is depicted in **Fig.5.2** (Chapter 4). FACS analysis of IEL revealed that HFD feeding did not alter the frequencies of any of the cell's subsets and neither did the ablation of AhRR and/or the three

CYP enzymes (Fig. 5.57). In terms of EpCAM⁺ IEC, there were no prominent differences across genotypes and treatment groups, but a mild induction was observed in the HFD-fed group (Fig. **5.57** A). In the TCR $\gamma\delta^+$ CD8 $\alpha\alpha^+$ subset, WT mice had the highest frequency in both diet groups. However, HFD slightly reduced the frequency of TCR $\gamma\delta^+$ CD8 $\alpha\alpha^+$ and TCR β^+ CD8 $\alpha\alpha^+$ particularly in Triple CYP-KO AhRR⁺/⁺ mice (Fig. 5.57 B and C). In both TCRβ⁺ IEL subsets, neither HFD nor the absence of AhRR and/or the three CYP enzymes led to alterations in frequencies (Fig. 5.57 C and D). In terms of AhRR expression, there was no difference in AhRR expression in EpCAM⁺ IEC and the three IEL subsets between AhRR^{E/E} and Triple CYP-KO AhRR^{E/E} mice in both HFD and CD groups (Fig. 5.58 A-D). Compared to the in-vivo ligand experiment in Chapter 4, there was an overall reduction in AhRR/EGFP expression in IEC and IEL subsets. In the ligand feeding experiment, the frequency of AhRR-expressing IEC reached ~10% in the control-treated Triple CYP-KO AhRR^{E/E} mice, whereas the frequencies of AhRRexpressing IEL subsets reached 60-80% (Fig 5.4 Chapter 4). Here, the frequency was around 5% or less in both CD- and HFD-treated AhRR $^{\rm E/E}$ and Triple CYP-KO AhRR $^{\rm E/E}$ mice (Fig. 5.58). In addition, the frequencies of AhRR-expressing IEL subsets were reduced to around 50% in CDand HFD-fed AhRR^{E/E} and Triple CYP-KO AhRR^{E/E} mice. In general, HFD feeding did not cause further reduction in the AhRR-expressing IEL frequencies compared to the CD group, although in the $TCR\beta^+$ $CD8\alpha\alpha^+$ subset, HFD seemed to slightly reduce the frequency in $AhRR^{E/E}$ mice. The frequencies of the AhRR-expressing IEL subsets in AhRR^{E/E} mice were also slightly lower, compared to the result shown by Schanz et al. (Schanz et al., 2020), in which the frequencies of EGFP+ TCRβ⁺ IEL in AhRR^{E/+} mice fed with ligand-reduced diet reached ~70% among all TCR β ⁺ IEL. However, the mice analyzed in this HFD experiment were ~12 weeks older than the ones used by Schanz et al., suggesting that age and AhRR expression could be inversely correlated.

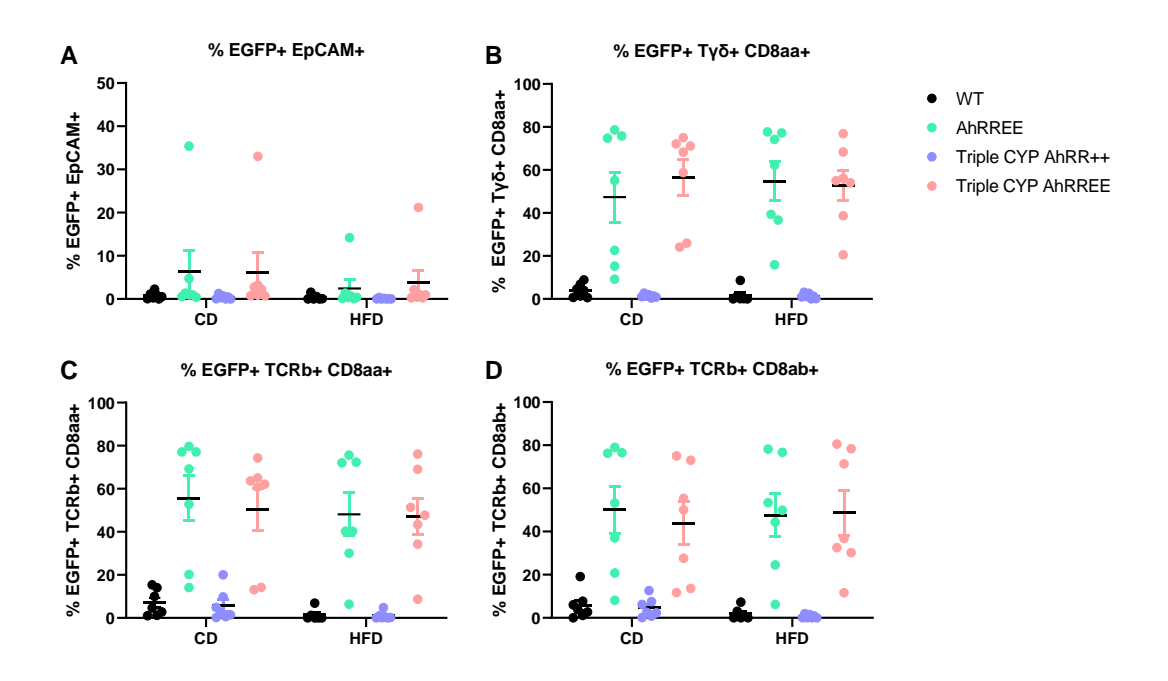


Fig. 5.58. HFD does not increase the frequencies of AhRR-expressing IEL SI was isolated from mice that were fed with either a CD or HFD for 14 weeks. The cells from the epithelial layer were then gated for EpCAM⁺, TCRγδ⁺ CD8αα⁺, TCRβ⁺ CD8αβ⁺, and TCRβ⁺ CD8αα⁺. The EGFP⁺ EpCAM and IEL subsets were analyzed by flow cytometry and their frequencies were quantified. Results are shown as mean \pm SEM and significance was analyzed by two-way ANOVA corrected for multiple comparisons by the Bonferroni's method. Data was pooled from two independent experiments (n=7).

5.5.2.2. Cellular composition in SI Lamina Propria

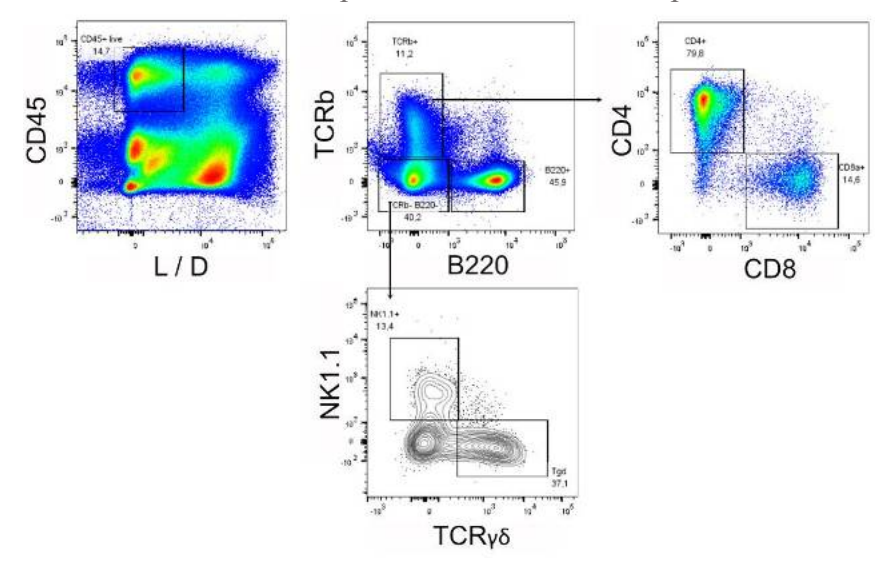


Fig. 5.59 Gating strategy of lymphocytes in SI lamina propria. SI cells were isolated from lamina propria and gated for living single CD45⁺ cells. Single cell gating was performed twice prior to gating the CD45⁺ subset. Then, B- and T cells, both conventional CD4⁺ and CD8⁺ TCRβ⁺ cells, as well as TCRγδ cells.

Following the isolation of immune cells in lamina propria, the cells were gated for B cells, $TCR\beta^+$ T cells (both conventional CD4⁺ and CD8⁺ $TCR\beta^+$ cells and $T\gamma\delta$ cells), macrophages, Mo-Mac, and cDC. B- and T cells were identified by their expression of B220 and $TCR\beta$, respectively.

Mo-Mac were identified as Ly6C⁺ Lc6G- F4/80⁺ cells, whereas macrophages were identified as F4/80⁺ CD64⁺ Ly6C- cells, and cDC were identified as MHCII⁺ CD11c⁺ cells. The lamina propria DC were further divided into four subsets, CD103⁻ CD11b⁻, CD103⁺ CD11b⁺, CD103⁺ CD11b, and CD103 CD11b DC, but the double negative population was omitted in the analysis, due to extremely low cell number. The gating strategy for the myeloid subset is depicted in Fig 5.7 (Chapter 4), whereas the gating strategy for the lymphocytes is depicted in Fig. 5.59. There was no significant difference in the frequency of conventional T cells (both CD4⁺ and CD8⁺), although the frequency of CD8⁺ T cells tended to increase in the HFD group (**Fig. 5.60**) **A-C**). The frequency of Tyδ cells was slightly increased in AhRR^{E/E} mice under HFD, whereas the ablation of triple CYP enzymes slightly reduced the Tyδ cell frequency in both HFD and CD groups (Fig. 5.60 D). A significant difference in the frequency of Ty δ cells was observed between the HFD-fed AhRR^{E/E} and Triple CYP-KO AhRR^{+/+}mice. Further, HFD did not alter the frequency of B cells across all genotypes (Fig. 5.60 E). In contrast, the ablation of either AhRR and/or the Triple CYP enzymes reduced the frequency of B cells compared to WT mice regardless of diet groups. In terms of total macrophages and MHCII⁺ macrophages, there were no significant differences observed (Fig. 5.60 F and G). HFD seemed to slightly increase the frequency of Mo-Mac in Triple CYP-KO AhRR+/+ mice, which led to a significant difference between Triple CYP-KO AhRR+/+ and Triple CYP-KO AhRRE/E mice (Fig. 5.60 H). Also, the Mo-Mac frequency was reduced in AhRR^{E/E} mice to a level observed in CD-fed mice, indicating that deficiency of AhRR inhibits the accumulation of Mo-Mac under HFD. In terms of DC, the frequencies of each subset were rather low (~0.5-2%). Regarding CD103⁺ CD11b⁺ cDC, HFD slightly reduced their frequency across all genotypes, compared to the frequencies in the CD group (Fig. 5.60 I), whereas the frequency of CD103⁺ CD11b⁻DC was slightly enhanced under HFD conditions in Triple CYP-KO AhRR^{E/E} mice (Fig. 5.60 ^J). In contrast, HFD slightly reduced the frequency of CD103⁻ CD11b⁺ DC in AhRR^{E/E} mice (Fig. 5.60 K). These diverse effects on frequencies of various immune cells further showed the cell-type specificity of AhRR regulation and it also indicated that the ablation of AhRR and/or the Triple CYP enzymes could directly alter the frequency of intestinal immune cells.

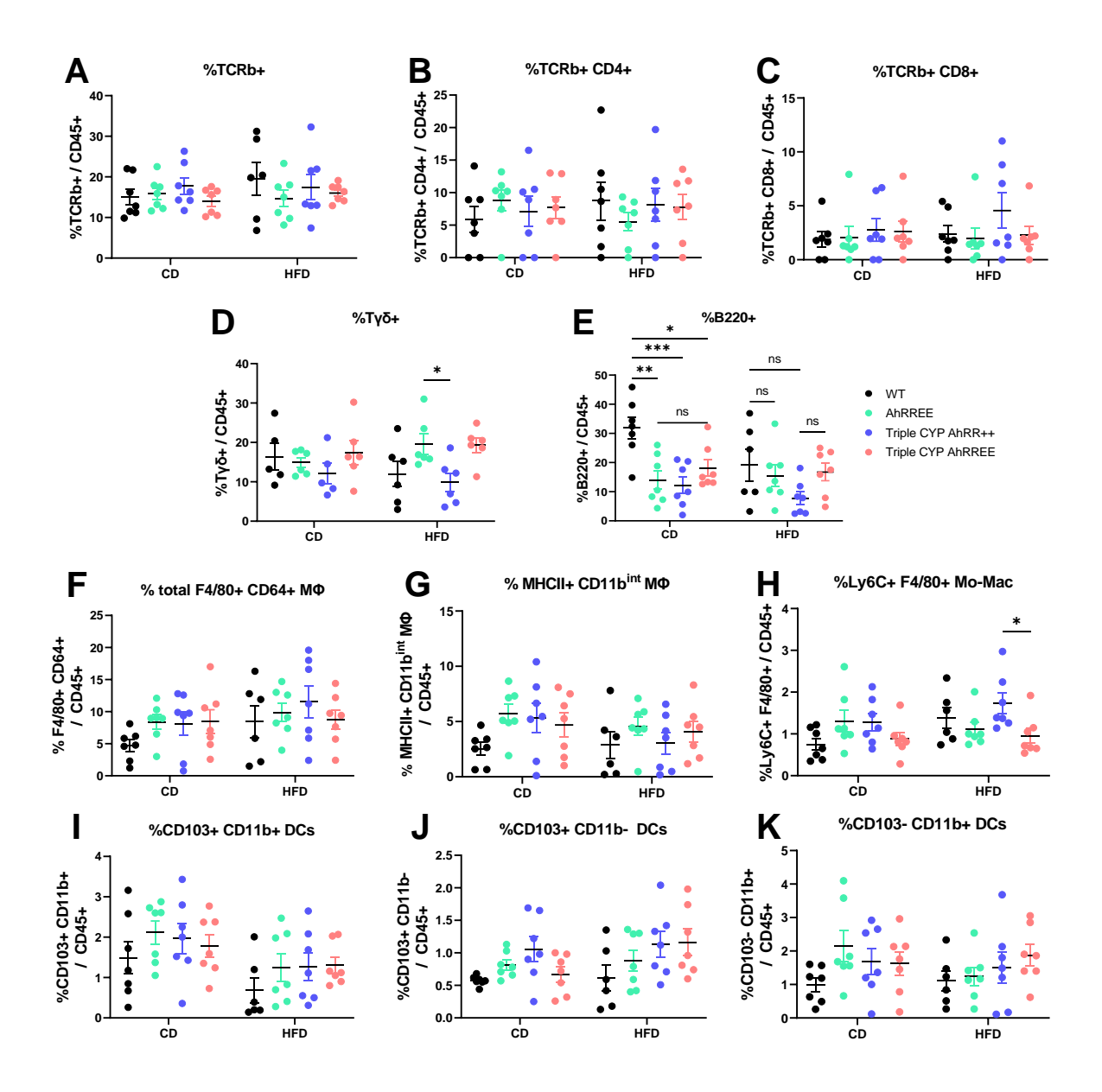


Fig. 5.60 HFD slightly altered the frequencies of $\gamma\delta$ T cells and Mo-Mac in SI lamina propria. SI lamina propria cells were isolated from mice that were fed either by HFD or CD for 14 weeks. The cells were then gated for B- and T cells (both conventional and $\gamma\delta$ T cells), macrophages, Mo-Mac, and DC. The frequencies of the immune cell subsets were analyzed by means of flow cytometry. The frequencies of myeloid cells were quantified out of the total CD45⁺ cells. Results are shown as mean \pm SEM and significance was analyzed by two-way ANOVA corrected for multiple comparisons by the Bonferroni's method. Data was pooled from two independent experiments (n=7).

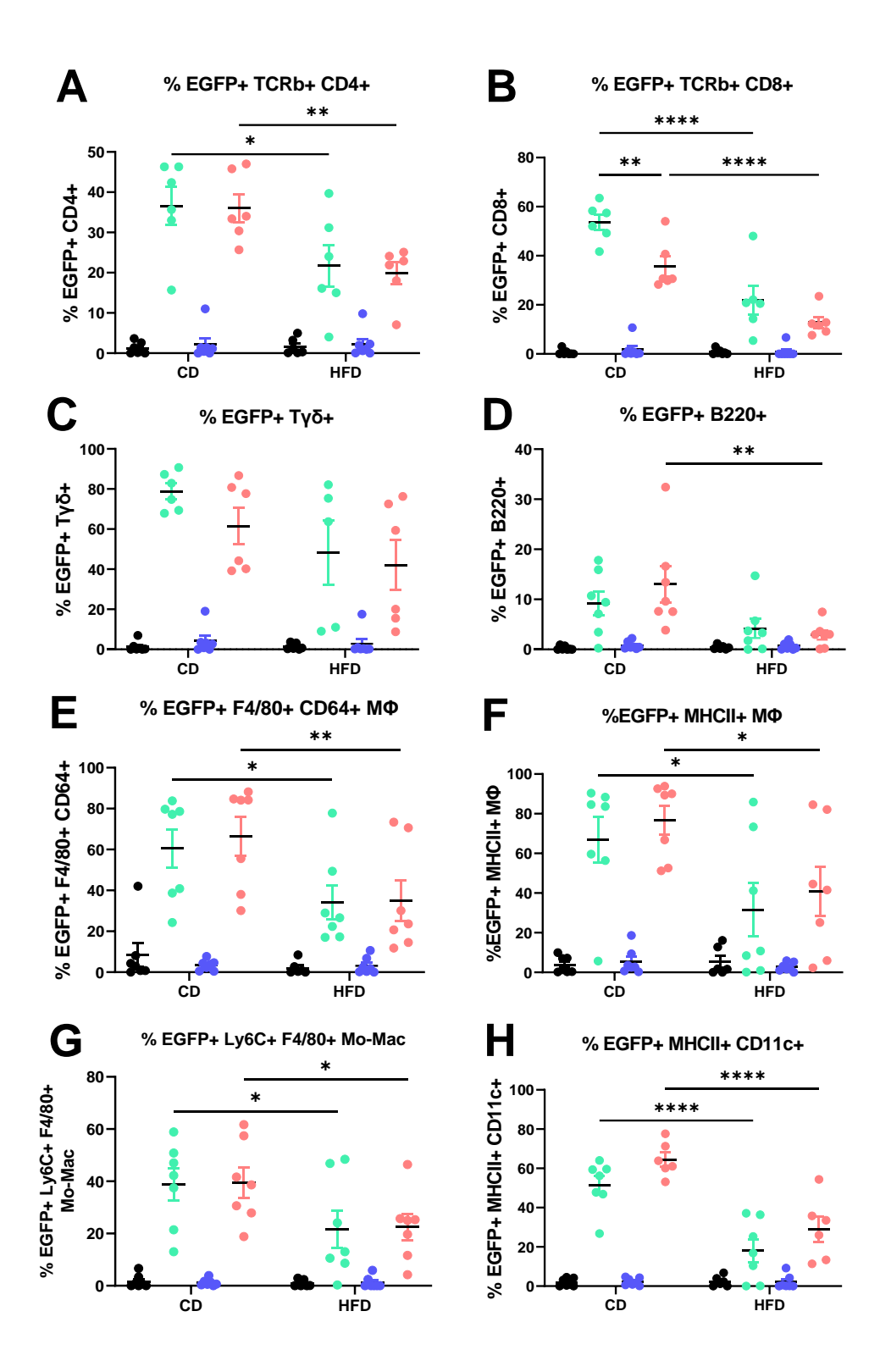


Fig. 5.61 HFD markedly reduced the frequencies of AhRR-expressing immune cells in SI lamina propria. The frequencies of AhRR/EGFP-expressing immune cell subsets were analyzed by flow cytometry. Results are shown as mean \pm SEM and significance was analyzed by two-way ANOVA corrected for multiple comparisons by the Bonferroni's method. Data was pooled from two independent experiments (n=7).

HFD reduced the AhRR/EGFP expression in most of the immune cell subsets, both in lymphoid and myeloid subsets of AhRR^{E/E} and Triple CYP-KO AhRR^{E/E} mice. HFD reduced the frequency of AhRR-expressing CD4⁺ T cells from a mean value of around 35% to 20% in both AhRR^{E/E}

and Triple CYP-KO AhRR^{E/E} mice, compared to the CD-fed mice, but there was no inherent difference between the two genotypes (Fig. 5.61 A). Similarly, HFD also reduced AhRRexpressing CD8⁺ T cells from mean values of 58% and 38% to ~20% and ~10% in AhRR^{E/E} and Triple CYP-KO AhRR^{E/E} mice, respectively (Fig. 5.61 B). Interestingly, the frequency of AhRRexpressing cells in AhRR^{E/E} mice was significantly higher than Triple CYP-KO AhRR^{E/E} mice in the CD group. Regarding Ty δ cells, there was also a tendency that HFD reduced the frequency of these cells in both AhRR^{E/E} and Triple CYP-KO AhRR^{E/E} mice, and the frequency of AhRRexpressing Ty δ cells was also slightly higher in AhRR^{E/E} mice (Fig. 5.61 C). This result differed from the result shown in Chapter 4, where AhRR expression was higher in Triple CYP-KO AhRR^{E/E} mice both in lymphocytes and myeloid cells, but the mice used here were around 22– 24-week-old, much older than the 8-week-old mice used in the previous experiment. This may suggest that the combination of lack of AhR ligands, aging, and ablation of the three CYP enzymes might mediate such a reduction in AhRR/EGFP expression. Apart from T cells, HFD also significantly reduced the frequency of AhRR/EGFP+ B cells in Triple CYP-KO AhRR^{E/E} mice (Fig. 5.61 D). In the myeloid compartment, the frequency of AhRR-expressing cells was comparable between AhRRE/E and Triple CYP-KO AhRRE/E mice and feeding a HFD also significantly reduced the frequency of AhRR-expressing macrophages, Mo-Mac, and DC in both genotypes (Fig. 5.61 E-H).

In addition to FACS analysis, a qualitative histological analysis of SI from CD- and HFD-fed AhRR^{E/E} and Triple CYP-KO AhRR^{E/E} mice was conducted (**Fig. 5.62**). In this case, however, it was harder to observe the HFD-mediated reduction of AhRR expression on tissue level. One explanation could be that the AhRR is also expressed in intestinal stromal cells, and it could be that the AhRR expression in these cells was not as affected as in the immune cells. In fact, the previous chapter showed that AhRR is differentially regulated in stromal versus immune cells. Nevertheless, it seems that AhRR expression in mice fed with purified diets (both CD and HFD) was reduced both in terms of intensity and frequency, as the AhRR-expressing stromal cells in the pericryptal areas that were normally observed in NC-fed mice were not visible in the CD-and HFD-fed Triple CYP-KO AhRR^{E/E} mice, as shown in **Fig. 5.62**. In the future, an isolation method for the stromal cells in lamina propria should be developed to determine if HFD can also reduce the AhRR expression in various stromal cells subsets.

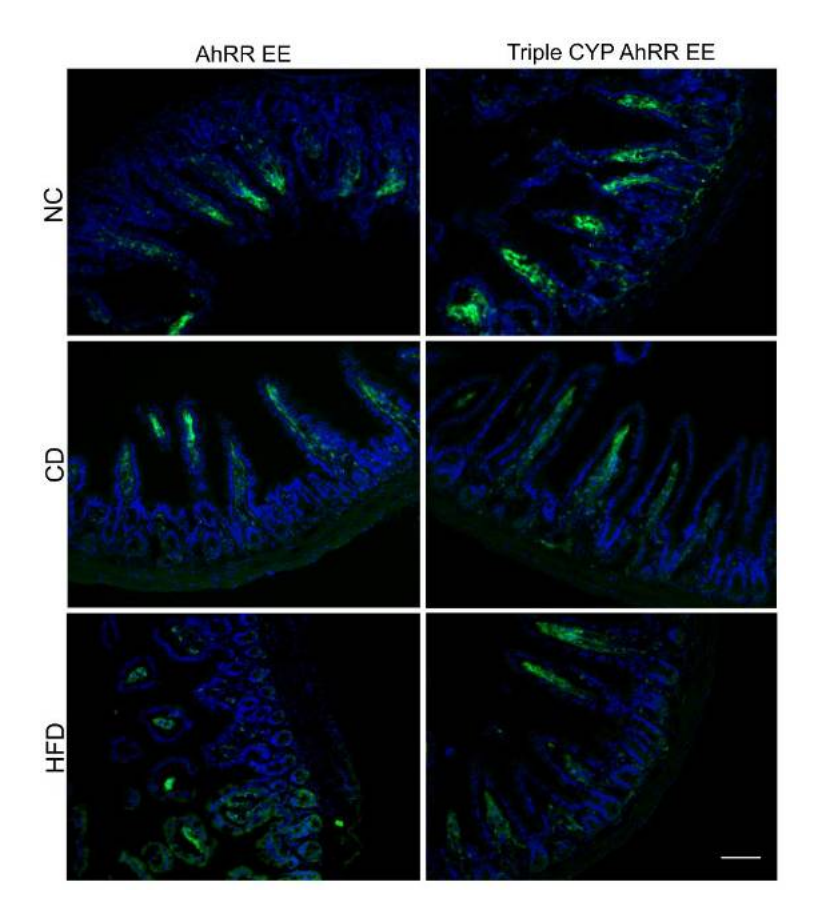


Fig. 5.62 AhRR expression in SI of CD- or HFD-fed mice. SI cryosections were prepared from AhRR^{E/E} and Triple CYP-KO AhRR^{E/E} mice that had been fed with either CD or HFD for 14 weeks and AhRR expression was compared to the one from NC-fed 8-week-old female mice. Representative images of one mouse from each treatment group and genotype are shown here. Images were taken at 20x magnification with similar exposure time. Scale bar = $50\mu m$.

5.5.3. AhRR and CYP-dependent cellular and metabolic alterations in the liver after dietary challenge

In liver, AhR and the three AhR-dependent CYP enzymes are highly expressed, and they all play a role in xenobiotic metabolism, which takes place in the liver. AhR expression, particularly of the high-affinity AhR which is present in C57BL/6J mice, and activation by kynurenine has been shown to induce not only increased body weight gain and hyperglycemia, but also liver steatosis (Kerley-Hamilton et al., 2012; Rojas et al., 2021). The three AhR-dependent CYP enzymes as mentioned earlier also have been shown to mediate the synthesis of lipid mediators (Divanovic et al., 2013). To assess if enhanced AhR activation in mice fed a HFD for 14 weeks would also result in NASH, a more progressive form of liver inflammation, we sought to investigate if DIO and ablation of AhRR and/or the three CYP enzymes would affect the frequencies of hepatic immune cells and if this alters liver pathology at large.

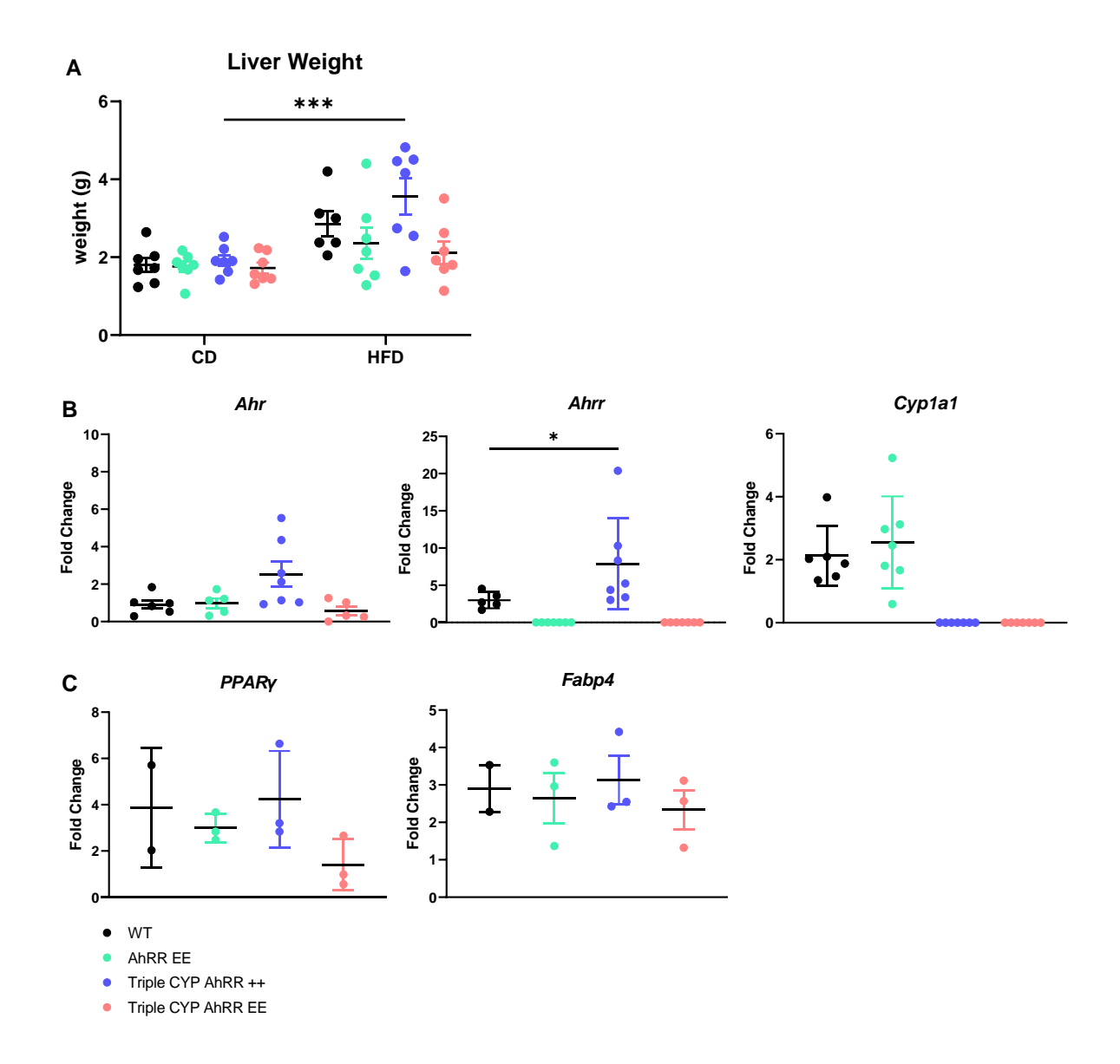


Fig. 5.63 Loss of Triple CYP enzymes increased liver weight and hepatic *Ahrr* **expression.** WT, AhRR^{E/E}, Triple CYP-KO AhRR^{E/E} increased liver weight and hepatic *Ahrr* expression. WT, AhRR^{E/E}, Triple CYP-KO AhRR^{E/E} mice were fed with either CD or HFD for 14 weeks. A) Liver was isolated and weighed at the end of week 14, and the expression of B) *Ahr* and its target genes, as well as C) genes involved in obesity progression were quantified by qPCR. Data was normalized to the expression of the reference gene and to the CD-fed mice from the respective genotype. Gene expression of *Ahr*, *Ahrr*, *Cyp1a1*, *Ppary*, and *Fabp4* is depicted as fold change ($2^{-\Delta\Delta Ct}$). Error bars represent mean \pm SEM. Significance was analyzed by oneway ANOVA corrected for multiple comparisons by the Bonferroni's method, * p<0,05, *** p<0,001. Data was pooled from two independent experiments in figure A and B (n=7), whereas in figure C, data was obtained from one experiment (n=4).

At a gross level, HFD slightly increased the liver weight of WT mice and to a lesser extent the liver weights of AhRR^{E/E} and Triple CYP-KO AhRR^{E/E} mice, but only the liver weight of Triple CYP-KO AhRR^{+/+} mice was significantly increased compared to the CD-fed counterpart (**Fig. 5.63 A**). Neither the loss of AhRR nor the three CYP enzymes altered the liver weight in the CD group. At mRNA level, Triple CYP-KO mice fed with HFD had a slightly increased *Ahr*

expression in liver compared to the other genotypes. The *Ahrr* expression of these mice was also significantly increased by ~8-fold relative to the CD-fed mice, suggesting that AhR activation was occurring. However, such induction was more than three times lower compared to the induction of *Ahrr* expression in the NC-fed mice used in the ligand stimulation experiment (**Fig. 5.63 B**), which showed more than 30 times higher expression of *Ahrr* following 3MC application (**Fig. 5.44**). Moreover, *Cyp1a1* expression in AhRR^{E/E} mice fed with HFD was comparable to WT mice, further alluding to reduced AhR signaling in mice fed a purified diet. In terms of obesity-related genes, the loss of AhRR mildly reduced *Ppary* expression in liver and it was further reduced by 2.5-fold when both AhRR and Triple CYP were absent (**Fig. 5.63 C**). To a lesser extent, the loss of AhRR also slightly reduced *Fabp4* expression in liver.

To see if HFD feeding induced structural alterations and changes in lipid accumulation in liver, H&E and Oil-red-O stainings of liver sections were performed. Overall, both stainings showed similar phenotypes, matching the ones in the body and liver weights. The H&E staining demonstrated that WT and Triple CYP-KO AhRR+/+ mice exhibited slightly more fat accumulation in the liver lobules than AhRR^{E/E} mice (Fig. 5.64 A and B, upper row). Interestingly, the liver of Triple CYP-KO AhRR^{E/E} mice appeared to be most protected against HFD-induced hepatosteatosis. In the CD-fed mice, no apparent lipid accumulation was observed, except for the liver of Triple CYP-KO AhRR+/+ mice (Fig. 5.64 A and B, lower row). Furthermore, Oil-red-O (ORO) staining was performed to detect neutral lipids, such as triglycerides, cholesteryl esters, and lipoproteins (Du et al., 2022). Overall, preliminary staining results from two or three sections/mouse demonstrated more extensive lipid droplet accumulation in HFD-fed WT and Triple CYP-KO AhRR+/+ mice compared to AhRR-deficient mice, as evident in the more intense ORO staining and larger lipid droplets (Fig. 5.65 A and B, upper row). Interestingly, lipid accumulation was also visible in the CD-fed WT and Triple CYP-KO AhRR^{+/+} mice, but not in AhRR^{E/E} and Triple CYP-KO AhRR^{E/E} mice (Fig. 5.65 A and B, lower row). Nevertheless, quantification of lipid droplet size still needs to be conducted with ImageJ AdipoQ plugin and more sections should be stained and analyzed.

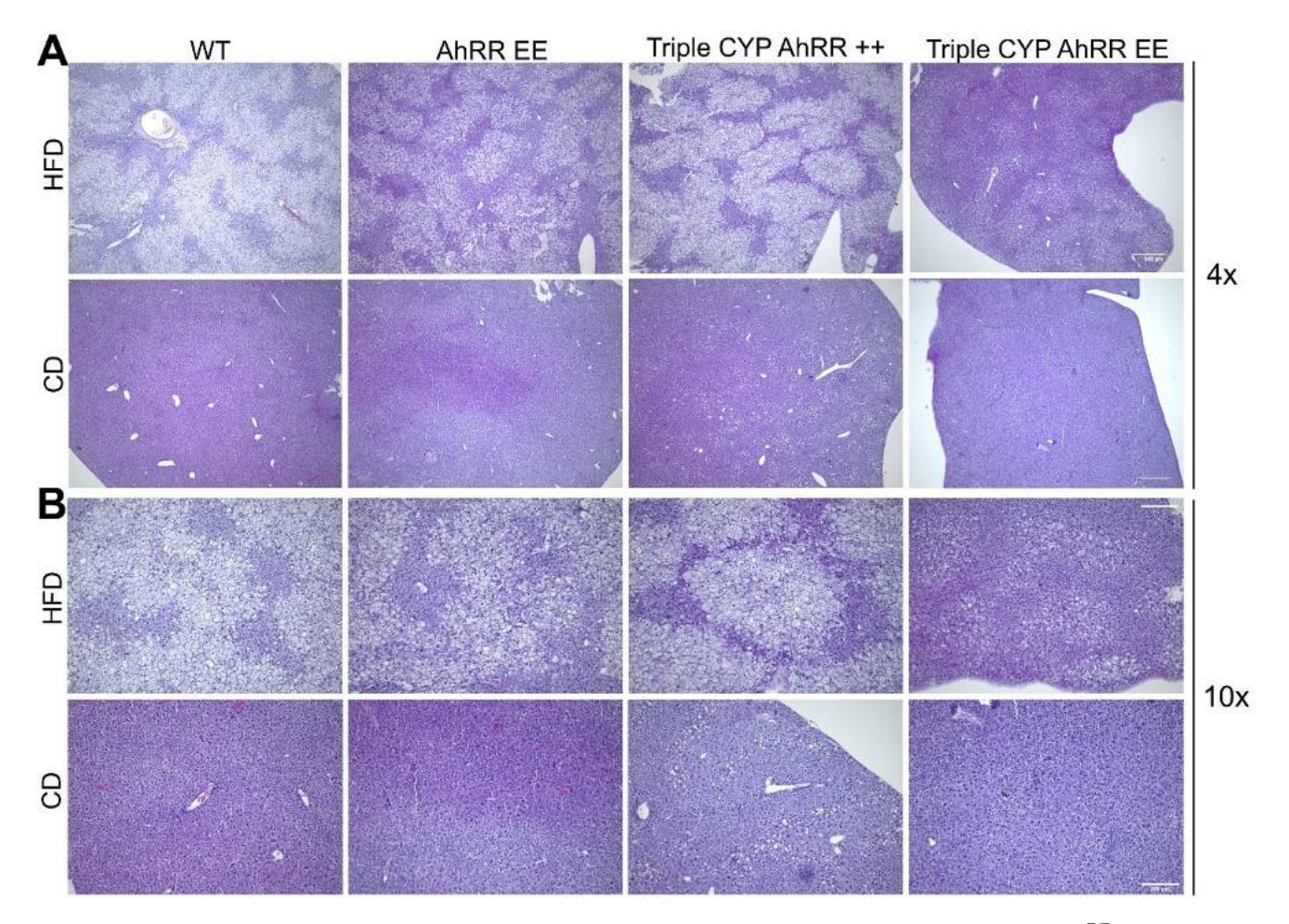


Fig. 5.64 Liver histology in response to HFD and CD feeding. Livers were isolated from WT, AhRR^{E/E}, Triple CYP-KO AhRR^{E/E}, and Triple CYP-KO AhRR^{E/E} mice were fed with either CD or HFD for 14 weeks. They were then paraffinized and H&E staining was performed on the paraffin sections. Representative images from one mouse / genotype are shown here. Sections were visualized at A) 4x and B) 10x magnification. Scale bar = $500\mu m$ in A and $200\mu m$ in B.

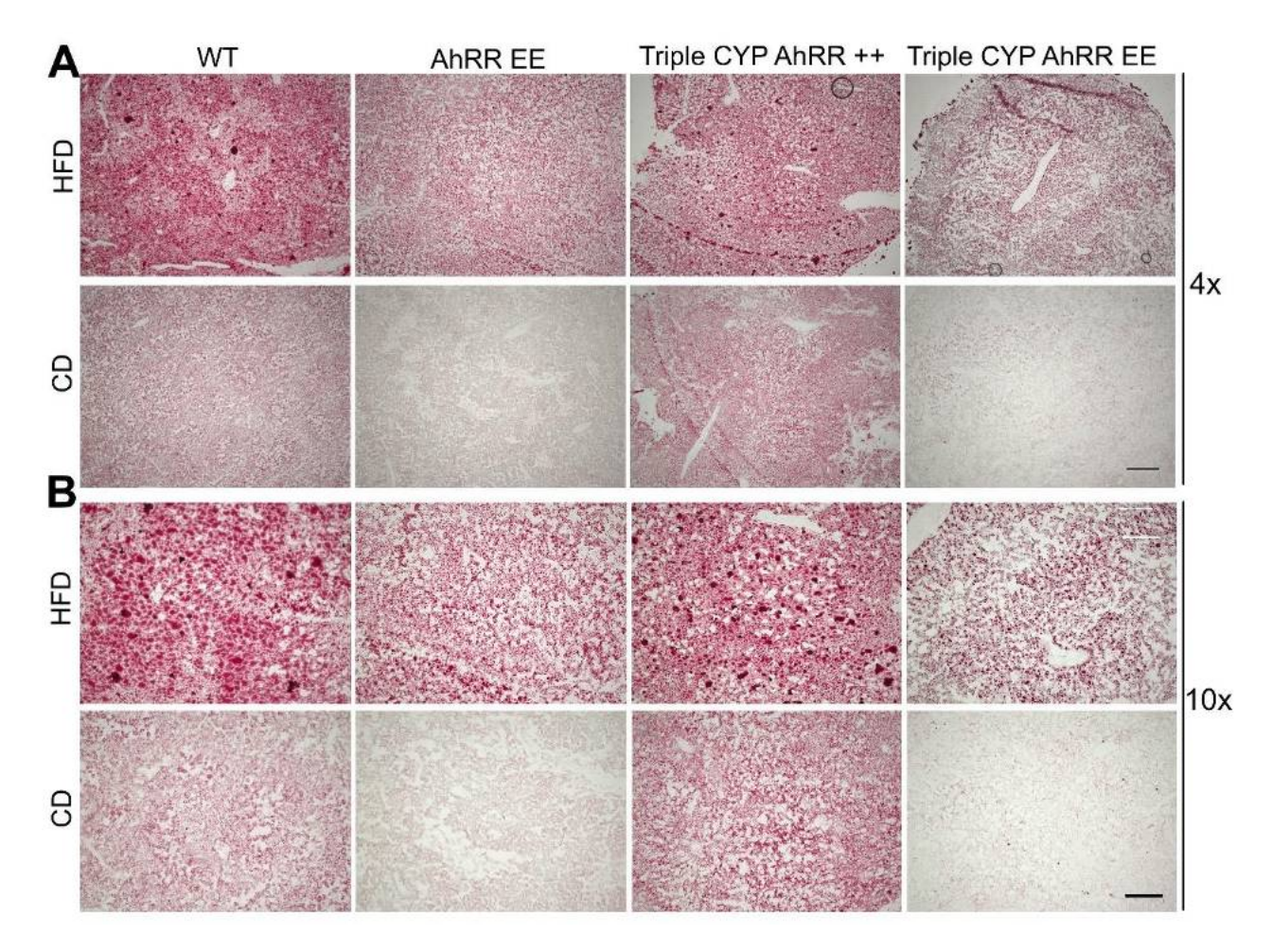


Fig. 5.65 Loss of AhRR reduces lipid accumulation and lipid droplet size. Livers were isolated from WT, AhRR^{E/E}, Triple CYP-KO AhRR^{+/+}, and Triple CYP-KO AhRR^{E/E} mice fed with either CD or HFD for 14 weeks. Cryosections were then obtained, and Oil-Red-O staining was performed to detect neutral lipids, cholesterols, and lipoprotein. Images are representative of three mice/genotype, of which one image/genotype is shown here. Sections were visualized at A) 4x and B) 10x magnification. Scale bar = 500μm in A and 200μm in B.

Although the HFD-fed mice exhibited increased lipid accumulation and hepatosteatosis/NAFLD developed, it was unclear if the HFD feeding also resulted in development of fibrosis, which is also a sign of NASH. Hence, Picrosirius Red staining was conducted on paraffin liver sections. This staining detects type I and type III collagen. Collagen I is expressed by fibroblasts, but also large vessels contain type I and III collagen (Schwarz, 2015; Xu & Shi, 2014). Nevertheless, the staining showed no extensive collagen deposition in HFD-fed mice (Fig. 5.66 A and B). Like the ORO staining, the Picrosirius Red staining was performed on two sections/mouse and showed some variations between animals, correlating with their body and liver weights. In general, only mild fibrosis was observed across all genotypes, there was accumulation of collagen observed in some tissue areas, but fibrotic bridges could hardly be detected. Hence, the ORO and Picrosirius Red stainings suggested that feeding the mice with HFD for 14 weeks in our animal facility resulted in NAFLD/hepatic steatosis but did not lead to NASH. Nevertheless, more sections need to be stained and an objective method for scoring needs to be employed.

Taken together, ablation of the three CYP enzymes led to an altered energy homeostasis and lipid metabolism, as evident in the increased body mass, glucose intolerance, as well as hepatic lipid accumulation and larger lipid droplet size. On the contrary, ablation of AhRR rather protected against symptoms of DIO and this effect was dominant over Triple-CYP deficiency.

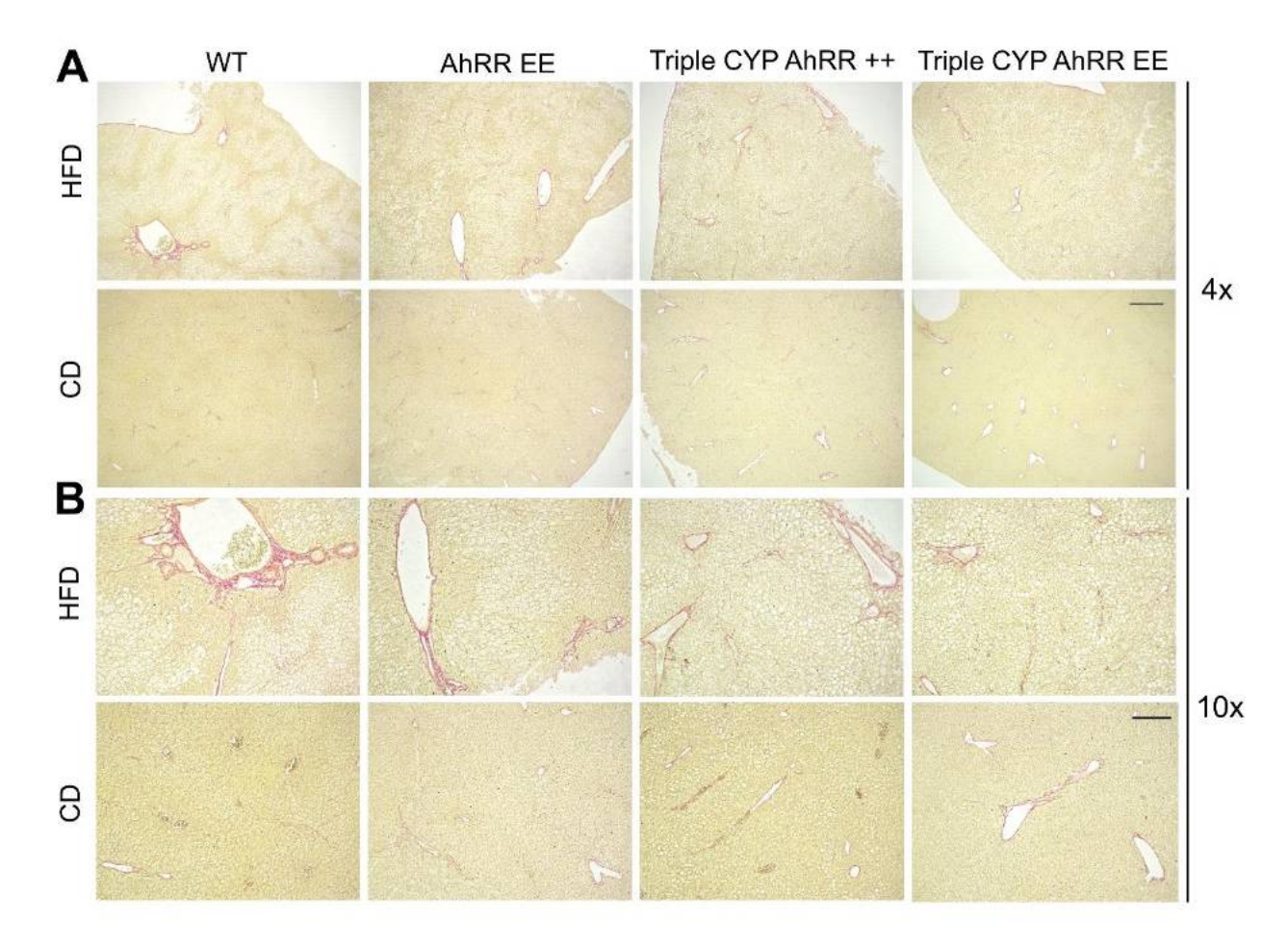


Fig. 5.66 HFD feeding did not cause extensive liver fibrosis. Livers were isolated from WT, AhRR^{E/E}, Triple CYP-KO AhRR^{+/+}, and Triple CYP-KO AhRR^{E/E} mice were fed with either CD or HFD for 14 weeks. Paraffin sections were obtained and Picrosirius red staining was performed to detect type I and III collagen. Images are representative of three mice/genotype, of which one image/genotype is shown. Sections were visualized at A) 4x and B) 10x magnification. Scale bar = 500μ m in A and 200μ m in B.

Obesity has been shown to perturb not only the molecular architecture of liver cells, but also the homeostasis of the hepatic immune system (Parlakgül et al., 2022; Remmerie, Martens, & Scott, 2020). Hence, the frequencies of hepatic immune cells, from both the lymphoid and myeloid compartments, were analyzed by flow cytometry. Hepatic immune cells were gated based on the strategy shown in **Figure 5.13** (**Chapter 4**). The myeloid subset was first gated based on the lack of CD19 and NK1.1 expression. Then, KC were identified as CD11b^{int} F4/80^{hi} Tim4⁺ CD31⁻ cells and cDCs were identified as Ly6^{lo} MHCII⁺ CD11c^{hi} cells. Mo-Mac subsets were divided into two subpopulations, based on the expression of F4/80 and Ly6C: either as F4/80⁺ Ly6C⁺ CD11b⁺- or F4/80⁺ Ly6C⁻ CD11b⁺ cells. Monocytes were identified as

Ly6C⁺ MHCII^{+/-}. Lastly, cDC were identified as Ly6C⁻ MHCII⁺ CD11c^{hi} cells. The cDC subsets were distinguished by the presence or absence of CD11b; CD11b⁻ cDC belong to cDC1 and CD11b⁺ belong to cDC2.

HFD-feeding induced some alterations in the immune cell subsets of the different genotypes on top of the alterations induced by the ablation of AhRR and/or the three CYP enzymes. In the lymphocyte subsets, no alteration was observed in the T cell subset across genotypes and treatment groups (Fig. 5.67 A), whereas HFD slightly reduced NKT frequency in AhRR^{E/E} and Triple CYP-KO AhRR^{E/E} mice compared to WT mice, but the reduction was only significant in the latter (Fig. 5.67 B). Remarkably, the frequency of NK cells in Triple CYP-KO AhRR^{+/+} mice in the CD group was significantly higher compared to the other genotypes, but HFD reduced the proportion of NK cells and made it more comparable to that in Triple CYP-KO AhRR^{E/E} mice, although it was still significantly higher than in AhRR^{E/E} mice (Fig. 5.67 C). In the myeloid compartment, the KC frequency in AhRR^{E/E} mice reached 9% out of the total CD45⁺ cells (Fig. **5.67 D**). It was significantly higher compared to the other three genotypes, which was different to the previous experiments (Figure 5.14 D, Chapter 4). HFD feeding, in turn, significantly reduced the frequency on KC in AhRR^{E/E} mice down to ~2% and to a lesser extent also in WT and Triple CYP-KO AhRR^{E/E} mice. Of note, the KC frequency in Triple CYP-KO AhRR^{+/+} mice was the lowest among the four genotypes regardless of the diet. In contrast, HFD markedly increased Ly6C⁺ Mo-Mac frequency from around 1,6% to 3,0% in Triple CYP-KO AhRR^{+/+} mice (Fig. 5.67 E). HFD also tended to increase the Ly6C⁺ Mo-Mac frequency in WT and to a lesser extent, in AhRR^{E/E} mice. Interestingly, the Ly6C⁺ Mo-Mac frequency in Triple CYP-KO AhRR^{E/E} mice consistently remained low despite the HFD feeding. In the more mature Mo-Mac, in which Ly6C expression has already been downregulated, HFD markedly increased the frequency of Ly6C⁻ MHCII⁺-, but not MHCII⁻ Mo-Mac (Fig. 5.67 F and G). Moreover, HFD slightly increased the hepatic MHCII⁺ monocyte frequency from 2% to 3-3,5% in AhRR^{E/E}, Triple CYP-KO AhRR^{+/+}, and Triple CYP-KO AhRR^{E/E} mice (Fig. 5.67 H), but did not notably alter the MHCII⁻ monocyte frequency (Fig. 5.67 I). There were also no significant alterations in the MHCII monocyte frequency caused by the ablation of AhRR and/or the three CYP enzymes. Lastly, in terms of cDC, HFD significantly increased the frequency of cDC2 in Triple CYP-KO AhRR^{E/E} mice, so that it was also significantly higher than in WT mice (Fig. 5.67 J). In contrast, neither HFD nor the loss of AhRR and/or Triple CYP altered the cDC1 frequency (Fig. 5.67 K).

The increase in KC frequency in CD-fed mice was not observed in untreated NC-fed mice as shown in Chapter 4. When comparing the two experiments, it should be considered that the CD-

and HFD-fed mice were of male sex, and they were already 22-24 weeks old at the end of the experiment, whereas the mice used in the ligand experiment were 8-week-old female mice. NC contains more phytochemicals and flavonoids that have AhR-activating properties; hence it was interesting to determine if age-matched male mice fed NC diet would also exhibit alterations in KC frequency. Therefore, 24-week-old male mice fed with NC throughout their lifetime were used and the hepatic immune cells were isolated. The gating strategy depicted in **5.13** (Chapter 4) was used to identify KC. The result showed that the KC frequency of WT and AhRR^{E/E} mice were comparable in NC fed mice (**Fig. 5.68**), suggesting that the presence of AhR ligands, not the age or sex of mice may modulate KC maintenance and frequency.

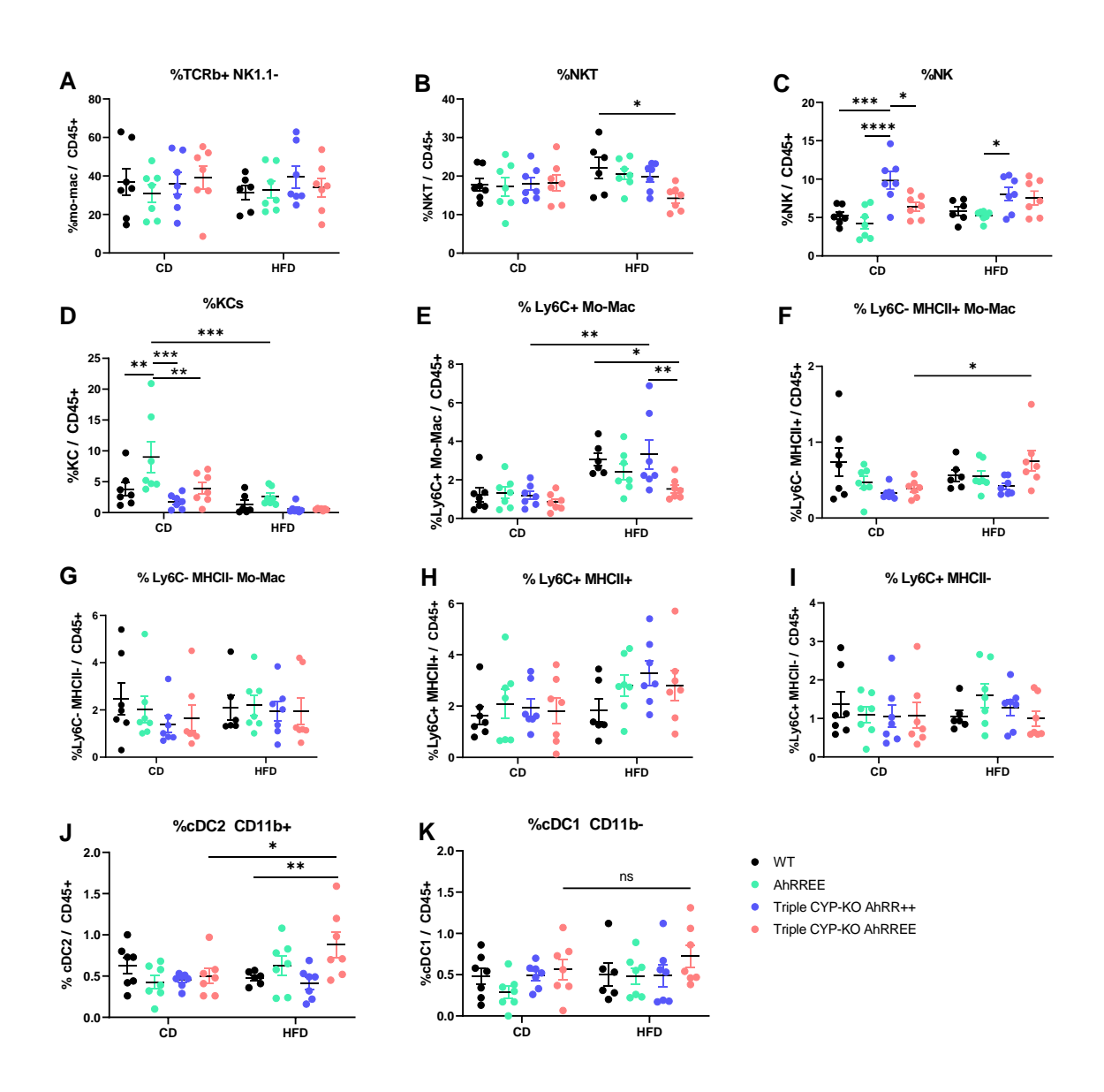


Fig. 5.67 Comparison of hepatic immune cell frequencies between CD- and HFD-fed mice. Liver cells were isolated from mice that were fed with either CD or HFD for 14 weeks. They were gated for NKT-, T cells, NK cells, as well as KC, Mo-Mac, monocytes, as well as cDC1 & cDC2. The frequencies of the cell subsets were analyzed by

flow cytometry and were quantified out of the total CD45 $^+$ cells. Results are shown as mean \pm SEM and significance was analyzed by two-way ANOVA corrected for multiple comparisons by the Bonferroni's method. Data was pooled from two independent experiments (n=7).

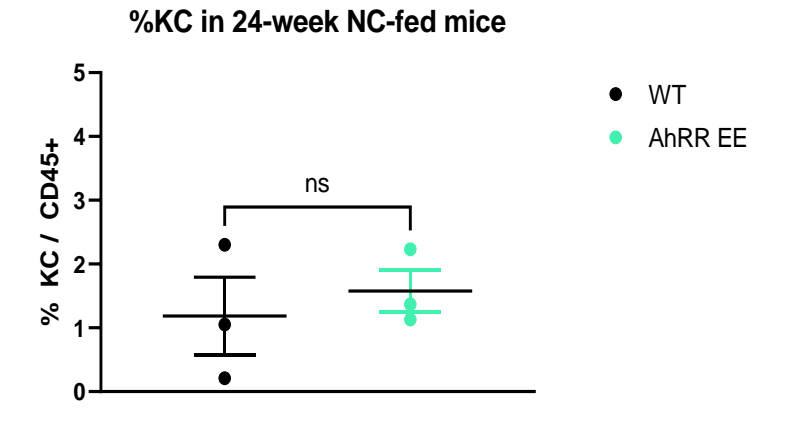


Fig. 5.68 The absence of AhRR does not increase KC frequency in NC-fed mice. Liver cells were isolated from 24-week-old WT and AhRR^{E/E} mice that were fed with NC. The frequencies of the cell subsets were analyzed by flow cytometry and were quantified out of the total CD45⁺ cells. Results are shown as mean \pm SEM and significance was analyzed by two-tailed paired t-test.

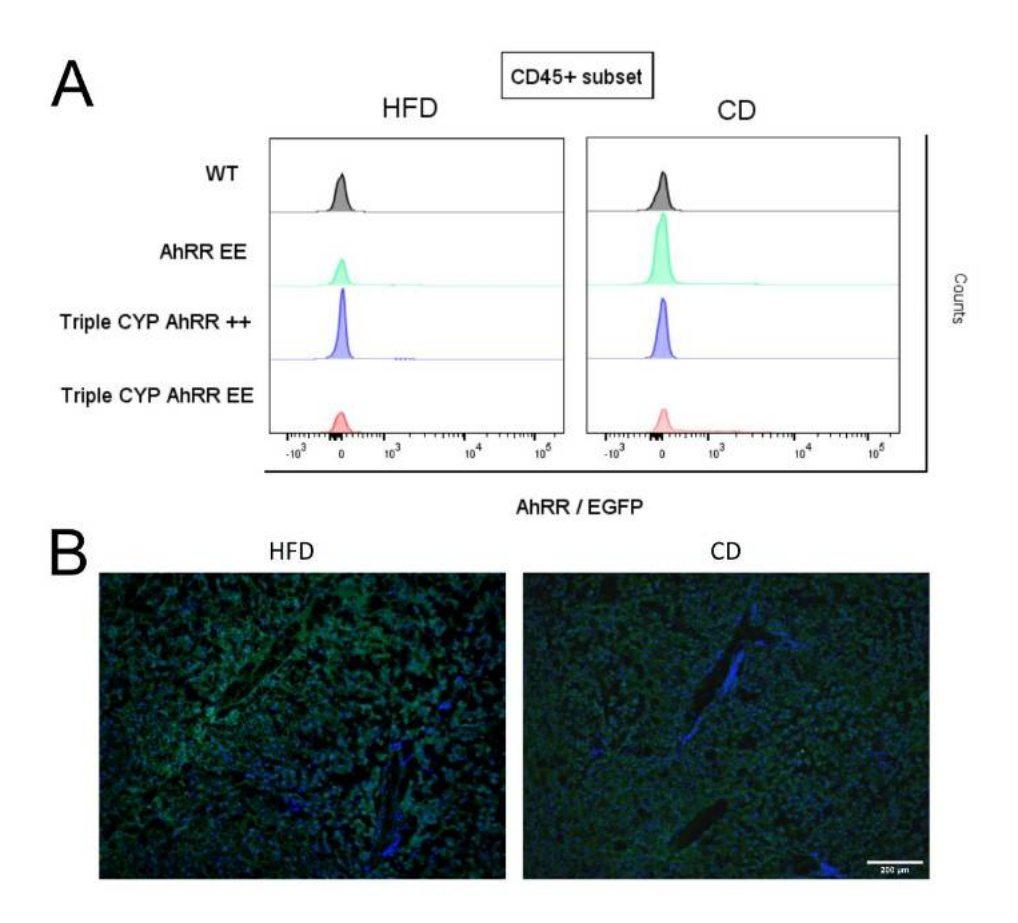


Fig. 5.69 Both HFD and CD feeding greatly reduced AhRR expression in hepatic immune and stromal cells. Following liver cell isolation, the AhRR/EGFP expression in each genotype and treatment group was analyzed in A) in living CD45 $^+$ subset by FACS. B) Liver cryosections of Triple CYP-KO AhRR^{E/E} mice were also analyzed for EGFP expression. In both A) and B), representative images from one mouse from each treatment group and genotype are shown. In B), scale bar represents 200 μ m.

Previously, Brandstätter et al. (Brandstätter et al., 2016a) showed that AhRR/EGFP was not expressed in the liver of AhRR^{E/+} and AhRR^{E/E} mice. In this organ, AhRR/EGFP has been only observed so far in some immune and perivascular stromal cells of NC-fed Triple CYP-KO AhRR^{E/E} mice, as shown in Chapter 4. However, expression of AhRR/EGFP was no longer observed in mice fed with CD or HFD (**Fig. 5.69 A and B**). This result is consistent with the finding of Schanz et al. (Schanz et al., 2020b), which showed that HFD and CD, which both are purified diets that contain less AhR-activating phytochemicals, greatly reduced AhRR/EGFP expression (**Fig. 5.69**). Hence, the AhRR/EGFP expression in individual immune subsets were not plotted here. Taken together, purified diets caused a low AhR activation state in liver, hence the alterations that were observed in some immune cell subsets here may have been directly or indirectly mediated by non-canonical AhR signaling.

5.5.4. AhRR and CYP-dependent cellular and metabolic alterations in WATg after dietary challenge

AhRR is expressed in immune cells of WATg, as shown in **Fig 5.19** (Chapter 4). Besides, a previous publication also showed that conditional ablation of AhR in Pdgfrα-expressing cells, such as preadipocytes, protected mice from DIO and liver steatosis (Gourronc et al., 2020). AhR activation by TCDD, BaP, and PCB-like dioxins led to different metabolic complications in murine models, such as AT inflammation, increased lipid levels, impaired glucose homeostasis, and reduced glucose tolerance (Baker et al., 2015; Enan et al., 1992; Lou et al., 2022). Among the three AhR-dependent CYP enzymes, CYP1b1 has been shown to be increased in human WAT following adipogenic stimulation and its deficiency protected against DIO and glucose intolerance in mice (Liu et al., 2015). However, the role of *Ahrr* as an AhR target gene in modulating lipid metabolism is still not well elucidated. Hence, it was of our interest to investigate if AhRR ablation with or without the ablation of the three AhR-dependent CYP enzymes, would alter the physiology of the AT, as well as immune cell frequencies in DIO-induced metainflammation.

HFD feeding for 14 weeks increased the overall WATg weight by 1-1.5g compared to CD-fed mice and the ablation of the three CYP enzymes with or without AhRR ablation also led to a slightly increased WATg weight upon HFD challenge (**Fig. 5.70 A**). To assess lipid metabolism, a lipolysis assay was performed by Dr. Laia Reverte-Salisa. In this assay, norepinephrine, a catecholamine, was used to stimulate sympathetic nerves that innervate WATg via the three beta-adrenergic (beta 1-, beta 2-, and beta 3-adrenergic) receptors. Stimulated sympathetic nerves can

in turn promote the release of energy in the form of FFAs, as well as glycerol (Malfacini & Pfeifer, 2023). The amount of glycerol released from the tissue was quantified following norepinephrine administration and normalized to the tissue weight. Baseline levels of lipolysis in CD and HFD groups were comparable, but the NE-induced increase in lipolysis was lower in the HFD- compared to the CD-fed mice (**Fig. 5.70 B**). This might suggest that neither AhRR nor the three CYP enzymes played major roles in lipolysis in WATg.

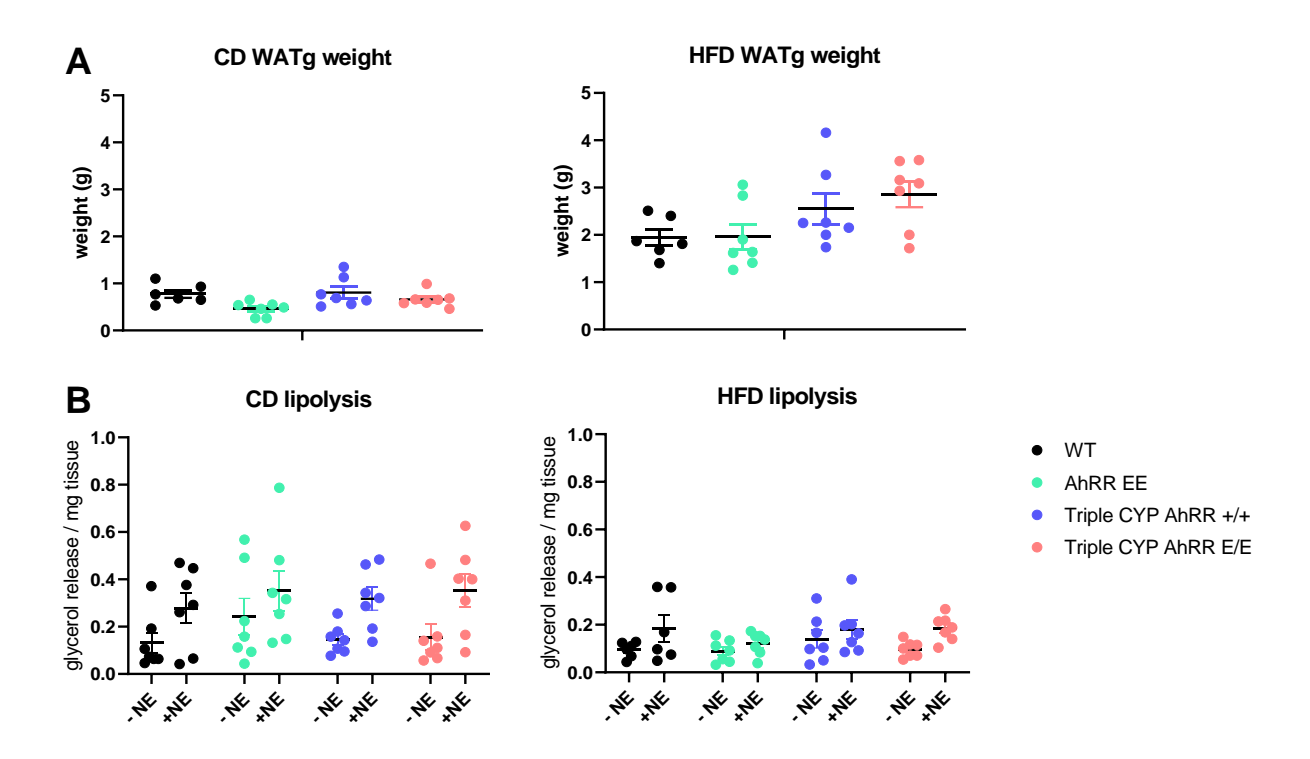


Fig. 5.70 Loss of Triple CYP enzymes tended to increase WATg mass after HFD. WT, AhRR^{E/E}, Triple CYP-KO AhRR^{E/E} mice were fed with either CD or HFD for 14 weeks. A) WATg was isolated and weighed at the end of week 14. B) A lipolysis assay was conducted Dr. Laia Reverte-Salisa to measure the amount of glycerol released upon norepinephrine (NE) stimulation. The glycerol amount was normalized to the tissue weight.

Moreover, H&E staining was performed to see if HFD had altered the cellular and tissue architecture of WATg (**Fig. 5.71 A and B**). WT and Triple CYP-KO AhRR^{+/+} mice exhibited more advanced adipose tissue pathogenesis than AhRR^{E/E} and Triple CYP-KO AhRR^{E/E} mice, as there appeared to be more Crown-Like Structures (CLS) surrounding the adipocytes. This was most prominent in the Triple CYP-KO AhRR^{+/+} mice, although variations were observed between animals. CLS are macrophages mostly derived from monocytes in blood surrounding dead or dying adipocytes. The presence of CLS is a hallmark of the proinflammatory process in adipose tissue (Wang et al., 2019). Nevertheless, additional immunohistochemical staining of

macrophages needs to be conducted in the future to confirm if the cell infiltrations surrounding the adipocytes are indeed comprised of macrophages.

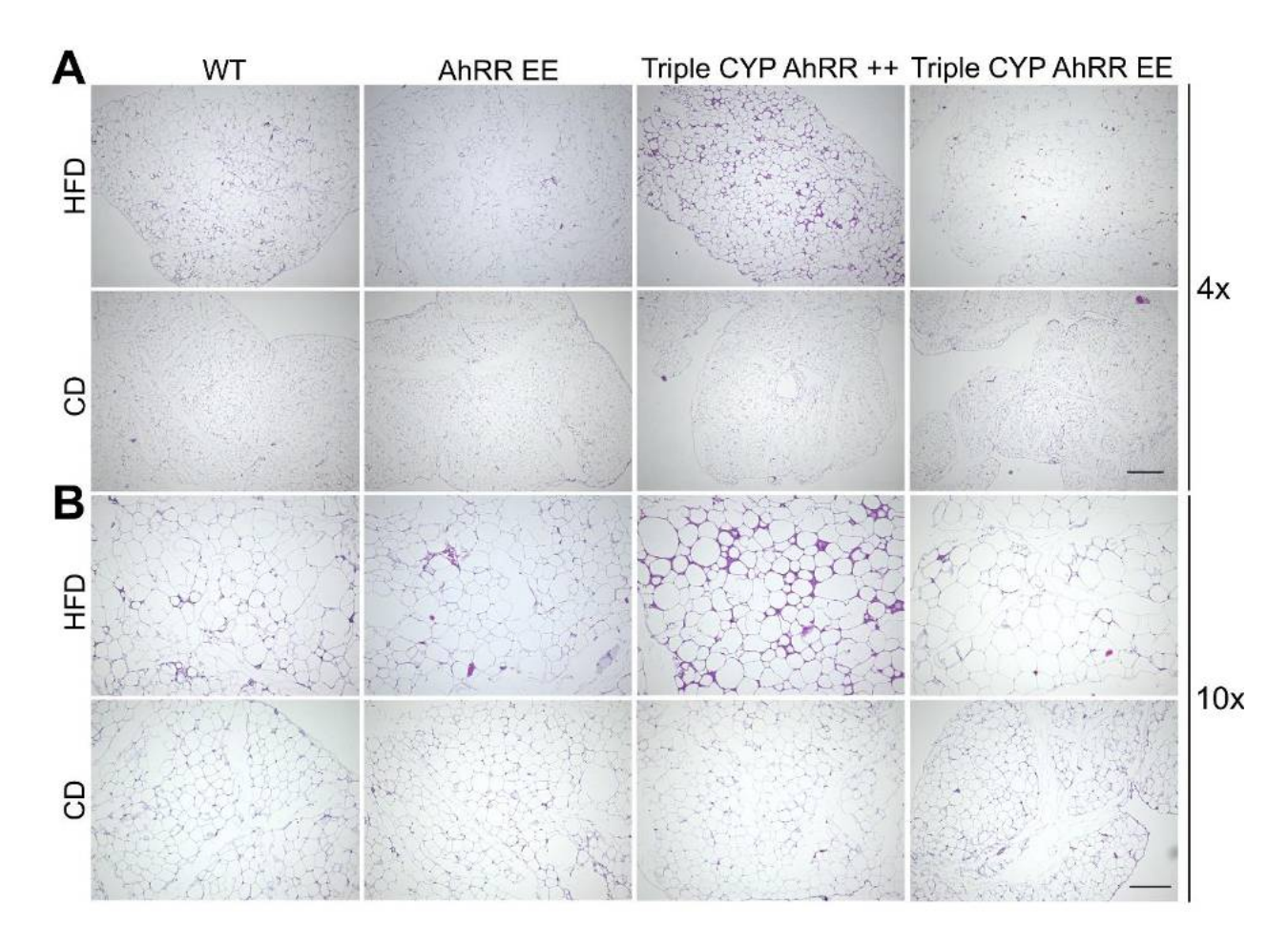


Fig. 5.71 WATg histology of WATg after CD or HFD feeding. WATg was isolated from WT, AhRR^{E/E},Triple CYP-KO AhRR^{+/+}, and Triple CYP-KO AhRR^{E/E} mice fed with either CD or HFD for 14 weeks. H&E staining was performed on paraffin sections of the adipose tissue. Representative images from one mouse/genotype are shown here. Sections were visualized at A) 4x and B) 10x magnification. Scale bar = 500μm in A and 200μm in B.

Consistent with the H&E staining, the Picrosirius Red staining showed that WT and Triple CYP-KO AhRR^{+/+} mice exhibited a more severe phenotype, as a higher deposition of collagen was observed compared to AhRR^{E/E} and Triple CYP-KO AhRR^{E/E} mice (**Fig. 5.72 A and B**). The preliminary scoring of Picrosirius Red staining obtained from three sections/mouse showed that the results also varied between animals (**Fig. 5.72 C**). The scoring was based on the method described by Lassen et al. (Lassen et al., 2017), where fibrosis in adipose tissue was divided into two main categories, pericellular and perilobular fibrosis (PCF and PLF, respectively). Based on the severity of the fibrosis in both categories, the fibrosis score of adipose tissue (FAT scores) was determined, which is further divided into four stages: stage 0, where neither PLF and PCF are observed; stage 1, where moderate PLF and/or moderate PCF are observed; stage 2, where either severe PLF or severe PCF was observed; and stage 3, where severe PLF and severe PCF

is observed. 14-week HFD feeding in our mice facility only led to moderate PCF in WT and Triple CYP-KO AhRR^{+/+} mice (stage 1) (**Fig. 5.72 C**). In AhRR^{E/E} and Triple CYP-KO AhRR^{E/E} mice, a mild to moderate fibrosis was observed (stage 0-1). In CD-fed mice, mild fibrosis in some WT and Triple CYP-KO AhRR^{+/+} mice was detected.

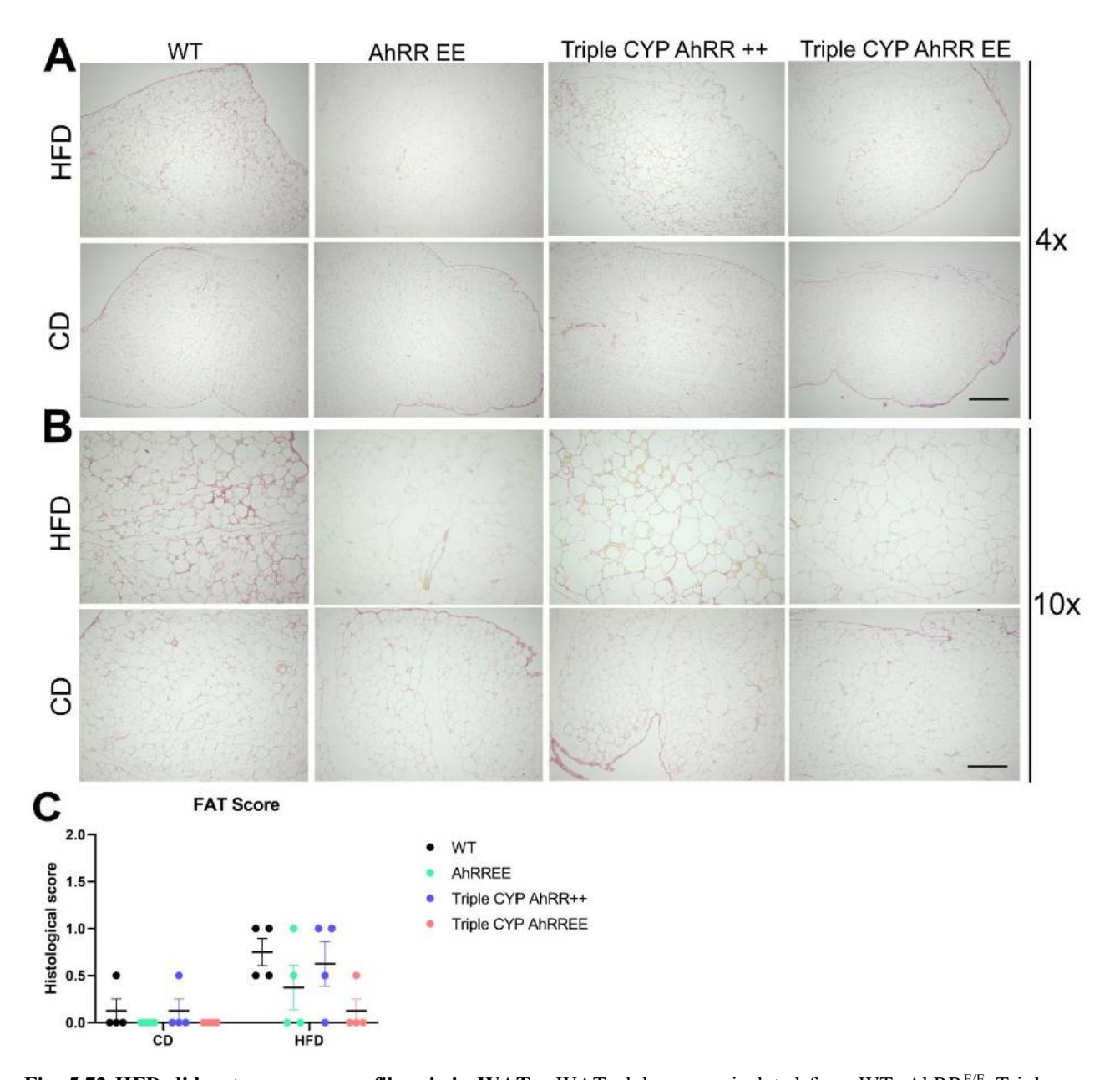


Fig. 5.72 HFD did not cause severe fibrosis in WATg. WATg lobes were isolated from WT, AhRR^{E/E}, Triple CYP-KO AhRR^{+/+}, and Triple CYP-KO AhRR^{E/E} mice were fed either CD or HFD for 14 weeks. Paraffin sections were obtained from adipose tissue, and Picrosirius red staining was performed to detect type I and III collagen. Images are representative of three mice/genotype, of which one image/genotype is shown here. Sections were visualized at A) 4x and B) 10x magnification. Scale bar = $500\mu m$ in A and $200\mu m$ in B. C) Three sections obtained from each mouse/genotype were scored based on the fibrosis severity and the average scores were plotted in the graph. The scores were determined as described in the methods section. Data was derived from one experiment (n =4).

On the cellular level, it was also necessary to quantify the presence of immune cells that resided in the SVF of WATg, as it had been shown that obesity and aging altered the immune milieu of visceral AT (Khan et al., 2020). Hence, the frequencies of various immune cell subsets from lymphoid and myeloid compartments were quantified by flow cytometry. The gating strategy for myeloid cells has been depicted in **Fig 5.17** (Chapter 4), whereas the gating strategy for lymphocytes is shown in **Fig. 5.73**. The lymphocytes were gated for CD19⁺ B cells, TCRβ⁺ T cells (both conventional CD4⁺ and CD8⁺ TCRβ⁺ cells and Tγδ cells), as well NK1.1⁺ TCRβ⁺ CD11b⁺ NKT cells and NK1.1⁺ TCRβ⁻ CD11b⁻ NK cells. For the myeloid cells, eosinophils were identified as CD11b⁺ SiglecF⁺ Ly6G⁻ cells, monocytes were identified as Ly6C⁺ cells, whereas ATM were identified as F4/80⁺ CD64⁺ cells. ATM were further divided into 4 subsets: ATM 1a, b, 2, and 3. ATM 1a and 1b were identified as CD11c⁺ CD206⁻ and CD206⁺, respectively. ATM 2 were defined as CD206⁺ CD11c⁻ cells, whereas ATM 3 were defined as CD206⁻ CD11c⁻ cells. cDCs were identified as F4/80^{lo} CD64⁺ MHCII⁺ cells.

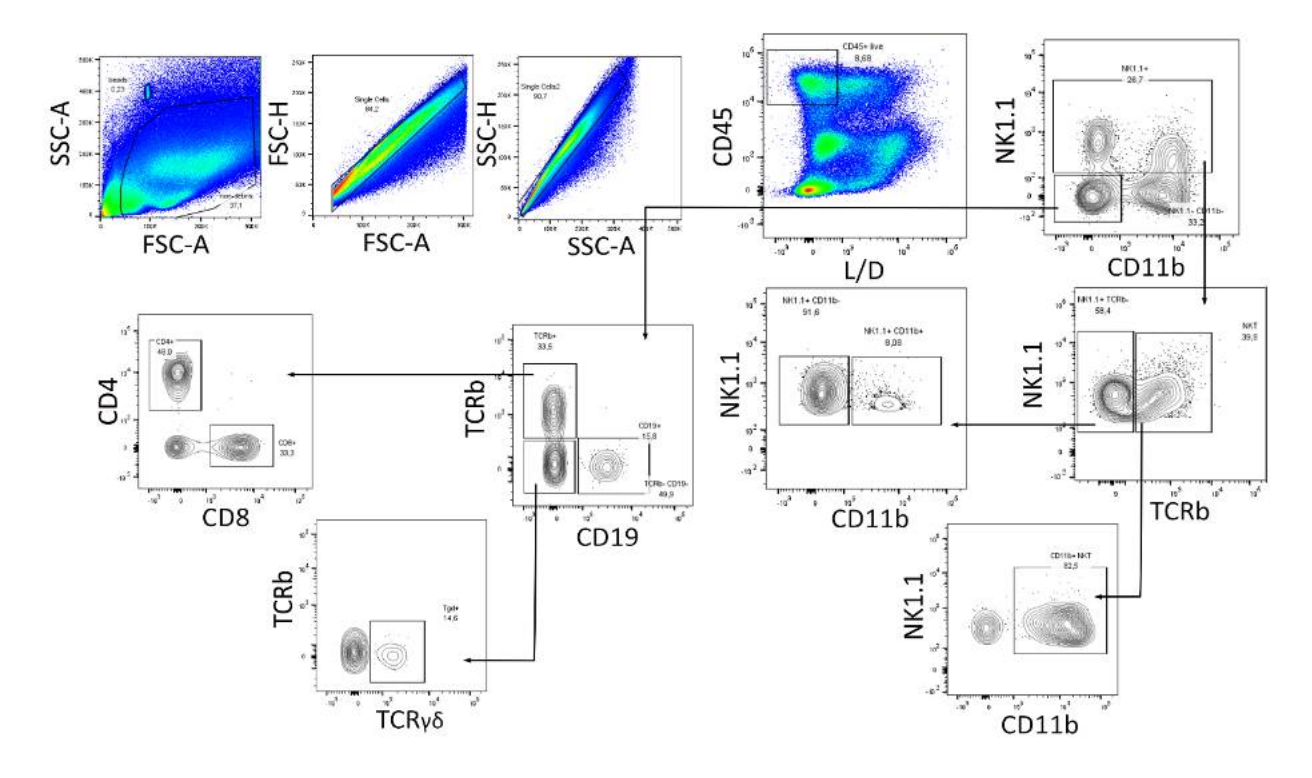


Fig. 5.73 Gating strategy of lymphocytes in the SVF of WATg. Stromal vascular fraction (SVF) was isolated from WATg of mice fed with either CD or HFD for 14 weeks and single SVF cells were gated for living single CD45⁺ cells. Then, T cells were identified as either conventional $TCR\beta^+$ cells (CD4⁺ and CD8⁺ T cells) or Tγδ cells. B cells were identified as $CD19^+$ cells. NKT cells were identified as $NK1.1^+$ $TCR\beta^+$ CD11b⁺, whereas NK cells were identified as $TCR\beta^-$ CD11b⁻ cells.

There was no inherent alteration of either NKT- and NK-cell subsets caused by the ablation of AhRR or the three CYP enzymes, and HFD also did not significantly alter the frequencies of

NKT- and NK cells across all genotypes (**Fig. 5.74 A and B**). In contrast, the ablation of the three CYP enzymes in Triple CYP-KO AhRR^{+/+} and Triple CYP-KO AhRR^{E/E} mice significantly reduced CD4 T cells frequency to around 8% compared to 15% cell frequency in CD-fed WT mice (**Fig. 5.74 C**). Meanwhile, HFD reduced the CD4 T cells frequency in WT, but not in the other three Moreover, HFD primarily affected the frequency of CD8 T cells in Triple CYP-KO AhRR^{+/+} mice to an extent that was significantly higher than the one in Triple CYP-KO AhRR^{E/E} mice (**Fig. 5.74 D**). HFD also slightly increased the frequency of CD8 T cells in WT and AhRR^{E/E} mice. Further, there was a tendency that HFD increased the B cell frequency in WT mice, but not in the mice that lacked AhRR or the three CYP enzymes (**Fig. 5.74 E**). Interestingly, the ablation of the three CYP enzymes was sufficient to markedly increase the T $\gamma\delta$ cells frequency to around 5% compared to 2% in WT, whereas the ablation of AhRR only slightly increased the frequency of T $\gamma\delta$ cells (**Fig. 5.74 F**). Nevertheless, the T $\gamma\delta$ cell frequency in Triple CYP-KO AhRR^{E/E} mice was not higher than the one in Triple CYP-KO AhRR^{+/+} mice.

Of note, HFD strongly reduced the frequency of eosinophils in WT mice from 12% to around 2%, as well as in Triple CYP-KO AhRR^{+/+} and Triple CYP-KO AhRR^{E/E} mice from around 7,5-8% to 2,5-3%, respectively (**Fig. 5.74 G**). Besides, in the CD group, the eosinophil frequency in WT mice tended to be higher than in the other three genotypes. Interestingly, HFD increased all cDC subpopulations across all genotypes, especially in AhRR^{E/E} and Triple CYP-KO AhRR^{E/E} mice, suggesting that AhRR depletion elevated cDC frequencies in AT (**Fig. 5.74 H**). This increase was primarily attributed to the CD24⁺ cDC rather than the CD24⁺ cDC (**Fig. 5.74 I and J**, respectively). Regarding CD24⁺ cDC, HFD increased their frequency in AhRR^{E/E}, Triple CYP-KO AhRR^{E/E} mice, whereas HFD only slightly reduced the CD24⁺ cDC frequency in Triple CYP-KO AhRR^{E/E} mice (**Fig. 5.74 J**). HFD also significantly increased the frequencies of both MHCII⁻ and MHCII⁺ monocytes (**Fig. 5.74 K and L**, respectively). In the MHCII⁻ subset, HFD increased the cell frequency from 2% to 5,8% (WT), 4% (AhRR^{E/E}), and 5% (Triple CYP-KO AhRR^{+/+}). In the MHCII⁺ subset, HFD increased the frequency from around 1,5% to around 4% in WT and around 3% in AhRR^{E/E} and Triple CYP-KO AhRR^{+/+} mice.

Further, the frequency of MHCII⁻ monocytes in WT and Triple CYP-KO AhRR^{+/+} mice was slightly higher than the one in AhRR^{E/E} and Triple CYP-KO AhRR^{E/E} mice (**Fig. 5.74 K**). The frequency of total F4-80⁺ Ly6C⁺ Mo-Mac, was not altered by either different diet or different genotypes (**Fig. 5.74 M**). Also, HFD did not induce the expression of CD11c in ATM, thus only ATM 2 and -3 (both were lacking CD11c) frequencies were quantified (**Fig. 5.74 N and O**, respectively). In general, HFD increased the frequencies of both ATM subsets across all

genotypes, but the increase was not significant in the ATM subsets of WT mice (**Fig. 5.74 N and O**).

As shown in **Fig. 5.19** (Chapter 4), AhRR/EGFP was expressed by immune cells, particularly myeloid cells of WATg, but this was exclusively observed in the Triple CYP-KO AhRR^{E/E} mice. Feeding HFD and CD greatly reduced the AhRR/EGFP expression in the CD45⁺ immune cells in WATg SVF of AhRR^{E/E} and Triple CYP-KO AhRR^{E/E} mice, as already described for the hepatic immune cell subsets (**Fig. 5.75**). Hence, the AhRR/EGFP expression in individual immune subsets of WATg were alos not plotted here. Unfortunately, for the histology it was hard to obtain intact WATg sections particularly from the HFD-fed mice, thus it was not possible to analyze AhRR/EGFP expression by histology. Therefore, it could also not be determined whether AhRR expression was changed in the AT. All in all, HFD induced many alterations across various immune cell subsets, but the absence of AhRR and/or the three CYP enzymes fed CD altered frequencies in only two immune subsets, namely CD4⁺ T cells and Tyô cells).

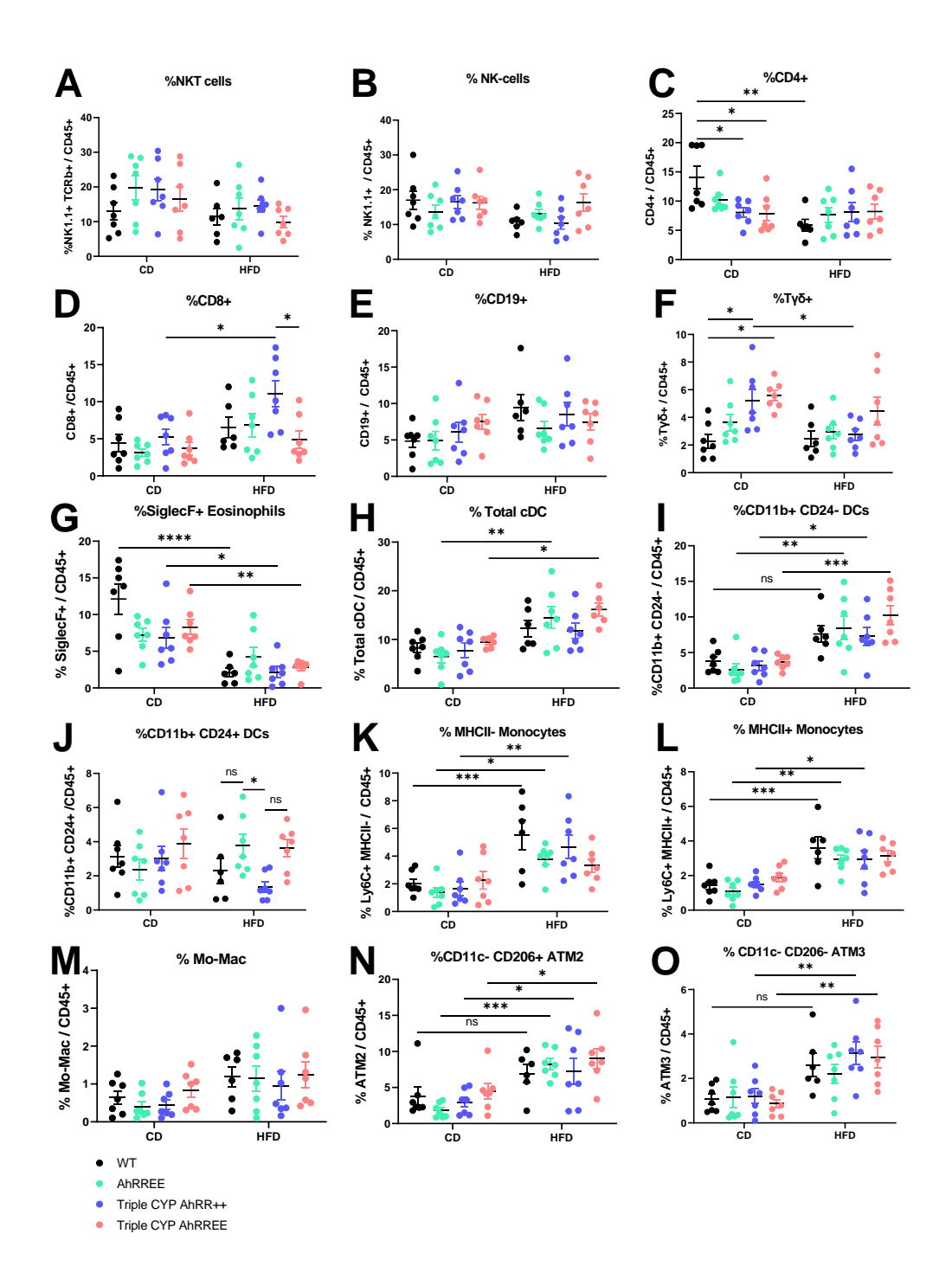


Fig. 5.74 HFD altered the frequencies of multiple lymphoid and myeloid subsets. WATg SVF cells were isolated from mice that were fed with either CD or HFD for 14 weeks. Cells were t gated for NKT-, T cells, NK cells, as well as KC, Mo-Mac, monocytes, as well as cDC1 & cDC2. The frequencies of the cell subsets were analyzed by flow cytometry and were quantified out of the total CD45 $^+$ cells. Results are shown as mean \pm SEM and significance was analyzed by two-way ANOVA corrected for multiple comparisons by the Bonferroni's method. Data was pooled from two independent experiments (n=7).

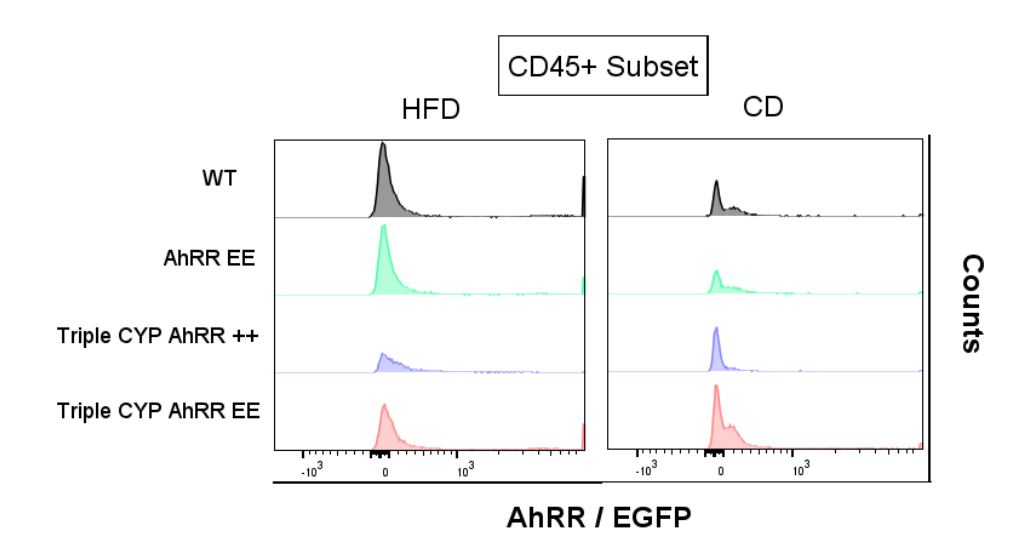


Fig. 5.75 HFD and CD diminished AhRR-expressing immune cells in WATg SVF. Following the isolation of WATg SVF, the AhRR/EGFP expression in each genotype and treatment group was analyzed in the living CD45⁺ subset by flow cytometry

6. Discussion

The AhR is expressed widely in cells of the immune system and its activity is particularly high in different cell types of barrier organs (Esser & Rannug, 2015), in line with its main function as an environmental sensor. AhR activation leads to the transcription of target genes, such as Ahrr, Cyp1a1, Cyp1a2, and Cyp1b1, all of which are negative regulators of AhR. The function of the AhRR is highly context- and organ dependent. During intestinal inflammation, AhRR and AhR react in a similar way to attenuate inflammation, whereas in the LPS shock model, the AhRR antagonizes the anti-inflammatory function of the AhR (Brandstaetter et al., 2016). Furthermore, CYP1A1, CYP1A2, CYP1B1, three enzymes of the cytochrome P450 family that metabolize most of AhR ligands except for TCDD, are all expressed in an AhR-dependent manner (Nebert et al., 2004). The overarching aim of my project was to assess AhR activation and AhR-dependent trasncriptional regulation in different ways. To elucidate the role of the AhRR during AhR signaling, V5-epitope tagged mice were generated as a potential tool to trace the AhRR protein within cells. To characterize this new reporter mouse line, AhRR-V5 expression was analyzed. In addition, to gain a better understanding of AhR signaling, both concentration and time kinetics were conducted, and a mathematical modeling approach was initiated in collaboration with the group of J. Hasenauer. In addition, AhR signaling in the absence of the negative regulators AhRR and the three AhR-dependent CYP enzymes was analyzed under multiple conditions, comparing steady-state, enhanced AhR activation following application of AhR ligands, and obesity-induced metaflammation.

6.1. Validation of AhRR-V5 protein expression in mice

To analyze the expression and function of the AhRR on the protein level, V5-tagged AhRR mice were generated, as there is no commercially available antibody against AhRR. To test the functionality of the mice, AhRR-V5 expression was first analyzed by Western blot using V5-specific antibodies in primary cells and organs isolated ex vivo. Unfortunately, AhRR-V5 expression could not be detected by this method even after stimulating BMDC with 3MC for 12 and 20 hours. Also, after increasing the cell number to 20 million cells/sample, AhRR expression could not be detected. Then, another approach using IP was used to pull down the V5-tagged AhRR protein from 20 million 3MC-treated BMDC, as well as bladder and mLN prior to detection by Western blot. Bladder and mLN were used, as these organs were previously shown to moderately express AhRR (Brandstätter et al., 2016; Tsuchiya et al., 2003).

However, only the positive control, AhRR-V5 overexpressing HEK293T cells, yielded a AhRR-V5 specific band. This indicates that either the physiological expression level of the AhRR was generally too low to be detected, or that the AhRR mRNA or protein might have been rapidly degraded on post-transcriptional and post-translational level, respectively, during the procedure. It is known that *Ahrr* mRNA contains 2 AU-rich elements (ARE) in the 3'UTR. RNA binding proteins can bind to these AREs, and these proteins can either stabilize or destabilize mRNA (Kramer & Carrington, 2014; Lee et al., 2013). TTP is one of the mRNA binding proteins that can destabilize Ahrr mRNA, hence also reduces AhRR expression. Therefore, *Ttp* expression on mRNA level was analyzed. *Ttp* expression peaked earlier than AhRR expression peaked, thus it is unclear whether TTP would be able to interfere with AhRR mRNA stability. It would be more ideal to measure TTP expression on the protein level, since it is the TTP protein that binds to the AREs. To assess if Ahrr is unstable at the mRNA level, an mRNA decay assay was conducted. In this assay, HepG2 cells were either treated with ActD only, a DNA intercalator that inhibits RNA polymerase-mediated transcription or co-treated with 3MC and ActD. The co-treatment of 3MC and ActD slightly induced Cyp1a1 mRNA decay, but not that of Ahr and Ahrr. When treated with ActD alone, the half-lives of Ahrr and Ahr were comparable and they were slightly shorter than the one of *Cyp1a1*, making it unlikely that Ahrr mRNA is regulated by enhanced mRNA decay. Nevertheless, the half-lives of Ahr, Ahrr, and Cyp1a1 may be different in BMDC.

Apart from post-transcriptional regulation, there is also post-translational regulation by ubiquitination-mediated proteasomal degradation by the 26S proteasome that can degrade a broad array of proteins, including AhR and AhRR. An earlier study showed that TCDD-mediated AhR activation leads to the degradation of AhR via the ubiquitin-proteasome pathway (Ma & Baldwin, 2000) and hence would also lead to reduced AhRR expression. Nevertheless, UbCM4 acts on many proteins and can possibly also degrade AhRR directly. Another AhR repressor, TiPARP represses AhR using a similar mechanism, as its overexpression could enhance TCDD-mediated proteolytic degradation of the AhR (MacPherson et al., 2013). Thus, the possibility of enhanced proteasomal degradation of AhR and AhRR cannot be excluded. Therefore, the proteasomal inhibitor MG132 was also used in one of the Western blot experiments to treat the cells post 3MC treatment. However, also here, no AhRR-V5 protein could be observed. It might be that the dose and or the timing of MG132 treatment was not optimal. In addition, dose and time course is also dependent on the cell type analyzed (Dang et al., 2014; Sun et al., 2018). In further experiments, a time and dose kinetic for MG132 in BMDC should be performed, as well as testing the optimal time point for 3MC treatment. It seems that

pre-treatment is favored over co- or post-treatment, as previous findings have shown that 2-hour pre-treatment of MG132 at 10µM could efficiently prevent p53 degradation in HeLa and SiHa cervical-cancer-derived cells (Hougardy et al., 2005), and 1-hour pre-treatment at the same concentration could prevent the degradation of the Topoisomerase II cleavage complex (Sciascia et al., 2020). Besides, one also does not know if MG132 treatment would confound the interpretation of the ChIP-seq result. Hence, we decided not to continue to work with this model and another approach to increase AhRR mRNA and protein expression was chosen. One way to achieve that is by generating a mouse model, in which the enzymes that metabolize AhR ligands are ablated. This mouse model could be used not only to increase AhRR expression, but also to elucidate the functional properties that may be elicited by the enhanced expression of AhRR.

6.2. Expression kinetics of *Ahr* and its target genes after stimulation with different AhR ligands

The aims of the kinetics experiment were to determine the optimal concentration and stimulation time of various ligands, and to investigate the expression dynamics of Ahr and its target genes at the optimal time point. From the concentration kinetics, it was concluded that the most optimal concentration for most ligands is $1\mu M$, as they could elicit all the target genes except *Tiparp* at this concentration. *Tiparp* was induced 5-7.5 times higher compared to the control at a concentration of 100µM after 16 hours, depending on the ligands. In addition, Ahr expression appeared to be upregulated by lower concentrations of the different ligands (10-100 nM), whereas the three target genes analyzed (Ahrr, Ahrr $\Delta 8$, Cyp1a1) were upregulated by higher concentrations (100nM -10μM). Furthermore, the concentration kinetics results of Ahrr and Ahrr $\Delta 8$, a splice variant of the full length AhRR are also not entirely similar; for the Ahrr, 3MC and DIM were the most potent stimulants, whereas for the Ahrr∆8, FICZ and ICZ were the most potent ones. The underlying reason for this discrepancy is unclear, as they are supposed to be induced in a similar manner following AhR activation. In human cells, the Ahrr $\Delta 8$ is more prominent compared to the full-length form and can repress the endogenous HepG2 Ahr expression by 61%, whereas Ahrr barely represses it (Karchner et al., 2009). For the analysis of Cypla1, not only mRNA levels were determined but also the activation of the Cyplal promoter was accessed using a reporter cell line. In this case, the expression levels of Cyplal after stimulation with different ligands were largely in agreement with the result of the reporter assay, except for the fact that in the latter 3MC at a concentration of 100µM elicited the highest Cyp1a1 promoter activation, but it was 3MC at 10µM that elicited the highest Cypla1 transcript. Such a discrepancy should be interpreted with caution, as both assays

measured different aspects of gene expression. It might be that a larger amount of Cyp1a1 mRNA was degraded at the $100\mu\text{M}$ concentration of 3MC and such an effect did not affect the Luciferase experiment, as it only measured the Cyp1a1 promoter activation and not the amount of transcript. For most ligands and target genes, the $100\mu\text{M}$ concentration might elicit toxic effects on the cells, as the expression levels of most of the target genes dropped at this concentration. All in all, 3MC elicited the highest expression of all AhR target genes analyzed, except $Ahrr\Delta 8$, whereas DIM was the most potent stimulus to induce Ahrr and Ahr. Meanwhile, ICZ and FICZ had a similar kinetic, but they were not as potent as 3MC and DIM in inducing most target genes, except $Ahrr\Delta 8$ and in the case of FICZ, also Cyp1a1. Nevertheless, these experiments showed variations between the independent experiments performed. Each of the three experiments was conducted with around 2-3 weeks in between, increasing the passage number of the cells overtime. This might have altered the properties of the HepG2 cell line and caused the large variations between the experiments.

For the time kinetics experiment, the three independent experiments were done with only a week interval in between to minimize the unwanted effects of over-passaging cells that could cause larger variations. The time kinetics data was also used to generate a mathematical model of AhR signaling following ligand binding. Upon 3MC stimulation, Cyp1a1 was induced up to 50-fold after 24-hour stimulation, showing the highest expression level compared to the other AhR target genes, probably due to its constitutive expression and high inducibility in hepatic tissue (Klomp et al., 2020; Ye et al., 2019). In the same setting, Ahr and Tiparp were induced only up to 2.5- and 2.3-fold at 12- and 24 -hours, respectively. When comparing this to the results published by MacPherson et al. (MacPherson et al., 2013), who treated T-47D human breast cancer cells with TCDD, the Cyp1a1 kinetics is similar, as it also peaked 24-hours after stimulation. However, discrepancies were observed in terms of Ahrr and Tiparp expression. In TCDD-treated MCF7 human breast cancer cells, Ahrr had already reached its peak at 2.5-hours and this was sustained up to 24-hours (MacPherson et al., 2014). In contrast, *Tiparp* expression reached its peak (~6-fold) within 1.5 hours post treatment, but this only lasted for 30 minutes, and its expression had already declined from 2.5 hours onwards. This is intriguing, as TCDD could sustain the peak expression of Ahrr but not Tiparp. The sustained Ahrr expression can be attributed to the high stability of TCDD (Denison and Nagy, 2003), even though the binding affinity of TCDD is comparable to 3MC (Giani Tagliabue et al., 2019). Thus, it was expected that TCDD could have induced *Tiparp* also for a longer time period. It is possible that *Tiparp* is even more unstable than Ahrr on mRNA level, but a mRNA decay assay should be conducted to prove this notion. Furthermore, 3MC triggered the *Cyp1a1* promoter activity the most 8 hours after stimulation, whereas the amount of *Cyp1a1* transcript peaked at 24-hour. An explanation for this could be that promoter activation is detected earlier than the transcripts, as the Luciferase assay monitors promoter activation, whereas qPCR measures gene expression.

6.3. Increased AhR signaling through elimination of CYP- and/or AhRR- mediated negative feedback regulation

Several publications have shown that AhR signaling is tightly controlled, as its prolonged activation either by ligands that resist metabolic clearance, e.g., TCDD (Bock, 2016, Kerkvliet et al., 2002) or by the expression of a constitutively active AhR has detrimental effects on cellular physiology (Mitchell and Elferink, 2009, Andersson et al., 2002). A proof-of-concept experiment (Schiering et al., 2017) had shown that both systemic and IEC-restricted constitutive expression of Cyp1a1 alone were sufficient to increase the metabolic clearance of AhR ligands in the small intestine and therefore curtailed the duration of AhR signaling in this organ. The net effect of constitutive activation of Cypla1 mimicked an AhR-deficient state, in which the AhR-dependent ILC3 and Th17 cells were depleted. The reduced Th17 level also led to a reduced IL-22 level in the small intestine of mice with systemic or IEC-restricted constitutive Cyplal expression. However, most AhR ligands are metabolized not only by CYP1A1, but also by CYP1A2 and CYP1B1 (Nebert et al., 2004). Moreover, Nebert et al. (Nebert et al., 2004) have also shown that the ablation of these three CYP enzymes caused alterations in both gross conditions (e.g. lower body weight, higher serum ALT and AST) and at the cellular level (e.g. increased neutrophils and macrophages numbers in zymosan-induced peritonitis). Hence, we aimed to further investigate the cellular phenotype of these mice and crossed the Triple CYP-KO mice with AhRR^{E/E} mice to further enhance AhR activity and to quantify and visualize AhRR expression. We analyzed the Triple CYP-KO mice in the presence of the homozygous AhRR^{E/E} knockin only and no heterozygous mice were analyzed, different from the study conducted by Brandstaetter et al (Brandstätter et al., 2016a). The reason for this was that the phenotype of AhRR^{E/+} mice is quite unpredictable, as cell-type specific gene dosage effects were observed in the AhRR^{E/+} heterozygous mice. Moreover, the AhRR^{E/+} mice also possessed weaker EGFP signal strength compared to the AhRR^{E/E} mice. In addition, by breeding the mice using homozygous as opposed to heterozygous breeding pairs, we could reduce the number of mice required for breeding, which is in accordance with the 3R principle.

These animal models enabled us to conduct a proof-of-concept experiment that showed enhanced expression of AhRR/EGFP in the Triple CYP-deficient mice in various cell subsets and in multiple organs under physiological condition. Such enhanced expression was also accompanied by altered frequencies of specific immune cell subsets.

6.3.1. Triple CYP deficiency enhanced AhRR expression in immune and stromal non-immune cells in different organs

In general, there were obvious differences both in the AhRR/EGFP expression level and in the distribution of AhRR/EGFP-expressing cells in various organs comparing Triple CYP-KO AhRR^{E/E} and AhRR^{E/E} mice. These differences were observed by both histology and FACS analysis. For gallbladder and small intestine only histological analysis was conducted, whereas for the rest of the organs, similar results could be achieved by both methods. Overall, AhRR/EGFP expression was readily detected in immune cells, which is in line with the findings of Brandstätter et al. (Brandstätter et al., 2016a). In some organs (e.g S.I. and gallbladder), however, AhRR/EGFP could also be detected in CD45⁻ stromal cells in the Triple CYP-KO AhRR^{E/E} mice, but not in AhRR^{E/E} mice. This increase in AhRR/EGFP expression in stromal cells makes sense, as CYP1A1 and CYP1B1 expression could be found in hepatocytes, endothelial cells, hepatic LSEC (Dragin et al., 2006), lung epithelial cells (Alessandrini et al., 2022), and vascular endothelial cells (Conway et al., 2009). Hence, the ablation of the three CYP enzymes could also lead to elevated AhR ligand levels, upregulating AhRR (Dragin et al., 2006). In most of the immune cell subsets in these organs, AhRR/EGFP expression was detected in both Triple CYP-KO AhRR^{E/E} and AhRR^{E/E} mice, with an enhanced level of AhRR/EGFP expression in Triple CYP-KO AhRR^{E/E} mice. This shows that ablating the three CYP enzymes has successfully increased AhR activation, hence also AhRR/EGFP expression. Remarkably, such an increase in AhRR/EGFP expression did not occur in IEC. This result is very interesting, as AhR and the three CYP enzymes are expressed by IEC in both SI and colon (Schiering et al., 2017; Shah et al., 2022; Stockinger et al., 2021; Yoshimatsu et al., 2022), indicating that AhRR expression is specifically prevented in IEC by an additional, so far unknown mechanism.

In the SI of Triple CYP-KO AhRR^{E/E} mice, AhRR/EGFP expression was detected in the PDGFR α^+ , CD34 $^+$, and gp38 $^+$ stromal cells in the villi and crypts. However, the identity of these cells was hard to determine. The PDGFR α^+ AhRR/EGFP-expressing cells could be telocytes, but these EGFP $^+$ cells are localized more in the superficial villi and not at the crypt-villus junction like intestinal telocytes (McCarthy et al., 2020). McCarthy et al. also suggested

that there are CD81⁺ PDGFRα^{lo} trophocytes at the crypt base. Hence, further staining with CD81 would be required to determine if some of the AhRR/EGFP-expressing cells are trophocytes. Also, an upregulation of AhRR in the immune cell subsets should be visible, as AhRR is expressed in intestinal cDC, macrophages, and T cells (Brandstaetter et al., 2016, Schanz et al., 2020). But in this experiment, it could not be determined if there are more AhRR/EGFP-expressing immune cell subsets in the Triple CYP-KO AhRR^{E/E} due to the lack of a FACS analysis.

In the skin, AhRR/EGFP was expressed in more immune cell subsets in Triple CYP-KO AhRR^{E/E} than AhRR^{E/E} mice, such as in cDC1, CCR2⁻-monocyte-derived cells, and TCRβ⁺ cells. In the other subsets, such as Langerhans cells, cDC2, CCR2+-monocyte-derived cells, dermal γδ T cells, and DETC, AhRR/EGFP was expressed in both Triple CYP-KO AhRR^{E/E} and AhRR^{E/E} mice with a higher level in the former mice. There were more AhRR/EGFPexpressing cells among $\gamma\delta$ T cells than in TCR β^+ T cells in both genotypes. This may complement previous findings that showed that ~15% of dermal MHCII⁻ cells in AhRR^{E/E} mice expressed AhRR/EGFP (Brandstaetter et al., 2016). These MHCII⁻ cells contain both, T cells and fibroblasts. Therefore, the reported AhRR-expressing T cells could also be $\gamma\delta$ T cells (Brandstätter et al. 2016). Based on the previous finding by Brandstaetter et al., it can also be hypothesized that some of the AhRR/EGFP-expressing cells could be fibroblasts and that AhRR/EGFP expression can also be enhanced in dermal fibroblasts in Triple CYP-KO AhRR^{E/E} mice. Therefore, multiplex staining is required in the future to determine if AhRR/EGFP expression is enhanced in one or more fibroblast subsets. In DETC, there was a comparable level of AhRR/EGFP expression in both Triple CYP-KO AhRR^{E/E} and AhRR^{E/E} mice, as most of the cells (~60% of total DETC) were already AhRR/EGFP⁺ in AhRR^{E/E} mice. The expression of the AhRR also changed during development, as AhRR/EGFP expression was higher in DETC of p2 neonates than in 8-week adult mice, suggesting that AhRR may play a role in supporting the development of this cell subset. Nevertheless, how or if AhRR is regulated during development is still not well elucidated.

Similar to the skin, in BMDC cultures, there was a comparable level of AhRR/EGFP expression in both Triple CYP-KO AhRR^{E/E} and AhRR^{E/E} mice, as most of the cells (~80-95% of total BMDC) were already AhRR/EGFP⁺ in AhRR^{E/E} mice. BMDC cultures generated by GM-CSF stimulation consist not only of DC (GM-DC) but also of macrophages (GM-Macs). The expression of AhRR/EGFP in the CD11c⁺ MHCII⁺ subset, double-negative cells (GM-DN), and GM-Macs in control- and 3MC-treated samples were comparable. However, AhRR/EGFP

expression in LPS-treated samples was reduced in CD11c⁺ MHCII⁺ cells and GM-Macs, particularly in AhRR^{E/E} mice. This contradicts previous finding by Brandstätter et al. (Brandstätter et al., 2016a), who showed that LPS increased AhRR/EGFP expression in DC and macrophage subsets in BMDC cultures of AhRR^{E/+} mice. It is unclear what contributes to such discrepancy, but it could be that the presence of one allele that encodes functional AhRR in heterozygous AhRR^{E/+} mice may account for this. Furthermore, LPS is also known to reduce the expression of CD115 (M-CSFR1) in PBMC-derived monocytes, but this effect was inhibited by co-treating the cells with TMI005, an ADAM17 inhibitor. This suggests that LPSinduced CD115 shedding was mediated by ADAM17 (Waller et al., 2019). Furthermore, the AhRR/EGFP expression in the MerTK+ F4/80+ GM-Mac subset of AhRRE/E mice was significantly reduced after LPS-treatment, compared to the control and the 3MC-treated samples. However, this did not occur in the BMDC of Triple CYP-KO AhRR^{E/E} mice, and it is not clear what caused this effect and if it is mediated by the downregulation of CD115. Thus, it might be conceivable that the already very high AhRR/EGFP expression could not be further enhanced by elevated AhR activation in the Triple CYP-KO mice. This may suggest that AhRR expression is strictly regulated, i.e. its expression will be limited once it reaches a certain threshold.

In contrast, in the liver, spleen, and gallbladder, AhRR/EGFP was only expressed in the cells of Triple CYP-KO AhRR^{E/E} mice and not in those of AhRR^{E/E} mice, based on both FACS and histological analyses. In these organs, the AhRR/EGFP was mainly expressed in non-immune cells, for example in CD34⁺ interstitial cells of Cajal/telocytes in gallbladder and in CD73⁺ cells in the liver. Expression of CD73 is associated with hepatic stellate cells and portal vein fibroblasts (Vuerich et al., 2019). Like for IEC, as discussed above, it is not clear why there was no enhanced AhRR/EGFP expression in hepatocytes of Triple CYP-KO AhRR^{E/E} mice. Again, this was unexpected, as AhR and its associated CYP enzymes are highly inducible in hepatocytes (Klomp et al., 2020).

In the WATg SVF, only SiglecF⁺ eosinophils and CD206⁺ CD11c⁻ ATM2 macrophages of Triple CYP-KO AhRR^{E/E} mice expressed AhRR/EGFP. Both immune cell subsets have been shown to modulate inflammation in AT, particularly in obesity or other related metabolic diseases (Vieira-Potter, 2014; Brigger et al., 2020). In the gallbladder, the AhRR/EGFP-expressing cells were mainly the CD34⁺ stromal cells. According to Diaz-Flores et al. (Diaz-Flores et al., 2020), these cells are telocytes, which have multiple region-specific functions, such as to modulate the proliferation and maturation of parenchymal stem cells during tissue

regeneration and act as one of the main sources of mesenchymal precursor cells during tissue repair (Diaz-Flores et al. 2020). In the gallbladder, the altered amino acid composition of bile in gall stone patients could reduce the number of telocytes (Bugajska et al., 2023). Nevertheless, the function of telocytes in gallbladder is not well elucidated. Lastly, the AhRR expression in the spleen was minimal (<5%) and AhRR/EGFP-expressing cells were largely found in T cells of Triple CYP-KO AhRR^{E/E} mice. This finding also supports the study conducted by Brandstaetter et al. (Brandstaetter et al., 2016), as there was barely any AhRR/EGFP expression detected in spleens of AhRR^{E/E} mice.

In some cases, discrepancies between the FACS- and histological results were also observed. For instance, the liver histology from Triple CYP-KO AhRR^{E/E} mice showed that AhRR/EGFP expression was most pronounced in the stromal cells surrounding blood or lymphatic vessels, but the FACS result showed that no AhRR/EGFP-expressing cells were detected in the CD45⁻ fraction of the Triple CYP-KO AhRR^{E/E} mice. The underlying reason could be the preparation of the tissues for FACS analysis and immunohistology. Some of the CD45⁻ negative cells could have been lost during preparation of single cells or could have been damaged during the preparation, thus leading to a leakage of the cytoplasmic EGFP signal. Therefore, it would be crucial to test other preparation methods or develop methods that can capture the heterogeneity of stromal cells to identify and quantify the AhRR/EGFP-expressing cells, so that the FACS result can also complement the histological result.

In conclusion, AhRR and the three CYP enzymes are not co-expressed in IEC and hepatocytes, as no AhRR/EGFP signal was detected in AhRR^{E/E} mice. Moreover, AhRR/EGFP remained undetected in these cells despite the increase of ligand bioavailability resulting from knocking out the three CYP enzymes. It might be that a protective mechanism or a strict regulatory mechanism, e.g., by epigenetic means, exists that prevents AhRR expression in these cell types. One can also speculate that aberrant AhRR expression and inhibition of AhR signaling in these cell types is unfavorable, as AhR signaling is crucial in IEC and hepatocytes to maintain homeostasis. For instance, AhR activation prevents fibrogenesis and activation of hepatic stellate cells (Yan et al., 2019) and AhR signaling in IEC is necessary not only to maintain IEC, but also ILC3 and Th17 cells (Schiering et al., 2017). In the future, conducting an experiment that allows us to force the expression of AhRR in hepatocytes or IEC using newly generated Rosa26-LSL-AhRR mice will be interesting, as one can see if such forced expression may lead to deleterious effects on health.

6.3.2. Lack of AhRR and/or deficiency of the three AhR-dependent CYP enzymes alters the frequency of immune cell subsets

Apart from an increased AhRR/EGFP expression in Triple CYP-KO AhRR^{E/E} mice compared to AhRR^{E/E} mice, the lack of AhRR and/or AhR-dependent CYP enzymes led to alterations in the cellularity of different organs. For instance, in the SVF of WATg, none of the immune cell subsets in the Triple CYP-KO mice and/or AhRR^{E/E} mice was altered across all genotypes. According to Divanovic et al. (Divanovic et al., 2013), the three CYP enzymes are present in this tissue and supposed to play a role in lipid metabolism. In addition, this study also showed that under homeostatic conditions there were no significant differences between WT and Triple CYP-KO mice in the immune cell numbers as well as in the level of ω -6 and ω -3 polyunsaturated fatty acids, as well as leukotriene B (LTB) 4, which are lipid mediators in the peritoneal cavity. Only following zymosan-induced peritonitis there was an enhanced neutrophil recruitment in the Triple CYP-KO mice compared to WT mice, due to increased peritoneal levels of LTB4 in these mice (Divanovic et al, 2013).

In liver and spleen, the lack of either AhRR or the three CYP enzymes was sufficient to alter the frequencies of immune cells. Thus, the absence of AhR-dependent CYP enzymes led to a slightly lower frequency of KCs in the liver compared to WT and AhRR^{E/E} mice. This finding is plausible, as 55% of CYP isozymes are highly expressed in liver, including the three CYP enzymes (Renaud et al., 2011). Moreover, systemic ablation of the three AhR-dependent CYP enzymes has been shown to increase neutrophil frequency in peripheral blood following benzo(a)pyrene (BaP) induction (Divanovic et al., 2013; Dragin et al., 2008). Unfortunately, the FACS panel used in the current experiments did not include Ly6G, hence the frequency of neutrophils could not be analyzed. Interestingly, AhRR-deficiency also increased the frequency of hepatic CD172⁺ cDC2 only in the AhRR^{E/E} but not in Triple CYP-KO AhRR^{E/E} mice. Hence, it is possible that AhRR and the three CYP enzymes engage in different downstream signaling pathways that subsequently affect immune subsets in a differential manner. In the spleen, the absence of either AhRR or Triple CYP increased the NK cell frequency compared to WT mice, but interestingly, the absence of all of these proteins in the Triple CYP-KO AhRR^{E/E} mice did not further increase the NK-cell frequency. In skin, a reduced frequency in the DETC subset of 8-week-old mice could be seen in both AhRR^{E/E} and Triple CYP-KO AhRR^{E/E} mice, therefore the reduced DETC frequency was most likely mediated by AhRR-deficiency rather than by the deficiency of the three CYP enzymes.

In other subsets, however, the altered immune cell frequencies could not be explained by the absence of either AhRR or AhR-dependent CYP enzymes alone. For instance, in skin cDC2 and conventional T cells, the absence of AhRR or AhR-dependent CYP enzymes was not sufficient to alter their frequencies, but in the absence of all of them in Triple CYP-KO AhRR^{E/E} mice the frequencies of cDC2 and T cells was enhanced. Similarly, a reduction of GM-Macs in BMDC only occurred in the absence of the three AhR-dependent CYP enzymes and AhRR. It is known that the three CYP enzymes are present in bone-marrow and skin, in which they play a role in the metabolism of not only AhR ligands but also fatty acids (Divanovich et al., 2013; Slominski et al, 2014). Nevertheless, it has not yet been investigated how the metabolic alterations caused by the absence of these three CYP enzymes affect the canonical AhR signaling in steady state. Lastly, FACS analysis of the SI could not be conducted due to time restraints. Hence, the frequencies of intestinal immune cells (e.g, ILC3 and Th17 cells) that were analyzed in the experiment by Schiering et al. (Schiering et al., 2017b) could not be quantified and compared in the present study to determine if the alteration of immune subsets in CYP1A1-deficient mice would be similar to the one of Triple CYP KO.

Taken together, it is still unclear why deficiency in AhRR or Triple CYP was sufficient to alter cell frequencies in some cells and organs, but in others, the deficiency of both was required. One possibility is that this depends on differences in the baseline expression of AhRR and Triple CYP in each organ and cell type. In some cell types either AhRR or CYP enzymes are expressed, and AhRR expression might therefore be restricted to distinct cell types. For instance, in the liver, CYP enzymes are abundant (Renaud et al., 2011), but AhRR is minimally expressed (Brandstaetter et al., 2016). In the intestine, both AhRR and CYP enzymes are highly expressed, but not in the same cell types (Brandstaetter et al., 2016; Uno et al., 2018). In the skin, AhRR expression is also high in immune cells (Brandstaetter et al., 2016; Divanovich et al., 2013), whereas CYP1A1 expression is high in keratinocytes (Kyoreva et al., 2021). Therefore, the regulation of AhR signaling would also differ in these cell types. Alternatively, it might also be that the absence of the three CYP enzymes affects the expression of other CYP enzymes, as the ablation of Cyp1a2 caused reduced expression of Cyp4a14 and Cyp4a10 mRNA (Smith et al., 2003). Also, it might be that other CYP enzymes produce metabolites that eventually can influence AhR signaling. We cannot exclude the possibility that such influence may lead to the induction of other signal cascades that influence the presence of immune cell subsets. Thus, single-cell transcriptomics and metabolic profiling of these cell subsets might be helpful to elucidate which other genes are affected by the AhRR and/or the three CYP-enzymes.

Another aspect that still warrants further investigation is the question whether alterations in AhRR and/or CYP expression would affect the cytokine profiles, since AhR activation or inhibition has been shown to modulate the expression level of numerous cytokines in different cells, e.g., IL-33 in macrophages (Ishihara et al., 2019) and IL-10 in Foxp3⁺ T cells (Gandhi et al., 2010). Such alterations in cytokine expression may in turn modulate the microenvironment and cellularity of an organ. It can also affect the crosstalk between immune and stromal cells. For instance, in the gut, macrophages and Treg produce IL-10 which targets IEC to foster their proliferation and the homeostasis of the gut barrier, whereas IEC can also produce IL-33 under perturbed conditions, which targets ILC2 and Tregs among others, leading to Type 2 immune responses and intestinal inflammation (Mahapatro et al., 2021). Apart from cytokines, immune cells can also generate lipid mediators under certain conditions, for example following zymosan challenge depending on the three AhR-dependent CYP enzymes (Divanovich et al., 2013). Hence, in Triple CYP-KO mice or in Triple CYP-KO AhRR^{E/E} mice dysregulated metabolic processes in both immune and stromal cells, could occur. In line with this notion, a study by Uno et al. (Uno et al., 2018) showed that the absence of CYP1A1 could exacerbate the progression of NAFLD in mice fed a BaP-supplemented Western diet. This was mediated by elevated expression of the genes involved in bile acid export (Abcc4 and Slc51b) and reduction in bile-acid-synthesizing genes (*Cyp7a1* and *Cyp8b1*).

6.3.3. Deficiency for AhRR and Triple CYP inhibit proliferation of skin epidermal DETC under physiological conditions

FACS analysis of skin epidermal DETC showed that in adult, 8-week-old mice, there was a reduction in the DETC frequency in both AhRR^{E/E} and Triple CYP-KO AhRR^{E/E} mice, suggesting that the DETC reduction was mediated by AhRR deficiency. It was not clear though if this reduction was caused by impaired proliferation, premature cell death, or impaired migration of DETC to the skin, as DETC also migrate from thymus to peripheral organs once they are differentiated, like conventional T lymphocytes (Fiala et al., 2020). Kadow et al., (Kadow et al., 2011) showed that the reduction of DETC numbers in AhR-KO mice can already be observed in the thymus during the embryonic phase. In contrast, the seeding of DETC into the skin was not affected, as DETC numbers were comparable with WT on postnatal day 2 (p2). Interestingly, there were more cycling cells in AhR^{+/-} mice than in AhR-KO mice, suggesting that the reduced DETC numbers were caused by impaired proliferation rather than cell death or impaired seeding.

Based on these earlier findings, epidermal cells from Triple CYP-KO AhRR^{E/E} mice at p2 were isolated and stained with Ki-67, a proliferation marker, and their frequencies were quantified by flow cytometry. There was no significant difference in total DETC numbers in epidermal immune cells, which is similar to the result for AhR-KO mice (Kadow et al. 2011). However, there was a significant reduction in Ki67⁺ proliferating DETC but not Ki67⁻ non-proliferating DETC in the Triple CYP-KO AhRR^{E/E} mice already at p2. Therefore, the reduced DETC frequency at 8 weeks of age was most likely due to impaired proliferation and not to increased cell death or impaired migration. Moreover, the time point at which the DETC reduction was observed differs between the AhR-KO and Triple CYP-KO AhRR^{E/E} mice; DETC numbers in AhR-KO mice are lower than in WT starting from p7 onwards, whereas DETC in Triple CYP-KO AhRR^{E/E} mice are already lower at p2 compared to WT. This result suggests that the absence of AhRR and the three CYP enzymes depleted the DETC by a mechanism other than the absence of the AhR per se. Unfortunately, because there were no data from the AhRR^{E/E} mice at p2, it cannot be concluded that the reduced frequency of proliferating DETC is due to AhRR deficiency, as it is in the adult 8-week-old mice. Nevertheless, it is interesting that DETC are reduced in both AhR-KO and Triple CYP-KO AhRR^{E/E} mice already at the neonatal phase.

The reduced DETC frequency has been reported to impair the maturation of Langerhans cells, since DETC are a major source of GM-CSF that is required for Langerhans cell maturation (Kadow et al., 2011). Nevertheless, the Langerhans cells frequency was not reduced in this experiment, and it is not clear if they use an alternative GM-CSF source or other growth factors to sustain their maturation. It is also possible that the Langerhans cells reach maturation by simply expressing AhR. Hence, GM-CSF measurement by ELISA needs to be done in the future to see if there's a reduction of GM-CSF.

6.4. 3MC treatment in vivo can upregulate AhRR expression in myeloid cells of various organs

AhR ligands are derived from various sources; they can be endogenous, like tryptophan metabolites, such as FICZ, kynurenine, and kynurenic acid (Murray & Perdew, 2020) or exogenous carcinogenic polycyclic aromatic hydrocarbons, like 3MC or BaP (Stejskalova et al., 2011). For the current experiments, 3MC, a synthetic ligand, also found as a byproduct of industrial combustion processes, was used because of its high potency and binding affinity to AhR (Giani Tagliabue et al., 2019; Tsuchiya et al., 2003). Previous data demonstrated that 16-

hour 3MC treatment of mice following i.p. injection in a concentration of 10mg/kg upregulated AhRR expression mostly in myeloid cells in skin, intestine, and secondary lymphoid organs (Brandstätter et al., 2016a). However, the oral/intragastric bypass is more physiologically relevant than the i.p route, even though the ligands applied are subjected to both hepatic and gastrointestinal first-pass metabolism (Al Shoyaib et al., 2019). Besides, this method also allows direct administration of 3MC to the small intestine, where high expression of AhR and its target genes has been observed. The main aim of these experiments was to investigate the effect of acute 3MC treatment administered by oral gavage on the AhRR expression in immune cells.

6.4.1. 3MC activates AhR and induces AhR target genes on mRNA level in several peripheral organs

3MC administered by gavage for 16 hours was sufficient to enhance AhR signaling, therefore also AhRR expression in various immune cell populations in liver, SI, and WATg. In liver and SI, the increase was also measured on mRNA level. 3MC significantly enhanced the expression of both AhR target genes, Ahrr and Cyplal in the liver of Triple CYP-KO AhRR+/+ and AhRR^{E/E} mice, respectively. In SI, 3MC significantly enhanced Ahrr in Triple CYP-KO AhRR^{+/+} mice and slightly increased Cyp1a1 in AhRR^{E/E} mice. Interestingly, Ahr expression in SI was also upregulated post 3MC treatment in Triple CYP-KO AhRR+/+ mice, but not in in Triple CYP-KO AhRR^{E/E} mice. It is unclear what might have caused this increase, but there are several possible reasons. First, it can be hypothesized that enhanced Ahr activation caused by the ablation of the three AhR controlled CYP enzymes led to an increased Ahr expression. However, if this was true, such an increase should also have been observed in the Triple CYP-KO AhRR^{E/E} mice, in which the highest AhR activation was taking place. Moreover, the increase also did not occur in liver, where 30-fold-upregulation of Ahrr was observed, further suggesting an organ- or cell type-specific effect of AhR. Previous publications have also reported that IDO1/TDO expression does not only activate the AhR, but also increases AhR expression (Solvay et al., 2023). They postulated that such an increase could be mediated by Nrf2, as it can bind to AhR antioxidant response elements in the AhR promoter (Raghunath et al., 2018; Shin et al., 2007). In general, Nrf2 is an AhR-target and it can be induced by AhR ligands (Wen et al., 2014), although FICZ treatment does not induce its expression (Mohammadi et al., 2021). So far it has only been reported that Nrf2 expression can be induced by tryptophan (Wen et al., 2014). Nevertheless, Nrf2 also responds to thiol reactive compounds (both xenobiotics and endogenous compounds) and subsequently alters the redox balance in cells (Hayes et al., 2009), which could influence AhR expression.

Another reason for enhanced *Ahr* expression could be that functional AhRR expression might have counteracted other competing pathways, such as the Rel B subunit of NF-kappaB (Vogel & Haarmann-Stemmann, 2017), that could have been induced by 3MC or its metabolites and subsequently inhibited not only AhR activation, but also *Ahr* expression. This would explain the absence of an increased *Ahr* expression in Triple CYP-KO AhRR^{E/E} mice. On the other hand, it is largely unknown whether *Ahr* expression can also be inhibited by other pathways. The pregnane X receptor (PXR), another transcription factor that plays a role in xenobiotic metabolism, can directly bind AhR at its DNA-binding domain, thereby preventing AhR from binding to its target genes and reducing *Cyp1a1*, *1a2*, and *1b1* expression (Cui et al., 2017). Nevertheless, activation of neither the canonical AhR signaling pathway nor other unknown pathways can fully explain the increase in *Ahr* expression in Triple CYP-KO AhRR^{+/+} mice. In the future, transcriptomic and ChIP-seq analyses of SI derived from mice that lack Triple CYP and/or AhRR would be helpful to see which other transcription factors are up/down-regulated and which potential binding partners of the AhRR can be detected.

6.4.2. AhRR expression is induced by 3MC treatment in immune cells in several peripheral organs

In addition to the transcriptomic analysis, the increase in AhRR expression was also measured by flow cytometry and histological analysis using the AhRR/EGFP reporter mouse model. AhRR/EGFP expression was particularly pronounced in different myeloid subsets (e.g. macrophages, DC, and Mo-Mac) of 3MC-treated Triple CYP-KO AhRR^{E/E} mice in liver, SI lamina propria, and WATg. In liver, AhRR/EGFP expression was also upregulated in lymphocytes (e.g. T cells, NKT- and NK cells). In contrast, in most cases 3MC only marginally increased AhRR/EGFP reporter expression in AhRR^{E/E} mice, in liver and SI. In WATg SVF, 3MC treatment significantly increased the AhRR/EGFP-expressing myeloid subsets both in AhRR^{E/E} and Triple CYP-KO AhRR^{E/E} mice. Unfortunately, this result was only partially confirmed by histology, mainly due to the high autofluorescence of adipocytes. In addition, the sensitivity of the detection method also differs, as FACS is more sensitive than the epifluorescence microscopy and because of the exclusion of adipocytes from the SVF also allows to put a better focus on the analysis of immune cells. Besides, the mechanical shear force inflicted by the sectioning procedure can also cause EGFP to leak from the cell cytoplasm. Furthermore, 3MC upregulated AhRR/EGFP expression not only in a cell type-specific manner,

but it also did so in differential magnitudes. Thus, in the SI, the AhRR/EGFP upregulation was more pronounced than in WATg. This may indicate that the amount of 3MC and its metabolites that ended up in each organ might differ. Measurement and quantification of 3MC and its metabolites in each organ by means of LC-MS could be conducted to prove this hypothesis. Regarding the intensity of staining, 3MC did not so much enhance the MFI of AhRR/EGFP on a per cell basis, which was also apparent in histology based on qualitative analysis. Only in the ATM2 and DC population in WATg 3MC treatment could markedly increase the MFI of AhRR/EGFP. In some of the immune subsets, there were not many AhRR-expressing cells to begin with, but they had an artificially high MFI due to autofluorescence. Nevertheless, in terms of the frequency of AhRR/EGFP⁺ cells, the present results are in agreement with previous findings, as a higher frequency of Ahrr and AhRR/EGFP-expressing DC and macrophages in mesenteric lymph nodes (mLN) of AhRR^{E/+} mice were also observed following 3MC treatment (Brandstätter et al., 2016a). This was also the case for DC, macrophages, and T cells in intestinal lamina propria following 4-week feeding with I3C-supplemented diet (Schanz et al., 2020). The upregulation of AhRR/EGFP expression was greatly mediated by AhR activation, as AhR-/- AhRR^{E/+} mice had a strongly reduced, barely detectable frequency of AhRR/EGFP-expressing cells in secondary lymphoid organs (Schanz et al., 2020). Taken together, 3MC treatment increased the frequency of AhRR/EGFP expressing cells but not necessarily the intensity of EGFP fluorescence in different immune cell subsets in various peripheral organs. Furthermore, in SI IEL, which already showed a very high basal AhRR/EGFP expression, 3MC could not further increase the expression, further implying that AhRR/EGFP expression is limited per cell once it reached a certain level.

Apart from immune cells, AhRR/EGFP was also found to be expressed in endothelial cells in liver and SI of Triple CYP-KO AhRR^{E/E} mice as shown in Chapter 3, as well as in WAT tissue (unpublished data). As the FACS analysis done here mainly focused on the immune cell analysis, additional analyses to capture the stromal cell subset should be performed in future. Qualitative analysis by means of histology showed that the AhRR/EGFP expression in the hepatic endothelial cells of control- and 3MC-treated Triple CYP-KO AhRR^{E/E} mice appeared to be similar, and 3MC did not induce AhRR/EGFP expression in hepatic endothelial cells of AhRR^{E/E} mice. This might be because AhR and its target genes (e.g. *Cyp1a1*, *Cyp1b1*) are highly expressed in hepatic endothelial cells (Lano et al., 2020; Li et al., 2020) and the AhR-dependent CYP enzymes limit the AhR activation in endothelial cells of AhRR^{E/E} mice (Major et al., 2023; Wiggins et al., 2023). Furthermore, the expression of the individual CYP enzymes

may not be identical in all cell types or organs. For instance, the inducible expression of CYP1A1 and CYP1A2 was the highest in the proximal small intestine, whereas the CYP1B1 expression was the highest in stomach and esophagus (Uno et al., 2008). Therefore, 3MC might have been metabolized by different combinations of the three AhR-dependent CYP enzymes in different organs.

In the SI, 3MC induced an overall increase of AhRR/EGFP expression in the lamina propria of AhRR^{E/E} mice, as the EGFP expression was extended down to the base of the villi and not just in the upper regions of the villi. The additional AhRR/EGFP-expressing cells could be immune cells, as there were increments of AhRR/EGFP-expressing macrophages and Mo-Mac in the lamina propria of AhRR^{E/E} mice. Besides, AhRR expression can also occur in stromal cells, as the result in Chapter 3 showed that AhRR/EGFP is also expressed by endothelial cells and possibly by PDGFRα⁺ telocytes. In the Triple CYP-KO AhRR^{E/E} mice, there were even more AhRR/EGFP-expressing cells in the cryptal area, but not in the villi. The exact identity of these additional AhRR-expressing cells at the villus base and crypt areas is not yet known. Because of their sub-epithelial localization, they might be fibroblasts, α-SMA⁺ myofibroblasts, telocytes, or PDGFRA10 mesenchymal cells (McCarthy et al., 2020; Powell et al., 2011). Regardless of their identity, the maintenance of cells at the villus base and in crypts was shown to be mediated by Wnt and EGF signaling rather than BMP signaling and they further rely on TRPA1, TAC1, and GLP1 hormones (Y. Wang et al., 2022). Interestingly, Wnt signaling has been shown to be mediated by AhR signaling in the intestine (Metidji et al., 2018). Nevertheless, most AhRR/EGFP expressing cells in the epithelial layer did not overlap with EpCAM⁺ IEC, suggesting that they are more likely to be IEL.

The histological analysis and FACS results permit several conclusions: First, 3MC did not induce AhRR/EGFP expression in cells of AhRR^{E/E} mice that did not anyways have basal AhRR/EGFP expression, like hepatocytes, hepatic endothelial cells, and IEC. The possible reasons for the absence of AhRR expression in the aforementioned cell types has been explained at the end of Chapter 6.3. Second, this result may also imply that 3MC treatment activated other pathways that are independent of canonical AhR signaling, which might have hampered AhRR expression. One of the possible pathways affected is the NF-κB pathway, as the promoter sequence of the AhRR contains three GC box sequences and one NF-κB site on top of the XRE site (Baba et al., 2001). Alternatively, it can simply be that the 3MC-mediated AhR activation was not sufficient to induce AhRR expression in these cells. Hence, activating AhR with either

longer stimulation time, higher dose, or more potent ligands like TCDD would also be crucial to prove this notion.

6.4.3. 3MC treatment alters the frequency of eosinophils and double negative ATM in WATg SVF

In general, enhanced AhR signaling and AhRR expression by 3MC treatment did not lead to alterations in the frequency of immune cells in liver and SI. However, in WATg SVF, the frequencies of both eosinophils and CD206⁻ CD11c⁻ ATM3 in the 3MC-treated AhRR^{E/E} mice were reduced or increased, respectively. Interestingly, AhRR/EGFP expression in eosinophils of AhRR^{E/E} mice was not significantly upregulated by 3MC and only ~4.5% of eosinophils expressed AhRR/EGFP in 3MC-treated AhRR^{E/E} mice, as shown by the FACS analysis. In contrast, AhRR/EGFP expression in the ATM3 subset was upregulated in the 3MC-treated AhRR^{E/E} mice such that ~60% of the ATM3 in AhRR^{E/E} mice expressed AhRR/EGFP after 3MC treatment, similar to the AhRR-expressing ATM2 subset. It is not clear if the alteration of eosinophil- and ATM3 cell numbers were mediated by different AhR target genes. Alternatively, both upregulation and downregulation of ATM3 and eosinophils, respectively were mediated by AhR activation. Nevertheless, the involvement of other signaling pathways cannot be excluded.

It is well possible that the three CYP enzymes are the ones that mediate this effect, as the altered frequencies only occurred in AhRR^{E/E} mice and not in the Triple-CYP KO AhRR^{E/E} mice. Alternatively, it can be that the AhR signaling in the Triple-CYP KO AhRR^{E/E} mice was too strong, and this prevented the eosinophils from declining via an unknown mechanism. Quantification of the expression levels of *Ahr* and other *Ahr* target genes should also be done in future. It is also unfortunate that the frequency of eosinophils was not measured and analyzed in liver and SI, as such information might also be helpful to see if the reduction of eosinophils following 3MC treatment occurs systemically or whether it is restricted to WATg. Lastly, further investigation is required to see if AhR signaling *per se* accounts for such reduction in eosinophils (both in WATg and systemically).

6.5. Dysregulated AhR signaling affects the onset of obesity and immune cell frequencies

Long-term consumption of HFD causes an excess energy intake, which is stored in fat (Hill et al., 2013). Thus, it triggers excessive fat accumulation mostly in adipose tissue and liver, which

eventually leads to systemic chronic low-grade inflammation and insulin resistance among other symptoms (Balistreri et al., 2010). DIO also alters the functions of intestinal stem cells, enhances cell death in adipocytes, causes fatty liver/NAFLD, as well as inflammation in liver and adipose tissue (Aliluev et al., 2021; Eguchi & Feldstein, 2014; Hildebrandt et al., 2023). The latter is known to be mediated by the NF-κB signaling pathway (Catrysse & Loo, 2017).

Moreover, numerous publications demonstrated the intricate role of the AhR and its activation in energy homeostasis and DIO. Mice carrying the high-affinity AhR allele, such as C57BL/6J mice, had higher weight gain and gonadal fat mass following 28-week Western diet feeding compared to mice with the low affinity AhR allele (Kerley-Hamilton et al., 2012). Global AhRdeficiency consistently resulted in reduced body weight in the context of DIO and in some studies also in increased glucose tolerance (Moyer et al., 2016; Rojas et al., 2021; Wang et al., 2011). The three AhR-controlled CYP enzymes might contribute to this effect as they also mediate the biosynthesis of some lipid mediators, which are conversion byproducts of ω -6 and ω -3 fatty acids (Divanovic et al., 2013). Some of these lipid mediators participate in either the initiation or resolution phase of inflammation. AhR plays a role in DIO as inhibition of AhR activation by alpha-naphthoflavone (aNF) could also reverse DIO and liver steatosis in mice fed with Western diet (Rojas et al., 2020). Previous findings showed that the absence of either CYP1A1 or CYP1B1 is sufficient to influence the DIO onset; CYP1A1 depletion exacerbated hepatic steatosis following BaP-supplemented HFD (Uno et al., 2018), whereas CYP1B1 depletion attenuated HFD-induced obesity and liver steatosis (Liu et al., 2015). In contrast, inhibition of the enzymatic activity of CYP1A1 by 5-methoxyflavone, a flavonoid, ameliorated NAFLD by reducing triglyceride deposition (Zhang et al., 2023). Interestingly, the AhRR has been shown to regulate adipocyte differentiation in vitro (Ishihara et al., 2019) and previous findings in our lab showed that loss of AhRR protected against DIO (unpublished data). Nevertheless, the consequences of dysregulated AhR signaling caused by the absence of AhRR and/or the three CYP enzymes in the context of DIO is still not well elucidated. Therefore, mice lacking AhRR and/or the three CYP enzymes were fed for 14 weeks with either CD or HFD. The overall aim of this study was to test if the ablation of the three AhR-dependent CYP enzymes and/or AhRR would lead to alterations of systemic metabolism, cellular architecture on tissue level, and gene expression in SI, liver, and WATg.

6.5.1. Purified diets significantly reduce AhRR/EGFP expression

As shown in Chapter 3 and 4, ablating AhR target genes that participate in feedback control of AhR signaling, such as Ahrr and genes encoding the three AhR-controlled CYP enzymes, led to increased AhR activation in AhRRE/E and Triple CYP-KO AhRRE/E mice fed with normal chow (NC), as evident by the increased expression of the AhRR/EGFP reporter. However, both histology and FACS analysis demonstrated that AhRR/EGFP expression in AhRR^{E/E} and Triple CYP-KO AhRR^{E/E} mice was reduced when mice were fed with either HFD or CD. In immune cell subsets of liver and WATg, only minimal AhRR/EGFP expression was observed in both AhRR^{E/E} and Triple CYP-KO AhRR^{E/E} mice. Besides, AhRR/EGFP expression was also no longer observed in hepatic stromal cells in Triple CYP-KO AhRR^{E/E} mice that were fed with CD or HFD, although this was clearly observed in NC-fed mice, as shown in Chapter 4. This loss of Ahrr expression was due to a low AhR activation state that was caused by the purified diets, which differ from NC diet regarding nutrient composition. NC is a grain-based diet, as it contains unprocessed plant ingredients, such as 'ground corn', 'ground wheat', 'ground oats', and 'soybean meal'. On top of that, vitamin and mineral premixes are supplemented to these diets, further adding undefined levels of micronutrients provided inherently from other ingredients (Pellizzon & Ricci, 2018). Such ingredients contain multiple sources of AhR ligands. The dietary fibers can also be fermented by microbiota in the gut, leading to the production of short-chain fatty acids (SCFA) that include butyrate, a recently described AhR ligand (Venter et al., 2022). In addition to the dietary fibers, phytoestrogens can also be found in some ingredients, e.g., 'soybean meal' and can also serve as AhR ligands. On the contrary, purified diets like CD and HFD are comprised of highly refined ingredients, such as casein, corn starch, sucrose, cellulose, and soybean oil, which contain one main nutrient and only few non-nutrient chemicals. Most importantly, they are deprived of phytoestrogens, which are known AhR ligands. Hence, CD and HFD feeding caused a low AhR activation state and subsequently low AhRR/EGFP expression.

Nevertheless, in the SI IEL, AhRR/EGFP expression was comparable between AhRR^{E/E} and Triple CYP-KO AhRR^{E/E} mice, and also between diet groups. In contrast, in the SI lamina propria, HFD strongly reduced the proportion of AhRR/EGFP-expressing T- and B lymphocytes, as well as myeloid cells. In most of the subsets, the reduction occurred in both AhRR^{E/E} and Triple CYP-KO AhRR^{E/E} mice. This result is in line with a previous publication, which also showed an overall reduction in AhRR/EGFP expression in the SI lamina propria of mice fed with a special ligand-reduced diet (LRD), as well as CD and HFD (Schanz et al., 2020). In this publication, AhRR^{E/+} mice were used, and they were only fed with the aforementioned diets for 4 weeks, hence the age of the mice at the end of the experiment was

younger than in the present HFD experiments. Moreover, the present work shows that AhRR/EGFP expression in Triple CYP-KO AhRR^{E/E} mice was also reduced across all immune subsets after CD and HFD feeding. Prostaglandin E2 (PGE2), a lipid mediator derived from ω6-fatty acids that are abundant in HFD has also been reported to be able to activate AhR, which would not fit with the HFD-induced reduction of AhRR expression (Seidel et al., 2001). Nevertheless, the fact that PGE2 contained in HFD can activate AhR may explain the qPCR result of the liver, as a ~7.5-fold induction of Ahrr transcripts between CD- and HFD-fed Triple CYP-KO AhRR+/+ mice was observed. This was also significantly higher than the Ahrr induction in WT mice. This notion that PGE2 can activate AhR is also supported by another finding of Divanovich et al. (Divanovic et al., 2013) who also showed that PGE2 is increased in Triple CYP-KO mice. However, no AhRR/EGFP expression was detected in the liver of AhRR^{E/E} and Triple CYP-KO AhRR^{E/E} mice in the CD or HFD group. It is not clear what has caused the discrepancy between the qPCR and FACS results. Furthermore, HFD also slightly elevated Ahr transcripts by $\sim 3\%$. It is also unclear what is the underlying cause of this increase, but it could be that HFD caused increased NFkB signaling, hence RelA availability, which can also upregulate the Ahr expression via binding of RelA/p50 to an NF-κB binding site in the Ahr promoter (Vogel et al., 2014).

6.5.2. Ablation of AhRR but not Triple CYP protects against weight gain and liver steatosis

As mentioned previously, systemic ablation of the AhR protects against DIO, as it resulted in reduced body weight in the context of DIO and in some studies also in increased glucose tolerance (Moyer et al., 2016; Rojas et al., 2021; Wang et al., 2011). Here, the ablation of the AhRR both in AhRR^{E/E} and Triple CYP-KO AhRR^{E/E} mice, which is supposed to enhance AhR activation (Brandstätter et al., 2016; Schanz et al., 2020) also protected from enhanced body-and liver weight, as well as glucose intolerance in the HFD-fed mice. Interestingly, a similar tendency was also observed in the CD-fed mice. Based on this, it seems that both ablation and enhanced activation of AhR can protect against DIO.

In line with the weight reduction and glucose tolerance, the serum levels of AST and ALT, but not of triglycerides tended to be lower in both AhRR^{E/E} and Triple CYP-KO AhRR^{E/E} mice. Increases in serum AST and ALT levels are hallmarks of NAFLD. Sometimes the AST/ALT ratio is also calculated and it should be <1 in NAFLD, unless cirrhosis is present (Hall & Cash, 2012; Sattar et al., 2014). In this experiment, only the Triple CYP-KO AhRR^{+/+} mice had an AST/ALT ratio of 1.5 on average, whereas the mean ratio in the other genotypes was around 1.

Accordingly, more extensive lipid droplet accumulation was observed in HFD-fed WT and Triple CYP-KO AhRR^{+/+} mice compared to AhRR-deficient mice, and the lipid droplets seemed larger in these mouse lines. Interestingly, in the CD-fed WT and Triple CYP-KO AhRR^{+/+} mice, a more intense Oil-Red-O staining was observed compared to the two AhRR-deficient groups, suggesting that some lipid accumulation in the liver had already occurred in the 24-week-old mice even in the absence of high fat diet.

In contrast to AhRR deficiency, the ablation of the three CYP enzymes slightly exacerbated the DIO, as they had slightly more weight gain, worsened liver steatosis, and less glucose tolerance compared to the other three genotypes. Moreover, Triple CYP-KO AhRR^{E/E} mice that were deficient in AhRR and the three CYP enzymes showed less severe symptoms than the Triple CYP-KO AhRR+/+ mice, showing that the protection from DIO through AhRR-ablation is dominant over the absence of the Triple CYP enzymes. This is intriguing, as both AhRR and the three CYP enzymes are negative regulators of AhR signaling, hence ablating one or all would result in enhanced AhR signaling. However, it appears that AhRR depletion attenuates DIO, whereas Triple CYP depletion has an opposite tendency. Thus, merely enhanced AhR signaling cannot be causative for the reduced weight gain, it is more likely the differential organ- or cell-type specific expression of the AhR and its target genes that is the key to the observed response of the different knockout mouse lines to high caloric diet. It could be that constitutive hepatic AhR activation induced spontaneous hepatic steatosis due to upregulation of CD36, encoded by another AhR target gene, and other fatty acid transport proteins, which inhibited the export of hepatic triglycerides (J. H. Lee et al., 2010). It is therefore intriguing to see that Triple CYP-KO AhRR^{E/E} mice, which are supposed to have the highest AhR activation showed an attenuated phenotype in DIO compared to Triple CYP-KO AhRR+/+ mice. Therefore, the expression level of CD36 in Triple CYP-KO AhRR^{E/E} mice was analysed. Both *Ppary* and its target *Fabp4* were slightly lower in AhRR^{E/E} and Triple CYP-KO AhRR^{E/E} mice, but HFD did not highly upregulate their expression. Both Fabp4 and Cd36 are among the downstream targets of $PPAR\gamma$, hence they are upregulated upon $PPAR\gamma$ activation. However, the *Ppary* primers used were able to detect all *Ppary* isoforms, including $\gamma 1$ that is expressed ubiquitously and not necessarily upregulated because of DIO and *Ppary* expression is also more predominant in WAT than liver (Wang et al., 2020). Hence, measuring Ppary and its target genes in WAT should also be done in the future. Moreover, a previous experiment in our lab using metabolic cages has also shown that the reduced weight gain in these mice was not due to reduced food intake, suggesting that it is not mediated by alteration of the hypothalamicpituitary-adrenal (HPA)-axis. Nevertheless, it is not yet known if the reduced weight gain was caused by altered lipid metabolism and if it was, it would be interesting to know how the lipid metabolism is altered. The exacerbated DIO exhibited by Triple CYP-KO AhRR^{+/+} mice also highlights the complicated relationship between the individual CYP1 enzymes in the context of obesity. While CYP1B1 deficiency alone was protective against weight gain and glucose intolerance induced by 6-weeks HFD feeding (Liu et al., 2015), CYP1A1 deficiency was associated with increased cholesterol, triglyceride and bile acid levels following Western diet feeding (Uno et al., 2018). The role of CYP1A2 in obesity is not as well elucidated as the other two CYP1 enzymes and it is also unclear which one of the three CYP enzymes played the most dominant role in the regulation of obesity.

Apart from body- and liver weight, WATg weight was also measured. It has been shown that adipose precursor cells of WATg are more resistant to differentiation into adipocytes and are more sensitive to cell death than the ones from subcutaneous AT (Macotela et al., 2012). This phenomenon can also greatly contribute to inflammation and metabolic syndrome (Ghaben & Scherer, 2019), although it is unclear if adipocyte death is required to elicit inflammation. The WATg weights of Triple CYP-KO AhRR+/+ and Triple CYP-KO AhRRE/E mice were similar and even slightly higher than the ones of $AhRR^{E/E}$ and WT mice. This points out, together with the enhanced weight gain, that the three CYP enzymes are also involved in lipid metabolism in WATg. As shown in this thesis, the increased WATg weight in Triple CYP-KO AhRR+/+ and Triple CYP-KO AhRR^{E/E} mice was not caused by reduced lipolysis. This is in line with previous findings that obesity blunted the catecholamine-induced lipolysis in female humans (Horowitz & Klein, 2000) possibly mediated by leptin resistance, reduced expression of β-adrenergic receptors or increased expression of α2-adrenergic receptors (Mowers et al., 2013). Moreover, obesity causes a dynamic remodeling of WAT in which adipocytes can either increase in size (hypertrophy) or in number (hyperplasia) (Hildebrandt et al., 2023). It would be interesting to determine if the increase in WATg weight in Triple CYP-KO AhRR+/+ and Triple CYP-KO AhRR^{E/E} mice was caused by adipocyte hypertrophy or increased adipocyte numbers, as such an analysis has not been conducted, yet. In the future, body composition analysis, for instance by Dual Energy X-ray Absorptiometry (DEXA) scan, should be conducted to see in which fat depot the Triple CYP-KO AhRR+/+ mice have more mass, which contributes to the overall higher body weight compared to the Triple CYP-KO AhRR^{E/E} mice. Alternatively, mice can be kept in metabolic cages to determine which physiological parameters (e.g. O2 consumption, energy expenditure, indirect calorimetry) are affected the most by the HFD and the genetic alterations.

6.5.3. HFD did not lead to extensive fibrosis in liver and WATg

The spectrum of NAFLD can be manifested in the form of fatty liver disease (non-alcoholic fatty liver, NAFL) or progression to non-alcoholic steatohepatitis (NASH), which is steatosis accompanied by chronic inflammation and cell damage (Heyens et al., 2021). On the histological level, NASH is characterized by pericellular and /or perilobular collagen deposition (Bel Lassen et al., 2017), lobular inflammation, and ballooning of hepatocytes, the latter being the driving force of fibrosis. Even though the 14-week HFD feeding caused liver steatosis and elevated levels of serum AST and ALT, particularly in WT and Triple CYP-KO AhRR^{+/+} mice, it only led to mild fibrosis in liver and WATg across all genotypes. Only mild pericellular fibrosis that did not lead to adipocyte trapping occurred in the WATg of WT and Triple CYP-KO AhRR^{+/+} mice, whereas it was nearly absent in AhRR^{E/E} and Triple CYP-KO AhRR^{E/E} mice. In the literature there is evidence that not all long-term HFD treatments lead to development of fibrosis (Matsumoto et al., 2013). Whereas one study showed that 10-week HFD feeding was sufficient to induce liver fibrosis in WT mice (Wada et al., 2016b), another study showed that extensive liver fibrosis only occurred in mice fed with HFD for 80 weeks, in which both age and HFD contributed to obesity and liver fibrosis (Velázquez et al., 2019). In some studies, WT mice were fed with a Western diet for 12 weeks or with a choline-deficient, L-amino aciddefined, high-fat diet (CDAHFD) to induce fibrosis (Matsumoto et al., 2013; Yang et al., 2023). In this study, rats fed with the CDAHFD diet showed rapid progression of fibrosis followed by a rise in ALT (Matsumoto et al., 2013).

DIO has been shown to cause an accumulation of crown like structures (CLS) in WAT that is induced by WAT inflammation. CLS formation consists of macrophages that have a metabolically activated phenotype, and they normally surround the dying adipocytes. Hence, the presence of CLS signifies that adipocyte death and inflammation have occurred (Lindhorst et al., 2021; Wang et al., 2019). In the case of WATg in our experiment, there were CLS observed particularly in Triple CYP-KO AhRR^{+/+} and WT mice, which is in agreement with the more severe DIO onset observed in these mice. Besides CLS, the pro-inflammatory response in WATg should be determined, as it is unclear if the levels of pro-inflammatory cytokines in our HFD experiment were not high enough to induce a more severe fibrosis phenotype. Quantifying the expression levels of pro-inflammatory genes is also necessary to determine the involvement of NF-kB and non-canonical AhR signaling or other pathways that mediate the pro-inflammatory process in liver and WATg. The non-canonical AhR signaling

pathway has been shown to be influenced by inflammation; LPS-induced inflammation enhances AhR expression via RelA activation and the binding of RelA/p50 complex to an NFkB binding site in the AhR promoter (Vogel et al., 2014). Nevertheless, supplementing the HFD with high sugar as in Western diet may be able to induce more extensive fibrosis, which may also be accompanied by stronger activation of pro-inflammatory pathways and subsequently more alterations in immune cell subsets both in terms of frequencies and cytokine expression.

6.5.4. Ablation of AhRR and/or Triple CYP deficiency alters immune cell frequencies after dietary challenge

As mentioned earlier, CD and HFD reduced AhRR/EGFP expression and hence AhR activation strongly. Therefore, it was interesting to investigate the effect of the low AhR-activation state on the frequency of immune cells subsets in the DIO model, as there could be other signaling pathways involved, e.g pro-inflammatory signaling like NF-kB activation that can also mediate non-canonical AhR signaling. Therefore, we also analyzed the frequencies of myeloid cells and lymphocytes in SI, liver, and WATg in this model.

6.5.4.1. Ablation of AhRR reduces the lamina propria Mo-Mac after HFD

Feeding mice with HFD did not significantly affect the IEC, IEL, and immune cells in the lamina propria. IEC, however, slightly increased in HFD-fed WT and AhRR^{E/E} mice compared to the CD-fed counterparts. This result is similar to a published finding that showed an increase (~7%) in enterocytes in WT mice following 11-13 weeks HFD feeding, which is caused by an increase in enterocyte progenitors. In addition, it could be shown that HFD induces intestinal stem cell (ISC) differentiation and turnover, as evident by reduced ISC frequency, but increased Goblet- and enteroendocrine cells (Aliluev et al., 2021). (Wang et al., 2023). For IEL, it has been reported that their function depends on the activation state, as activated TCRγδ IEL might modulate levels of GLP-1 and possibly other gut hormones (Bank, 2022; Park et al., 2019), and can contribute to insulin resistance and obesity. Mice lacking IEL following ablation of $\alpha 4\beta 7$ and αeβ7 integrins are resistant to DIO (He et al., 2019). HFD-fed Triple CYP-KO AhRR^{+/+} mice tended to have reduced frequencies of natural (CD8 $\alpha\alpha^+$ TCR $\gamma\delta$ and TCR β^+) IEL, but increased frequencies of induced (CD8 $\alpha\beta^+$ TCR β^+) IEL. In contrast, the frequencies of both natural and induced IEL between the HFD-fed and CD-fed WT mice were comparable. This is in agreement with a published study, which demonstrated that 18-22 weeks of HFD feeding reduced the absolute numbers of both $\gamma\delta$ and $\alpha\beta$ T cells, but their frequencies were comparable

to the CD counterparts (Park et al., 2019). Such a reduction in $\alpha\beta$ T cells, but not $\gamma\delta$ T cells, was attributed to the reduced frequencies of proliferating cells. Further, another publication showed that a 12-week Western diet regimen induced a 25% reduction in CD8 $\alpha\alpha^+$ TCR $\gamma\delta$ and CD8 $\alpha\alpha^+$ TCR $\alpha\beta$ IELs combined and ~5% reduction in CD8 $\alpha\beta^+$ TCR $\gamma\delta$ and CD8 $\alpha\beta^+$ TCR $\alpha\beta^+$ IELs following IEL sorting (Wang et al., 2023). This also further highlights the different effects exerted by Western diet compared to HFD. Overall, IEL numbers may not be the main reason of the differences in DIO onsets between different genotypes, but transcriptional and cytokines profiles of sorted IEL post HFD treatment need to be analyzed in the future.

In terms of the immune cells in SI lamina propria, there were some alterations observed across genotypes but not treatment groups. The $T\gamma\delta^+$ cells were higher in AhRR^{E/E} mice and Triple CYP-KO AhRR^{E/E} mice compared to WT and Triple CYP-KO AhRR^{+/+} mice, suggesting such increase was mediated by AhRR deficiency. Nevertheless, such increase in $T\gamma\delta^+$ cells has only been observed in mice with HFD or CD, as $T\gamma\delta^+$ cells were not analyzed in the previous experiment involving NC-fed mice. Furthermore, it has been shown that HFD reduced the frequency of CD8 $\alpha\alpha^+$ and CD8 $\alpha\beta^+$ TCR $\gamma\delta$ /TCRb⁺ cells in lamina propria due to increased cell death (Wang et al., 2023). Hence, the higher frequency of TCR $\gamma\delta^+$ in AhRR-deficient mice could be caused by increased resistance to cell death or TCR $\gamma\delta^+$ cells compensate for increased cell death by enhancing proliferation. Also, the frequency of B cells was reduced in mice deficient of AhRR and/ or the three CYP enzymes significantly reduced their frequency compared to WT mice in the CD group, suggesting that enhanced AhR signaling mediated by these ablations may account for the B cells reduction.

Interestingly, HFD-fed Triple CYP-KO AhRR^{+/+} mice had a markedly higher macrophage frequency compared to Triple CYP-KO AhRR^{E/E} mice. Macrophages differentiated from recruited blood monocytes produce TNF, which promotes loss of barrier function that contributes to local inflammation as well as systemic immunometabolic dysfunction in DIO (Breznik et al., 2023). Enhanced frequencies of inflammatory Mo Mac would be in line with the enhanced DIO observed in Triple CYP-KO AhRR^{+/+} compared to Triple CYP-KO AhRR^{E/E} mice. In contrast, in the study conducted by Wang et al. (Wang et al., 2023), the 12-week Western Diet feeding markedly increased the frequencies of plasma cells, CD4 T-cells, and to a lesser extent also cDC and ILC1-3 in WT mice and reduced CD8aa⁺ TCRγδ /TCRb⁺ T cells frequency. This finding alludes that the combination of high fat and high-sugar components of Western Diet might have exerted more pro-inflammatory stimuli on IEL and lamina propria immune cells.

6.5.4.2. DIO and dysregulated AhR signaling alter the frequencies of hepatic KC and Mo-Mac

DIO and NAFLD have been reported to alter the hepatic immune milieu by triggering inflammatory cascades, as well as by activating endothelial and hepatic stellate cells among many other processes (Huby & Gautier, 2022; Méndez-Sánchez et al., 2021). Hepatocytes can also contribute to inflammation by secreting HMGB1, PGE2, and activating the NRLP3 inflammasome and NF-kB pathways. Subsequently, NLRP3 activation can cause hepatocyte death following secretion of DAMPs, which in turn activate other downstream signaling molecules, such as STAT3 in hepatocytes that may lead to hepatocarcinogenesis (Méndez-Sánchez et al., 2021).

Hence, FACS analysis was conducted on cell suspensions of the liver to analyze the frequencies of hepatic immune cell subsets post HFD treatment. In the current experiments, HFD reduced the frequency of KC in AhRR^{E/E} mice compared to the CD-fed control mice, although AhRR^{E/E} mice had the highest KC frequency among all genotypes in the CD group. The impact of a reduction of KC during DIO is still unclear. Previous findings showed that a lack of KC led to enhanced steatosis, STAT3 signaling, and insulin resistance (Clementi et al., 2009). This work also demonstrated that 15-week HFD feeding neither increased expression of KC markers nor caused classical activation of KC. In contrast, another study demonstrated that DIO induces proinflammatory polarization of KC, which can inhibit insulin signaling and activate hepatic glucose production leading to the development of insulin resistance (Jager et al., 2016). Furthermore, alternative activation of KC that is mediated by hematopoetic PPARδ confers protection against DIO (Odegaard et al., 2008). Interestingly, the increased KC frequency observed in CD fed mice could not be observed in 24-week-old AhRR^{E/E} mice fed with NC obtained from a separate experiment. This suggests that AhR signaling may directly or indirectly influence the frequency of KC. Apart from KC, HFD also altered the frequencies of Ly6C⁺ and Ly6C⁻ Mo-Mac. HFD significantly increased the frequency of Ly6C⁺ Mo-Mac in Triple CYP-KO AhRR+/+ mice and also slightly increased it in WT mice, whereas the frequency of Ly6C- Mo-Mac was elevated in Triple CYP-KO AhRR^{E/E} mice. These two Mo-Mac subsets have been shown to originate from Ly6chi and Ly6cho monocytes, respectively. The former are proinflammatory and pro-fibrotic, whereas the latter are restorative and involved in tissue repair (Cho et al., 2023; Ramachandran et al., 2012). Some cells of the Ly6C- Mo-Mac subset also express MHCII, which enables antigen presentation between macrophages and IFNγ-producing lymphoid populations (Buxadé et al., 2018). The result of our experiment showed that Ly6chi Mo-Mac were more highly represented in Triple CYP-KO AhRR^{+/+}- and WT mice, whereas Ly6c^{lo} Mo-Mac were more predominantly expressed in Triple CYP-KO AhRR^{E/E} mice. Since it is postulated that Ly6c^{hi} Mo-Mac have more proinflammatory properties, whereas Ly6c^{lo} have a rather restorative function, this result may fit to the phenotype of the WT, Triple CYP-KO AhRR^{+/+} mice and the Triple CYP-KO AhRR^{E/E} mice, respectively. Furthermore, hepatic immune cells, particularly myeloid cells like KC (in activated state), monocytes and Mo-Mac, have been shown to be recruited during inflammation or infection (Devisscher et al., 2017; Zigmond et al., 2014) and can drive the progression of liver steatosis to NASH (Devisscher et al., 2016).

In addition, HFD significantly increased the frequency of CD11b⁺ cDC2 in Triple CYP-KO AhRR^{E/E} mice and also slightly increased their frequency in AhRR^{E/E} mice. The hepatic cDC2 subset has been shown to induce a pro-inflammatory environment, inducing CD4⁺ T-cell-mediated immunity, as well as recruiting macrophages into the liver (Méndez-Sánchez et al., 2021). Therefore, the increased cDC2 frequency in Triple CYP-KO AhRR^{E/E} mice may also contribute to the increase of Ly6c^{lo} Mo-Mac.

Apart from the alterations solely induced by HFD, the ablation of AhRR and/or the three CYP enzymes also altered the immune cell frequencies under CD conditions. The frequency of NKT cells was significantly lower in HFD-fed Triple CYP-KO AhRR^{E/E} mice compared to WT mice, whereas the NK-cell frequency was significantly higher in Triple CYP-KO AhRR+/+ mice compared to the other genotypes in the CD group and it was significantly higher than AhRR^{E/E} mice in HFD group. However, the roles of both hepatic NKT and NK cells in DIO are not well elucidated, but it is thought that they are pivotal regulators of inflammation (Highton et al., 2021; Martin-Murphy et al., 2014). It has been reported that 12-week HFD feeding did not alter the frequency of NK cells but the cells were less cytotoxic than the ones from CD-fed control mice (Cuff et al., 2019). Such reduction in NK cell cytotoxicity was considered protective against DIO. In line, ablation of NKT cells in mice conferred less protection against DIO (Martin-Murphy et al., 2014). However, another study showed that feeding mice with a cholinedeficient HFD activated NKT cells and CD8⁺ T cells, but not myeloid cells, which was shown to promote not only NASH but also hepatocellular carcinoma (Wolf et al., 2014). Therefore, it is possible that NKT cells play a dual role in the progression of NAFLD, depending on the stimuli from the microenvironment or diet.

6.5.4.3. HFD alters both lymphoid and myeloid immune compartments in WATg

During the course of DIO, AT, particularly WAT inflammation precedes liver inflammation (Stanton et al., 2011; van der Heijden et al., 2015). This process involves adipokine and cytokine secretion, which affect not only the inflammatory response but also lipid metabolism (Harwood, 2012; Kawai et al., 2021). Hence, FACS analysis was conducted to investigate if DIO and dysregulated AhR signaling would differentially alter the frequency of immune cells in WATg.

FACS analysis revealed that more HFD-induced changes in immune cell frequencies were observed in WATg compared to liver or SI. Here, a reduced CD4⁺ T-cell frequency was observed in HFD-fed WT mice. This however, did not go in line with a previous publication that showed an increase of CD4⁺ T-lymphocytes in epididymal AT in DIO (Kintscher et al., 2008). Different from the present experiments, this study used histology and qPCR to detect the CD4⁺ T cells, which can be inaccurate as NKT- and NK cells can also express CD3 and CD4, depending on their activation state (Krijgsman et al., 2018; Milush et al., 2009). Further, HFD increased the frequency of CD8⁺ T cells in WT, AhRR^{E/E}, and Triple CYP-KO AhRR^{+/+} mice, although this was significant only in the latter. This result is supported by a study, which showed that obesity (both diet- and genetically-induced) elevated infiltrating CD8⁺ T cells in AT, driving ATM polarization towards a pro-inflammatory phenotype (Rausch et al., 2008). Moreover, HFD reduced the TCRγδ frequency in Triple CYP-KO AhRR^{+/+} mice, but not in the other three genotypes including Triple CYP-KO AhRRE/E mice, suggesting a Triple-CYPspecific effect that is somehow counter-regulated by AhRR deficiency. Previous findings support this result, as they also showed that DIO does not only reduce TCRγδ cells, but also reduces TNFα upregulation by TCRγδ cells, which alters their homeostasis and also impairs their ability to promptly retract their dendrites upon wounding (Costanzo et al., 2015; Taylor et al., 2010). However, other studies showed the opposite: HFD increased both the frequency and absolute number of Tyδ cells (Bruno et al., 2022; Mehta et al., 2015) and promoted the accumulation of ATM, inflammation, and insulin resistance in obese mice (Mehta et al., 2015).

Along this line, HFD increased CD206⁺ CD11c⁻ ATM2 (resident macrophages) and CD206⁻ CD11c⁻ ATM3 macrophages across all genotypes with no significant differences observed between genotypes. There are four known ATM subsets (Li et al., 2023). First, ATM1, which express CD11c, possess a pro-inflammatory phenotype and can be subdivided into

ATM1a and 1b that are CD206 and CD206, respectively. Second, ATM2, the resident macrophages that possess an alternatively activated phenotype. Lastly, ATM3, which may possess more pro-inflammatory phenotype, as they also accumulate in CLS and uniquely express chemokine receptor CCR7. DIO has been shown to induce the CD11c⁺ ATM1 macrophages (Li et al., 2023), but this did not occur in our experiments. Such lack of CD11c expression was not caused by digestion buffer, as collagenase I and II contained in the Liberase solution used for the WATg digestion cannot cleave CD11c (Autengruber et al., 2012; Botting et al., 2017). Additionally, Bailin et al. (Bailin et al., 2022) suggested that CD206⁺ CD11c⁻ ATMs are primarily perivascular macrophages (PVM), whereas intermediate macrophages (IM) are among the CD206⁻ CD11c⁺ population and lipid-associated macrophages (LAM) are within the double-positive CD206⁺ CD11c⁺ cells. ATM2 can produce inflammatory cytokines but the expression of CD206 has been perceived as a marker of an alternatively activated phenotype and CD206⁺ M2-like macrophages modulate insulin sensitivity by inhibiting proliferation and differentiation of adipocyte progenitors (Li et al., 2023; Nawaz et al., 2017). Moreover, a previous study showed that CD206 can also be internalized in a Clathrin-dependent manner upon ligand binding or proteolytically cleaved and shed by an unknown metalloprotease (van der Zande et al., 2021). This shedding occurs constitutively and depends on Dectin-1mediated signaling. The level of soluble CD206 correlates with the amount of total CD206 expressed in the cells. Thus, we can speculate that the HFD-induced increases in ATM2 and 3 could have been caused by increased cleavage and shedding of surface CD206 receptor, which in turn also increased the turnover of the mannose receptor. In our experiment, AhRR^{E/E} mice had more CD206⁺ ATM2 and less CD206⁻ ATM. It is possible that the CD206 turnover and shedding occurs at a lower rate in these mice, but it is not clear if AhRR deficiency can directly influence the turnover rate. Soluble CD206 has been shown to induce pro-inflammatory macrophage activation, which subsequently leads to a cellular reprogramming towards an inflammatory phenotype mediated by Src/Akt/NF-κB (Embgenbroich et al., 2020). In DIO, this soluble form of CD206 is increased. Hence, further quantification of soluble CD206 by ELISA needs to be conducted to confirm this notion and to determine if the level of soluble CD206 correlates with the DIO severity between the different genotypes in our experiments. In DIO-induced metaflammation, ATM subsets, particularly the CD11c⁺ ATM1 that express CCR7 and CD11c⁻ CD206⁻ ATM3, also contribute to the CLS formation (Morris et al., 2011; Shaul et al., 2010). As CLS formation was most pronounced in the Triple CYP-KO AhRR^{+/+} mice, the ATM1 and 3 subsets should be the highest here, but the CD11c⁺ expressing ATM1 subset was not observed in my experiment. An in vivo pulse experiment by Shaul et al. (Shaul et al., 2010) using the lipophilic dye PKH26 also showed that the MGL1^{med} CD11c⁺ ATM1 are not derived from resident MGL1⁺ CD11c⁻ cells (PKH26⁺), they are rather derived from the recruited MGL1⁺ CD11c⁻ (PKH26⁻) cells. This might also be the cause of the increased CD206⁺/- CD11c⁻ ATM post HFD feeding in our experiment. Nevertheless, it would be interesting to also check the transcriptional profiles of the ATM from the mice deficient of AhRR and/or three CYP enzymes.

Furthermore, HFD also led to a reduced eosinophil frequency in WT, Triple CYP-KO AhRR^{E/E}, and Triple CYP-KO AhRR+/+ mice, and to a lesser extent in AhRRE/E mice. This result is in agreement with previous findings; eosinophils are reduced in HFD-fed mice and this decrease is accompanied by increased weight gain and glucose intolerance (Hams et al., 2013; Li et al., 2019). Another study also showed that eosinophils play a role in dampening age-related localand systemic low-grade inflammation (Brigger et al., 2020). Nevertheless, the protective role of eosinophils in DIO is still disputable, as contradicting evidence arose from other murine studies (Calco et al., 2020). Eosinophils have been reported to regulate axonal plasticity in WAT, leading to enhanced sympathetic innervation and increased energy expenditure (Meng et al., 2022). Intestinal eosinophils contributed to transcriptional upregulation of genes related to the immune response, cell-cell communication, and extracellular matrix remodeling (Diny et al., 2022). In addition, AhR expression was essential for eosinophil degranulation and survival. However, it is not known if WAT eosinophils also play similar roles as their intestinal counterparts. When comparing the eosinophil frequency from the HFD experiments with the one from the AhR ligand feeding experiments shown in Chapter 4, there was an overall reduction in eosinophil frequency in both CD and HFD (~2.5-12.5%), compared to the control group in the ligand feeding experiment (18-38%). This indicates that survival and or proliferation of WAT eosinophils may also depend on AhR activation.

HFD also increased the cDC frequency across all genotypes and this increment was mostly attributed to the increased frequency of CD24⁻ cDC with no differences between genotypes. However, the frequency of CD24⁺ cDC was higher in AhRR^{E/E} and Triple CYP-KO AhRR^{E/E} mice compared to AhRR-proficient mice. CD24 has been shown to interact with SiglecE, which is also expressed in hematopoetic cells and this interaction negatively regulated DIO-associated metaflammation (Wang et al., 2022). Therefore, the reduction in CD24⁺ cDC might have contributed to the attenuated DIO phenotype of the two AhRR-deficient mouse lines. Lastly, HFD also increased MHCII⁺- and MHCII⁻ monocytes, except in Triple CYP-KO AhRR^{E/E} mice.

It is expected that the Triple CYP-KO AhRR^{E/E} mice had lower monocyte infiltration, as recruited monocyte-derived ATM have been suggested to cause low-grade systemic inflammation and insulin resistance (Félix et al., 2021). In ATM, MHCII expression also plays a role in T cell maturation and metaflammation, but it is not known if MHCII on monocytes also assumes similar roles (Cho et al., 2014).

6.6 Conclusion

Taken together, the reduction in DIO symptoms (increased body and liver weights, as well as glucose intolerance, and liver steatosis) in AhRR^{E/E} and Triple CYP-KO AhRR^{E/E} mice could not simply be attributed to enhanced AhR signaling. If this would be the case, Triple CYP-KO AhRR+/+ mice should also have shown ameliorated DIO symptoms compared to WT, but these mice even had a worse phenotype than WT mice. This suggests that the three CYP enzymes also exert AhR-independent effects, possibly in lipid metabolism. Moreover, altered expression levels of proteins involved in lipid metabolism might be the contributing factors to the differences in the severity of DIO between genotypes. Both AhRRE/E and Triple CYP-KO AhRR^{E/E} mice had slightly lower levels of both FabP4 and PPARy and they both exhibited attenuated DIO symptoms in terms of body weight, liver steatosis, and glucose tolerance. The altered frequencies of various immune cells in peripheral organs that may be caused by the combination of altered AhR signaling and altered microenvironments (e.g., hepatokines and adipokines profile) are likely to further contribute to the attenuated and exacerbated DIO onsets caused by AhRR and Triple-CYP depletion, respectively. In the future, transcriptomic- and cytokine profiling analyses need to be performed to better understand how the dysregulated AhR signaling exerts its effect and to also investigate the effects of AhRR and Triple-CYP depletion on the non-canonical AhR signaling pathway in DIO.

7. References

Abdelrahim, M., Ariazi, E., Kim, K., Khan, S., Barhoumi, R., Burghardt, R., Liu, S., Hill, D., Finnell, R., Wlodarczyk, B., Jordan, V. C., & Safe, S. (2006). 3-Methylcholanthrene and other aryl hydrocarbon receptor agonists directly activate estrogen receptor alpha. *Cancer Research*, *66*(4), 2459–2467. https://doi.org/10.1158/0008-5472.CAN-05-3132

Aguilera-Montilla, N., Blas, M., Lopez-Santalla, M., & Villa, J. M. (2004). Mucosal immune system: A brief review. *Inmunologia*, *23*, 207–216.

Ahima, R. S., & Flier, J. S. (2000). Adipose tissue as an endocrine organ. *Trends in Endocrinology and Metabolism: TEM*, 11(8), 327–332. https://doi.org/10.1016/s1043-2760(00)00301-5

Ahmed, S., Bott, D., Gomez, A., Tamblyn, L., Rasheed, A., Cho, T., MacPherson, L., Sugamori, K. S., Yang, Y., Grant, D. M., Cummins, C. L., & Matthews, J. (2015). Loss of the Mono-ADP-ribosyltransferase, Tiparp, Increases Sensitivity to Dioxin-induced Steatohepatitis and Lethality. *The Journal of Biological Chemistry*, 290(27), 16824–16840. https://doi.org/10.1074/jbc.M115.660100

Al Shoyaib, A., Archie, S. R., & Karamyan, V. T. (2019). Intraperitoneal Route of Drug Administration: Should it Be Used in Experimental Animal Studies? *Pharmaceutical research*, *37*(1), 12. https://doi.org/10.1007/s11095-019-2745-x

Alessandrini, F., de Jong, R., Wimmer, M., Maier, A.-M., Fernandez, I., Hils, M., Buters, J. T., Biedermann, T., Zissler, U. M., Hoffmann, C., Esser-von-Bieren, J., Schmidt-Weber, C. B., & Ohnmacht, C. (2022). Lung Epithelial CYP1 Activity Regulates Aryl Hydrocarbon Receptor Dependent Allergic Airway Inflammation. *Frontiers in Immunology*, *13*, 901194. https://doi.org/10.3389/fimmu.2022.901194

Aliluev, A., Tritschler, S., Sterr, M., Oppenländer, L., Hinterdobler, J., Greisle, T., Irmler, M., Beckers, J., Sun, N., Walch, A., Stemmer, K., Kindt, A., Krumsiek, J., Tschöp, M. H., Luecken, M. D., Theis, F. J., Lickert, H., & Böttcher, A. (2021). Diet-induced alteration of intestinal stem cell function underlies obesity and prediabetes in mice. *Nature Metabolism*, *3*(9), Article 9. https://doi.org/10.1038/s42255-021-00458-9

Alonso-Magdalena, P., Quesada, I., & Nadal, A. (2011). Endocrine disruptors in the etiology of type 2 diabetes mellitus. *Nature Reviews Endocrinology*, 7(6), Article 6. https://doi.org/10.1038/nrendo.2011.56

Anderson, C. M., & Ren, J. (2002). Leptin, leptin resistance and endothelial dysfunction in pre-eclampsia. *Cellular and Molecular Biology (Noisy-Le-Grand, France)*, 48 Online Pub, OL323-329.

Arita, Y., Kihara, S., Ouchi, N., Takahashi, M., Maeda, K., Miyagawa, J., Hotta, K., Shimomura, I., Nakamura, T., Miyaoka, K., Kuriyama, H., Nishida, M., Yamashita, S., Okubo, K., Matsubara, K., Muraguchi, M., Ohmoto, Y., Funahashi, T., & Matsuzawa, Y. (1999). Paradoxical decrease of an adipose-specific protein, adiponectin, in obesity. *Biochemical and Biophysical Research Communications*, 257(1), 79–83. https://doi.org/10.1006/bbrc.1999.0255

Autengruber, A., Gereke, M., Hansen, G., Hennig, C., & Bruder, D. (2012). Impact of enzymatic tissue disintegration on the level of surface molecule expression and immune cell function. *European Journal of Microbiology & Immunology*, 2(2), 112–120. https://doi.org/10.1556/EuJMI.2.2012.2.3

- Baba, T., Mimura, J., Gradin, K., Kuroiwa, A., Watanabe, T., Matsuda, Y., Inazawa, J., Sogawa, K., & Fujii-Kuriyama, Y. (2001). Structure and expression of the Ah receptor repressor gene. *The Journal of Biological Chemistry*, *276*(35), 33101–33110. https://doi.org/10.1074/jbc.M011497200
- Bailin, S. S., Kropski, J. A., Gangula, R. D., Hannah, L., Simmons, J. D., Mashayekhi, M., Ye, F., Fan, R., Mallal, S., Warren, C. M., Kalams, S. A., Gabriel, C. L., Wanjalla, C. N., & Koethe, J. R. (2022). White Adipose Tissue Compositional and Transcriptional Patterns with Progressive Glucose Intolerance in Persons with HIV (S. 2022.03.21.484794). bioRxiv. https://doi.org/10.1101/2022.03.21.484794
- Bain, C. C., Bravo-Blas, A., Scott, C. L., Perdiguero, E. G., Geissmann, F., Henri, S., Malissen, B., Osborne, L. C., Artis, D., & Mowat, A. M. (2014). Constant replenishment from circulating monocytes maintains the macrophage pool in the intestine of adult mice. *Nature Immunology*, *15*(10), 929–937. https://doi.org/10.1038/ni.2967
- Bain, C. C., Montgomery, J., Scott, C. L., Kel, J. M., Girard-Madoux, M. J. H., Martens, L., Zangerle-Murray, T. F. P., Ober-Blöbaum, J., Lindenbergh-Kortleve, D., Samsom, J. N., Henri, S., Lawrence, T., Saeys, Y., Malissen, B., Dalod, M., Clausen, B. E., & Mowat, A. M. (2017). TGFβR signalling controls CD103+CD11b+ dendritic cell development in the intestine. *Nature Communications*, 8(1), Article 1. https://doi.org/10.1038/s41467-017-00658-6
- Bain, C. C., & Mowat, A. M. (2014). Macrophages in intestinal homeostasis and inflammation. *Immunological Reviews*, 260(1), 102–117. https://doi.org/10.1111/imr.12192
- Bain, C. C., & Schridde, A. (2018). Origin, Differentiation, and Function of Intestinal Macrophages. *Frontiers in Immunology*, 9. https://www.frontiersin.org/articles/10.3389/fimmu.2018.02733
- Bain, C. C., Scott, C. L., Uronen-Hansson, H., Gudjonsson, S., Jansson, O., Grip, O., Guilliams, M., Malissen, B., Agace, W. W., & Mowat, A. M. (2013). Resident and pro-inflammatory macrophages in the colon represent alternative context-dependent fates of the same Ly6Chi monocyte precursors. *Mucosal Immunology*, *6*(3), 498–510. https://doi.org/10.1038/mi.2012.89
- Baker, N. A., Shoemaker, R., English, V., Larian, N., Sunkara, M., Morris, A. J., Walker, M., Yiannikouris, F., & Cassis, L. A. (2015). Effects of Adipocyte Aryl Hydrocarbon Receptor Deficiency on PCB-Induced Disruption of Glucose Homeostasis in Lean and Obese Mice. *Environmental Health Perspectives*, *123*(10), 944–950. https://doi.org/10.1289/ehp.1408594
- Balistreri, C. R., Caruso, C., & Candore, G. (2010). The Role of Adipose Tissue and Adipokines in Obesity-Related Inflammatory Diseases. *Mediators of Inflammation*, 2010, 802078. https://doi.org/10.1155/2010/802078
- Bank, I. (2022). Obesity and cancer: The gammadelta T cell link. *Exploration of Immunology*, *2*(3), 320–333. https://doi.org/10.37349/ei.2022.00053
- Bayerl, F., Bejarano, D. A., Bertacchi, G., Doffin, A.-C., Gobbini, E., Hubert, M., Li, L., Meiser, P., Pedde, A.-M., Posch, W., Rupp, L., Schlitzer, A., Schmitz, M., Schraml, B. U., Uderhardt, S., Valladeau-Guilemond, J., Wilflingseder, D., Zaderer, V., & Böttcher, J. P. (2023). Guidelines for visualization and analysis of DC in tissues using multiparameter fluorescence microscopy imaging methods. *European Journal of Immunology*, *53*(11), e2249923. https://doi.org/10.1002/eji.202249923
- Bekiaris, V., Persson, E. K., & Agace, W. W. (2014). Intestinal dendritic cells in the regulation of mucosal immunity. *Immunological Reviews*, 260(1), 86–101. https://doi.org/10.1111/imr.12194
- Bel Lassen, P., Charlotte, F., Liu, Y., Bedossa, P., Le Naour, G., Tordjman, J., Poitou, C., Bouillot, J.-L., Genser, L., Zucker, J.-D., Sokolovska, N., Aron-Wisnewsky, J., & Clément, K. (2017). The FAT Score, a

Fibrosis Score of Adipose Tissue: Predicting Weight-Loss Outcome After Gastric Bypass. *The Journal of Clinical Endocrinology & Metabolism*, 102(7), 2443–2453. https://doi.org/10.1210/jc.2017-00138

Belkaid, Y., & Naik, S. (2013). Compartmentalized and systemic control of tissue immunity by commensals. *Nature immunology*, *14*(7), 10.1038/ni.2604. https://doi.org/10.1038/ni.2604

Berg, A. H., Combs, T. P., Du, X., Brownlee, M., & Scherer, P. E. (2001). The adipocyte-secreted protein Acrp30 enhances hepatic insulin action. *Nature Medicine*, *7*(8), 947–953. https://doi.org/10.1038/90992

Bilzer, M., Roggel, F., & Gerbes, A. L. (2006). Role of Kupffer cells in host defense and liver disease. Liver International: Official Journal of the International Association for the Study of the Liver, 26(10), 1175–1186. https://doi.org/10.1111/j.1478-3231.2006.01342.x

Blaszczak, A. M., Jalilvand, A., & Hsueh, W. A. (2021). Adipocytes, Innate Immunity and Obesity: A Mini-Review. *Frontiers in Immunology*, *12*, 650768. https://doi.org/10.3389/fimmu.2021.650768

Blériot, C., Barreby, E., Dunsmore, G., Ballaire, R., Chakarov, S., Ficht, X., De Simone, G., Andreata, F., Fumagalli, V., Guo, W., Wan, G., Gessain, G., Khalilnezhad, A., Zhang, X. M., Ang, N., Chen, P., Morgantini, C., Azzimato, V., Kong, W. T., ... Ginhoux, F. (2021). A subset of Kupffer cells regulates metabolism through the expression of CD36. *Immunity*, *54*(9), 2101-2116.e6. https://doi.org/10.1016/j.immuni.2021.08.006

Bolus, W. R., Kennedy, A. J., & Hasty, A. H. (2018). Obesity-induced reduction of adipose eosinophils is reversed with low-calorie dietary intervention. *Physiological Reports*, *6*(22), e13919. https://doi.org/10.14814/phy2.13919

Bonilla, F. A., & Oettgen, H. C. (2010). Adaptive immunity. *The Journal of Allergy and Clinical Immunology*, 125(2 Suppl 2), S33-40. https://doi.org/10.1016/j.jaci.2009.09.017

Borger, J. G., Lau, M., & Hibbs, M. L. (2019). The Influence of Innate Lymphoid Cells and Unconventional T Cells in Chronic Inflammatory Lung Disease. *Frontiers in Immunology*, *10*. https://www.frontiersin.org/articles/10.3389/fimmu.2019.01597

Botting, R. A., Bertram, K. M., Baharlou, H., Sandgren, K. J., Fletcher, J., Rhodes, J. W., Rana, H., Plasto, T. M., Wang, X. M., Lim, J. J. K., Barnouti, L., Kohout, M. P., Papadopoulos, T., Merten, S., Olbourne, N., Cunningham, A. L., Haniffa, M., & Harman, A. N. (2017). Phenotypic and functional consequences of different isolation protocols on skin mononuclear phagocytes. *Journal of Leukocyte Biology*, *101*(6), 1393–1403. https://doi.org/10.1189/jlb.4A1116-496R

Boverhof, D. R., Burgoon, L. D., Tashiro, C., Chittim, B., Harkema, J. R., Jump, D. B., & Zacharewski, T. R. (2005). Temporal and dose-dependent hepatic gene expression patterns in mice provide new insights into TCDD-Mediated hepatotoxicity. *Toxicological Sciences: An Official Journal of the Society of Toxicology*, 85(2), 1048–1063. https://doi.org/10.1093/toxsci/kfi162

Bradford, B. M., Sester, D. P., Hume, D. A., & Mabbott, N. A. (2011). Defining the anatomical localisation of subsets of the murine mononuclear phagocyte system using integrin alpha X (Itgax, CD11c) and colony stimulating factor 1 receptor (Csf1r, CD115) expression fails to discriminate dendritic cells from macrophages. *Immunobiology*, *216*(11), 1228–1237. https://doi.org/10.1016/j.imbio.2011.08.006

Brandstätter, O., Schanz, O., Vorac, J., König, J., Mori, T., Maruyama, T., Korkowski, M., Haarmann-Stemmann, T., von Smolinski, D., Schultze, J. L., Abel, J., Esser, C., Takeyama, H., Weighardt, H., & Förster, I. (2016a). Balancing intestinal and systemic inflammation through cell type-specific

expression of the aryl hydrocarbon receptor repressor. *Scientific Reports*, *6*(1), Article 1. https://doi.org/10.1038/srep26091

Brandstätter, O., Schanz, O., Vorac, J., König, J., Mori, T., Maruyama, T., Korkowski, M., Haarmann-Stemmann, T., von Smolinski, D., Schultze, J. L., Abel, J., Esser, C., Takeyama, H., Weighardt, H., & Förster, I. (2016b). Balancing intestinal and systemic inflammation through cell type-specific expression of the aryl hydrocarbon receptor repressor. *Scientific Reports*, *6*(1), Article 1. https://doi.org/10.1038/srep26091

Breznik, J. A., Jury, J., Verdú, E. F., Sloboda, D. M., & Bowdish, D. M. E. (2023). Diet-induced obesity alters intestinal monocyte-derived and tissue-resident macrophages and increases intestinal permeability in female mice independent of tumor necrosis factor. *American Journal of Physiology-Gastrointestinal and Liver Physiology*, 324(4), G305–G321. https://doi.org/10.1152/ajpgi.00231.2022

Brigger, D., Riether, C., van Brummelen, R., Mosher, K. I., Shiu, A., Ding, Z., Zbären, N., Gasser, P., Guntern, P., Yousef, H., Castellano, J. M., Storni, F., Graff-Radford, N., Britschgi, M., Grandgirard, D., Hinterbrandner, M., Siegrist, M., Moullan, N., Hofstetter, W., ... Eggel, A. (2020). Eosinophils regulate adipose tissue inflammation and sustain physical and immunological fitness in old age. *Nature metabolism*, *2*(8), 688–702. https://doi.org/10.1038/s42255-020-0228-3

Bruno, M. E. C., Mukherjee, S., Powell, W. L., Mori, S. F., Wallace, F. K., Balasuriya, B. K., Su, L. C., Stromberg, A. J., Cohen, D. A., & Starr, M. E. (2022). Accumulation of $\gamma\delta$ T cells in visceral fat with aging promotes chronic inflammation. *GeroScience*, *44*(3), 1761–1778. https://doi.org/10.1007/s11357-022-00572-w

Bugajska, J., Berska, J., Pasternak, A., & Sztefko, K. (2023). Biliary Amino Acids and Telocytes in Gallstone Disease. *Metabolites*, *13*(6), Article 6. https://doi.org/10.3390/metabo13060753

Bunte, K., & Beikler, T. (2019). Th17 Cells and the IL-23/IL-17 Axis in the Pathogenesis of Periodontitis and Immune-Mediated Inflammatory Diseases. *International Journal of Molecular Sciences*, 20(14), 3394. https://doi.org/10.3390/ijms20143394

Buonocore, S., Ahern, P. P., Uhlig, H. H., Ivanov, I. I., Littman, D. R., Maloy, K. J., & Powrie, F. (2010). Innate lymphoid cells drive interleukin-23-dependent innate intestinal pathology. *Nature*, *464*(7293), 1371–1375. https://doi.org/10.1038/nature08949

Cai, B., Thorp, E. B., Doran, A. C., Subramanian, M., Sansbury, B. E., Lin, C.-S., Spite, M., Fredman, G., & Tabas, I. (2016). MerTK cleavage limits proresolving mediator biosynthesis and exacerbates tissue inflammation. *Proceedings of the National Academy of Sciences*, *113*(23), 6526–6531. https://doi.org/10.1073/pnas.1524292113

Calco, G. N., Fryer, A. D., & Nie, Z. (2020). Unraveling the connection between eosinophils and obesity. *Journal of leukocyte biology*, 108(1), 123–128. https://doi.org/10.1002/JLB.5MR0120-377R

Cassado, A. dos A., D'Império Lima, M. R., & Bortoluci, K. R. (2015). Revisiting Mouse Peritoneal Macrophages: Heterogeneity, Development, and Function. *Frontiers in Immunology*, *6*. https://www.frontiersin.org/articles/10.3389/fimmu.2015.00225

Catrysse, L., & Loo, G. van. (2017). Inflammation and the Metabolic Syndrome: The Tissue-Specific Functions of NF-κB. *Trends in Cell Biology*, *27*(6), 417–429. https://doi.org/10.1016/j.tcb.2017.01.006

Cerovic, V., Bain, C. C., Mowat, A. M., & Milling, S. W. F. (2014). Intestinal macrophages and dendritic cells: What's the difference? *Trends in Immunology*, *35*(6), 270–277. https://doi.org/10.1016/j.it.2014.04.003

Chen, D.-Z., Qi, M., Auborn, K. J., & Carter, T. H. (2001). Indole-3-Carbinol and Diindolylmethane Induce Apoptosis of Human Cervical Cancer Cells and in Murine HPV16-Transgenic Preneoplastic Cervical Epithelium. *The Journal of Nutrition*, *131*(12), 3294–3302. https://doi.org/10.1093/jn/131.12.3294

Chen, Y., Wang, Y., Fu, Y., Yin, Y., & Xu, K. (2023). Modulating AHR function offers exciting therapeutic potential in gut immunity and inflammation. *Cell & Bioscience*, *13*(1), 85. https://doi.org/10.1186/s13578-023-01046-y

Cheroutre, H., Lambolez, F., & Mucida, D. (2011). The light and dark sides of intestinal intraepithelial lymphocytes. *Nature reviews. Immunology*, *11*(7), 445–456. https://doi.org/10.1038/nri3007

Cho, K. W., Morris, D. L., DelProposto, J. L., Geletka, L., Zamarron, B., Martinez-Santibanez, G., Meyer, K. A., Singer, K., O'Rourke, R. W., & Lumeng, C. N. (2014). An MHC II-Dependent Activation Loop between Adipose Tissue Macrophages and CD4+ T Cells Controls Obesity-Induced Inflammation. *Cell Reports*, *9*(2), 605–617. https://doi.org/10.1016/j.celrep.2014.09.004

Cho, Y. E., Kwon, Y. S., & Hwang, S. (2023). Heterogeneous population of macrophages in the development of non-alcoholic fatty liver disease. *Liver Research*, 7(1), 16–25. https://doi.org/10.1016/j.livres.2022.06.001

Cipolletta, D., Feuerer, M., Li, A., Kamei, N., Lee, J., Shoelson, S. E., Benoist, C., & Mathis, D. (2012). PPARy is a major driver of the accumulation and phenotype of adipose-tissue Treg cells. *Nature*, *486*(7404), 549–553. https://doi.org/10.1038/nature11132

Cirillo, F., Lappano, R., Bruno, L., Rizzuti, B., Grande, F., Guzzi, R., Briguori, S., Miglietta, A. M., Nakajima, M., Di Martino, M. T., & Maggiolini, M. (2019). AHR and GPER mediate the stimulatory effects induced by 3-methylcholanthrene in breast cancer cells and cancer-associated fibroblasts (CAFs). *Journal of Experimental & Clinical Cancer Research*, *38*(1), 335. https://doi.org/10.1186/s13046-019-1337-2

Clementi, A. H., Gaudy, A. M., van Rooijen, N., Pierce, R. H., & Mooney, R. A. (2009). Loss of Kupffer cells in diet-induced obesity is associated with increased hepatic steatosis, STAT3 signaling, and further decreases in insulin signaling. *Biochimica et biophysica acta*, *1792*(11), 1062–1072. https://doi.org/10.1016/j.bbadis.2009.08.007

Conway, D. E., Sakurai, Y., Weiss, D., Vega, J. D., Taylor, W. R., Jo, H., Eskin, S. G., Marcus, C. B., & McIntire, L. V. (2009). Expression of CYP1A1 and CYP1B1 in human endothelial cells: Regulation by fluid shear stress. *Cardiovascular Research*, *81*(4), 669–677. https://doi.org/10.1093/cvr/cvn360

Costanzo, A. E., Taylor, K. R., Dutt, S., Han, P. P., Fujioka, K., & Jameson, J. M. (2015). Obesity Impairs $\gamma\delta$ T Cell Homeostasis and Antiviral Function in Humans. *PLoS ONE*, *10*(3), e0120918. https://doi.org/10.1371/journal.pone.0120918

Cox, N., & Geissmann, F. (2020). Macrophage ontogeny in the control of adipose tissue biology. *Current opinion in immunology*, *62*, 1–8. https://doi.org/10.1016/j.coi.2019.08.002

Crews, S. T. (1998). Control of cell lineage-specific development and transcription by bHLH–PAS proteins. *Genes & Development*, *12*(5), 607–620.

Crispe, I. N. (2009). The liver as a lymphoid organ. *Annual Review of Immunology*, *27*, 147–163. https://doi.org/10.1146/annurev.immunol.021908.132629

Cuff, A. O., Sillito, F., Dertschnig, S., Hall, A., Luong, T. V., Chakraverty, R., & Male, V. (2019). The Obese Liver Environment Mediates Conversion of NK Cells to a Less Cytotoxic ILC1-Like Phenotype. *Frontiers in Immunology*, *10*, 2180. https://doi.org/10.3389/fimmu.2019.02180

Cui, H., Gu, X., Chen, J., Xie, Y., Ke, S., Wu, J., Golovko, A., Morpurgo, B., Yan, C., Phillips, T. D., Xie, W., Luo, J., Zhou, Z., & Tian, Y. (2017). Pregnane X receptor regulates the AhR/Cyp1A1 pathway and protects liver cells from benzo-[α]-pyrene-induced DNA damage. *Toxicology Letters*, *275*, 67–76. https://doi.org/10.1016/j.toxlet.2017.03.028

Curry, M. P., Golden-Mason, L., Doherty, D. G., Deignan, T., Norris, S., Duffy, M., Nolan, N., Hall, W., Hegarty, J. E., & O'Farrelly, C. (2003). Expansion of innate CD5pos B cells expressing high levels of CD81 in hepatitis C virus infected liver. *Journal of Hepatology*, *38*(5), 642–650. https://doi.org/10.1016/s0168-8278(03)00075-8

da Silva, J. F., Bolsoni, J. A., da Costa, R. M., Alves, J. V., Bressan, A. F. M., Silva, L. E. V., Costa, T. J., Oliveira, A. E. R., Manzato, C. P., Aguiar, C. A., Fazan Jr, R., Cunha, F. Q., Nakaya, H. I., Carneiro, F. S., & Tostes, R. C. (2022). Aryl hydrocarbon receptor (AhR) activation contributes to high-fat dietinduced vascular dysfunction. *British Journal of Pharmacology*, *179*(12), 2938–2952. https://doi.org/10.1111/bph.15789

Dantsuka, A., Ichii, O., Hanberg, A., Elewa, Y. H. A., Otsuka-Kanazawa, S., Nakamura, T., & Kon, Y. (2019). Histopathological features of the proper gastric glands in FVB/N-background mice carrying constitutively-active aryl-hydrocarbon receptor. *BMC Gastroenterology*, *19*(1), 102. https://doi.org/10.1186/s12876-019-1009-x

De Rosa, V., Procaccini, C., Calì, G., Pirozzi, G., Fontana, S., Zappacosta, S., La Cava, A., & Matarese, G. (2007). A key role of leptin in the control of regulatory T cell proliferation. *Immunity*, *26*(2), 241–255. https://doi.org/10.1016/j.immuni.2007.01.011

De Simone, G., Andreata, F., Bleriot, C., Fumagalli, V., Laura, C., Garcia-Manteiga, J. M., Di Lucia, P., Gilotto, S., Ficht, X., De Ponti, F. F., Bono, E. B., Giustini, L., Ambrosi, G., Mainetti, M., Zordan, P., Bénéchet, A. P., Ravà, M., Chakarov, S., Moalli, F., ... lannacone, M. (2021). Identification of a Kupffer cell subset capable of reverting the T cell dysfunction induced by hepatocellular priming. *Immunity*, 54(9), 2089-2100.e8. https://doi.org/10.1016/j.immuni.2021.05.005

Delves, P. J., & Roitt, I. M. (2000). The immune system. First of two parts. *The New England Journal of Medicine*, 343(1), 37–49. https://doi.org/10.1056/NEJM200007063430107

Deng, Y., & Scherer, P. E. (2010). Adipokines as novel biomarkers and regulators of the metabolic syndrome. *Annals of the New York Academy of Sciences*, *1212*, E1–E19. https://doi.org/10.1111/j.1749-6632.2010.05875.x

Denison, M. S., & Nagy, S. R. (2003). Activation of the aryl hydrocarbon receptor by structurally diverse exogenous and endogenous chemicals. *Annual Review of Pharmacology and Toxicology*, *43*, 309–334. https://doi.org/10.1146/annurev.pharmtox.43.100901.135828

Denison, M. S., Pandini, A., Nagy, S. R., Baldwin, E. P., & Bonati, L. (2002). Ligand binding and activation of the Ah receptor. *Chemico-Biological Interactions*, *141*(1–2), 3–24. https://doi.org/10.1016/s0009-2797(02)00063-7

Denison, M. S., Soshilov, A. A., He, G., DeGroot, D. E., & Zhao, B. (2011). Exactly the same but different: Promiscuity and diversity in the molecular mechanisms of action of the aryl hydrocarbon

(dioxin) receptor. *Toxicological Sciences: An Official Journal of the Society of Toxicology*, 124(1), 1–22. https://doi.org/10.1093/toxsci/kfr218

DePaolo, R. W., Kamdar, K., Khakpour, S., Sugiura, Y., Wang, W., & Jabri, B. (2012). A specific role for TLR1 in protective TH17 immunity during mucosal infection. *The Journal of Experimental Medicine*, 209(8), 1437–1444. https://doi.org/10.1084/jem.20112339

Devisscher, L., Scott, C. L., Lefere, S., Raevens, S., Bogaerts, E., Paridaens, A., Verhelst, X., Geerts, A., Guilliams, M., & Van Vlierberghe, H. (2017). Non-alcoholic steatohepatitis induces transient changes within the liver macrophage pool. *Cellular Immunology*, *322*, 74–83. https://doi.org/10.1016/j.cellimm.2017.10.006

Devisscher, L., Verhelst, X., Colle, I., Van Vlierberghe, H., & Geerts, A. (2016). The role of macrophages in obesity-driven chronic liver disease. *Journal of Leukocyte Biology*, *99*(5), 693–698. https://doi.org/10.1189/jlb.5RU0116-016R

Diny, N. L., Schonfeldova, B., Shapiro, M., Winder, M. L., Varsani-Brown, S., & Stockinger, B. (2022). The aryl hydrocarbon receptor contributes to tissue adaptation of intestinal eosinophils in mice. *The Journal of Experimental Medicine*, *219*(4), e20210970. https://doi.org/10.1084/jem.20210970

Divanovic, S., Dalli, J., Jorge-Nebert, L. F., Flick, L. M., Gálvez-Peralta, M., Boespflug, N. D., Stankiewicz, T. E., Fitzgerald, J. M., Somarathna, M., Karp, C. L., Serhan, C. N., & Nebert, D. W. (2013). Contributions of the Three CYP1 Monooxygenases to Pro-Inflammatory and Inflammation-Resolution Lipid-Mediator Pathways. *Journal of immunology (Baltimore, Md. : 1950), 191*(6), 10.4049/jimmunol.1300699. https://doi.org/10.4049/jimmunol.1300699

Dou, H., Duan, Y., Zhang, X., Yu, Q., Di, Q., Song, Y., Li, P., & Gong, Y. (2019). Aryl hydrocarbon receptor (AhR) regulates adipocyte differentiation by assembling CRL4B ubiquitin ligase to target PPARγ for proteasomal degradation. *Journal of Biological Chemistry*, *294*(48), Article 48. https://doi.org/10.1074/jbc.RA119.009282

Dragin, N., Shi, Z., Madan, R., Karp, C. L., Sartor, M. A., Chen, C., Gonzalez, F. J., & Nebert, D. W. (2008). Phenotype of the Cyp1a1/1a2/1b1(-/-) Triple-Knockout Mouse. *Molecular pharmacology*, 73(6), 1844–1856. https://doi.org/10.1124/mol.108.045658

Du, J., Zhao, L., Kang, Q., He, Y., & Bi, Y. (o. J.). An optimized method for Oil Red O staining with the salicylic acid ethanol solution. *Adipocyte*, *12*(1), 2179334. https://doi.org/10.1080/21623945.2023.2179334

Du, W., & Wang, L. (2022). The Crosstalk Between Liver Sinusoidal Endothelial Cells and Hepatic Microenvironment in NASH Related Liver Fibrosis. *Frontiers in Immunology*, *13*. https://www.frontiersin.org/articles/10.3389/fimmu.2022.936196

Eberl, G., Colonna, M., Di Santo, J. P., & McKenzie, A. N. J. (2015). Innate Lymphoid Cells: A new paradigm in immunology. *Science (New York, N.Y.)*, *348*(6237), aaa6566. https://doi.org/10.1126/science.aaa6566

Eguchi, A., & Feldstein, A. E. (2014). Adipocyte Cell Death, Fatty Liver Disease and Associated Metabolic Disorders. *Digestive diseases (Basel, Switzerland)*, *32*(5), 579–585. https://doi.org/10.1159/000360509

Elchaninov, A., Vishnyakova, P., Menyailo, E., Sukhikh, G., & Fatkhudinov, T. (2022). An Eye on Kupffer Cells: Development, Phenotype and the Macrophage Niche. *International Journal of Molecular Sciences*, *23*(17), Article 17. https://doi.org/10.3390/ijms23179868

Ellulu, M. S., Patimah, I., Khaza'ai, H., Rahmat, A., & Abed, Y. (2017). Obesity and inflammation: The linking mechanism and the complications. *Archives of Medical Science : AMS*, *13*(4), 851–863. https://doi.org/10.5114/aoms.2016.58928

Embgenbroich, M., Zande, H. J. P. van der, Hussaarts, L., Schulte-Schrepping, J., Pelgrom, L. R., García-Tardón, N., Schlautmann, L., Stoetzel, I., Händler, K., Lambooij, J. M., Zawistowska-Deniziak, A., Hoving, L., Ruiter, K. de, Wijngaarden, M., Pijl, H., Dijk, K. W. van, Everts, B., Harmelen, V. van, Yazdanbakhsh, M., ... Burgdorf, S. (2020). *Soluble mannose receptor induces pro-inflammatory macrophage activation and metaflammation* (S. 2020.09.29.315598). bioRxiv. https://doi.org/10.1101/2020.09.29.315598

Enan, E., Liu, P. C., & Matsumura, F. (1992). 2,3,7,8-Tetrachlorodibenzo-p-dioxin causes reduction of glucose transporting activities in the plasma membranes of adipose tissue and pancreas from the guinea pig. *The Journal of Biological Chemistry*, *267*(28), 19785–19791.

Esser, C., & Rannug, A. (2015). The Aryl Hydrocarbon Receptor in Barrier Organ Physiology, Immunology, and Toxicology. *Pharmacological Reviews*, *67*(2), Article 2. https://doi.org/10.1124/pr.114.009001

Etzerodt, A., Moulin, M., Doktor, T. K., Delfini, M., Mossadegh-Keller, N., Bajenoff, M., Sieweke, M. H., Moestrup, S. K., Auphan-Anezin, N., & Lawrence, T. (2020). Tissue-resident macrophages in omentum promote metastatic spread of ovarian cancer. *The Journal of Experimental Medicine*, 217(4), e20191869. https://doi.org/10.1084/jem.20191869

Falero-Perez, J., Song, Y.-S., Zhao, Y., Teixeira, L., Sorenson, C. M., & Sheibani, N. (2018). Cyp1b1 expression impacts the angiogenic and inflammatory properties of liver sinusoidal endothelial cells. *PLOS ONE*, *13*(10), e0206756. https://doi.org/10.1371/journal.pone.0206756

Félix, I., Jokela, H., Karhula, J., Kotaja, N., Savontaus, E., Salmi, M., & Rantakari, P. (2021). Single-Cell Proteomics Reveals the Defined Heterogeneity of Resident Macrophages in White Adipose Tissue. *Frontiers in Immunology*, *12*. https://www.frontiersin.org/articles/10.3389/fimmu.2021.719979

Frueh, F. W., Hayashibara, K. C., Brown, P. O., & Whitlock, J. P. (2001). Use of cDNA microarrays to analyze dioxin-induced changes in human liver gene expression. *Toxicology Letters*, *122*(3), 189–203. https://doi.org/10.1016/s0378-4274(01)00364-2

Fuchs, A., Vermi, W., Lee, J. S., Lonardi, S., Gilfillan, S., Newberry, R. D., Cella, M., & Colonna, M. (2013). Intraepithelial type 1 innate lymphoid cells are a unique subset of IL-12- and IL-15-responsive IFN-γ-producing cells. *Immunity*, *38*(4), 769–781. https://doi.org/10.1016/j.immuni.2013.02.010

Gao, B., Jeong, W.-I., & Tian, Z. (2008). Liver: An organ with predominant innate immunity. Hepatology (Baltimore, Md.), 47(2), 729–736. https://doi.org/10.1002/hep.22034

Garly, M.-L., Martins, C. L., Balé, C., Baldé, M. A., Hedegaard, K. L., Gustafson, P., Lisse, I. M., Whittle, H. C., & Aaby, P. (2003). BCG scar and positive tuberculin reaction associated with reduced child mortality in West Africa. A non-specific beneficial effect of BCG? *Vaccine*, *21*(21–22), 2782–2790. https://doi.org/10.1016/s0264-410x(03)00181-6

Ghaben, A. L., & Scherer, P. E. (2019). Adipogenesis and metabolic health. *Nature Reviews Molecular Cell Biology*, 20(4), Article 4. https://doi.org/10.1038/s41580-018-0093-z

Giani Tagliabue, S., Faber, S. C., Motta, S., Denison, M. S., & Bonati, L. (2019). Modeling the binding of diverse ligands within the Ah receptor ligand binding domain. *Scientific Reports*, *9*(1), Article 1. https://doi.org/10.1038/s41598-019-47138-z

Girer, N. G., Tomlinson, C. R., & Elferink, C. J. (2020). The Aryl Hydrocarbon Receptor in Energy Balance: The Road from Dioxin-Induced Wasting Syndrome to Combating Obesity with Ahr Ligands. *International Journal of Molecular Sciences*, 22(1), 49. https://doi.org/10.3390/ijms22010049

Goode, G., Pratap, S., & Eltom, S. E. (2014). Depletion of the aryl hydrocarbon receptor in MDA-MB-231 human breast cancer cells altered the expression of genes in key regulatory pathways of cancer. *PloS One*, *9*(6), e100103. https://doi.org/10.1371/journal.pone.0100103

Goodman, T., & Lefrançois, L. (1988). Expression of the gamma-delta T-cell receptor on intestinal CD8+ intraepithelial lymphocytes. *Nature*, *333*(6176), 855–858. https://doi.org/10.1038/333855a0

Gourronc, F. A., Markan, K. R., Kulhankova, K., Zhu, Z., Sheehy, R., Quelle, D. E., Zingman, L. V., Kurago, Z. B., Ankrum, J. A., & Klingelhutz, A. J. (2020). Pdgfrα-Cre mediated knockout of the aryl hydrocarbon receptor protects mice from high-fat diet induced obesity and hepatic steatosis. *PLOS ONE*, *15*(7), e0236741. https://doi.org/10.1371/journal.pone.0236741

Gregory, S. H., Sagnimeni, A. J., & Wing, E. J. (1996). Bacteria in the bloodstream are trapped in the liver and killed by immigrating neutrophils. *Journal of Immunology (Baltimore, Md.: 1950), 157*(6), 2514–2520.

Grimaldi, G., Rajendra, S., & Matthews, J. (2018). The aryl hydrocarbon receptor regulates the expression of TIPARP and its cis long non-coding RNA, TIPARP-AS1. *Biochemical and Biophysical Research Communications*, 495(3), 2356–2362. https://doi.org/10.1016/j.bbrc.2017.12.113

Guzik, T. J., Korbut, R., & Adamek-Guzik, T. (2003). Nitric oxide and superoxide in inflammation and immune regulation. *Journal of Physiology and Pharmacology: An Official Journal of the Polish Physiological Society*, *54*(4), 469–487.

Haarmann-Stemmann, T., Esser, C., & Krutmann, J. (2015). The Janus-Faced Role of Aryl Hydrocarbon Receptor Signaling in the Skin: Consequences for Prevention and Treatment of Skin Disorders. *The Journal of Investigative Dermatology*, 135(11), 2572–2576. https://doi.org/10.1038/jid.2015.285

Haldar, M., & Murphy, K. M. (2014). Origin, development, and homeostasis of tissue-resident macrophages. *Immunological Reviews*, 262(1), 25–35. https://doi.org/10.1111/imr.12215

Halim, T. Y. F., Rana, B. M. J., Walker, J. A., Kerscher, B., Knolle, M. D., Jolin, H. E., Serrao, E. M., Haim-Vilmovsky, L., Teichmann, S. A., Rodewald, H.-R., Botto, M., Vyse, T. J., Fallon, P. G., Li, Z., Withers, D. R., & McKenzie, A. N. J. (2018). Tissue-Restricted Adaptive Type 2 Immunity Is Orchestrated by Expression of the Costimulatory Molecule OX40L on Group 2 Innate Lymphoid Cells. *Immunity*, *48*(6), 1195-1207.e6. https://doi.org/10.1016/j.immuni.2018.05.003

Hall, P., & Cash, J. (2012). What is the Real Function of the Liver 'Function' Tests? *The Ulster Medical Journal*, 81(1), 30–36.

Hams, E., Locksley, R. M., McKenzie, A. N. J., & Fallon, P. G. (2013). IL-25 elicits innate lymphoid type 2 and type II natural killer T cells that regulate obesity in mice1. *Journal of immunology (Baltimore, Md.: 1950)*, 191(11), 10.4049/jimmunol.1301176. https://doi.org/10.4049/jimmunol.1301176

Haque, N., Ojo, E. S., Krager, S. L., & Tischkau, S. A. (2023). Deficiency of Adipose Aryl Hydrocarbon Receptor Protects against Diet-Induced Metabolic Dysfunction through Sexually Dimorphic Mechanisms. *Cells*, *12*(13), Article 13. https://doi.org/10.3390/cells12131748

Harwood, H. J. (2012). The adipocyte as an endocrine organ in the regulation of metabolic homeostasis. *Neuropharmacology*, *63*(1), 57–75. https://doi.org/10.1016/j.neuropharm.2011.12.010

Hayday, A., Theodoridis, E., Ramsburg, E., & Shires, J. (2001). Intraepithelial lymphocytes: Exploring the Third Way in immunology. *Nature Immunology*, *2*(11), 997–1003. https://doi.org/10.1038/ni1101-997

Hayes, J. D., Dinkova-Kostova, A. T., & McMahon, M. (2009). Cross-talk between Transcription Factors AhR and Nrf2: Lessons for Cancer Chemoprevention from Dioxin. *Toxicological Sciences*, 111(2), 199–201. https://doi.org/10.1093/toxsci/kfp168

He, S., Kahles, F., Rattik, S., Nairz, M., McAlpine, C. S., Anzai, A., Selgrade, D., Fenn, A. M., Chan, C. T., Mindur, J. E., Valet, C., Poller, W. C., Halle, L., Rotllan, N., Iwamoto, Y., Wojtkiewicz, G. R., Weissleder, R., Libby, P., Fernández-Hernando, C., ... Swirski, F. K. (2019). Gut intraepithelial T cells calibrate metabolism and accelerate cardiovascular disease. *Nature*, *566*(7742), Article 7742. https://doi.org/10.1038/s41586-018-0849-9

Heyens, L. J. M., Busschots, D., Koek, G. H., Robaeys, G., & Francque, S. (2021). Liver Fibrosis in Non-alcoholic Fatty Liver Disease: From Liver Biopsy to Non-invasive Biomarkers in Diagnosis and Treatment. *Frontiers in Medicine*, *8*. https://www.frontiersin.org/articles/10.3389/fmed.2021.615978

Highton, A. J., Schuster, I. S., Degli-Esposti, M. A., & Altfeld, M. (2021). The role of natural killer cells in liver inflammation. *Seminars in Immunopathology*, *43*(4), 519–533. https://doi.org/10.1007/s00281-021-00877-6

Hildebrandt, X., Ibrahim, M., & Peltzer, N. (2023). Cell death and inflammation during obesity: "Know my methods, WAT(son)". *Cell Death & Differentiation*, *30*(2), Article 2. https://doi.org/10.1038/s41418-022-01062-4

Hill, J. O., Wyatt, H. R., & Peters, J. C. (2013). The Importance of Energy Balance. *European Endocrinology*, *9*(2), 111–115. https://doi.org/10.17925/EE.2013.09.02.111

Hooper, L. V. (2011). You AhR what you eat: Linking diet and immunity. *Cell*, *147*(3), 489–491. https://doi.org/10.1016/j.cell.2011.10.004

Horowitz, J. F., & Klein, S. (2000). Whole body and abdominal lipolytic sensitivity to epinephrine is suppressed in upper body obese women. *American Journal of Physiology. Endocrinology and Metabolism*, *278*(6), E1144-1152. https://doi.org/10.1152/ajpendo.2000.278.6.E1144

Hosoya, T., Harada, N., Mimura, J., Motohashi, H., Takahashi, S., Nakajima, O., Morita, M., Kawauchi, S., Yamamoto, M., & Fujii-Kuriyama, Y. (2008). Inducibility of cytochrome P450 1A1 and chemical carcinogenesis by benzo[a]pyrene in AhR repressor-deficient mice. *Biochemical and Biophysical Research Communications*, *365*(3), 562–567. https://doi.org/10.1016/j.bbrc.2007.11.016

Hotamisligil, G. S. (1999). The role of TNFalpha and TNF receptors in obesity and insulin resistance. *Journal of Internal Medicine*, *245*(6), 621–625. https://doi.org/10.1046/j.1365-2796.1999.00490.x

Hu, W., & Pasare, C. (2013). Location, location: Tissue-specific regulation of immune responses. *Journal of Leukocyte Biology*, *94*(3), 409–421. https://doi.org/10.1189/jlb.0413207

Huby, T., & Gautier, E. L. (2022). Immune cell-mediated features of non-alcoholic steatohepatitis. *Nature Reviews Immunology*, *22*(7), Article 7. https://doi.org/10.1038/s41577-021-00639-3

Hue, S., Ahern, P., Buonocore, S., Kullberg, M. C., Cua, D. J., McKenzie, B. S., Powrie, F., & Maloy, K. J. (2006). Interleukin-23 drives innate and T cell–mediated intestinal inflammation. *The Journal of Experimental Medicine*, 203(11), 2473–2483. https://doi.org/10.1084/jem.20061099

Hume, D. A., Offermanns, S., & Bonnavion, R. (2022). Contamination of isolated mouse Kupffer cells with liver sinusoidal endothelial cells. *Immunity*, *55*(7), 1139–1140. https://doi.org/10.1016/j.immuni.2022.06.010

Ireland, H., Kemp, R., Houghton, C., Howard, L., Clarke, A. R., Sansom, O. J., & Winton, D. J. (2004). Inducible cre-mediated control of gene expression in the murine gastrointestinal tract: Effect of loss of β-catenin. *Gastroenterology*, *126*(5), Article 5. https://doi.org/10.1053/j.gastro.2004.03.020

Ishihara, Y., Kado, S. Y., Hoeper, C., Harel, S., & Vogel, C. F. A. (2019). Role of NF-kB RelB in Aryl Hydrocarbon Receptor-Mediated Ligand Specific Effects. *International Journal of Molecular Sciences*, 20(11), 2652. https://doi.org/10.3390/ijms20112652

Jager, J., Aparicio-Vergara, M., & Aouadi, M. (2016). Liver innate immune cells and insulin resistance: The multiple facets of Kupffer cells. *Journal of Internal Medicine*, *280*(2), 209–220. https://doi.org/10.1111/joim.12483

Jain, S., Dolwick, K. M., Schmidt, J. V., & Bradfield, C. A. (1994). Potent transactivation domains of the Ah receptor and the Ah receptor nuclear translocator map to their carboxyl termini. *The Journal of Biological Chemistry*, *269*(50), 31518–31524.

Janeway, C. A. (1992). The immune system evolved to discriminate infectious nonself from noninfectious self. *Immunology Today*, *13*(1), 11–16. https://doi.org/10.1016/0167-5699(92)90198-G

Johansson-Lindbom, B., Svensson, M., Pabst, O., Palmqvist, C., Marquez, G., Förster, R., & Agace, W. W. (2005). Functional specialization of gut CD103+ dendritic cells in the regulation of tissue-selective T cell homing. *The Journal of Experimental Medicine*, *202*(8), 1063–1073. https://doi.org/10.1084/jem.20051100

Jr, C. A. J., Travers, P., Walport, M., Shlomchik, M. J., Jr, C. A. J., Travers, P., Walport, M., & Shlomchik, M. J. (2001). *Immunobiology* (5th Aufl.). Garland Science.

Kadow, S., Jux, B., Zahner, S. P., Wingerath, B., Chmill, S., Clausen, B. E., Hengstler, J., & Esser, C. (2011). Aryl Hydrocarbon Receptor Is Critical for Homeostasis of Invariant $\gamma\delta$ T Cells in the Murine Epidermis. *The Journal of Immunology*, *187*(6), Article 6. https://doi.org/10.4049/jimmunol.1100912

Kadowaki, T., Yamauchi, T., Kubota, N., Hara, K., Ueki, K., & Tobe, K. (2006). Adiponectin and adiponectin receptors in insulin resistance, diabetes, and the metabolic syndrome. *Journal of Clinical Investigation*, *116*(7), 1784–1792. https://doi.org/10.1172/JCl29126

Kaech, S. M., Hemby, S., Kersh, E., & Ahmed, R. (2002). Molecular and functional profiling of memory CD8 T cell differentiation. *Cell*, *111*(6), 837–851. https://doi.org/10.1016/s0092-8674(02)01139-x

Kaestner, K. H. (2019). The Intestinal Stem Cell Niche: A Central Role for Foxl1-Expressing Subepithelial Telocytes. *Cellular and Molecular Gastroenterology and Hepatology*, 8(1), 111–117. https://doi.org/10.1016/j.jcmgh.2019.04.001

Karchner, S. I., Jenny, M. J., Tarrant, A. M., Evans, B. R., Kang, H. J., Bae, I., Sherr, D. H., & Hahn, M. E. (2009). The Active Form of Human Aryl Hydrocarbon Receptor (AHR) Repressor Lacks Exon 8, and Its Pro185 and Ala185 Variants Repress both AHR and Hypoxia-Inducible Factor. *Molecular and Cellular Biology*, *29*(13), Article 13. https://doi.org/10.1128/MCB.00206-09

Kawai, T., Autieri, M. V., & Scalia, R. (2021). Adipose tissue inflammation and metabolic dysfunction in obesity. *American Journal of Physiology - Cell Physiology*, *320*(3), C375–C391. https://doi.org/10.1152/ajpcell.00379.2020 Kelly, A., Fahey, R., Fletcher, J. M., Keogh, C., Carroll, A. G., Siddachari, R., Geoghegan, J., Hegarty, J. E., Ryan, E. J., & O'Farrelly, C. (2014). CD141⁺ myeloid dendritic cells are enriched in healthy human liver. *Journal of Hepatology*, *60*(1), 135–142. https://doi.org/10.1016/j.jhep.2013.08.007

Kennedy, G. C. (1953). The role of depot fat in the hypothalamic control of food intake in the rat. *Proceedings of the Royal Society of London. Series B, Biological Sciences*, *140*(901), 578–596. https://doi.org/10.1098/rspb.1953.0009

Kerley-Hamilton, J. S., Trask, H. W., Ridley, C. J. A., DuFour, E., Ringelberg, C. S., Nurinova, N., Wong, D., Moodie, K. L., Shipman, S. L., Moore, J. H., Korc, M., Shworak, N. W., & Tomlinson, C. R. (2012). Obesity Is Mediated by Differential Aryl Hydrocarbon Receptor Signaling in Mice Fed a Western Diet. *Environmental Health Perspectives*, *120*(9), 1252–1259. https://doi.org/10.1289/ehp.1205003

Kewley, R. J., Whitelaw, M. L., & Chapman-Smith, A. (2004). The mammalian basic helix-loophelix/PAS family of transcriptional regulators. *The International Journal of Biochemistry & Cell Biology*, *36*(2), 189–204. https://doi.org/10.1016/s1357-2725(03)00211-5

Khan, S., Chan, Y. T., Revelo, X. S., & Winer, D. A. (2020). The Immune Landscape of Visceral Adipose Tissue During Obesity and Aging. *Frontiers in Endocrinology*, *11*, 267. https://doi.org/10.3389/fendo.2020.00267

Khan, S., Luck, H., Winer, S., & Winer, D. A. (2021). Emerging concepts in intestinal immune control of obesity-related metabolic disease. *Nature Communications*, *12*, 2598. https://doi.org/10.1038/s41467-021-22727-7

Kintscher, U., Hartge, M., Hess, K., Foryst-Ludwig, A., Clemenz, M., Wabitsch, M., Fischer-Posovszky, P., Barth, T. F. E., Dragun, D., Skurk, T., Hauner, H., Blüher, M., Unger, T., Wolf, A.-M., Knippschild, U., Hombach, V., & Marx, N. (2008). T-lymphocyte Infiltration in Visceral Adipose Tissue. *Arteriosclerosis, Thrombosis, and Vascular Biology*, 28(7), 1304–1310. https://doi.org/10.1161/ATVBAHA.108.165100

Klomp, F., Wenzel, C., Drozdzik, M., & Oswald, S. (2020). Drug–Drug Interactions Involving Intestinal and Hepatic CYP1A Enzymes. *Pharmaceutics*, *12*(12), 1201. https://doi.org/10.3390/pharmaceutics12121201

Klose, C. S. N., Kiss, E. A., Schwierzeck, V., Ebert, K., Hoyler, T., d'Hargues, Y., Göppert, N., Croxford, A. L., Waisman, A., Tanriver, Y., & Diefenbach, A. (2013). A T-bet gradient controls the fate and function of CCR6-RORγt+ innate lymphoid cells. *Nature*, *494*(7436), 261–265. https://doi.org/10.1038/nature11813

Knudson, J. D., Dincer, U. D., Zhang, C., Swafford, A. N., Koshida, R., Picchi, A., Focardi, M., Dick, G. M., & Tune, J. D. (2005). Leptin receptors are expressed in coronary arteries, and hyperleptinemia causes significant coronary endothelial dysfunction. *American Journal of Physiology. Heart and Circulatory Physiology*, 289(1), H48-56. https://doi.org/10.1152/ajpheart.01159.2004

Kolodin, D., van Panhuys, N., Li, C., Magnuson, A. M., Cipolletta, D., Miller, C. M., Wagers, A., Germain, R. N., Benoist, C., & Mathis, D. (2015). ANTIGEN- AND CYTOKINE-DRIVEN ACCUMULATION OF REGULATORY T CELLS IN VISCERAL ADIPOSE TISSUE OF LEAN MICE. *Cell metabolism*, *21*(4), 543–557. https://doi.org/10.1016/j.cmet.2015.03.005

Konopka, R. J., & Benzer, S. (1971). Clock Mutants of Drosophila melanogaster. *Proceedings of the National Academy of Sciences of the United States of America*, 68(9), 2112–2116.

Konturek, S. J., Konturek, J. W., Pawlik, T., & Brzozowski, T. (2004). Brain-gut axis and its role in the control of food intake. *Journal of Physiology and Pharmacology: An Official Journal of the Polish Physiological Society*, *55*(1 Pt 2), 137–154.

Kramer, S., & Carrington, M. (2014). An AU-rich instability element in the 3'UTR mediates an increase in mRNA stability in response to expression of a dhh1 ATPase mutant. *Translation*, *2*(1), Article 1. https://doi.org/10.4161/trla.28587

Krijgsman, D., Hokland, M., & Kuppen, P. J. K. (2018). The Role of Natural Killer T Cells in Cancer—A Phenotypical and Functional Approach. *Frontiers in Immunology*, *9*. https://www.frontiersin.org/articles/10.3389/fimmu.2018.00367

Kubes, P., & Mehal, W. Z. (2012). Sterile inflammation in the liver. *Gastroenterology*, 143(5), 1158–1172. https://doi.org/10.1053/j.gastro.2012.09.008

Kubota, A., Goldstone, J. V., Lemaire, B., Takata, M., Woodin, B. R., & Stegeman, J. J. (2015). Role of pregnane X receptor and aryl hydrocarbon receptor in transcriptional regulation of pxr, CYP2, and CYP3 genes in developing zebrafish. *Toxicological Sciences: An Official Journal of the Society of Toxicology*, 143(2), 398–407. https://doi.org/10.1093/toxsci/kfu240

Kwon, O., Kim, K. W., & Kim, M.-S. (2016). Leptin signalling pathways in hypothalamic neurons. *Cellular and Molecular Life Sciences: CMLS*, 73(7), 1457–1477. https://doi.org/10.1007/s00018-016-2133-1

Kyoreva, M., Li, Y., Hoosenally, M., Hardman-Smart, J., Morrison, K., Tosi, I., Tolaini, M., Barinaga, G., Stockinger, B., Mrowietz, U., Nestle, F. O., Smith, C. H., Barker, J. N., & Di Meglio, P. (2021). CYP1A1 Enzymatic Activity Influences Skin Inflammation Via Regulation of the AHR Pathway. *The Journal of Investigative Dermatology*, *141*(6), 1553-1563.e3. https://doi.org/10.1016/j.jid.2020.11.024

Lamas, B., Natividad, J. M., & Sokol, H. (2018). Aryl hydrocarbon receptor and intestinal immunity. *Mucosal Immunology*, *11*(4), 1024–1038. https://doi.org/10.1038/s41385-018-0019-2

Lano, G., Laforêt, M., Von Kotze, C., Perrin, J., Addi, T., Brunet, P., Poitevin, S., Burtey, S., & Dou, L. (2020). Aryl Hydrocarbon Receptor Activation and Tissue Factor Induction by Fluid Shear Stress and Indoxyl Sulfate in Endothelial Cells. *International Journal of Molecular Sciences*, *21*(7), Article 7. https://doi.org/10.3390/ijms21072392

Larigot, L., Juricek, L., Dairou, J., & Coumoul, X. (2018). AhR signaling pathways and regulatory functions. *Biochimie Open*, 7, 1–9. https://doi.org/10.1016/j.biopen.2018.05.001

Lee, H. H., Kim, W.-T., Kim, D. H., Park, J. W., Kang, T.-H., Chung, J. W., & Leem, S.-H. (2013). Tristetraprolin suppresses AHRR expression through mRNA destabilization. *FEBS Letters*, *587*(10), 1518–1523. https://doi.org/10.1016/j.febslet.2013.03.031

Lee, J. H., Wada, T., Febbraio, M., He, J., Matsubara, T., Lee, M. J., Gonzalez, F. J., & Xie, W. (2010). A novel role for the dioxin receptor in fatty acid metabolism and hepatic steatosis. *Gastroenterology*, 139(2), 653–663. https://doi.org/10.1053/j.gastro.2010.03.033

Lentz, A. K., & Feezor, R. J. (2003). Principles of immunology. *Nutrition in Clinical Practice: Official Publication of the American Society for Parenteral and Enteral Nutrition*, *18*(6), 451–460. https://doi.org/10.1177/0115426503018006451

Li, D., & Wu, M. (2021). Pattern recognition receptors in health and diseases. *Signal Transduction and Targeted Therapy*, *6*(1), Article 1. https://doi.org/10.1038/s41392-021-00687-0

- LI, T., LESUER, W., SINGH, A., HERNANDEZ, J. D., ZHANG, X., JELINEK, D., LIU, J., VELLA, A., JACOBSEN, E. A., & DEFILIPPIS, E. (2019). 2006-P: The Role of Adipose Tissue-Resident Eosinophils in Adipocyte Metabolism and Whole-Body Energy Homeostasis. *Diabetes*, *68*(Supplement_1), 2006-P. https://doi.org/10.2337/db19-2006-P
- Li, X., Duan, X., Jiang, H., Sun, Y., Tang, Y., Yuan, Z., Guo, J., Liang, W., Chen, L., Yin, J., Ma, H., Wang, J., & Zhang, D. (2006). Genome-Wide Analysis of Basic/Helix-Loop-Helix Transcription Factor Family in Rice and Arabidopsis. *Plant Physiology*, *141*(4), 1167–1184. https://doi.org/10.1104/pp.106.080580
- Li, X., Ren, Y., Chang, K., Wu, W., Griffiths, H. R., Lu, S., & Gao, D. (2023). Adipose tissue macrophages as potential targets for obesity and metabolic diseases. *Frontiers in Immunology*, *14*. https://www.frontiersin.org/articles/10.3389/fimmu.2023.1153915
- Li, Y., Zhou, C., Lei, W., Wang, K., & Zheng, J. (2020). Roles of aryl hydrocarbon receptor in endothelial angiogenic responses†. *Biology of Reproduction*, *103*(5), 927–937. https://doi.org/10.1093/biolre/ioaa128
- Lin, Y.-H., Luck, H., Khan, S., Schneeberger, P. H. H., Tsai, S., Clemente-Casares, X., Lei, H., Leu, Y.-L., Chan, Y. T., Chen, H.-Y., Yang, S.-H., Coburn, B., Winer, S., & Winer, D. A. (2019). Aryl hydrocarbon receptor agonist indigo protects against obesity-related insulin resistance through modulation of intestinal and metabolic tissue immunity. *International Journal of Obesity*, *43*(12), Article 12. https://doi.org/10.1038/s41366-019-0340-1
- Liu, X., Huang, T., Li, L., Tang, Y., Tian, Y., Wang, S., & Fan, C. (2015). CYP1B1 deficiency ameliorates obesity and glucose intolerance induced by high fat diet in adult C57BL/6J mice. *American Journal of Translational Research*, 7(4), 761–771.
- Liu, Y., She, W., Wang, F., Li, J., Wang, J., & Jiang, W. (2014). 3, 3'-Diindolylmethane alleviates steatosis and the progression of NASH partly through shifting the imbalance of Treg/Th17 cells to Treg dominance. *International Immunopharmacology*, 23(2), 489–498. https://doi.org/10.1016/j.intimp.2014.09.024
- Longo, M., Zatterale, F., Naderi, J., Parrillo, L., Formisano, P., Raciti, G. A., Beguinot, F., & Miele, C. (2019). Adipose Tissue Dysfunction as Determinant of Obesity-Associated Metabolic Complications. *International Journal of Molecular Sciences*, 20(9), 2358. https://doi.org/10.3390/ijms20092358
- Lopategi, A., López-Vicario, C., Alcaraz-Quiles, J., García-Alonso, V., Rius, B., Titos, E., & Clària, J. (2016). Role of bioactive lipid mediators in obese adipose tissue inflammation and endocrine dysfunction. *Molecular and Cellular Endocrinology*, *419*, 44–59. https://doi.org/10.1016/j.mce.2015.09.033
- Lou, W., Zhang, M., Chen, Q., Bai, T.-Y., Hu, Y.-X., Gao, F., Li, J., Lv, X.-L., Zhang, Q., & Chang, F.-H. (2022). Molecular mechanism of benzo [a] pyrene regulating lipid metabolism via aryl hydrocarbon receptor. *Lipids in Health and Disease*, *21*(1), 13. https://doi.org/10.1186/s12944-022-01627-9
- Louwe, P. A., Gomez, L. B., Webster, H., Perona-Wright, G., Bain, C. C., Forbes, S. J., & Jenkins, S. J. (2020). *Recruited macrophages that colonise the post-inflammatory peritoneal niche convert into functionally divergent resident cells* (S. 2020.11.30.404988). bioRxiv. https://doi.org/10.1101/2020.11.30.404988
- Lu, P., Yan, J., Liu, K., Garbacz, W. G., Wang, P., Xu, M., Ma, X., & Xie, W. (2015). Activation of aryl hydrocarbon receptor dissociates fatty liver from insulin resistance by inducing fibroblast growth factor 21. *Hepatology*, *61*(6), 1908–1919. https://doi.org/10.1002/hep.27719

Ma, Q., & Baldwin, K. T. (2000). 2,3,7,8-Tetrachlorodibenzo-p-dioxin-induced Degradation of Aryl Hydrocarbon Receptor (AhR) by the Ubiquitin-Proteasome Pathway: ROLE OF THE TRANSCRIPTION ACTIVATON AND DNA BINDING OF AhR *. *Journal of Biological Chemistry*, *275*(12), 8432–8438. https://doi.org/10.1074/jbc.275.12.8432

Macdougall, C. E., Wood, E. G., Loschko, J., Scagliotti, V., Cassidy, F. C., Robinson, M. E., Feldhahn, N., Castellano, L., Voisin, M.-B., Marelli-Berg, F., Gaston-Massuet, C., Charalambous, M., & Longhi, M. P. (2018). Visceral Adipose Tissue Immune Homeostasis Is Regulated by the Crosstalk between Adipocytes and Dendritic Cell Subsets. *Cell Metabolism*, *27*(3), 588-601.e4. https://doi.org/10.1016/j.cmet.2018.02.007

Macotela, Y., Emanuelli, B., Mori, M. A., Gesta, S., Schulz, T. J., Tseng, Y.-H., & Kahn, C. R. (2012). Intrinsic Differences in Adipocyte Precursor Cells From Different White Fat Depots. *Diabetes*, *61*(7), 1691–1699. https://doi.org/10.2337/db11-1753

MacPherson, L., Ahmed, S., Tamblyn, L., Krutmann, J., Förster, I., Weighardt, H., & Matthews, J. (2014). Aryl Hydrocarbon Receptor Repressor and TiPARP (ARTD14) Use Similar, but also Distinct Mechanisms to Repress Aryl Hydrocarbon Receptor Signaling. *International Journal of Molecular Sciences*, *15*(5), Article 5. https://doi.org/10.3390/ijms15057939

Major, J., Crotta, S., Finsterbusch, K., Chakravarty, P., Shah, K., Frederico, B., D'Antuono, R., Green, M., Meader, L., Suarez-Bonnet, A., Priestnall, S., Stockinger, B., & Wack, A. (2023). Endothelial AHR activity prevents lung barrier disruption in viral infection. *Nature*, *621*(7980), 813–820. https://doi.org/10.1038/s41586-023-06287-y

Malfacini, D., & Pfeifer, A. (2023). GPCR in Adipose Tissue Function—Focus on Lipolysis. *Biomedicines*, 11(2), 588. https://doi.org/10.3390/biomedicines11020588

Martin-Murphy, B. V., You, Q., Wang, H., Houssaye, B. A. D. L., Reilly, T. P., Friedman, J. E., & Ju, C. (2014). Mice Lacking Natural Killer T Cells Are More Susceptible to Metabolic Alterations following High Fat Diet Feeding. *PLOS ONE*, *9*(1), e80949. https://doi.org/10.1371/journal.pone.0080949

Matsumoto, M., Hada, N., Sakamaki, Y., Uno, A., Shiga, T., Tanaka, C., Ito, T., Katsume, A., & Sudoh, M. (2013). An improved mouse model that rapidly develops fibrosis in non-alcoholic steatohepatitis. *International Journal of Experimental Pathology*, *94*(2), 93–103. https://doi.org/10.1111/iep.12008

Matsunawa, M., Amano, Y., Endo, K., Uno, S., Sakaki, T., Yamada, S., & Makishima, M. (2009). The aryl hydrocarbon receptor activator benzo[a]pyrene enhances vitamin D3 catabolism in macrophages. *Toxicological Sciences: An Official Journal of the Society of Toxicology, 109*(1), 50–58. https://doi.org/10.1093/toxsci/kfp044

Matthews, J. (2017). AHR toxicity and signaling: Role of TIPARP and ADP-ribosylation. *Current Opinion in Toxicology*, 2, 50–57. https://doi.org/10.1016/j.cotox.2017.01.013

McCarthy, N., Manieri, E., Storm, E. E., Saadatpour, A., Luoma, A. M., Kapoor, V. N., Madha, S., Gaynor, L. T., Cox, C., Keerthivasan, S., Wucherpfennig, K., Yuan, G.-C., Sauvage, F. J. de, Turley, S. J., & Shivdasani, R. A. (2020). Distinct Mesenchymal Cell Populations Generate the Essential Intestinal BMP Signaling Gradient. *Cell Stem Cell*, *26*(3), Article 3. https://doi.org/10.1016/j.stem.2020.01.008

McDole, J. R., Wheeler, L. W., McDonald, K. G., Wang, B., Konjufca, V., Knoop, K. A., Newberry, R. D., & Miller, M. J. (2012). Goblet cells deliver luminal antigen to CD103+ dendritic cells in the small intestine. *Nature*, *483*(7389), Article 7389. https://doi.org/10.1038/nature10863

McKenzie, A. N. J., Spits, H., & Eberl, G. (2014). Innate lymphoid cells in inflammation and immunity. *Immunity*, *41*(3), 366–374. https://doi.org/10.1016/j.immuni.2014.09.006

Meek, T. H., Matsen, M. E., Dorfman, M. D., Guyenet, S. J., Damian, V., Nguyen, H. T., Taborsky, G. J., & Morton, G. J. (2013). Leptin Action in the Ventromedial Hypothalamic Nucleus Is Sufficient, But Not Necessary, to Normalize Diabetic Hyperglycemia. *Endocrinology*, *154*(9), 3067–3076. https://doi.org/10.1210/en.2013-1328

Mehta, P., Nuotio-Antar, A. M., & Smith, C. W. (2015). Γδ T cells promote inflammation and insulin resistance during high fat diet-induced obesity in mice. *Journal of Leukocyte Biology*, *97*(1), 121–134. https://doi.org/10.1189/jlb.3A0414-211RR

Méndez-Sánchez, N., Córdova-Gallardo, J., Barranco-Fragoso, B., & Eslam, M. (2021). Hepatic Dendritic Cells in the Development and Progression of Metabolic Steatohepatitis. *Frontiers in Immunology*, *12*, 641240. https://doi.org/10.3389/fimmu.2021.641240

Meng, X., Qian, X., Ding, X., Wang, W., Yin, X., Zhuang, G., & Zeng, W. (2022). Eosinophils regulate intra-adipose axonal plasticity. *Proceedings of the National Academy of Sciences*, *119*(3), e2112281119. https://doi.org/10.1073/pnas.2112281119

Merches, K., Schiavi, A., Weighardt, H., Steinwachs, S., Teichweyde, N., Förster, I., Hochrath, K., Schumak, B., Ventura, N., Petzsch, P., Köhrer, K., & Esser, C. (2020). AHR Signaling Dampens Inflammatory Signature in Neonatal Skin $\gamma\delta$ T Cells. *International Journal of Molecular Sciences*, *21*(6), 2249. https://doi.org/10.3390/ijms21062249

Mestecky, J., Russell, M. W., & Elson, C. O. (1999). Intestinal IgA: Novel views on its function in the defence of the largest mucosal surface. *Gut*, 44(1), 2–5. https://doi.org/10.1136/gut.44.1.2

Metidji, A., Omenetti, S., Crotta, S., Li, Y., Nye, E., Ross, E., Li, V., Maradana, M. R., Schiering, C., & Stockinger, B. (2018). The Environmental Sensor AHR Protects from Inflammatory Damage by Maintaining Intestinal Stem Cell Homeostasis and Barrier Integrity. *Immunity*, *49*(2), 353-362.e5. https://doi.org/10.1016/j.immuni.2018.07.010

Milush, J. M., Long, B. R., Snyder-Cappione, J. E., Cappione, A. J., York, V. A., Ndhlovu, L. C., Lanier, L. L., Michaëlsson, J., & Nixon, D. F. (2009). Functionally distinct subsets of human NK cells and monocyte/DC-like cells identified by coexpression of CD56, CD7, and CD4. *Blood*, *114*(23), 4823–4831. https://doi.org/10.1182/blood-2009-04-216374

Misawa, T., Wagner, M., & Koyasu, S. (2022). ILC2s and Adipose Tissue Homeostasis: Progress to Date and the Road Ahead. *Frontiers in Immunology*, *13*, 876029. https://doi.org/10.3389/fimmu.2022.876029

Mittal, B. (2019). Subcutaneous adipose tissue & visceral adipose tissue. *The Indian Journal of Medical Research*, *149*(5), 571–573. https://doi.org/10.4103/ijmr.IJMR_1910_18

Mohammadi, H., Daryabor, G., Ghaffarian Bahraman, A., Keshavarzi, M., Kalantar, K., & Mohammadi-Bardbori, A. (2021). Aryl hydrocarbon receptor engagement during redox alteration determines the fate of CD4+ T cells in C57BL/6 mice. *Journal of Biochemical and Molecular Toxicology*, *35*(8), e22821. https://doi.org/10.1002/jbt.22821

Molofsky, A. B., Nussbaum, J. C., Liang, H.-E., Van Dyken, S. J., Cheng, L. E., Mohapatra, A., Chawla, A., & Locksley, R. M. (2013). Innate lymphoid type 2 cells sustain visceral adipose tissue eosinophils and alternatively activated macrophages. *The Journal of Experimental Medicine*, *210*(3), 535–549. https://doi.org/10.1084/jem.20121964

Morris, D. L., Singer, K., & Lumeng, C. N. (2011). Adipose tissue macrophages: Phenotypic plasticity and diversity in lean and obese states. *Current Opinion in Clinical Nutrition & Metabolic Care*, *14*(4), Article 4. https://doi.org/10.1097/MCO.0b013e328347970b

Movita, D., Kreefft, K., Biesta, P., van Oudenaren, A., Leenen, P. J. M., Janssen, H. L. A., & Boonstra, A. (2012). Kupffer cells express a unique combination of phenotypic and functional characteristics compared with splenic and peritoneal macrophages. *Journal of Leukocyte Biology*, *92*(4), 723–733. https://doi.org/10.1189/jlb.1111566

Mowat, A. M. (2003). Anatomical basis of tolerance and immunity to intestinal antigens. *Nature Reviews. Immunology*, *3*(4), 331–341. https://doi.org/10.1038/nri1057

Mowat, A. M., & Agace, W. W. (2014). Regional specialization within the intestinal immune system. *Nature Reviews Immunology*, *14*(10), Article 10. https://doi.org/10.1038/nri3738

Mowers, J., Uhm, M., Reilly, S. M., Simon, J., Leto, D., Chiang, S.-H., Chang, L., & Saltiel, A. R. (2013). Inflammation produces catecholamine resistance in obesity via activation of PDE3B by the protein kinases IKKε and TBK1. *eLife*, *2*, e01119. https://doi.org/10.7554/eLife.01119

Moyer, B. J., Rojas, I. Y., Kerley-Hamilton, J. S., Hazlett, H. F., Nemani, K. V., Trask, H. W., West, R. J., Lupien, L. E., Collins, A. J., Ringelberg, C. S., Gimi, B., Kinlaw, W. B., & Tomlinson, C. R. (2016). Inhibition of the aryl hydrocarbon receptor prevents Western diet-induced obesity. Model for AHR activation by kynurenine via oxidized-LDL, TLR2/4, TGFβ, and IDO1. *Toxicology and Applied Pharmacology*, *300*, 13–24. https://doi.org/10.1016/j.taap.2016.03.011

Muir, L. A., Cho, K. W., Geletka, L. M., Baker, N. A., Flesher, C. G., Ehlers, A. P., Kaciroti, N., Lindsly, S., Ronquist, S., Rajapakse, I., O'Rourke, R. W., & Lumeng, C. N. (o. J.). Human CD206+ macrophages associate with diabetes and adipose tissue lymphoid clusters. *JCI Insight*, 7(3), e146563. https://doi.org/10.1172/jci.insight.146563

Murray, I. A., & Perdew, G. H. (2020). How Ah Receptor Ligand Specificity Became Important in Understanding Its Physiological Function. *International Journal of Molecular Sciences*, *21*(24), Article 24. https://doi.org/10.3390/ijms21249614

Nagashima, R., Maeda, K., Imai, Y., & Takahashi, T. (1996). Lamina propria macrophages in the human gastrointestinal mucosa: Their distribution, immunohistological phenotype, and function. *The Journal of Histochemistry and Cytochemistry: Official Journal of the Histochemistry Society, 44*(7), 721–731. https://doi.org/10.1177/44.7.8675993

Navrátilová, V., Paloncýová, M., Berka, K., Mise, S., Haga, Y., Matsumura, C., Sakaki, T., Inui, H., & Otyepka, M. (2017). Molecular insights into the role of a distal F240A mutation that alters CYP1A1 activity towards persistent organic pollutants. *Biochimica et Biophysica Acta (BBA) - General Subjects*, 1861(11, Part A), 2852–2860. https://doi.org/10.1016/j.bbagen.2017.08.002

Nawaz, A., Aminuddin, A., Kado, T., Takikawa, A., Yamamoto, S., Tsuneyama, K., Igarashi, Y., Ikutani, M., Nishida, Y., Nagai, Y., Takatsu, K., Imura, J., Sasahara, M., Okazaki, Y., Ueki, K., Okamura, T., Tokuyama, K., Ando, A., Matsumoto, M., ... Tobe, K. (2017). CD206+ M2-like macrophages regulate systemic glucose metabolism by inhibiting proliferation of adipocyte progenitors. *Nature Communications*, 8(1), Article 1. https://doi.org/10.1038/s41467-017-00231-1

Nebert, D. W., Dalton, T. P., Okey, A. B., & Gonzalez, F. J. (2004). Role of Aryl Hydrocarbon Receptor-mediated Induction of the CYP1 Enzymes in Environmental Toxicity and Cancer *. *Journal of Biological Chemistry*, *279*(23), Article 23. https://doi.org/10.1074/jbc.R400004200

Netea, M. G., Joosten, L. A. B., Latz, E., Mills, K. H. G., Natoli, G., Stunnenberg, H. G., O'Neill, L. A. J., & Xavier, R. J. (2016). Trained immunity: A program of innate immune memory in health and disease. *Science (New York, N.Y.)*, 352(6284), aaf1098. https://doi.org/10.1126/science.aaf1098

Nguyen, V. T., Giannoni, F., Dubois, M.-F., Seo, S.-J., Vigneron, M., Kédinger, C., & Bensaude, O. (1996). In Vivo Degradation of RNA Polymerase II Largest Subunit Triggered by α -Amanitin. *Nucleic Acids Research*, *24*(15), 2924–2929. https://doi.org/10.1093/nar/24.15.2924

Norris, S., Collins, C., Doherty, D. G., Smith, F., McEntee, G., Traynor, O., Nolan, N., Hegarty, J., & O'Farrelly, C. (1998). Resident human hepatic lymphocytes are phenotypically different from circulating lymphocytes. *Journal of Hepatology*, *28*(1), 84–90. https://doi.org/10.1016/s0168-8278(98)80206-7

Odegaard, J. I., Ricardo-Gonzalez, R. R., Eagle, A. R., Vats, D., Morel, C. R., Goforth, M. H., Subramanian, V., Mukundan, L., Ferrante, A. W., & Chawla, A. (2008). Alternative M2 Activation of Kupffer Cells by PPARδ Ameliorates Obesity-Induced Insulin Resistance. *Cell Metabolism*, *7*(6), 496–507. https://doi.org/10.1016/j.cmet.2008.04.003

Ohashi, K., Parker, J. L., Ouchi, N., Higuchi, A., Vita, J. A., Gokce, N., Pedersen, A. A., Kalthoff, C., Tullin, S., Sams, A., Summer, R., & Walsh, K. (2010). Adiponectin Promotes Macrophage Polarization toward an Anti-inflammatory Phenotype. *The Journal of Biological Chemistry*, *285*(9), 6153–6160. https://doi.org/10.1074/jbc.M109.088708

Park, C., Cheung, K. P., Limon, N., Costanzo, A., Barba, C., Miranda, N., Gargas, S., Johnson, A. M. F., Olefsky, J. M., & Jameson, J. M. (2019). Obesity Modulates Intestinal Intraepithelial T Cell Persistence, CD103 and CCR9 Expression, and Outcome in Dextran Sulfate Sodium–Induced Colitis. *The Journal of Immunology*, 203(12), 3427–3435. https://doi.org/10.4049/jimmunol.1900082

Parks, A. J., Pollastri, M. P., Hahn, M. E., Stanford, E. A., Novikov, O., Franks, D. G., Haigh, S. E., Narasimhan, S., Ashton, T. D., Hopper, T. G., Kozakov, D., Beglov, D., Vajda, S., Schlezinger, J. J., & Sherr, D. H. (2014). In silico identification of an aryl hydrocarbon receptor antagonist with biological activity in vitro and in vivo. *Molecular Pharmacology*, *86*(5), 593–608. https://doi.org/10.1124/mol.114.093369

Parlakgül, G., Arruda, A. P., Pang, S., Cagampan, E., Min, N., Güney, E., Lee, G. Y., Inouye, K., Hess, H. F., Xu, C. S., & Hotamışlıgil, G. S. (2022). Regulation of liver subcellular architecture controls metabolic homeostasis. *Nature*, *603*(7902), Article 7902. https://doi.org/10.1038/s41586-022-04488-5

Pellizzon, M. A., & Ricci, M. R. (2018). The common use of improper control diets in diet-induced metabolic disease research confounds data interpretation: The fiber factor. *Nutrition & Metabolism*, 15(1), 3. https://doi.org/10.1186/s12986-018-0243-5

Poland, A. P., Glover, E., Robinson, J. R., & Nebert, D. W. (1974). Genetic expression of aryl hydrocarbon hydroxylase activity. Induction of monooxygenase activities and cytochrome P1-450 formation by 2,3,7,8-tetrachlorodibenzo-p-dioxin in mice genetically "nonresponsive" to other aromatic hydrocarbons. *The Journal of Biological Chemistry*, 249(17), 5599–5606.

Postal, B. G., Ghezzal, S., Aguanno, D., André, S., Garbin, K., Genser, L., Brot-Laroche, E., Poitou, C., Soula, H., Leturque, A., Clément, K., & Carrière, V. (2020). AhR activation defends gut barrier integrity against damage occurring in obesity. *Molecular Metabolism*, *39*, 101007. https://doi.org/10.1016/j.molmet.2020.101007

Powell, D. W., Pinchuk, I. V., Saada, J. I., Chen, X., & Mifflin, R. C. (2011). Mesenchymal Cells of the Intestinal Lamina Propria. *Annual review of physiology*, *73*, 213–237. https://doi.org/10.1146/annurev.physiol.70.113006.100646

Puga, A., Barnes, S. J., Dalton, T. P., Chang, C. y, Knudsen, E. S., & Maier, M. A. (2000). Aromatic hydrocarbon receptor interaction with the retinoblastoma protein potentiates repression of E2F-dependent transcription and cell cycle arrest. *The Journal of Biological Chemistry*, *275*(4), 2943–2950. https://doi.org/10.1074/jbc.275.4.2943

Qazi, A., Kumar, A., Sharma, A., Calzadilla, N., Weber, C. R., Mongan, K., Saksena, S., Dudeja, P. K., Alrefai, W. A., & Gill, R. K. (2022). Intestinal epithelial specific AhR deficient mice exhibit increased severity of experimentally induced chronic colitis. *The FASEB Journal*, *36*(S1). https://doi.org/10.1096/fasebj.2022.36.S1.R6171

Qin, Z., Kim, H.-J., Hemme, J., & Blankenstein, T. (2002). Inhibition of Methylcholanthrene-induced Carcinogenesis by an Interferon γ Receptor–dependent Foreign Body Reaction. *The Journal of Experimental Medicine*, *195*(11), 1479–1490. https://doi.org/10.1084/jem.20011887

Qiu, J., & Zhou, L. (2013). Aryl Hydrocarbon Receptor Promotes RORyt+ ILCs and Controls Intestinal Immunity and Inflammation. *Seminars in immunopathology*, *35*(6), 657–670. https://doi.org/10.1007/s00281-013-0393-5

Quintana, F. J. (2013). The aryl hydrocarbon receptor: A molecular pathway for the environmental control of the immune response. *Immunology*, 138(3), 183–189. https://doi.org/10.1111/imm.12046

Quintana-Hayashi, M. P., Padra, M., Padra, J. T., Benktander, J., & Lindén, S. K. (2018). Mucus-Pathogen Interactions in the Gastrointestinal Tract of Farmed Animals. *Microorganisms*, *6*(2), 55. https://doi.org/10.3390/microorganisms6020055

Racanelli, V., Sansonno, D., Piccoli, C., D'Amore, F. P., Tucci, F. A., & Dammacco, F. (2001). Molecular characterization of B cell clonal expansions in the liver of chronically hepatitis C virus-infected patients. *Journal of Immunology (Baltimore, Md.: 1950), 167*(1), 21–29. https://doi.org/10.4049/jimmunol.167.1.21

Raghunath, A., Sundarraj, K., Nagarajan, R., Arfuso, F., Bian, J., Kumar, A. P., Sethi, G., & Perumal, E. (2018). Antioxidant response elements: Discovery, classes, regulation and potential applications. *Redox Biology*, 17, 297–314. https://doi.org/10.1016/j.redox.2018.05.002

Ramachandran, P., Pellicoro, A., Vernon, M. A., Boulter, L., Aucott, R. L., Ali, A., Hartland, S. N., Snowdon, V. K., Cappon, A., Gordon-Walker, T. T., Williams, M. J., Dunbar, D. R., Manning, J. R., van Rooijen, N., Fallowfield, J. A., Forbes, S. J., & Iredale, J. P. (2012). Differential Ly-6C expression identifies the recruited macrophage phenotype, which orchestrates the regression of murine liver fibrosis. *Proceedings of the National Academy of Sciences*, *109*(46), E3186–E3195. https://doi.org/10.1073/pnas.1119964109

Randall, T. D., & Mebius, R. E. (2014). The development and function of mucosal lymphoid tissues: A balancing act with micro-organisms. *Mucosal Immunology*, 7(3), Article 3. https://doi.org/10.1038/mi.2014.11

Rasmussen, M. K., Daujat-Chavanieu, M., & Gerbal-Chaloin, S. (2017). Activation of the aryl hydrocarbon receptor decreases rifampicin-induced CYP3A4 expression in primary human hepatocytes and HepaRG. *Toxicology Letters*, *277*, 1–8. https://doi.org/10.1016/j.toxlet.2017.05.029

Rausch, M. E., Weisberg, S., Vardhana, P., & Tortoriello, D. V. (2008). Obesity in C57BL/6J mice is characterized by adipose tissue hypoxia and cytotoxic T-cell infiltration. *International Journal of Obesity (2005)*, *32*(3), 451–463. https://doi.org/10.1038/sj.ijo.0803744

Redondo-Urzainqui, A., Hernández-García, E., Cook, E. C. L., & Iborra, S. (2023). Dendritic cells in energy balance regulation. *Immunology Letters*, *253*, 19–27. https://doi.org/10.1016/j.imlet.2022.12.002

Remmerie, A., Martens, L., & Scott, C. L. (2020). Macrophage Subsets in Obesity, Aligning the Liver and Adipose Tissue. *Frontiers in Endocrinology*, *11*, 259. https://doi.org/10.3389/fendo.2020.00259

Remmerie, A., Martens, L., Thoné, T., Castoldi, A., Seurinck, R., Pavie, B., Roels, J., Vanneste, B., De Prijck, S., Vanhockerhout, M., Binte Abdul Latib, M., Devisscher, L., Hoorens, A., Bonnardel, J., Vandamme, N., Kremer, A., Borghgraef, P., Van Vlierberghe, H., Lippens, S., ... Scott, C. L. (2020). Osteopontin Expression Identifies a Subset of Recruited Macrophages Distinct from Kupffer Cells in the Fatty Liver. *Immunity*, *53*(3), 641-657.e14. https://doi.org/10.1016/j.immuni.2020.08.004

Robinson, M. W., Harmon, C., & O'Farrelly, C. (2016). Liver immunology and its role in inflammation and homeostasis. *Cellular & Molecular Immunology*, *13*(3), Article 3. https://doi.org/10.1038/cmi.2016.3

Rojas, I. Y., Moyer, B. J., Ringelberg, C. S., Wilkins, O. M., Pooler, D. B., Ness, D. B., Coker, S., Tosteson, T. D., Lewis, L. D., Chamberlin, M. D., & Tomlinson, C. R. (2021). Kynurenine-Induced Aryl Hydrocarbon Receptor Signaling in Mice Causes Body Mass Gain, Liver Steatosis, and Hyperglycemia. *Obesity*, *29*(2), 337–349. https://doi.org/10.1002/oby.23065

Rosa, I., Marini, M., & Manetti, M. (2021). Telocytes: An Emerging Component of Stem Cell Niche Microenvironment. *Journal of Histochemistry and Cytochemistry*, *69*(12), 795–818. https://doi.org/10.1369/00221554211025489

Saito, R., Miki, Y., Hata, S., Takagi, K., Iida, S., Oba, Y., Ono, K., Ishida, T., Suzuki, T., Ohuchi, N., & Sasano, H. (2014). Aryl hydrocarbon receptor in breast cancer—A newly defined prognostic marker. Hormones & Cancer, 5(1), 11–21. https://doi.org/10.1007/s12672-013-0160-z

Santos-Alvarez, J., Goberna, R., & Sánchez-Margalet, V. (1999). Human leptin stimulates proliferation and activation of human circulating monocytes. *Cellular Immunology*, *194*(1), 6–11. https://doi.org/10.1006/cimm.1999.1490

Sattar, N., Forrest, E., & Preiss, D. (2014). Non-alcoholic fatty liver disease. *The BMJ*, *349*, g4596. https://doi.org/10.1136/bmj.g4596

Schanz, O., Chijiiwa, R., Cengiz, S. C., Majlesain, Y., Weighardt, H., Takeyama, H., & Förster, I. (2020a). Dietary AhR Ligands Regulate AhRR Expression in Intestinal Immune Cells and Intestinal Microbiota Composition. *International Journal of Molecular Sciences*, *21*(9), Article 9. https://doi.org/10.3390/ijms21093189

Schanz, O., Chijiiwa, R., Cengiz, S. C., Majlesain, Y., Weighardt, H., Takeyama, H., & Förster, I. (2020b). Dietary AhR Ligands Regulate AhRR Expression in Intestinal Immune Cells and Intestinal Microbiota Composition. *International Journal of Molecular Sciences*, *21*(9), Article 9. https://doi.org/10.3390/ijms21093189

Schiering, C., Wincent, E., Metidji, A., Iseppon, A., Li, Y., Potocnik, A. J., Omenetti, S., Henderson, C. J., Wolf, C. R., Nebert, D. W., & Stockinger, B. (2017a). Feedback control of AHR signalling regulates intestinal immunity. *Nature*, *542*(7640), Article 7640. https://doi.org/10.1038/nature21080

- Schiering, C., Wincent, E., Metidji, A., Iseppon, A., Li, Y., Potocnik, A. J., Omenetti, S., Henderson, C. J., Wolf, C. R., Nebert, D. W., & Stockinger, B. (2017b). Feedback control of AHR signalling regulates intestinal immunity. *Nature*, *542*(7640), Article 7640. https://doi.org/10.1038/nature21080
- Schmidt, J. V., Su, G. H., Reddy, J. K., Simon, M. C., & Bradfield, C. A. (1996). Characterization of a murine Ahr null allele: Involvement of the Ah receptor in hepatic growth and development. *Proceedings of the National Academy of Sciences of the United States of America*, *93*(13), 6731–6736.
- Schwartz, M. W., Prigeon, R. L., Kahn, S. E., Nicolson, M., Moore, J., Morawiecki, A., Boyko, E. J., & Porte, D. (1997). Evidence that plasma leptin and insulin levels are associated with body adiposity via different mechanisms. *Diabetes Care*, *20*(9), 1476–1481. https://doi.org/10.2337/diacare.20.9.1476
- Schwarz, R. I. (2015). Collagen I and the fibroblast: High protein expression requires a new paradigm of post-transcriptional, feedback regulation. *Biochemistry and Biophysics Reports*, *3*, 38–44. https://doi.org/10.1016/j.bbrep.2015.07.007
- Seidel, S. D., Winters, G. M., Rogers, W. J., Ziccardi, M. H., Li, V., Keser, B., & Denison, M. S. (2001). Activation of the Ah receptor signaling pathway by prostaglandins. *Journal of Biochemical and Molecular Toxicology*, *15*(4), 187–196. https://doi.org/10.1002/jbt.16
- Shah, K., Maradana, M. R., Joaquina Delàs, M., Metidji, A., Graelmann, F., Llorian, M., Chakravarty, P., Li, Y., Tolaini, M., Shapiro, M., Kelly, G., Cheshire, C., Bhurta, D., Bharate, S. B., & Stockinger, B. (2022). Cell-intrinsic Aryl Hydrocarbon Receptor signalling is required for the resolution of injury-induced colonic stem cells. *Nature Communications*, *13*(1), Article 1. https://doi.org/10.1038/s41467-022-29098-7
- Shaul, M. E., Bennett, G., Strissel, K. J., Greenberg, A. S., & Obin, M. S. (2010). Dynamic, M2-like remodeling phenotypes of CD11c+ adipose tissue macrophages during high-fat diet—Induced obesity in mice. *Diabetes*, *59*(5), 1171–1181. https://doi.org/10.2337/db09-1402
- Shetty, S., Lalor, P. F., & Adams, D. H. (2018). Liver sinusoidal endothelial cells—Gatekeepers of hepatic immunity. *Nature Reviews. Gastroenterology & Hepatology*, *15*(9), 555–567. https://doi.org/10.1038/s41575-018-0020-y
- Shi, C., & Pamer, E. G. (2011). Monocyte recruitment during infection and inflammation. *Nature Reviews. Immunology*, *11*(11), 762–774. https://doi.org/10.1038/nri3070
- Shin, S., Wakabayashi, N., Misra, V., Biswal, S., Lee, G. H., Agoston, E. S., Yamamoto, M., & Kensler, T. W. (2007). NRF2 Modulates Aryl Hydrocarbon Receptor Signaling: Influence on Adipogenesis. *Molecular and Cellular Biology*, *27*(20), 7188–7197. https://doi.org/10.1128/MCB.00915-07
- Sierro, F., Evrard, M., Rizzetto, S., Melino, M., Mitchell, A. J., Florido, M., Beattie, L., Walters, S. B., Tay, S. S., Lu, B., Holz, L. E., Roediger, B., Wong, Y. C., Warren, A., Ritchie, W., McGuffog, C., Weninger, W., Le Couteur, D. G., Ginhoux, F., ... Bertolino, P. (2017). A Liver Capsular Network of Monocyte-Derived Macrophages Restricts Hepatic Dissemination of Intraperitoneal Bacteria by Neutrophil Recruitment. *Immunity*, *47*(2), 374-388.e6. https://doi.org/10.1016/j.immuni.2017.07.018
- Singla, P., Bardoloi, A., & Parkash, A. A. (2010). Metabolic effects of obesity: A review. *World Journal of Diabetes*, 1(3), 76–88. https://doi.org/10.4239/wjd.v1.i3.76
- Solvay, M., Pfänder, P., Klaessens, S., Pilotte, L., Stroobant, V., Lamy, J., Naulaerts, S., Spillier, Q., Frédérick, R., Plaen, E. D., Sers, C., Opitz, C. A., Eynde, B. J. V. den, & Zhu, J.-J. (2023). *Tryptophan depletion sensitizes the AHR pathway by increasing AHR expression and GCN2/LAT1-mediated*

kynurenine uptake, and potentiates induction of regulatory *T lymphocytes* (S. 2023.01.16.524177). bioRxiv. https://doi.org/10.1101/2023.01.16.524177

Spits, H., & Cupedo, T. (2012). Innate lymphoid cells: Emerging insights in development, lineage relationships, and function. *Annual Review of Immunology*, *30*, 647–675. https://doi.org/10.1146/annurev-immunol-020711-075053

Stanton, M. C., Chen, S.-C., Jackson, J. V., Rojas-Triana, A., Kinsley, D., Cui, L., Fine, J. S., Greenfeder, S., Bober, L. A., & Jenh, C.-H. (2011). Inflammatory Signals shift from adipose to liver during high fat feeding and influence the development of steatohepatitis in mice. *Journal of Inflammation*, 8(1), 8. https://doi.org/10.1186/1476-9255-8-8

Stejskalova, L., Dvorak, Z., & Pavek, P. (2011). Endogenous and Exogenous Ligands of Aryl Hydrocarbon Receptor: Current State of Art. *Current Drug Metabolism*, *12*(2), 198–212. https://doi.org/10.2174/138920011795016818

Steppan, C. M., Bailey, S. T., Bhat, S., Brown, E. J., Banerjee, R. R., Wright, C. M., Patel, H. R., Ahima, R. S., & Lazar, M. A. (2001). The hormone resistin links obesity to diabetes. *Nature*, *409*(6818), 307–312. https://doi.org/10.1038/35053000

Steppan, C. M., Wang, J., Whiteman, E. L., Birnbaum, M. J., & Lazar, M. A. (2005). Activation of SOCS-3 by Resistin. *Molecular and Cellular Biology*, *25*(4), 1569–1575. https://doi.org/10.1128/MCB.25.4.1569-1575.2005

Stockinger, B., Shah, K., & Wincent, E. (2021). AHR in the intestinal microenvironment: Safeguarding barrier function. *Nature Reviews Gastroenterology & Hepatology*, *18*(8), Article 8. https://doi.org/10.1038/s41575-021-00430-8

Stremmel, C., Schuchert, R., Wagner, F., Thaler, R., Weinberger, T., Pick, R., Mass, E., Ishikawa-Ankerhold, H. C., Margraf, A., Hutter, S., Vagnozzi, R., Klapproth, S., Frampton, J., Yona, S., Scheiermann, C., Molkentin, J. D., Jeschke, U., Moser, M., Sperandio, M., ... Schulz, C. (2018). Yolk sac macrophage progenitors traffic to the embryo during defined stages of development. *Nature Communications*, *9*(1), Article 1. https://doi.org/10.1038/s41467-017-02492-2

Surendar, J., Frohberger, S. J., Karunakaran, I., Schmitt, V., Stamminger, W., Neumann, A.-L., Wilhelm, C., Hoerauf, A., & Hübner, M. P. (2019). Adiponectin Limits IFN-γ and IL-17 Producing CD4 T Cells in Obesity by Restraining Cell Intrinsic Glycolysis. *Frontiers in Immunology*, *10*, 2555. https://doi.org/10.3389/fimmu.2019.02555

Taylor, K. R., Mills, R. E., Costanzo, A. E., & Jameson, J. M. (2010). $\Gamma\delta$ T Cells Are Reduced and Rendered Unresponsive by Hyperglycemia and Chronic TNF α in Mouse Models of Obesity and Metabolic Disease. *PLOS ONE*, *5*(7), e11422. https://doi.org/10.1371/journal.pone.0011422

Thomson, A. W., & Knolle, P. A. (2010). Antigen-presenting cell function in the tolerogenic liver environment. *Nature Reviews. Immunology*, *10*(11), 753–766. https://doi.org/10.1038/nri2858

Tijet, N., Boutros, P. C., Moffat, I. D., Okey, A. B., Tuomisto, J., & Pohjanvirta, R. (2006). Aryl hydrocarbon receptor regulates distinct dioxin-dependent and dioxin-independent gene batteries. *Molecular Pharmacology*, *69*(1), 140–153. https://doi.org/10.1124/mol.105.018705

Townsend, K., & Tseng, Y.-H. (2012). Brown adipose tissue: Recent insights into development, metabolic function and therapeutic potential. *Adipocyte*, 1(1), 13. https://doi.org/10.4161/adip.18951

Trim, W. V., & Lynch, L. (2022). Immune and non-immune functions of adipose tissue leukocytes. *Nature Reviews Immunology*, *22*(6), Article 6. https://doi.org/10.1038/s41577-021-00635-7

Tsuchiya, Y., Nakajima, M., Itoh, S., Iwanari, M., & Yokoi, T. (2003). Expression of Aryl Hydrocarbon Receptor Repressor in Normal Human Tissues and Inducibility by Polycyclic Aromatic Hydrocarbons in Human Tumor-Derived Cell Lines. *Toxicological Sciences*, *72*(2), Article 2. https://doi.org/10.1093/toxsci/kfg022

Uno, S., Dragin, N., Miller, M. L., Dalton, T. P., Gonzalez, F. J., & Nebert, D. W. (2008). Basal and inducible CYP1 mRNA quantitation and protein localization throughout the mouse gastrointestinal tract. *Free radical biology & medicine*, *44*(4), 570–583. https://doi.org/10.1016/j.freeradbiomed.2007.10.044

Uno, S., Nebert, D. W., & Makishima, M. (2018). Cytochrome P450 1A1 (CYP1A1) protects against nonalcoholic fatty liver disease caused by Western diet containing benzo[a]pyrene in mice. Food and chemical toxicology: an international journal published for the British Industrial Biological Research Association, 113, 73–82. https://doi.org/10.1016/j.fct.2018.01.029

van Beek, L., van Klinken, J. B., Pronk, A. C. M., van Dam, A. D., Dirven, E., Rensen, P. C. N., Koning, F., Willems van Dijk, K., & van Harmelen, V. (2015). The limited storage capacity of gonadal adipose tissue directs the development of metabolic disorders in male C57Bl/6J mice. *Diabetologia*, *58*(7), 1601–1609. https://doi.org/10.1007/s00125-015-3594-8

van der Heijden, R. A., Sheedfar, F., Morrison, M. C., Hommelberg, P. P., Kor, D., Kloosterhuis, N. J., Gruben, N., Youssef, S. A., de Bruin, A., Hofker, M. H., Kleemann, R., Koonen, D. P., & Heeringa, P. (2015). High-fat diet induced obesity primes inflammation in adipose tissue prior to liver in C57BL/6j mice. *Aging (Albany NY)*, 7(4), 256–267.

van der Zande, H. J. P., Nitsche, D., Schlautmann, L., Guigas, B., & Burgdorf, S. (2021). The Mannose Receptor: From Endocytic Receptor and Biomarker to Regulator of (Meta)Inflammation. *Frontiers in Immunology*, *12*, 765034. https://doi.org/10.3389/fimmu.2021.765034

Velázquez, K. T., Enos, R. T., Bader, J. E., Sougiannis, A. T., Carson, M. S., Chatzistamou, I., Carson, J. A., Nagarkatti, P. S., Nagarkatti, M., & Murphy, E. A. (2019). Prolonged high-fat-diet feeding promotes non-alcoholic fatty liver disease and alters gut microbiota in mice. *World Journal of Hepatology*, 11(8), 619–637. https://doi.org/10.4254/wjh.v11.i8.619

Venter, C., Meyer, R. W., Greenhawt, M., Pali-Schöll, I., Nwaru, B., Roduit, C., Untersmayr, E., Adel-Patient, K., Agache, I., Agostoni, C., Akdis, C. A., Feeney, M., Hoffmann-Sommergruber, K., Lunjani, N., Grimshaw, K., Reese, I., Smith, P. K., Sokolowska, M., Vassilopoulou, E., ... O'Mahony, L. (2022). Role of dietary fiber in promoting immune health—An EAACI position paper. *Allergy*, 77(11), 3185–3198. https://doi.org/10.1111/all.15430

Villa, M., Gialitakis, M., Tolaini, M., Ahlfors, H., Henderson, C. J., Wolf, C. R., Brink, R., & Stockinger, B. (2017). Aryl hydrocarbon receptor is required for optimal B-cell proliferation. *The EMBO Journal*, *36*(1), 116–128. https://doi.org/10.15252/embj.201695027

Vogel, C. F. A., & Haarmann-Stemmann, T. (2017). The aryl hydrocarbon receptor repressor – More than a simple feedback inhibitor of AhR signaling: Clues for its role in inflammation and cancer. *Current Opinion in Toxicology*, *2*, 109–119. https://doi.org/10.1016/j.cotox.2017.02.004

Vogel, C. F. A., Khan, E. M., Leung, P. S. C., Gershwin, M. E., Chang, W. L. W., Wu, D., Haarmann-Stemmann, T., Hoffmann, A., & Denison, M. S. (2014). Cross-talk between Aryl Hydrocarbon Receptor

- and the Inflammatory Response. *The Journal of Biological Chemistry*, 289(3), 1866–1875. https://doi.org/10.1074/jbc.M113.505578
- Vogel, C. F. A., Sciullo, E., & Matsumura, F. (2007). Involvement of RelB in aryl hydrocarbon receptor-mediated induction of chemokines. *Biochemical and Biophysical Research Communications*, *363*(3), 722–726. https://doi.org/10.1016/j.bbrc.2007.09.032
- Vuerich, M., Robson, S. C., & Longhi, M. S. (2019). Ectonucleotidases in Intestinal and Hepatic Inflammation. *Frontiers in Immunology*, *10*, 507. https://doi.org/10.3389/fimmu.2019.00507
- Wada, T., Sunaga, H., Miyata, K., Shirasaki, H., Uchiyama, Y., & Shimba, S. (2016a). Aryl Hydrocarbon Receptor Plays Protective Roles against High Fat Diet (HFD)-induced Hepatic Steatosis and the Subsequent Lipotoxicity via Direct Transcriptional Regulation of Socs3 Gene Expression. *The Journal of Biological Chemistry*, *291*(13), 7004–7016. https://doi.org/10.1074/jbc.M115.693655
- Wada, T., Sunaga, H., Miyata, K., Shirasaki, H., Uchiyama, Y., & Shimba, S. (2016b). Aryl Hydrocarbon Receptor Plays Protective Roles against High Fat Diet (HFD)-induced Hepatic Steatosis and the Subsequent Lipotoxicity via Direct Transcriptional Regulation of Socs3 Gene Expression. *The Journal of Biological Chemistry*, 291(13), Article 13. https://doi.org/10.1074/jbc.M115.693655
- Wang, C., Xu, C.-X., Krager, S. L., Bottum, K. M., Liao, D.-F., & Tischkau, S. A. (2011). Aryl Hydrocarbon Receptor Deficiency Enhances Insulin Sensitivity and Reduces PPAR-α Pathway Activity in Mice. *Environmental Health Perspectives*, *119*(12), 1739–1744. https://doi.org/10.1289/ehp.1103593
- Wang, Q., Yang, K., Han, B., Sheng, B., Yin, J., Pu, A., Li, L., Sun, L., Yu, M., Qiu, Y., Xiao, W., & Yang, H. (2018). Aryl hydrocarbon receptor inhibits inflammation in DSS-induced colitis via the MK2/p-MK2/TTP pathway. *International Journal of Molecular Medicine*, *41*(2), 868–876. https://doi.org/10.3892/ijmm.2017.3262
- Wang, X., Liu, M., Zhang, J., Brown, N. K., Zhang, P., Zhang, Y., Liu, H., Du, X., Wu, W., Devenport, M., Tao, W., Mao-Draayer, Y., Chen, G.-Y., Chen, Y. E., Zheng, P., & Liu, Y. (2022). CD24-Siglec axis is an innate immune checkpoint against metaflammation and metabolic disorder. *Cell Metabolism*, *34*(8), 1088-1103.e6. https://doi.org/10.1016/j.cmet.2022.07.005
- Wang, Y., Nakajima, T., Gonzalez, F. J., & Tanaka, N. (2020). PPARs as Metabolic Regulators in the Liver: Lessons from Liver-Specific PPAR-Null Mice. *International Journal of Molecular Sciences*, *21*(6), 2061. https://doi.org/10.3390/ijms21062061
- Wang, Y., Song, W., Yu, S., Liu, Y., & Chen, Y.-G. (2022). Intestinal cellular heterogeneity and disease development revealed by single-cell technology. *Cell Regeneration*, *11*, 26. https://doi.org/10.1186/s13619-022-00127-6
- Wang, Y.-C., Cao, Y., Pan, C., Zhou, Z., Yang, L., & Lusis, A. J. (2023). Intestinal cell type-specific communication networks underlie homeostasis and response to Western diet. *Journal of Experimental Medicine*, 220(5), e20221437. https://doi.org/10.1084/jem.20221437
- Wayne, D., Kwok, T. C., Ojha, S., Budge, H., & Symonds, M. E. (2020). Chapter 39—Origins of Adipose Tissue and Adipose Regulating Hormones. In C. S. Kovacs & C. L. Deal (Hrsg.), *Maternal-Fetal and Neonatal Endocrinology* (S. 663–672). Academic Press. https://doi.org/10.1016/B978-0-12-814823-5.00039-8
- Wei, Y. D., Helleberg, H., Rannug, U., & Rannug, A. (1998). Rapid and transient induction of CYP1A1 gene expression in human cells by the tryptophan photoproduct 6-formylindolo[3,2-b]carbazole. *Chemico-Biological Interactions*, 110(1–2), 39–55. https://doi.org/10.1016/s0009-2797(97)00111-7

Wen, H., Feng, L., Jiang, W., Liu, Y., Jiang, J., Li, S., Tang, L., Zhang, Y., Kuang, S., & Zhou, X. (2014). Dietary tryptophan modulates intestinal immune response, barrier function, antioxidant status and gene expression of TOR and Nrf2 in young grass carp (Ctenopharyngodon idella). *Fish & Shellfish Immunology*, *40*(1), 275–287. https://doi.org/10.1016/j.fsi.2014.07.004

Wensveen, F. M., Valentić, S., Šestan, M., Turk Wensveen, T., & Polić, B. (2015). Interactions between adipose tissue and the immune system in health and malnutrition. *Seminars in Immunology*, *27*(5), 322–333. https://doi.org/10.1016/j.smim.2015.10.006

Wentworth, J. M., Naselli, G., Brown, W. A., Doyle, L., Phipson, B., Smyth, G. K., Wabitsch, M., O'Brien, P. E., & Harrison, L. C. (2010). Pro-Inflammatory CD11c+CD206+ Adipose Tissue Macrophages Are Associated With Insulin Resistance in Human Obesity. *Diabetes*, *59*(7), 1648–1656. https://doi.org/10.2337/db09-0287

West, N. R. (2019). Coordination of Immune-Stroma Crosstalk by IL-6 Family Cytokines. *Frontiers in Immunology*, *10*. https://www.frontiersin.org/articles/10.3389/fimmu.2019.01093

West, N. R., Hegazy, A. N., Owens, B. M. J., Bullers, S. J., Linggi, B., Buonocore, S., Coccia, M., Görtz, D., This, S., Stockenhuber, K., Pott, J., Friedrich, M., Ryzhakov, G., Baribaud, F., Brodmerkel, C., Cieluch, C., Rahman, N., Müller-Newen, G., Owens, R. J., ... Powrie, F. (2017). Oncostatin M drives intestinal inflammation and predicts response to tumor necrosis factor—neutralizing therapy in patients with inflammatory bowel disease. *Nature Medicine*, *23*(5), Article 5. https://doi.org/10.1038/nm.4307

Wiggins, B. G., Wang, Y.-F., Burke, A., Grunberg, N., Vlachaki Walker, J. M., Dore, M., Chahrour, C., Pennycook, B. R., Sanchez-Garrido, J., Vernia, S., Barr, A. R., Frankel, G., Birdsey, G. M., Randi, A. M., & Schiering, C. (2023). Endothelial sensing of AHR ligands regulates intestinal homeostasis. *Nature*, 621(7980), Article 7980. https://doi.org/10.1038/s41586-023-06508-4

Wincent, E., Bengtsson, J., Mohammadi Bardbori, A., Alsberg, T., Luecke, S., Rannug, U., & Rannug, A. (2012). Inhibition of cytochrome P4501-dependent clearance of the endogenous agonist FICZ as a mechanism for activation of the aryl hydrocarbon receptor. *Proceedings of the National Academy of Sciences of the United States of America*, 109(12), 4479–4484. https://doi.org/10.1073/pnas.1118467109

Wisse, E., Braet, F., Luo, D., De Zanger, R., Jans, D., Crabbé, E., & Vermoesen, A. (1996). Structure and function of sinusoidal lining cells in the liver. *Toxicologic Pathology*, *24*(1), 100–111. https://doi.org/10.1177/019262339602400114

Wolf, M. J., Adili, A., Piotrowitz, K., Abdullah, Z., Boege, Y., Stemmer, K., Ringelhan, M., Simonavicius, N., Egger, M., Wohlleber, D., Lorentzen, A., Einer, C., Schulz, S., Clavel, T., Protzer, U., Thiele, C., Zischka, H., Moch, H., Tschöp, M., ... Heikenwalder, M. (2014). Metabolic activation of intrahepatic CD8+ T cells and NKT cells causes nonalcoholic steatohepatitis and liver cancer via cross-talk with hepatocytes. *Cancer Cell*, 26(4), 549–564. https://doi.org/10.1016/j.ccell.2014.09.003

Wong, C. K., Cheung, P. F.-Y., & Lam, C. W. K. (2007). Leptin-mediated cytokine release and migration of eosinophils: Implications for immunopathophysiology of allergic inflammation. *European Journal of Immunology*, *37*(8), 2337–2348. https://doi.org/10.1002/eji.200636866

Woods, S. C., Seeley, R. J., Porte, D., & Schwartz, M. W. (1998). Signals that regulate food intake and energy homeostasis. *Science (New York, N.Y.)*, *280*(5368), 1378–1383. https://doi.org/10.1126/science.280.5368.1378

Woolard, M. D., Hensley, L. L., Kawula, T. H., & Frelinger, J. A. (2008). Respiratory Francisella tularensis Live Vaccine Strain Infection Induces Th17 Cells and Prostaglandin E2, Which Inhibits Generation of Gamma Interferon-Positive T Cells. *Infection and Immunity*, *76*(6), 2651–2659. https://doi.org/10.1128/IAI.01412-07

Wright, E. J., De Castro, K. P., Joshi, A. D., & Elferink, C. J. (2017). Canonical and non-canonical aryl hydrocarbon receptor signaling pathways. *Current opinion in toxicology*, *2*, 87–92. https://doi.org/10.1016/j.cotox.2017.01.001

Xu, C.-X., Wang, C., Zhang, Z.-M., Jaeger, C. D., Krager, S. L., Bottum, K. M., Liu, J., Liao, D.-F., & Tischkau, S. A. (2015). ARYL HYDROCARBON RECEPTOR DEFICIENCY PROTECTS MICE FROM DIET-INDUCED ADIPOSITY AND METABOLIC DISORDERS THROUGH INCREASED ENERGY EXPENDITURE. *International journal of obesity (2005), 39*(8), Article 8. https://doi.org/10.1038/ijo.2015.63

Xu, J., & Shi, G.-P. (2014). Vascular wall extracellular matrix proteins and vascular diseases. *Biochimica et biophysica acta*, *1842*(11), 2106–2119. https://doi.org/10.1016/j.bbadis.2014.07.008

Yamauchi, T., Kamon, J., Minokoshi, Y., Ito, Y., Waki, H., Uchida, S., Yamashita, S., Noda, M., Kita, S., Ueki, K., Eto, K., Akanuma, Y., Froguel, P., Foufelle, F., Ferre, P., Carling, D., Kimura, S., Nagai, R., Kahn, B. B., & Kadowaki, T. (2002). Adiponectin stimulates glucose utilization and fatty-acid oxidation by activating AMP-activated protein kinase. *Nature Medicine*, *8*(11), 1288–1295. https://doi.org/10.1038/nm788

Yamauchi, T., Kamon, J., Waki, H., Terauchi, Y., Kubota, N., Hara, K., Mori, Y., Ide, T., Murakami, K., Tsuboyama-Kasaoka, N., Ezaki, O., Akanuma, Y., Gavrilova, O., Vinson, C., Reitman, M. L., Kagechika, H., Shudo, K., Yoda, M., Nakano, Y., ... Kadowaki, T. (2001). The fat-derived hormone adiponectin reverses insulin resistance associated with both lipoatrophy and obesity. *Nature Medicine*, *7*(8), 941–946. https://doi.org/10.1038/90984

Yan, J., Tung, H.-C., Li, S., Niu, Y., Garbacz, W. G., Lu, P., Bi, Y., Li, Y., He, J., Xu, M., Ren, S., Monga, S. P., Schwabe, R. F., Yang, D., & Xie, W. (2019). Aryl Hydrocarbon Receptor Signaling Prevents Activation of Hepatic Stellate Cells and Liver Fibrogenesis in Mice. *Gastroenterology*, *157*(3), 793-806.e14. https://doi.org/10.1053/j.gastro.2019.05.066

Yang, M., Qi, X., Li, N., Kaifi, J. T., Chen, S., Wheeler, A. A., Kimchi, E. T., Ericsson, A. C., Rector, R. S., Staveley-O'Carroll, K. F., & Li, G. (2023). Western diet contributes to the pathogenesis of non-alcoholic steatohepatitis in male mice via remodeling gut microbiota and increasing production of 2-oleoylglycerol. *Nature Communications*, *14*(1), Article 1. https://doi.org/10.1038/s41467-023-35861-1

Ye, W., Chen, R., Chen, X., Huang, B., Lin, R., Xie, X., Chen, J., Jiang, J., Deng, Y., & Wen, J. (2019). AhR regulates the expression of human cytochrome P450 1A1 (CYP1A1) by recruiting Sp1. *The FEBS Journal*, 286(21), Article 21. https://doi.org/10.1111/febs.14956

Yin, J., Sheng, B., Qiu, Y., Yang, K., Xiao, W., & Yang, H. (2016). Role of AhR in positive regulation of cell proliferation and survival. *Cell Proliferation*, 49(5), 554–560. https://doi.org/10.1111/cpr.12282

Yoshimatsu, Y., Sujino, T., Miyamoto, K., Harada, Y., Tanemoto, S., Ono, K., Umeda, S., Yoshida, K., Teratani, T., Suzuki, T., Mikami, Y., Nakamoto, N., Sasaki, N., Takabayashi, K., Hosoe, N., Ogata, H., Sawada, K., Imamura, T., Yoshimura, A., & Kanai, T. (2022). Aryl hydrocarbon receptor signals in epithelial cells govern the recruitment and location of Helios+ Tregs in the gut. *Cell Reports*, *39*(6), 110773. https://doi.org/10.1016/j.celrep.2022.110773

Zhang, Y., Fu, Q., Wu, T., Liu, K., Xiao, Y., Liao, Q., Qi, X., Li, Y., & Zhou, L. (2023). 5-Methoxyflavone ameliorates non-alcoholic fatty liver disease through targeting the cytochrome P450 1A1. *Free Radical Biology and Medicine*, *195*, 178–191. https://doi.org/10.1016/j.freeradbiomed.2022.12.093

Zhang, Y., & Huang, B. (2017). The Development and Diversity of ILCs, NK Cells and Their Relevance in Health and Diseases. *Advances in Experimental Medicine and Biology*, *1024*, 225–244. https://doi.org/10.1007/978-981-10-5987-2_11

Zhou, L. (2016). AHR Function in Lymphocytes: Emerging Concepts. *Trends in Immunology*, *37*(1), 17–31. https://doi.org/10.1016/j.it.2015.11.007

Zigmond, E., Samia-Grinberg, S., Pasmanik-Chor, M., Brazowski, E., Shibolet, O., Halpern, Z., & Varol, C. (2014). Infiltrating monocyte-derived macrophages and resident kupffer cells display different ontogeny and functions in acute liver injury. *Journal of Immunology (Baltimore, Md.: 1950), 193*(1), 344–353. https://doi.org/10.4049/jimmunol.14005

Publication

Parts of this thesis are included in:

Graelmann, F. J., Gondorf, F., Majlesain, Y., Niemann, B., Klepac, K., Gosejacob, D., Gottschalk, M., Mayer, M., Iriady, I., Hatzfeld, P., Lindenberg, S. K., Wunderling, K., Thiele, C., Abdullah, Z., He, W., Hiller, K., Händler, K., Beyer, M. D., Ulas, T., Pfeifer, A., Esser, C., Weighardt, H., Förster, I., & Reverte-Salisa, L. (2024). Differential cell type-specific function of the aryl hydrocarbon receptor and its repressor in diet-induced obesity and fibrosis. *Molecular Metabolism*, *85*, 101963. https://doi.org/10.1016/j.molmet.2024.101963

Acknowledgements

Foremost, I would like to appreciate Prof. Irmgard Förster for giving me a chance to carry out exciting research projects in her group, for supervising my PhD project, and for her support and understanding over the past years.

I would also like to express my gratitude to PD Dr. Heike Weighardt for all the valuable inputs and intellectually stimulating discussions throughout the years, as well as for proofreading this dissertation.

I further want to thank Prof. Christoph Wilhelm for being the second referee for my PhD dissertation.

Furthermore, I would like to thank all AG Förster/AG Weighardt members for being very collaborative and supportive, not only during experiments, but also during day-to-day life. I would also like to thank Philip Hatzfeld for technical assistance, particularly for helping me with western blot troubleshooting and for generating the mouse lines for my crucial experiments. I also want to thank other colleagues from LIMES institute for scientific advices and insightful discussion in the past years.

I would also like to thank Vincent Wieland and Dr. Dilan Pathirana from the group of Prof. Jan Hasenauer, for generating the mathematical model of AhR signaling, which help elucidating the signaling pathway. A special thank also goes to Prof. Andreas Schlitzer and Dr. David Bejerano for performing the spatial phenotyping method, which helped me greatly in answering an important scientific question.

I'm also thankful for my friends and family all over the world for the supports throughout my PhD journey. Lastly, I want to thank Jonathan, for always being there for me throughout the ups and downs.